# THE RESPONSE OF INDIVIDUAL LIVING CELLS OF *CHLAMYDOMONAS* SPP. TO HIGH LIGHT AND SINGLET OXYGEN

A Thesis Submitted to the College of

Graduate and Postdoctoral Studies

In Partial Fulfillment of the Requirements

For the Degree of Doctor of Philosophy

In the Department of Biology

University of Saskatchewan

Saskatoon

By Kira Leanne Goff

# PERMISSION TO USE

In presenting this thesis/dissertation in partial fulfillment of the requirements for a Postgraduate degree from the University of Saskatchewan, I agree that the Libraries of this University may make it freely available for inspection. I further agree that permission for copying of this thesis/dissertation in any manner, in whole or in part, for scholarly purposes may be granted by the professor or professors who supervised my thesis/dissertation work or, in their absence, by the Head of the Department or the Dean of the College in which my thesis work was done. It is understood that any copying or publication or use of this thesis/dissertation or parts thereof for financial gain shall not be allowed without my written permission. It is also understood that due recognition shall be given to me and to the University of Saskatchewan in any scholarly use which may be made of any material in my thesis/dissertation.

## DISCLAIMER

Reference in this thesis/ dissertation to any specific commercial products, process, or service by trade name, trademark, manufacturer, or otherwise, does not constitute or imply its endorsement, recommendation, or favouring by the University of Saskatchewan. The views and opinions of the author expressed herein do not state or reflect those of the University of Saskatchewan, and shall not be used for advertising or product endorsement purposes.

Requests for permission to copy or to make other uses of materials in this thesis/dissertation in whole or part should be addressed to:

Head of the Department of Biology
112 Science Place
University of Saskatchewan
Saskatoon, Saskatchewan S7N 5E2
Canada

OR

Dean
College of Graduate and Postdoctoral Studies
University of Saskatchewan
116 Thorvaldson Building, 110 Science Place
Saskatoon, Saskatchewan S7N 5C9
Canada

# ABSTRACT

Oxidation-reduction reactions are critical to life on earth as we know it, via photosynthesis and/or respiration. As life becomes more complex, these reactions become essential to gene expression, chemosignalling, and physiological stress responses. Imbalance in these reactions can result in disruption of these pathways, as well as damage to cellular components ranging from lipids to proteins to DNA. Photosynthetic organisms are especially prone to these conditions, given the nature of the reactions used to convert light energy to chemical energy. Exposure to high light (HL) results in the production of a number of dangerously reactive byproducts, chief amongst them singlet oxygen. We have a good understanding of how HL results in singlet oxygen production and a rudimentary knowledge of organisms' genetic responses. However, the response of individual living cells at the biochemical level following HL stress remains unexplored, largely due to a lack of tools.

In this thesis, green algae of three species of *Chlamydomonas* (*reinhardtii*, DJX-J, and DJX-H) and four photosynthetic mutants of *C. reinhardtii* were exposed to high light, the singlet-oxygen producing photosensitizer rose bengal (RB), or a combination of HL and RB. Synchrotron-based Fourier Transform Infrared Spectromicroscopy (FTIR) was used to study the biochemical response of individual living cells to these exposures, as well as to characterize differences between cell lines. The FTIR system I developed was able to discriminate between different species of *Chlamydomonas*, between the *C. reinhardtii* mutants, and even between different cultures of the same species.

The synchrotron-based FTIR system allowed me to observe biochemical responses to stress exposures. These were primarily in peaks related to proteins (changes in secondary structure) and lipids (changes in diversity, membrane fluidity, lipid oxidation byproducts, degree of unsaturation, and changes in membrane function). Observed *in vivo* biochemical changes in living cells were dependent upon species/photosynthetic mutation and route of stress exposure. Measurements were able to differentiate between cells exposed to HL, RB, and the combination of both. Exposure to RB/HLRB was more likely to result in observable changes in membrane function.

Overall, this work clearly demonstrates the power of FTIR in studying living systems. Not only could I discriminate between very similar cells, but it provided the first assessment of the biochemical responses of individual living cells to high light, rose bengal, and the combination of these factors.

# ACKNOWLEDGEMENTS

I would firstly like to thanks my supervisors, Drs. Kenneth Wilson and Thomas Ellis, for their support and guidance throughout my research, and for the many opportunities for professional and personal development throughout. I would further like to thank the other members of my graduate committee, Drs. Christ Ambrose, Som Niyogi, and Brian Bandy, for their assistance and expertise. They say it takes a village, and that's certainly true herein. There a number of people without whose input, guidance, and technical assistance this thesis would not have been possible. As such, I would also like to extend my deepest gratitude to Stuart Reed, Ron Zwarich, and Drs. Ferenc Borondics, Xia Liu, Tim May, Ewa Miskiewicz, Scott Rosendahl, and Christophe Sandt. Finally, I would like to acknowledge my friends, family, and fellow graduate students in the Biology Department at the University of Saskatchewan. Thank you so much for your support and encouragement over the last few years.

Funding for this project was provided by the Natural Sciences and Engineering Research Council of Canada, the Canadian Light Source, *Source Optimisée de Lumière d'Energie Intermédiaire du LURE*, and the University of Saskatchewan.

# TABLE OF CONTENTS

# TABLE OF FIGURES

# TABLE OF TABLES

# LIST OF ABBREVIATIONS

| | |
|---|---|
| Amide II' | Amide II prime/deuterated amide II peak |
| AU | Absorbance units |
| *C. reinhardtii* | *Chlamydomonas reinhardtii* |
| CC-1355 | *Chlamydmonas reinhardtii* mutant CC-1355 *cbn1-48* $mt^-$ |
| CC-4107 | *Chlamydmonas reinhardtii* mutant CC-4107 *npq2-5 lor1* $mt^+$ |
| Chl | Chlorophyll |
| Chl *a* | Chlorophyll *a*, primary photosynthetic pigment. Primary electron donor in electron transport chain. |
| Chl *b* | Chlorophyll *b* accessory photosynthetic pigment, primarily associated with PSII. Derived from Chl *a* through the addition of a carbonyl group. |
| $^1$Chl* | Excited chlorophyll |
| $^3$Chl | Triplet chlorophyll |
| $cm^{-1}$ | Wavenumber (per centimetre) |
| D | Deuterium |
| $D_2O$ | Heavy water/deuterated water |
| DAG | Diacylglycerol |
| DGDG | Digalactosyldiacylglycerol (glyceroglycolipid) |
| DJX- | *Chlamydomonas* DJX-H and DJX-J |
| DJX-H | *Chlamydomonas* DJX-H |
| DJX-J | *Chlamydomonas* DJX-J |
| DNA | Deoxyribonucleic acid |
| EMSC | Extended multiplicative scattering correction |
| ETC | Electron transport chain |
| FFA | Free fatty acid |
| FTIR | Fourier transform infrared spectromicroscopy |
| GPXH | Glutathione peroxidase homologous gene |
| GSTS1 | Sigma-class glutathione-S-transferase gene |
| H-D | Hydrogen-deuterium |
| HL | High light |
| HLRB | High light plus rose bengal |
| HOD | Semi-heavy water |
| IR | Infrared |
| LHC | Light harvesting complex |
| LHC II | Light harvesting complex II |
| LOP | Lipid oxidation products |

| | |
|---|---|
| MGDG | Monogalactosyldiacylglycerol (glyceroglycolipid) |
| OEC | Oxygen-evolving complex |
| P680 | Photosystem II primary donor chlorophyll dimer |
| $^{1}$P680* | Excited photosystem II primary donor chlorophyll dimer |
| $^{3}$P680 | Triplet photosystem II primary donor chlorophyll dimer |
| P700 | Photosystem I primary donor chlorophyll dimer |
| $^{1}$P700* | Excited photosystem I primary donor chlorophyll dimer |
| PC | Principal component |
| PC-1 | Principal component 1 |
| PC-2 | Principal component 2 |
| PC-3 | Principal component 3 |
| PCA | Principal component analysis |
| PG | Phosphatidylglycerol (phospholipid) |
| Phe | Pheophytin |
| PL | Phospholipid |
| PQ | Plastoquinone |
| $PQH_2$ | Plastoquinol |
| PSAF | Photosystem I reaction centre subunit III |
| *psaF* | *Chlamydomonas reinhardtii* mutant *psaF* |
| *psaF cbn1* | *Chlamydmonas reinhardtii* mutant CC-1355 *cbn1-48* mt$^{-}$x*psaF* |
| PSI | Photosystem I (component nomenclature Psa_) |
| PSII | Photosystem II (component nomeclature Psb_) |
| RB | Rose bengal |
| ROS | Reactive oxygen species |
| SQDG | Sulfoquinovosyldiacylglycerol (sulfolipid) |
| TAG | Triacylglycerol |
| TAP | Tris-acetate-phosphate nutrient media |
| W1-7 | Cell wall layers 1-7 |
| WT | Wild type *Chlamydomonas reinhardtii* CC-125 mt$^{+}$ |

# CHAPTER ONE
# INTRODUCTION AND BACKGROUND

## 1.1 Introduction to Oxidative Stress

Oxidation-reduction (redox) reactions are critical to cellular respiration, gene expression, and the energy generating reactions of photosynthesis. Redox reactions and their products not only provide sources of energy for the cell, but are also required in cellular signalling and the regulation of physiological responses (Dietz, Mittler, and Noctor 2016; Holmström and Finkel 2014; Sies, Berndt, and Jones 2017). For example, a number of redox-sensitive proteins are activated or deactivated in response to the cellular redox balance (Dietz et al. 2016; Holmström and Finkel 2014). To maintain biological homeostasis, redox reactions are carefully balanced. Reactive oxygen species (ROS) – chemically reactive species that contain oxygen – are continuously generated within cells as a by-product of normal cellular redox reactions; as such, cells have evolved a suite of systems that detect and detoxify ROS (Apel and Hirt 2004; Sies et al. 2017).

Oxidative stress has been defined in a number of ways over the years. A more recent and succinct definition proposed by Jones (2006) defines oxidative stress as "a disruption of redox signalling and control." In action this disruption will lead to a loss of homeostasis in the cell, damage of cellular components at a rate that exceeds repair mechanisms, and can lead to cell death (Holmström and Finkel 2014; Jones 2006; Sies et al. 2017).

In cells performing oxidative photosynthesis, redox reactions occurring in the chloroplast convert light energy into chemical energy (Asada 2006; Suzuki et al. 2012). When the redox reactions of the photosynthetic electron transport chain (ETC) are unable to proceed efficiently, reduced components can donate their electrons to oxygen (Asada 2006). The first product of this type of reaction is superoxide ($O_2^-$). Superoxide is quickly converted by enzymatic reactions to hydrogen peroxide ($H_2O_2$), which can be further detoxified by cellular systems to water. However, damage can occur if these ROS interact with cellular components such as lipids or proteins prior to their detoxification (Apel and Hirt 2004). If damaged lipids and proteins are allowed to accumulate, they can lead to decreased metabolic rates, diversion of cellular resources for repair,

and finally to cell death via apoptosis or necrosis. In the chloroplast, damage to the lipids and proteins of the thylakoid membrane can lead to a feed-forward loop (Sies 2016). Increased damage further slows the rate of electron transport, further increasing the redox potential of the chain components. This increases the likelihood that electrons will be donated to $O_2$. The end result of this is the production of more ROS and thus more damage.

Photosynthetic organisms are especially prone to oxidative stress, given the nature of the reactions used to convert light energy to chemical energy. The foundation of photosynthetic reactions is the excitation of electrons by photons of light absorbed by chlorophyll molecules. The fact that this process occurs at rates that are nearly instantaneous, regardless of whether that energy is being used by the cell, means that the slower biochemical redox reactions of the photosynthetic electron transport chain used to convert the light energy into chemical energy can be outpaced when cells are exposed to high light. In fact, even the term "high light" is a relative thing (Huner, Öquist, and Fathey 1998). Factors which slow the electron transport chain reactions can make what would normally be considered dim light dangerous to the cell (Huner et al. 1998).

The redox reactions of the chloroplast are not problematic only because of this temporal disconnection, but also because large amounts of oxygen are produced. Additionally, chlorophyll, the key pigment required for light absorption, is composed of a conjugated π-orbital system. This allows chlorophyll to absorb light in the visible spectrum, while it also making it an effective photosensitizer. The energy-stabilizing π-orbital system means that chlorophyll molecules that are excited by a photon of light can hold that energy for a long period of time (in photochemistry terms - on the order of picoseconds). While in this excited state, the chlorophyll molecule can reverse the spin on its excited electron and enter the triplet state. As the Section 1.1.1 describes more fully, this makes it capable of producing singlet oxygen, a particularly reactive form of ROS.

There has been much research on large-scale physiological damage induced by ROS and the genetic responses organisms use to mitigate cellular damage. However, technical limitations mean that most work has been done with extracted compounds, such as proteins or lipids. There are techniques capable of examining ROS accumulation, lipid peroxide localization, or protein damage. For example, a suite of fluorescent dyes make some such assays possible. However, a quantitative, statistically accessible, system for examining the entire cellular metabolic and biochemical pool simultaneously is of great interest. A key limitation to examining the effects of

oxidative stress in living cells or tissues is the development of the tools necessary to do so. Fourier-transform infrared spectromicroscopy is one such potential system.

Understanding the interplay and time course of physiological adaptation to oxidative stress is essential in parsing cellular responses to oxidative stress. There is still need for increased understanding of the physiological and metabolic responses of individual cells to different sources of oxidative stress, particularly to short-term and acute damage. This would build understanding of the variability of responses of different individual cells, as well as to study how the disruption of photosynthetic electron transport alters cellular responses to oxidative stress. However, a robust, reliable technique that can be used to compare cells or tissues that have been exposed to oxidative stress conditions is needed. As part of this thesis, I plan to explore such a system.

### 1.1.1 Singlet Oxygen

Singlet oxygen ($^1O_2$) is a molecular species of great concern in photobiology. Unlike the more common triplet oxygen ($^3O_2$, usually written $O_2$), it is highly reactive in the biological environment. Nearly all organic molecules in the environment occur in the singlet spin state, with molecular oxygen normally occurring in the triplet spin state. Triplet oxygen is stable because the reaction of molecules with different quantum spin values is forbidden. Thus, the conversion of triplet oxygen ($^3O_2$) to singlet oxygen ($^1O_2$) results in a much more reactive compound (Green and Hill 1984; Ledford and Niyogi 2005). Because it does not carry a charge, $^1O_2$ is a strong electrophile agent, and can participate in a variety of types of reactions (Edreva 2005; Triantaphylides et al. 2008; Triantaphylides and Havaux 2009). Unsaturated compounds such as the unsaturated fatty acids found in plant membranes are a common target (Girotti and Kriska 2004; Triantaphylides et al. 2008). As a result, $^1O_2$ produced when excited chlorophyll molecules cannot pass on their excited state energy results in membrane damage through lipid peroxidation (Edreva 2005; Moller, Jensen, and Hansson 2007; Salin 1988), and the modification of structural cholesterol (Salin 1988). Because any compound containing carbon-carbon double bonds is a target of $^1O_2$, the amino acid side chains of proteins are often impacted, specifically Cys, His, Met, Trp, and Tyr (Davies 2004; Ledford and Niyogi 2005; Moller et al. 2007), as are the nucleotides of DNA or RNA (Di Mascio, Murphy, and Sies 1991), primarily through guanine (Martinez et al. 2003; Moller et al. 2007). A variety of other compounds can also be targeted or destroyed, including secondary metabolites (Triantaphylides and Havaux 2009) and pigment compounds that

contain unsaturated double bonds, including chlorophyll itself (Edreva 2005). As a sum, thylakoid membranes and photosynthetic reaction centres are highly sensitive targets (Edreva 2005) due to both their large number of unsaturated organic molecules and proximity to $^1O_2$ production.

### 1.1.2 Photosynthesis, Singlet Oxygen, and PSII

Photosynthesis is truly the ultimate source of energy supporting most of the life on Earth. Oxygenic photosynthesis converts light energy into more stable chemical energy which is ultimately used to reduce $CO_2$ into carbohydrate molecules. A simplified overview of the ETC and light-dependent photosynthetic pathways is given in Figure 1.1.

Photosynthesis starts with the absorption of a photon by a chlorophyll. Once a photon is absorbed, the geometrically precise organization of chlorophyll molecules (Chl, Figure 1.2) allows the energy to be distributed across of a number of Chl at photosystem II (PSII) and its associated light-harvesting complex II (LHCII), which together form the PSII-LHCII holocomplex (Figure 1.3, from Minagawa and Tokutsu (2015)). The energy associated with the absorbed photon is moved between Chl molecules until it is dissipated or arrives at the P680 reaction centre, which consists of two special excitonic dimers of chlorophyll which can absorb light energy equal to a photon with a wavelength of 680 nm. The P680 chlorophyll, when excited ($P680^*$), initiates charge separation reactions by passing an electron down the electron transport chain (ETC). Under normal conditions, the electron from P680 is passed to a stable quinone, and an electron is taken from the oxygen-evolving complex (OEC), to reduce P680+ back to ground state. When this reaction has happened four times, two molecules of $H_2O$ are oxidized into one molecule of $O_2$ and four $H^+$ ions (Vass 2011). If there is any disruption to the flow of energy or electrons through the ETC, chlorophylls associated with the PSII-LHCII complex will stay in their excited forms ($^1Chl^*$, $^1P680^*$). Increased dwell time as $^1Chl^*$ increases the chance that it will be converted to the lower-energy excited state $^3Chl$ or that $^1P680^*$ will likewise be converted to $^3P680$. In their triplet state, these chlorophylls can react readily with triplet oxygen, leading to the formation of singlet oxygen and regeneration of ground-state chlorophyll molecules: $^3Chl + {}^3O_2 \rightarrow {}^1Chl + {}^1O_2$ (Krieger-Liszkay 2005; Ledford and Niyogi 2005; Telfer 2014; Vass 2011).

As mentioned above, photosynthesis is especially prone to producing singlet oxygen. The rates at which the photochemical and biochemical reactions of photosynthesis occur differ by

orders of magnitude, and the co-localization of the OEC and PSII – and therefore $O_2$ generation – means that when $^3$Chl is present, there will be a local, readily available supply of $^3O_2$.

Plants have evolved a variety of mechanisms to cope with high-light stress and its resultant effects, most problematic amongst them the generation of singlet oxygen. The most effective mechanisms diminish the amount of light absorbed by PSII (Horton, Ruban, and Walters 1996). They include state transitions (reversible changes to the distribution of chlorophylls and LHCs between PSI and PSII, (Figure 1.3)), increased thermal dissipation through chlorophyll de-energization, and photoinhibition (the programmed dismantling of PSII complexes) (Allorent et al. 2013). Despite this, singlet oxygen is produced continuously during photosynthesis (Apel and Hirt 2004). Unlike many forms of ROS, singlet oxygen cannot be scavenged by cellular enzymatic systems (Edreva 2005). As such, photosynthetic organisms have adaptations to mediate the effects of singlet oxygen. These include physical quenching (interaction with carotenoids or tocopherols, which contain large numbers of conjugated double bonds that allow uptake of energy from excited molecules and its dissipation as heat (Edreva 2005)) and chemical quenching through oxidative reactions involving the products of compounds excited by singlet oxygen (Triantaphylides and Havaux 2009).

The majority of the singlet oxygen generated in plant cells occurs within the P680 reaction centre of PS II (Krieger-Liszkay 2005; Krieger-Liszkay, Fufezan, and Trebst 2008). Though there are much higher numbers of chlorophylls presents in the greater PSII-LHC holocomplex, photoprotective compounds such as carotenoids also present (Krieger-Liszkay et al. 2008), with approximately one carotenoid for every five chlorophyll molecules (Knox and Dodge 1985). In addition, other protective compounds such as tocopherols, ascorbate, and glutathione are located in the chloroplast (Krieger-Liszkay et al. 2008). Carotenoids can be converted to their triplet states in reaction to energy transfer from other compounds in triplet states, such as $^3$Chl*, and rapidly decay to their ground state through the dissipation of that energy as heat (Triantaphylides and Havaux 2009). As discussed above, singlet oxygen damage often preferentially targets double bonds. These protective compounds included residues with numerous double bonds and phenyl groups with conjugated double bonds, making them sacrificial targets for attack that can dissipate excess energy as heat (Edreva 2005). When these protective mechanisms are overwhelmed, damage levels increase and signalling processes are ramped up as a reflection of the cellular

damage events. In *C. reinhardtii*, it is clear that cellular signalling events reprogram cellular metabolism to make the cells more tolerant of singlet oxygen (Brzezowski, Wilson, and Gray 2012; Dent et al. 2005; Leisinger et al. 2001). The cellular response to singlet oxygen damage occurs primarily through repair of damaged components and increased capacity for chemical quenching of excited by-products through redox chemistry (Horton et al. 1996; Triantaphylides and Havaux 2009).

### 1.1.3 Biological Consequences of Singlet Oxygen

As discussed above, singlet oxygen is much more reactive than triplet oxygen. As such, increases in singlet oxygen production will result in an increase in oxidation reactions within the cell – recall that the targets of these reactions are often unsaturated (C=C) bonds. The chloroplast lipid composition in *C. reinhardtii* is dominated by four primary membrane lipids associated with the thylakoids: the anionic phospholipid phosphatidylglycerol (PG, ~5-12% of thylakoid membrane lipids), the nonionic glyceroglycolipids monogalactosyldiacylglycerol (MGDG, ~50% of thylakoid membrane lipids) and digalactosyldiacylglycerol (DGDG, ~30% of thylakoid membrane lipids), and the anionic sulfolipid sulfoquinovosyldiacylglycerol (SQDG, ~5-12% of membrane lipids) (Vieler et al. 2007). Their general structure is shown in Figure 1.13, after Mizusawa and Wada (2012). Plants and green algae typically have high levels of unsaturation in thylakoid membrane lipids. This helps maintain membrane fluidity under fluctuating temperatures. As presented in Figure 1.4 (after Thompson (1996)), the fatty acid composition of the thylakoid lipids is predominately 18:3, 16:4, and 16:0 fatty acids, which together constitute ~72% of the total (~30%, 22%, and 20%, respectively) thylakoid fatty acids found in *C. reinhardtii* grown under lab-typical conditions (Figure 1.4, blue). The predominance of polyunsaturated fatty acids (PUFAs) in the thylakoid membranes, where photosynthesis takes place and singlet oxygen is generated, makes them an easily accessible target for oxidative damage.

When the cell absorbs more light than it can use, singlet oxygen production will increase and the reaction of singlet oxygen and other ROS with unsaturated fatty acid chains will give rise to a complex mixture of lipid oxidation products (LOP). Membrane lipid peroxidation causes a general decrease in membrane fluidity and thus increased leakiness. Other effects include altered membrane protein folding and cross-linking of membrane lipids and proteins. Membrane structure and function is further impacted by the reaction of singlet oxygen with cholesterol (Girotti 1985).

In addition to the effects of oxidative lipid modification on membrane function, PUFA peroxidation and degradation can trigger biochemical signalling cascades. The formation of aldehydes, and hydroxyl- and keto- fatty acids can themselves form conjugates with DNA and proteins, leading to loss of function (Edreva 2005; Moller et al. 2007). The resulting lipid hydroperoxides via type II reactions include direct reaction of singlet oxygen with PUFAs via "ene" reactions (Figure 1.6), wherein the oxygen is directly inserted at the ends of the double bonds, for example between $C_{12}$ and $C_{13}$ to form an allylic hydroperoxide in trans configuration (Girotti 1985; Girotti and Kriska 2004).

Direct interaction between DNA and singlet oxygen primarily involves chemical reactions with guanine, wherein the direct exposure of DNA to singlet oxygen causes the oxidation of guanine to 8-hydroxyguanine (Figure 1.5), leading to strand breaks. If not adequately repaired, mutations can occur during DNA replication, leading to altered gene expression, cellular malfunctions, cell death, or – in non-plant multicellular organisms – cancer.

Proteins can also be damaged by singlet oxygen. It is thought that the degradation and replacement of proteins following oxidative damage is more energetically expensive for the cell as compared to the net metabolic cost of modifying or replacing lipids (Edreva 2005; Girotti and Kriska 2004; Moller et al. 2007). In fact, unsaturated lipids have been found to be protective of membrane proteins because they tend to be more reactive, and perhaps more easily accessible to ROS. Thus, the PUFAs can act as antioxidants by accumulating oxidative damage and in turn protecting integral membrane proteins (Rokitskaya et al. 2014). Protein oxidation can result in damage to all parts of protein structure, including side chains, and protein backbones (Davies 2003, 2016). Oxidized proteins exhibit altered folding, secondary structure, hydrophilicity, and have altered interactions with the environment and other biological compounds (Anjum et al. 2015; Davies 2016). They can have increased rates of crosslinking, aggregation, and increased rates of reaction with various compounds, resulting in proteins functionalized with alcohol and carbonyl groups (Anjum et al. 2015; Davies 2016).

Overall, singlet oxygen can potentially impact all cellular systems, but lipids, proteins, and DNA are particularly vulnerable to oxidative attack. One of my primary goals of my research was to investigate the damage to these sensitive biochemical components in individual, living cells.

### 1.1.4 Singlet Oxygen and Gene Expression

Studies using *C. reinhardtii* have demonstrated that this model alga can acclimatize to singlet oxygen. Pre-exposure to low levels of the singlet oxygen-generating dye rose bengal (RB) results in cells which exhibit increased tolerance to subsequent, higher exposures of singlet oxygen when compared to naïve, untreated controls, as is seen in Figure 1.7 (Brzezowski et al. 2012; Ledford, Chin, and Niyogi 2007).

The acclimation of *C. reinhardtii* to singlet oxygen exposure occurs as a result of transcriptional reprogramming (Fischer et al. 2012; Ledford et al. 2007; Leisinger et al. 2001) and possible post-transcriptional regulation of protein production (Brzezowski et al. 2012; Khandal et al. 2009). The transcriptional changes are specific, and the best-studied singlet oxygen-responsive gene is the glutathione peroxidase homologous gene (GPXH or GPX5 in the new nomenclature). A sigma-class glutathione-S-transferase gene GSTS1 is also upregulated in response to singlet oxygen (Fischer et al. 2012; Fischer, Krieger-Liszkay, and Eggen 2004; Fischer, Wiesendanger, and Eggen 2006; Ledford et al. 2007; Leisinger et al. 2001). The increase in expression of these two genes is specific to singlet oxygen, with little overlap with resistance mechanisms induced by other ROS. Ledford et al. (2007) have shown that *C. reinhardtii* is capable of mounting a robust acclimatization response to singlet oxygen given pretreatment prior to exposure. This response, while transient, can be induced even by relatively short-term exposure to low concentrations of singlet oxygen, and is specific to singlet oxygen with little overlap with adaptive responses to pretreatment with other ROS. Pretreatment with high light (a known generator of singlet oxygen) was also shown to be capable of inducing acclimation to singlet oxygen. These changes were again correlated with altered GPXH expression. Cells showed no changes in their carotenoid or tocopherol composition, despite the importance of these compounds in the neutralization of singlet oxygen and its products. Fischer et al. (2009) have shown the *C. reinhardtii* GPXH protein to be a thioredoxin-dependent peroxidase involved in scavenging by-products of singlet oxygen, specifically organic hydroperoxides and hydrogen peroxide. GSTS1 belongs to a class of enzymes that catalyzes the conjugation of glutathione to cellular targets. It is generally thought that glutathionylation targets proteins for degradation. Fischer et al. (2012) were further able to isolate a *C. reinhardtii* mutant that exhibited increased tolerance to singlet oxygen and had higher expression of these two genes.

In sum, it appears that to counteract the damage and cellular threat caused by singlet oxygen exposure, *C. reinhardtii* cells upregulate the production of enzymes capable of removing or repairing damaged components. By expressing enzymes such as GPXh and GSTS1 the cells become more resistant to singlet oxygen. One would also predict that such cells would repair damage at a faster rate.

## 1.2 FTIR of Biomolecules

### 1.2.1 FTIR of Whole Living Cells

Fourier transform infrared spectromicroscopy (FTIR) offers a unique opportunity for observing the response of individual living cells to oxidative stress. It is a non-destructive technique that allows for simultaneous assessment of all biomolecules. Additionally, in a measurement system using a time-resolved system, one could also assess metabolism and changes in cellular compartments. Traditional work involving the extraction of individual cellular components such as lipids, proteins, or DNA allows for in-depth bulk analysis of one class of compound. Extraction processes kill cells and homogenize the compounds in question across large numbers of cells in order to obtain sufficient sample sizes. This type of process also removes other compounds of interest, limiting the ability to observe interactions between different cellular components. The study of individual living cells offers the opportunity to simultaneously observe differences in compounds of interest, particularly in proteins and lipids, providing us with the opportunity to study the functional impacts of changes in cellular components or metabolism. Previous studies have used FTIR to identify classes of biomolecules such as lipids and proteins and map their intracellular distribution (Heraud et al. 2005; Jamin et al. 1998), as well as track conformational changes over time (Birarda et al. 2010; Chen et al. 2001; Holman et al. 2000), accumulation or depletion of metabolic products (Goff et al. 2010; Goff, Quaroni, and Wilson 2009; Heraud et al. 2005; Sackett et al. 2016), and cellular responses to stress or the cell cycle (Alvarez-Ordóñez et al. 2011; Dean, Martin, and Sigee 2007; Holman et al. 2000; Holman, Martin, and McKinney 2003).

FTIR of algal cells has established it as a tool to study *in vivo* algal metabolism and fundamental differences in physical structure (Dean et al. 2007; Goff et al. 2013, 2009; Palmucci, Ratti, and Giordano 2011; Sackett et al. 2016; Sigee et al. 2007). Specifically, previous work with individual living cells of *C. reinhardtii* has observed the production of ethanol due to fermentative

anaerobic metabolism (Goff et al. 2009). This particular system was also used to demonstrate the effects of naphthenic acids from oil sands process water on the secondary structure of cell wall proteins (Goff et al. 2014). This makes FTIR of individual living cells of *C. reinhardtii* an interesting technique with which to assess the impact of oxidative stress on living systems. As such, I have experience using this system to observe changes in metabolism and protein damage caused by external environmental factors. Given current interest in improving our understanding of the impacts of environmental stress on the process of photosynthesis, I believe that Fourier-transform infrared spectromicroscopy (FTIR) measurements of *C. reinhardtii* cells can provide a unique insight. Not only should I be able to identify changes in metabolite accumulation, but because of the specific lipid and protein absorbance bands in the mid-IR region, I will be able to examine the impact of high light stress and rose bengal-induced singlet oxygen production on these sensitive target molecules.

### 1.2.2 General Band Assignment

A generalized overview of the spectra of biological systems is given in Figure 1.8, and definitions of commonly used symbols are provided in Table 1.1. Figure 1.8, reproduced from Baker et. al (2014) was obtained from a measurement of cryo-sectioned human breast carcinoma tissue with 60 μm apertures. There are significant structural and biochemical differences between animal cells and those of plants and algae, most notably the presence of a cell wall (glycoproteins, in the case of *C. reinhardtii*), large chloroplasts, and photosynthetic by-products. A more exhaustive peak assignment table can be found in Movasaghi et. al (2008), which provides an unfiltered overview of peak assignments from a large number of papers, primarily focused on the FTIR of animal systems. This 24-page table highlights the complex, overlapping nature of the absorbance peaks in an FTIR spectrum, particularly one obtained from cells or tissues, and especially in the fingerprint region (1500-500 $cm^{-1}$). For example, the $\nu_{as}\, PO_2^-$ around 1260 $cm^{-1}$ in Figure 1.8, is assigned to nucleic acids but overlaps with the amide III peaks of proteins that are caused by general NH deformation. The ~1400 $cm^{-1}$ $COO^-$ protein stretch can be assigned to individual amino acids, organic acids, or proteins, and overlaps with $\delta CH_3$ of proteins and general $\delta CH_3$ (Figure 1.8). The generalized band assignment used in this work is given in Table 1.2 and synthesizes the overviews found in a number of review articles (Baker et al. 2014; Barth 2000, 2007; Berterame et al. 2016; Garidel and Schott 2006; Movasaghi et al. 2008; Oleszko et al. 2015). The spectral region below 1200 $cm^{-1}$ is particularly complex. It is composed of overlapping

absorption spectra that reflect the complex mixture of bonds found in carbohydrates, nucleic acids, lipids, and other small molecules that make up a typical cell (Movasaghi et al. 2008). The level of complexity is such that very little, if any, information can be deduced with certainty. As such this region was not used during my studies and has been excluded from Table 1.2.

### 1.2.3 FTIR of Lipids

Lipids contain multiple IR-active functional groups in both the tail ($CH_2$, $CH_3$, CH) and head and backbone. The tails contain $CH_2$ and CH groups with a terminal $CH_3$ groups. The head group and backbone consist primarily of C=O, CH, and $CH_2$ groups, with other functionalization such as phosphate, sulfur, or nitrogen depending on lipid class. In *Chlamydomonas* spp., most lipids fall into glass with a glycerol backbone (Giroud, Gerber, and Eichenberger 1988). A very brief overview is given in Figure 1.9. Given that lipids – particularly unsaturated lipids – are one of the primary targets of oxidative damage in photosynthetic cells (Ledford and Niyogi 2005), FTIR offers an exciting opportunity for the *in vivo* study of structural and functional lipid changes induced by exposures to abiotic stress. Lipids absorb in both the 3050-2800 $cm^{-1}$ and 1800-1240 $cm^{-1}$ ranges. The CH stretching region (3050-2800 $cm^{-1}$) is dominated by absorption from the hydrophobic tails of lipids, while absorption in the 1800-1240 $cm^{-1}$ region is primarily related to head groups (Derenne et al. 2013).

Well-identified peaks in the CH stretching region include $\nu CH_{3as}$ (2955 $cm^{-1}$), $CH_{2as}$ (2922 $cm^{-1}$), $CH_{3s}$ (2870 $cm^{-1}$), and $CH_{2s}$ (2852 $cm^{-1}$) (Figure 1.8 and Table 1.2), as well as a relatively weak peak arising from $\nu$=CH in unsaturated lipid bonds (3010 $cm^{-1}$) (Movasaghi et al. 2008; Tamm and Tatulian 1997). Unidentified CH stretches can be found in this region as well (Table 1.2, 2985 $cm^{-1}$ and 2895 $cm^{-1}$ in algae). Together, these peaks are often used to monitor the degree of lipid unsaturation, chain lengths, phase transitions, and the degree of membrane disorder present (Derenne et al. 2013). As the relative strength of the 3010 $cm^{-1}$ peak is directly related to the degree of unsaturation present in lipids, changes in this peak can be used to observe changes in the unsaturation index. As unsaturated fatty acid chains are a primary target of ROS (Girotti and Kriska 2004; Triantaphylides et al. 2008), changes in the 3010 $cm^{-1}$ peak can be used to observe the accumulation of oxidative damage on unsaturated lipids, though the measurement of whole cells means it is incapable of identifying which pool of unsaturated lipids is targeted.

The $\nu CH_2$ and $\nu CH_3$ peaks yield further information about chain composition. The ratio of $\nu CH_2$:$\nu CH_3$ can be used to make observations regarding the relative chain lengths, with longer fatty acid chains having a higher ratio (see Figure 1.9). However, this is complicated by the degree of unsaturation present. The position and peak widths of the $\nu CH_2$ and $\nu CH_3$ peaks are related to a number of factors, including the overall chain length and the number of unsaturated bonds. A greater diversity of $\nu CH_2$ chain lengths within a membrane will result in broader peaks (Derenne et al. 2013). The position and width of $CH_2$ peaks ($\nu CH_{2as}$, $\nu CH_{2s}$) are very sensitive to changes confirmation of fatty acid chains, and therefore to lipid and membrane disordering. Increased membrane disorder, such as that caused by oxidative damage, results in an upshift in the position of $\nu CH_{2as}$ and $\nu CH_{2s}$, as well as broadening of these peaks (Derenne et al. 2013; Kiwi and Nadtochenko 2004; Lewis and McElhaney 2006, 2013). Some authors suggest that only the $\nu CH_{2s}$ should be used in monitoring changes in lipid and membrane disorder, due to overlapping contributions from $CH_3$ groups and potential Fermi resonances (Lewis and McElhaney 2006) while others utilized both $\nu CH_{2as}$ and $\nu CH_{2s}$ (Derenne et al. 2013; Nadtochenko et al. 2005).

The carbonyl peak around 1740 $cm^{-1}$ is predominantly due to absorption by C=O bonds located in lipid head groups (Derenne et al. 2013; Lewis and McElhaney 2006). Second derivative analysis of *C. reinhardtii* cells shows that it is composed of two components, one around 1740 $cm^{-1}$ (likely due to absorbance by ester groups in phospholipid, triacylglycerol, diacylglycerol) and one around 1718 $cm^{-1}$ (likely due to absorbance by free fatty acids, lipid oxidative breakdown products such as hydroperoxides, aldehydes, and ketones) (Ismail et al. 1993; Voort et al. 1994). Characteristic changes occur in the 1740 $cm^{-1}$ peak during oxidation of lipids, resulting in reshaping of the peak caused by changes in the relative contributions of the second derivative components. Formation and breakdown of hydroperoxides or lipid endoperoxides, and the resultant formation of aldehydes and peroxidation intermediates results in an increase in the 1720-1700 $cm^{-1}$ region and a decrease in the 1740-1720 $cm^{-1}$ components (Derenne et al. 2013; Gericke and Hühnerfuss 1995; Kiwi and Nadtochenko 2004; Nadtochenko et al. 2005; Sánchez-Alonso, Carmona, and Careche 2012). Together, the overall impact on IR spectra is a broadening and reshaping of the ~1740 $cm^{-1}$ peak, with decreased separation between this peak and the amide I peak when greater levels of damage occur. An overall increase in the ~1740 $cm^{-1}$ peak might also be indicative of increased overall lipid oxidation due to the increased number and variety of carbonyls formed by peroxidation of fatty acid chains (Hayati et al. 2005; Oleszko et al. 2015).

In addition to these well-characterized peaks in the 1740 $cm^{-1}$ region, there are peaks in the 1500-1200 $cm^{-1}$ region associated with $\delta CH_3$, $\delta CH_2$, and $\nu COO^-$ (Lewis and McElhaney 2006; Movasaghi et al. 2008). Some of these absorptions, particularly the $CH_2$ wagging progression at 1400-1300 $cm^{-1}$ and $CH_3$ umbrella at 1378 $cm^{-1}$, can be used to obtain more in-depth structural information from lipid mixtures (Berterame et al. 2016; Lewis and McElhaney 2013). However, in systems containing complex mixtures of lipids, proteins, and carbohydrates interpretation of the 1400-1300 $cm^{-1}$ region is more ambiguous.

Even without use of the lower wavenumber lipid peaks, the mid-IR region offers rich opportunities for observing predicted oxidative damage to lipids, including changes in unsaturation, membrane disorder, and the production and breakdown of oxidative by-products. Because this damage will be repaired by the cell, it should also be possible to observe changes that occur post-damage event, in a time-resolved manner, to better understand the repair processes that occur in living cells. Complex mixtures of lipids are present in the cell at any specific point in time. Our ability to detect all cellular lipids at a given point in time means that this complex mixture registers as a single cohort of lipids. When lipids are modified or damaged, the end result is the loss of one class or type of lipid and the creation of at least one more. These changes in the relative abundance of the many different types of lipids present are referred to in this work as changes in the lipid cohort.

### 1.2.4 FTIR of Proteins

Proteins have several structural regions that are active in the mid-IR region. These are primarily associated with the bonds of the protein backbone (Figure 1.10) and secondary protein structure (Figure 1.11), though there are regions in which amino acid side chains may contribute (Barth 2000, 2007). Of particular interest in studying oxidative protein damage are the amide I and amide II peaks. The amide III peaks are of potential interest, but the increased complexity of absorption modes makes them difficult to interpret. In addition, the amide II prime (amide II') peak is of interest in studying alterations in membrane dynamics and transport.

The amide I protein peak is the strongest peak in cells of *Chlamydomonas* spp. To study it in living cells necessitates the use of heavy water ($D_2O$) as a solvent, as the absorption of regular water ($H_2O$) overlaps and saturates the amide I region that occurs at 1700-1600 $cm^{-1}$. The amide I peak is primarily due to absorption of IR light by $\nu C{=}O$, with contributions from $\nu CN$, and lesser

contributions from ρNH and δCNN. This results in a strong, broad peak with multiple components derived from the effect of secondary structure on the chemical bonds composing the protein backbone (Krimm and Bandekart 1986). The most common application of FTIR in protein studies is in use of the amide I peak to study protein secondary structure (Barth 2007). Depending on the analytical approach used (second derivatives, curve fitting, or deconvolution of original spectra), degree of data preprocessing applied, and protein mixture in question, a number of contributing structures at various wavenumbers are assigned. The generation of second derivatives is the most unsupervised technique but may fail to resolve closely overlapping components. I believe this is a reasonable trade-off.

The primary amide I second derivative assignments in *Chlamydomonas* spp. systems are given in Table 1.2. In all measured cells, the strongest contribution comes from α-helixes (~1654 $cm^{-1}$), followed by that of β-sheets (1635 $cm^{-1}$). There is a ~1680 $cm^{-1}$ component associated with unordered and random turns, coils, and C=O groups sensitive to disruption of hydrogen bonds. Antiparallel β- and aggregate strand absorb around 1690-1700 $cm^{-1}$, which shares overlapping absorptions with ketones and carboxyls. The α-helix and β-sheet contributions share overlapping absorption with unordered structures and cellular water, respectively (Barth 2007; Berterame et al. 2016; Miller, Bourassa, and Smith 2013; Movasaghi et al. 2008). Knowing all this, FTIR study of the amide I peak is extremely useful for monitoring changes in protein secondary structure. Changes in the shape of the amide I peak and the ratio and shape of its second derivative components allow monitoring of protein folding, refolding, and damage accumulation. High light stress in *Chlamydomonas* cells triggers physiological adaptations such as state transitions and dismantling of PSII. Direct oxidative damage to proteins – which has been found to be more energetically expensive for cells than the modification and replacement of lipids (Edreva 2005; Girotti 1985; Moller et al. 2007) – will also result in changes in protein secondary structure, often from α-helix to β-sheet (Davies 2016; Liu et al. 2013; Santos et al. 2013). These conformational protein changes – in response to either adaptive refolding, protein disassembly, direct or indirect damage – should be visible by examination of the amide I peak.

The amide II peak has a significantly more complex relation to protein secondary structures. This peak is primarily due to out-of-phase coupling of the ρNH and νCN vibrations, with minor contributions from ρCO, νCC, and νNC (Table 1.2). Changes in the ratio of the amide I to amide

II can be a useful indicator of protein secondary structure and cell health (Holman et al. 2000). Another fundamental property of the amide II peak is its sensitivity to hydrogen-deuterium exchange. Exposure of proteins to heavy water results in time-dependent H-D exchange of the NH group, which decouples the ρNH and νCN vibrations (ρND occurs at wavenumbers below 1200 $cm^{-1}$) and results in downshifting of the amide II peak to what is known as the amide II', a νCN absorbance around 1460 $cm^{-1}$ (Barth 2007). Because the cells are suspended in a $D_2O$ solution, changes in the amide II absorbance due to H-D is an indirect measure of membrane integrity. Greater conversion of amide II to amide II' would be indicative of increased penetration of $D_2O$ into the cell due to altered membrane permeability. Such changes might be expected from oxidative damage to membrane lipids and proteins. The amide I peak is also impacted by H-D exchange, but in a much less significant way due to the minor contribution of ρNH to the overall peak (Barth 2007). Typically it exhibits a slight downshift of its second derivative component by 2-5 $cm^{-1}$ in response to N-deuteration (Barth 2007).

The amide I and amide II peaks are both relatively insensitive to changes in amino acid side chains (Barth 2007). Side chains/residues are frequent targets of oxidative protein damage (Barth 2007; Davies 2004; Moller et al. 2007). As such their oxidative modification is not expected to be directly observable in the amide I or amide II peaks, though the resulting changes in protein secondary structure will be. IR absorption by the side chains, along with δNH and νCN, contribute directly to the complex series of weak amide III peaks in the 1400-1200 $cm^{-1}$ range. In the spectra of *Chlamydomonas* spp. amide III peaks are present at 1308 $cm^{-1}$, 1285 $cm^{-1}$, 1260 $cm^{-1}$, and may overlap with the other peaks present in the 1400-1308 $cm^{-1}$ range. The δNH contribution means that these peaks could also potentially exhibit shifts in response to N-deuteration (Barth 2007; Cai and Singh 1999). In addition, peaks associated with protein bonds are present in the 1500-1378 $cm^{-1}$ region ($\delta CH_2$, $\delta CH_3$, and $\nu COO^-$). It is not feasible to directly correlate changes in these peaks to secondary or other structural changes in complex systems, though it is possible to observe changes in them.

As with any technique, using FTIR to study proteins offers both opportunities and challenges. It does not allow for direct measurement of protein levels or relative abundance, nor can one examine a specific protein in the cellular mixture. However, it does allow the study of relative changes in protein conformation and secondary structure in individual cells, including

those induced by oxidative stress. The interconversion of the amide II and amide II' peaks in response to heavy water exposure also offers a chance to observe evidence of functional changes in cellular membranes.

### 1.2.5 FTIR of Other Biomolecules

Numerous other cellular components and compounds are IR-active, though for a variety of reasons their infrared spectra are of less use in this investigation. This may be due to complex, overlapping absorbance bands or their making up a relatively small proportion of cellular components. For example, the IR spectra of starch is complex. It contains a sharp, isolated peak around 1160 $cm^{-1}$. Absorption between this peak and 1000 $cm^{-1}$ is complex and varies significantly with source and the degree of hydration (Kacurakova et al. 2000; Kizil, Irudayaraj, and Seetharaman 2002). However, as nearly all characteristic starch bands occur below 1200 $cm^{-1}$ they are of limited use for this work. Other polysaccharides also absorb primarily in this region as well, and it is possible – through extremely difficult – to differentiate between various sugars (Coimbra et al. 1999; Hopkinson et al. 1987). Literature reviews also suggest absorption around 1370 $cm^{-1}$ and 1444 $cm^{-1}$, and from ring sugars around 1336 $cm^{-1}$ (Movasaghi et al. 2008). The spectra of proteins and glycoproteins are very similar, dominated by the amide I and amide II peaks. The spectra of glycoproteins contains absorption from carbohydrates, however, resulting in stronger peaks at ~1375 $cm^{-1}$, ~1310 $cm^{-1}$, and 1240 $cm^{-1}$ (Lewis, Lewis, and Lewis 2013; Wang et al. 2007) and may trigger a shoulder in the CH region around 2880-2870 $cm^{-1}$ (Clède, Policar, and Sandt 2014).

The absorption spectra of chlorophylls and their related and derived compounds (examples given in Figure 1.2, 1.12) varies significantly depending on extraction method, solvent, hydration, and specific pigment (Holt and Jacobs 1955; Katz et al. 1963; Sherman and Wang 1967). However, there are some commonly observed absorptions around 2920 $cm^{-1}$ ($\nu CH_2$); 1740 $cm^{-1}$ and 1718 $cm^{-1}$ (C=O ester); 1700 $cm^{-1}$ (C=O ketone); 1655 (aldehyde); 1610 $cm^{-1}$ (C=C), 1465, 1444, 1380 $cm^{-1}$ (mix of $\delta CH_2$, $\delta CH_3$); 1290-1270 $cm^{-1}$ (unassigned) (Holt and Jacobs 1955; Katz et al. 1963; Sherman and Wang 1967; Weigl and Livingston 1953). Examination of chlorophyll spectra from the literature indicates the strongest FTIR absorbance peaks are typically those associated with C=O carbonyl peaks, which exhibit significant overlap with the lipid esters in the 1740-1700 $cm^{-1}$ range (Gruszecki et al. 2012; Nabedryk et al. 1990; Noguchi, Tomo, and Inoue

1998). The best indicator band in the spectra of *Chlamydomonas* spp. appears to be the second derivative component at 1610 $cm^{-1}$; this component is significantly decreased in mutants of *C. reinhardtii* lacking Chl *b* (Figure 5.1). In addition, a tetrapyrrole absorption is present around 1285 $cm^{-1}$ (Derenne et al. 2013), which would include chlorophylls and similar compounds such as heme, siroheme, and phytochromobilin (cytochromes) (Klasek and Inoue 2016).

In addition to their previously described FTIR spectral contributions, DNA, RNA, and phospholipids also absorb in the 1240-1220, 1080, 1050, and 970 $cm^{-1}$ regions, as a result of their phosphate bonds (Machana et al. 2012; Movasaghi et al. 2008; Wang et al. 2007). The phosphate peak around 1240 $cm^{-1}$ also contains contributions from other phosphorylated and phosphorous-containing compounds, including membrane phospholipids (Movasaghi et al. 2008; Tamm and Tatulian 1997), and as discussed above, these peaks overlap with the amide III peak. While it is known that DNA and RNA are amongst the three cellular compounds most targeted by oxidative stressors and singlet oxygen, the significant overlap of their IR active peaks with other cellular components makes it difficult to directly observe related changes. In addition, there is very significant variation in the spectra of individual phospholipids. The relative strength of this 1260-1240 $cm^{-1}$ peak can vary significantly – and even be entirely absent – in the spectra of different individual phospholipids, or as a result of membrane phospholipid hydrolysis (Berterame et al. 2016; Derenne et al. 2013; Sánchez-Alonso et al. 2012). These peaks can also contain spectral contributions from other phosphate-containing compounds within the cell, including polyphosphate and phosphorylated sugars or proteins.

## 1.3 Research Objectives

The overall objectives of this research were twofold: first, to investigate the effects of high light and singlet oxygen exposure on individual living cells of *Chlamydomonas* spp. and examine the biochemical and metabolic responses. Second, to expand the body of literature on the use of FTIR in the study of complex systems exhibiting subtle responses. It was hypothesized that different species of algae would exhibit varying capacities to protect themselves from high light exposure. As singlet oxygen is the primary damaging agent in photosynthetic cells exposed to high light, it was thought that exposure to a singlet oxygen producing dye would produce a biochemical response in the cells similar to that of HL and could be used as a positive control during my experiments. To investigate further, the following hypotheses were identified:

1) Individual cells will exhibit variation. Variation will exist between cells within the same culture (intracultural differences), between cells of different cultures but the same species (intercultural differences), and between cells of different species. The more similar growth and experimental conditions are, the more similar the individual cells should be. I expect that cells within a culture will exhibit greater similarity than those in different cultures or grown on different days. While these spectral differences have the potential to interfere with comparison measurements, I will be able to understand and control for them such that I can still differentiate between algal species and different stress responses.

2) Oxidative stress will impact proteins, lipids, and DNA. This damage will be observable in individual living algal cells using synchrotron-based FTIR spectroscopy. The biochemical components that are damaged and the magnitude of the damage will vary between species, and in response to the specific oxidative stressor.

3) Photosynthetic mutations will impact photosynthetic capacity and processes. As a result, the cell lines should exhibit altered sensitivity to the effects of high-light stress. Because we can theorize on the impact each specific mutation should have on the cellular capacity to tolerate high light, these cells will allow us to test whether the changes in FTIR absorbance spectra match our predictions.

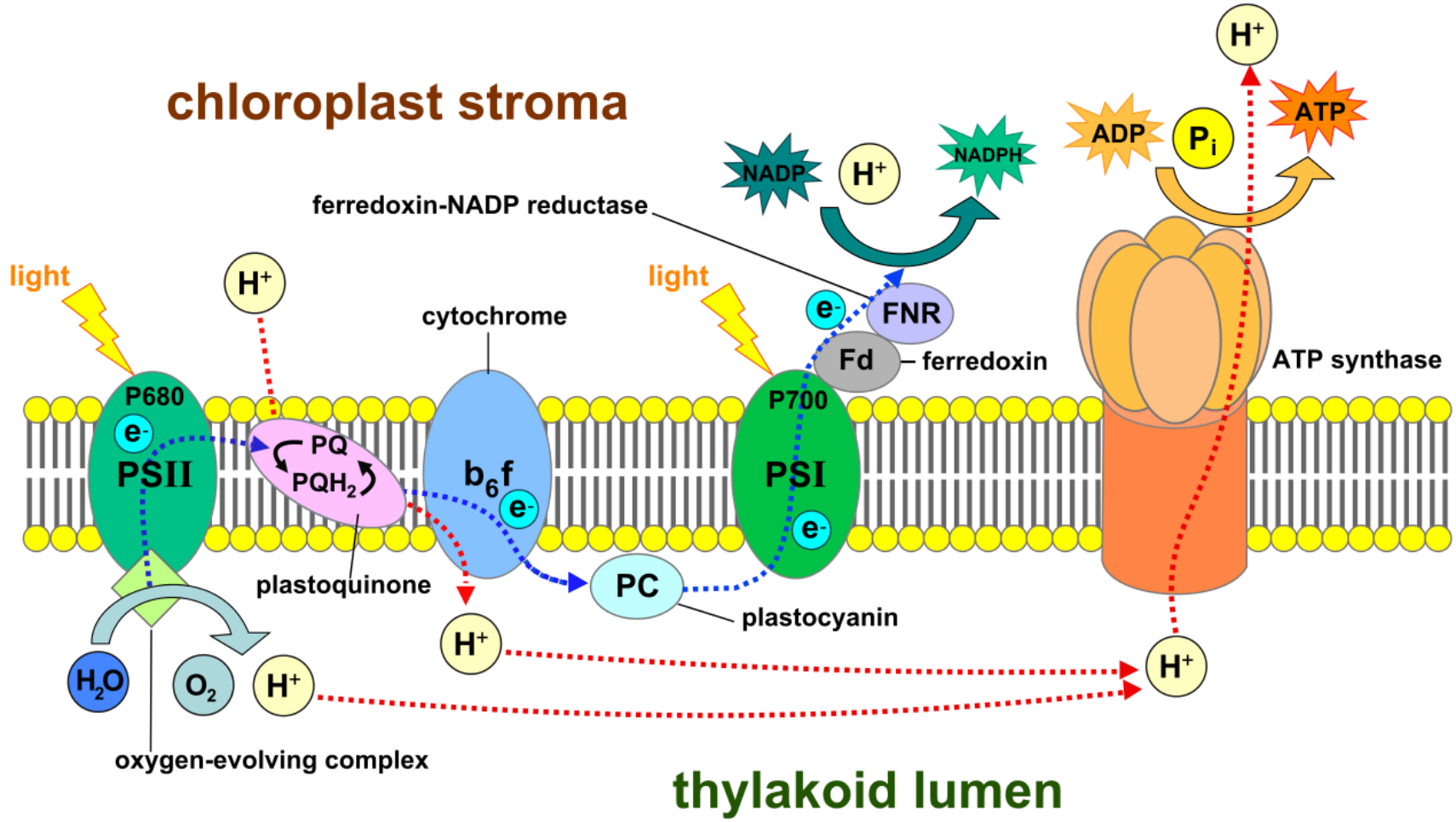


*Figure 1.1 – Schematic overview of light-dependent photosynthetic reactions and the electron transport chain (ETC). Image by Somepics, distributed under a CC BY-SA 4.0 license.*

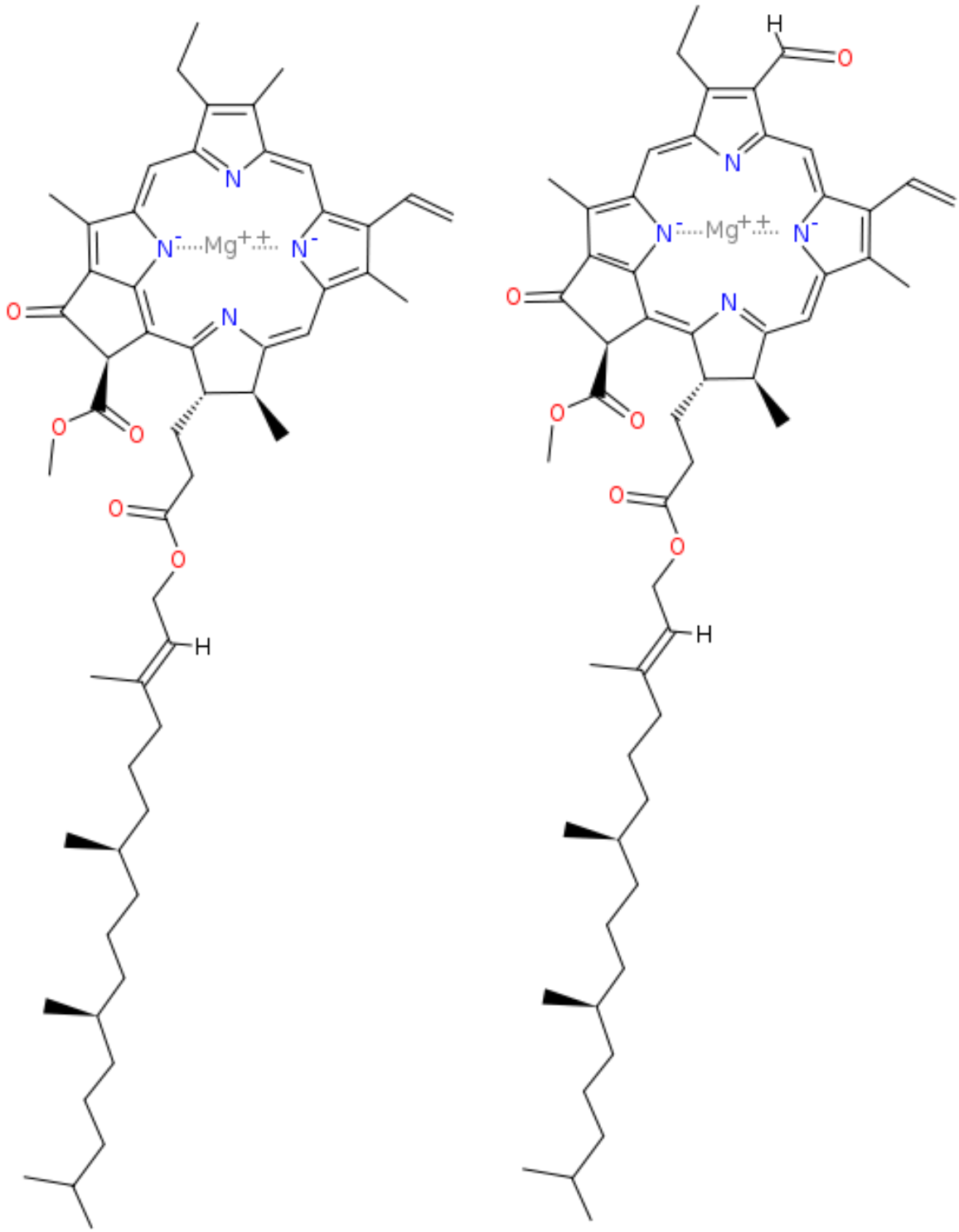


*Figure 1.2 - Structure of chlorophyll* a *(left) and* b *(right). Image by Wc010394, distributed under a CC BY-SA 4.0 license.*

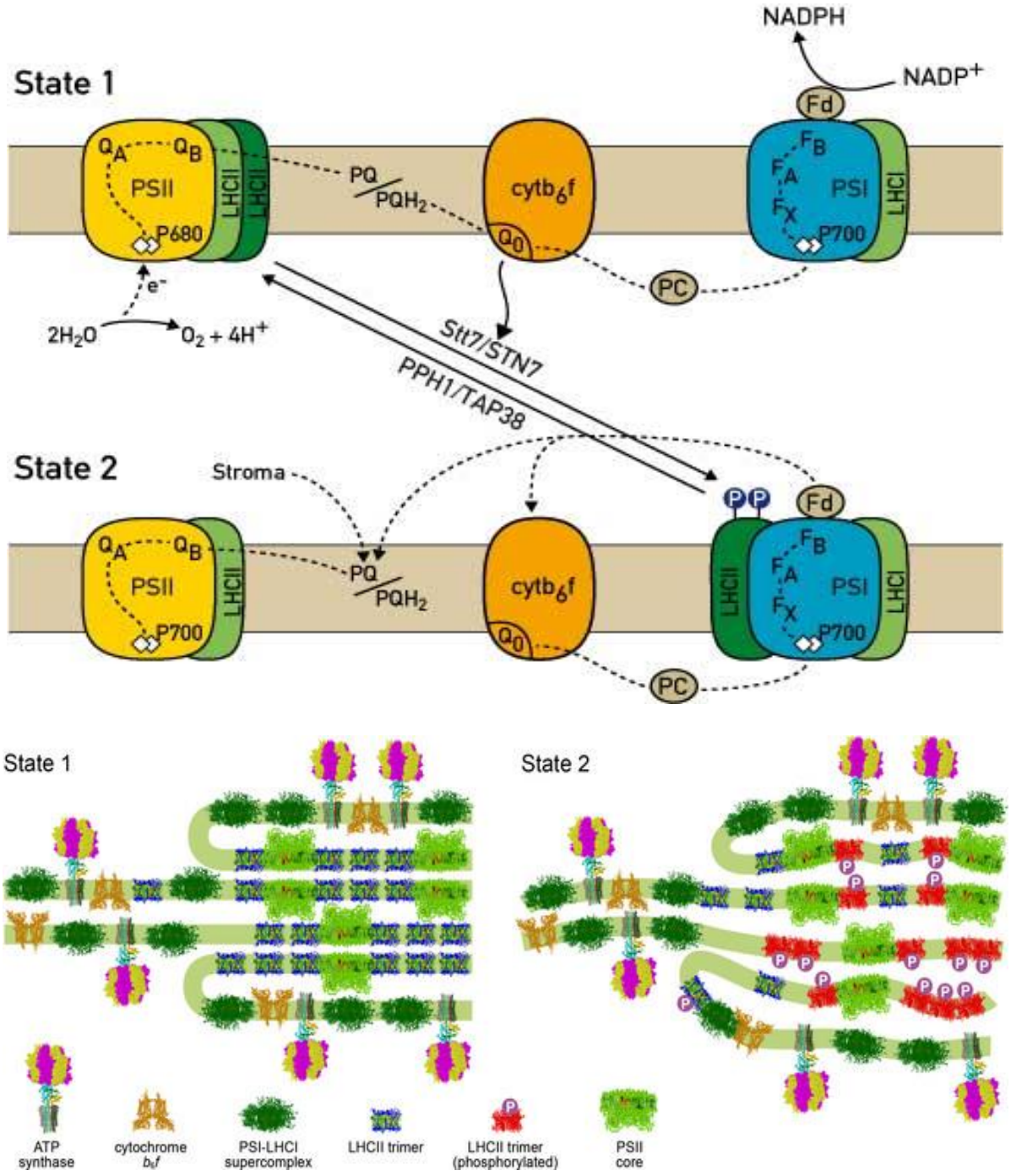


*Figure 1.3 - State transitions in* C. reinhardtii, *showing the reversible phosphorylation and movement of LCHII and associated changes in thylakoid stacking (from Minagawa & Tokutsu, 2015).*

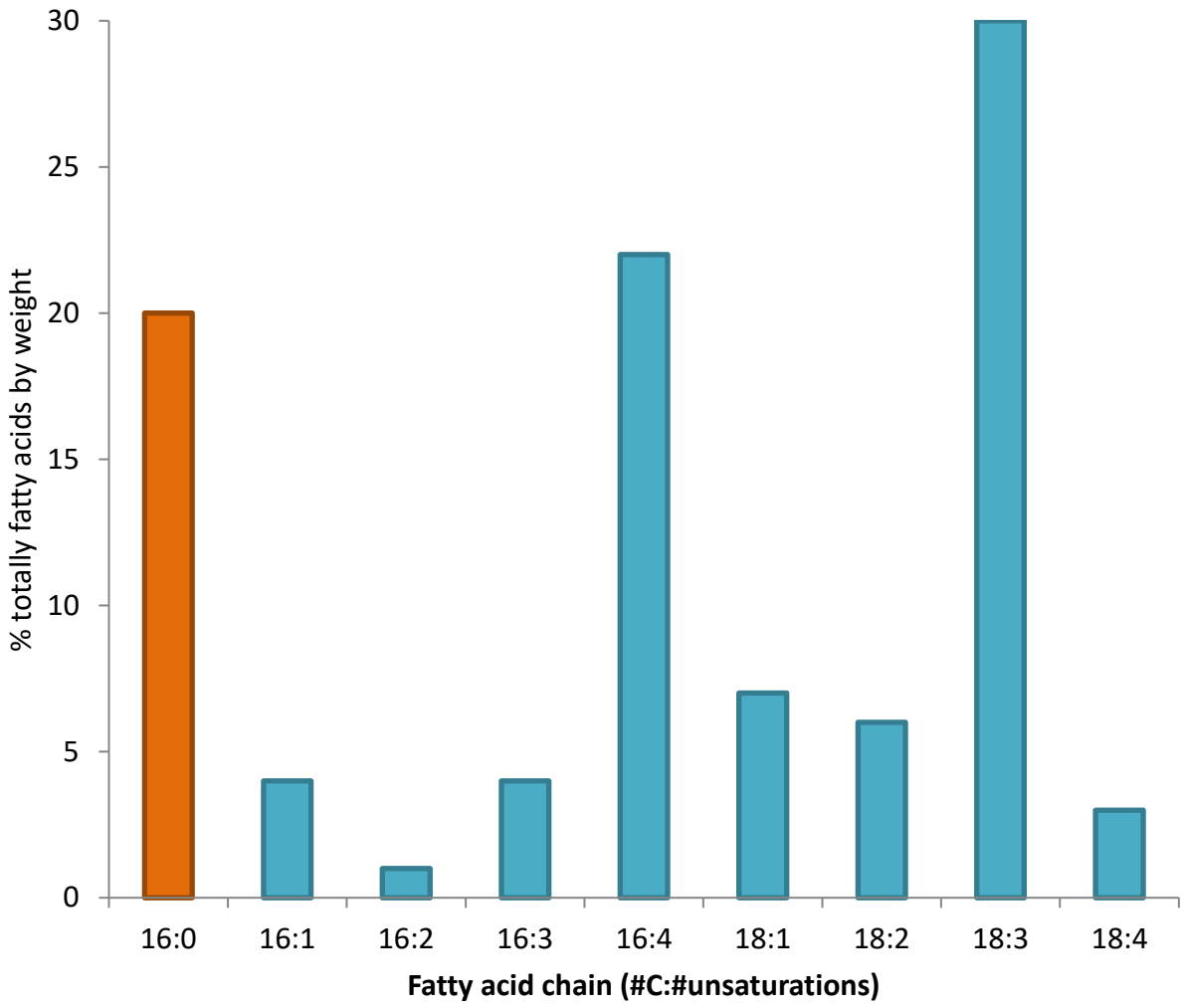


*Figure 1.4 – Saturation of fatty acids in* C. reinhardtii *thylakoid membranes, after Thompson (1996). Saturated fatty acids in orange, unsaturated fatty acids in blue.*

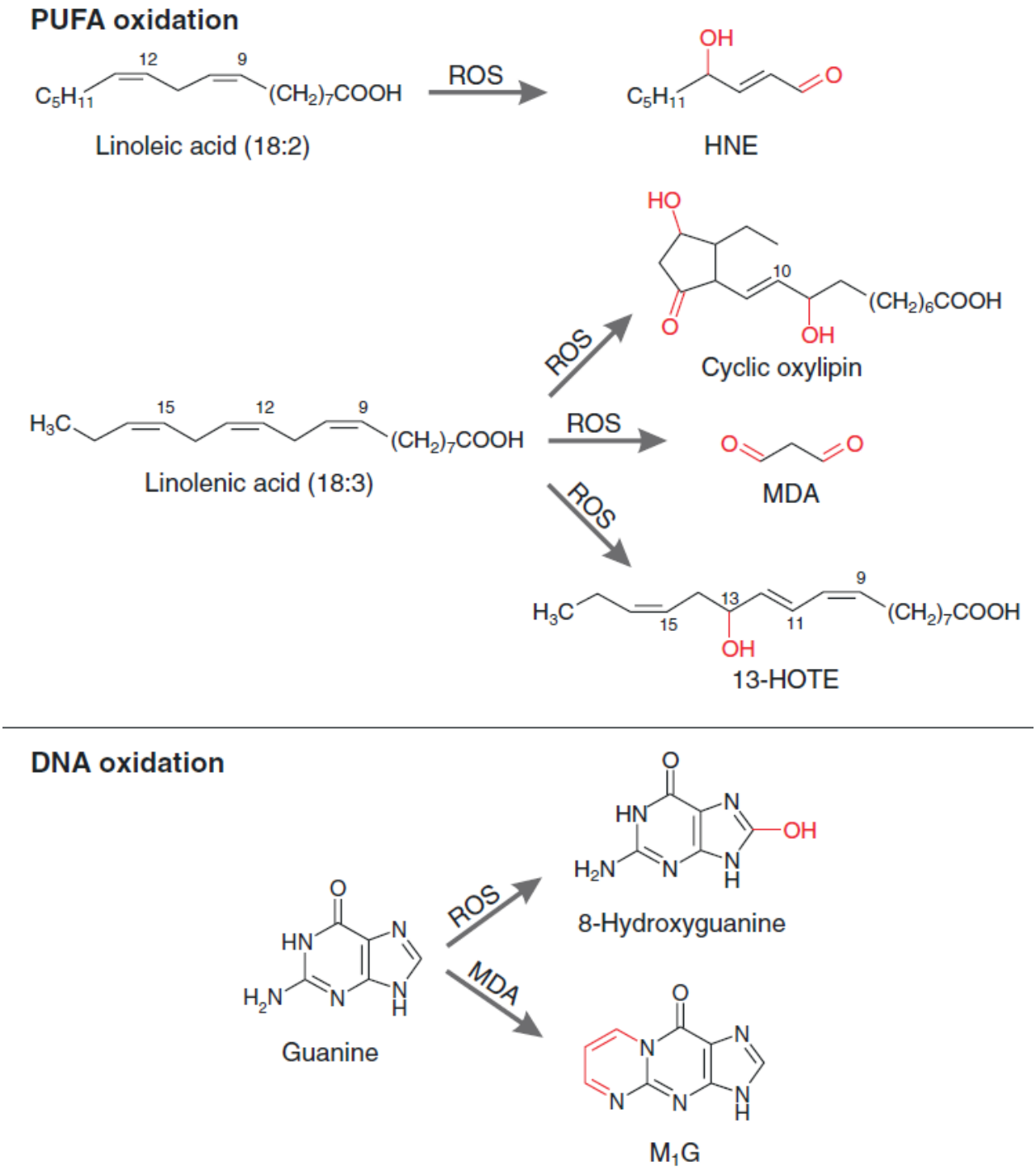


*Figure 1.5 – Common oxidation reactions in polyunsaturated fatty acids (PUFAs) and DNA via type II reactions. Taken from Moller, Jensen, and Hansson (2007).*

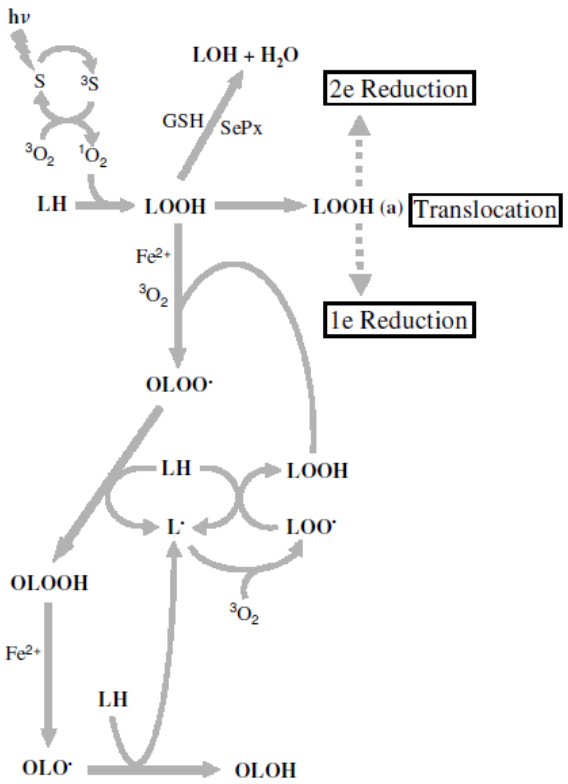


*Figure 1.6 – Singlet oxygen generation of lipid hydroperoxides (LOOH) and possible knock-on reactions. Taken from Girotti and Kriska (2004).*

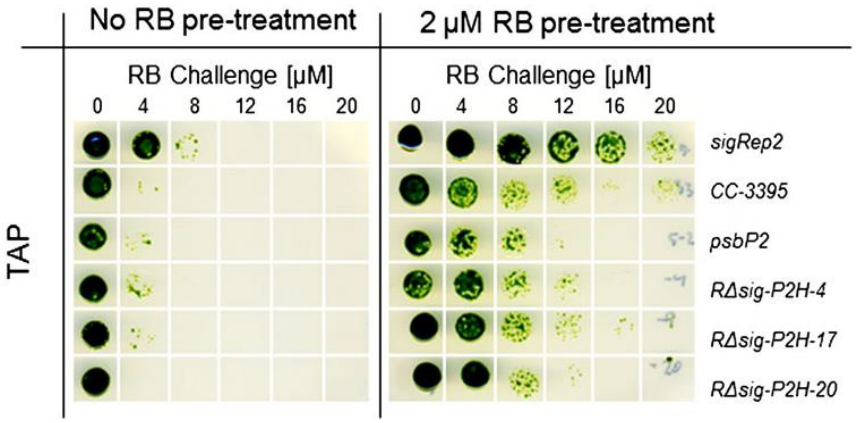


*Figure 1.7 - Response of* C. reinhardtii *mutants to oxidative stress with and without acclimatization pre-treatment. From Brzezowski, Wilson, and Gray (2012).*

*Table 1.1- Symbols used in Fourier transform infrared spectromicroscopy.*

| Symbol | FTIR assignment |
|---|---|
| δ | Deformation/bending/scissoring |
| ν | Stretching vibration |
| ρ | In plane bending (rocking) |
| τ | Out of plane bending (twisting) |
| ω | Out of plane bending (wagging) |
| *s* | Symmetrical |
| *as* | Asymmetrical |

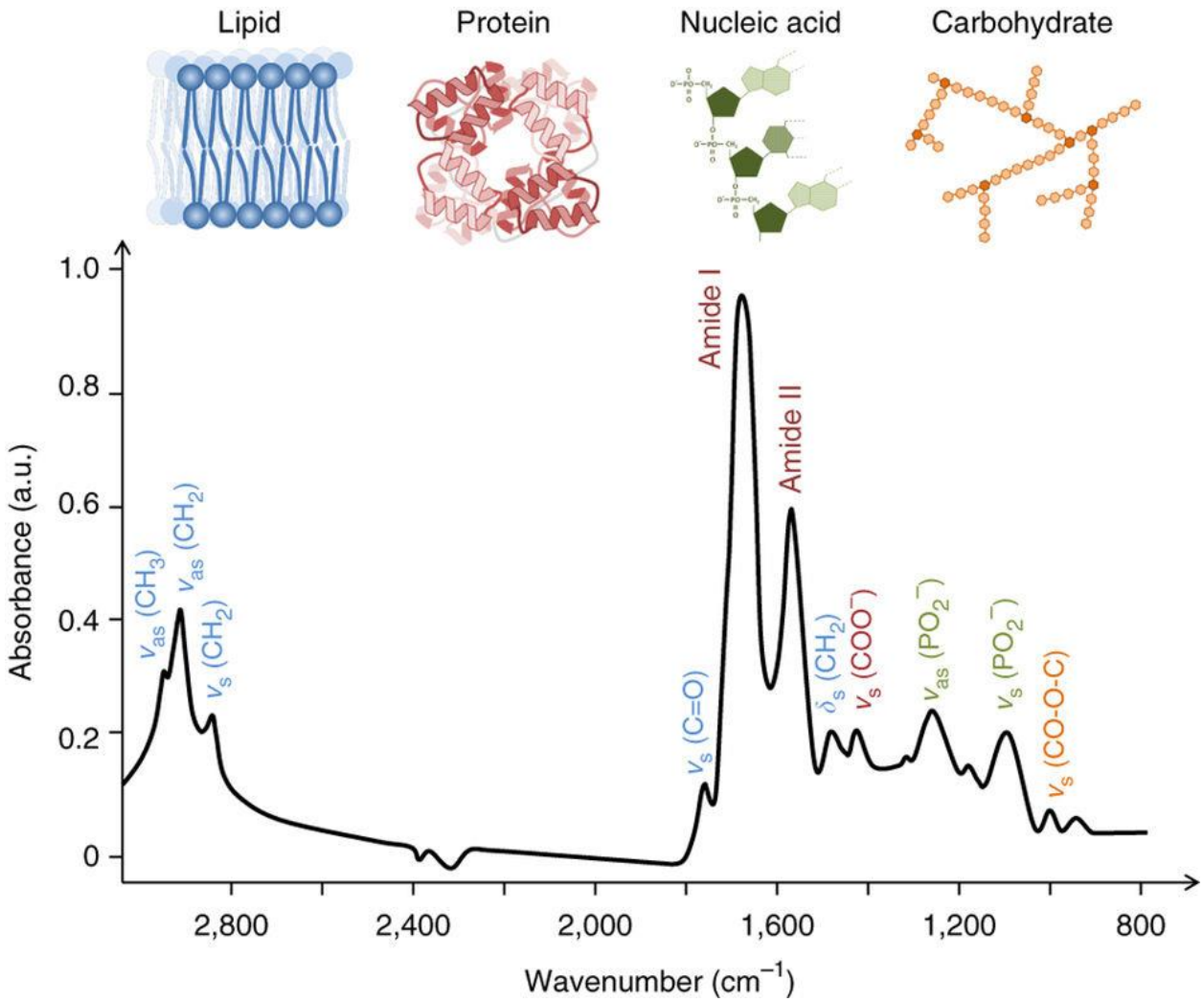


*Figure 1.8 - Simplified overview of the spectra of biological systems, animal cells. This figure, reproduced from Baker et. al (2014) is a cryosection of human breast carcinoma taken with 60 μm apertures.*

*Table 1.2 - Generalized peak assignments for biological spectra.*

| Spectral Region | Name | Description | | 2nd Deriv | Specific Assignment |
|---|---|---|---|---|---|
| 3050-2800 | CH stretching region | νCH | Primarily lipids | 3010 | =C-H Unsaturated lipids |
| | | | | *2985* | Unassigned CH |
| | | | | 2855 | $\nu_{as}$ $CH_3$ Fatty acid chains methyl groups |
| | | | | 2923 | $\nu_{as}$ $CH_2$ Fatty acid chains |
| | | | | *2895* | Unassigned CH, short chain alkanes |
| | | | | 2870 | $\nu_{s}$ $CH_3$ Fatty acid chains methyl groups |
| | | | | 2852 | $\nu_{as}$ $CH_2$ Fatty acid chains |
| 1750-1700 | Carbonyl | ν(C=O) | Primarily lipids | *1740* | Ester Phospholipids, tri- and diacylglycerol, chlorophyll |
| | | | | *1718* | Carboxylate Free fatty acids, lipid hydroperoxides, aldehydes, hydroxyl-and keto fatty acids |
| 1700-1600 | Amide I | Primarily νC=O; minor νCN, δCCN, ρNH | Primarily protein | 1700 | Unknown carbonyl |
| | | | | 1680 | Unordered/random turns and coils, H-bonded C=O sensitive to H-bond disruption |
| | | | | 1654 | α-helixes, minor contriubtion from unordered random coils and turns |
| | | | | 1635 | β-sheets; overlapping $H_2O$ absorption |
| | | | | 1608 | C=C of chlorophyll and derivative compounds |
| 16-1500 | Amide II | ρNH + νCN; minor ρCO, νCC, νNC | Primarily protein | 1580 | Ring stretch, C=N, $COO^-$ |
| | | | | 1547 | α-helixes |
| | | | | 1515 | Tyrosine, ring structures in carotenoids |
| | | ρCH, C=C, $\delta NCH_3$ | | 1494 | |
| 15-1400 | 1450 | HOD, amide II'; $\delta CH_2$ and $\delta CH_3$ | Protein, lipid, deuterated protein, semi heavy water | 1467 | $\delta CH_2$ lipids |
| | | | | 1457 | $\delta_{as}CH_3$ |
| | | | | 1440 | $\delta CH_{2/3}$ |
| | | νCN, δCH, δNH | | 1417 | |
| 1400-1240 | 1398 | | Primarily proteins, some lipids | 1398 | νCOO- |
| | | | | 1386-1378 | **$\delta_s CH_3$**, νCO, δCH, δNH |
| | | νCO, δCH, δNH | | 1363 | |
| | 1340 | | $\omega CH_2$, ring sugars, minor δCH | 1340 | |
| | | | | 1328 | |
| | Amide III | | | 1308 | AA residues, H-bonding. Coupling of νCN to dNH. |
| | Amide III | | | 1285 | Tetrapyrroles. |
| | Amide III/$PO_2$- | Phosphate | (phosophlipids, DNA/RNA), amide III | 1260 | |
| | | | | 1254 | |
| | | | | 1245 | |

**A)**

**B)**

**C)**

**D)**

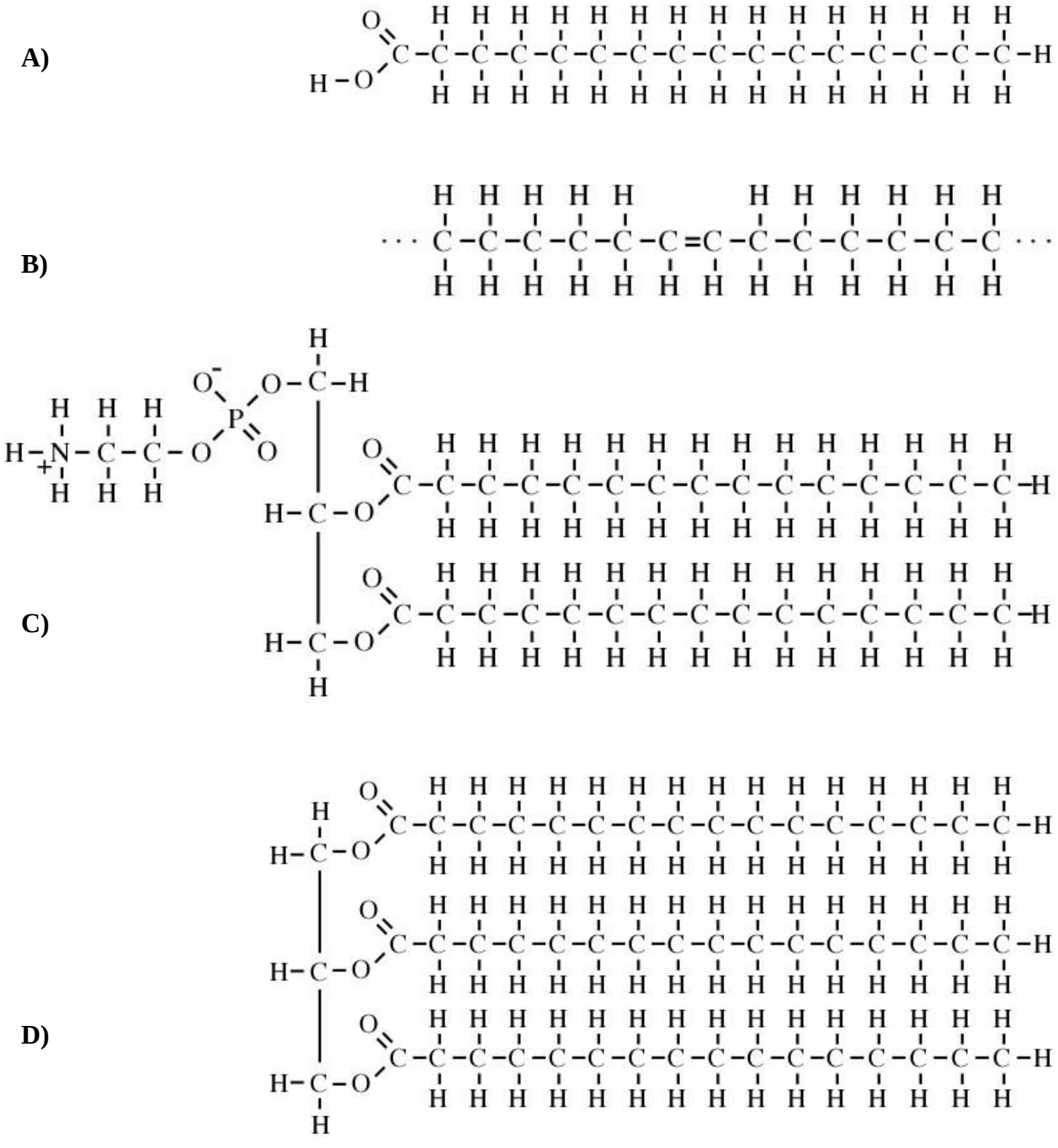

*Figure 1.9 – Basic lipid chemical structures. A) Free fatty acid, saturated. B) Fatty acid chain with one unsaturation. B) Phospholipid (phosphatidylcholine), saturated. C) Triglyceride, saturated.*

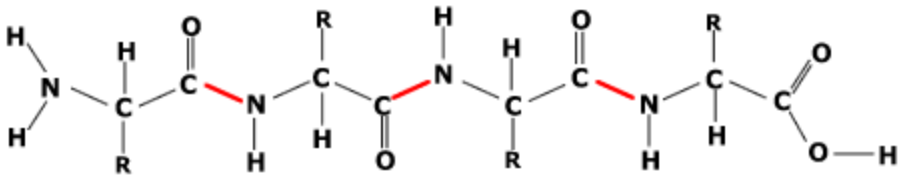

*Figure 1.10 - Structure of a protein. Peptide bonds between amino acid residues are in red. 'R' indicated amino acid side chains.*

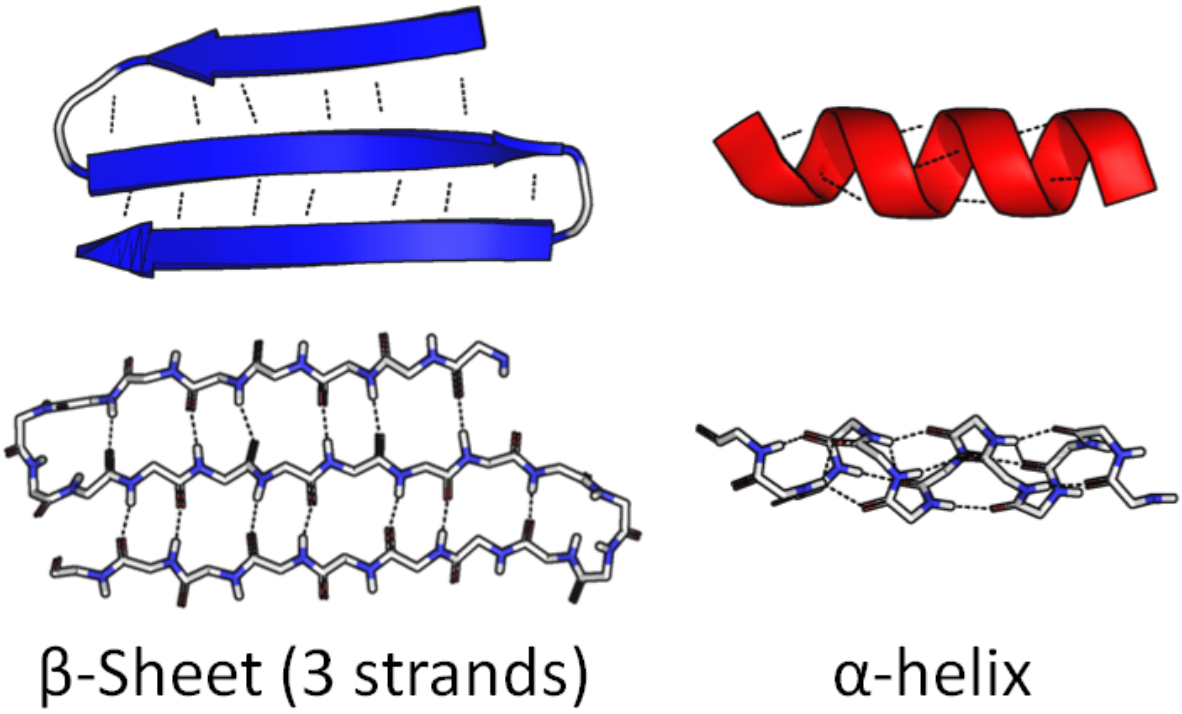


*Figure 1.11 - Protein secondary structure. Image by Thomas Shafee, distributed under a CC BY-SA 4.0 license.*

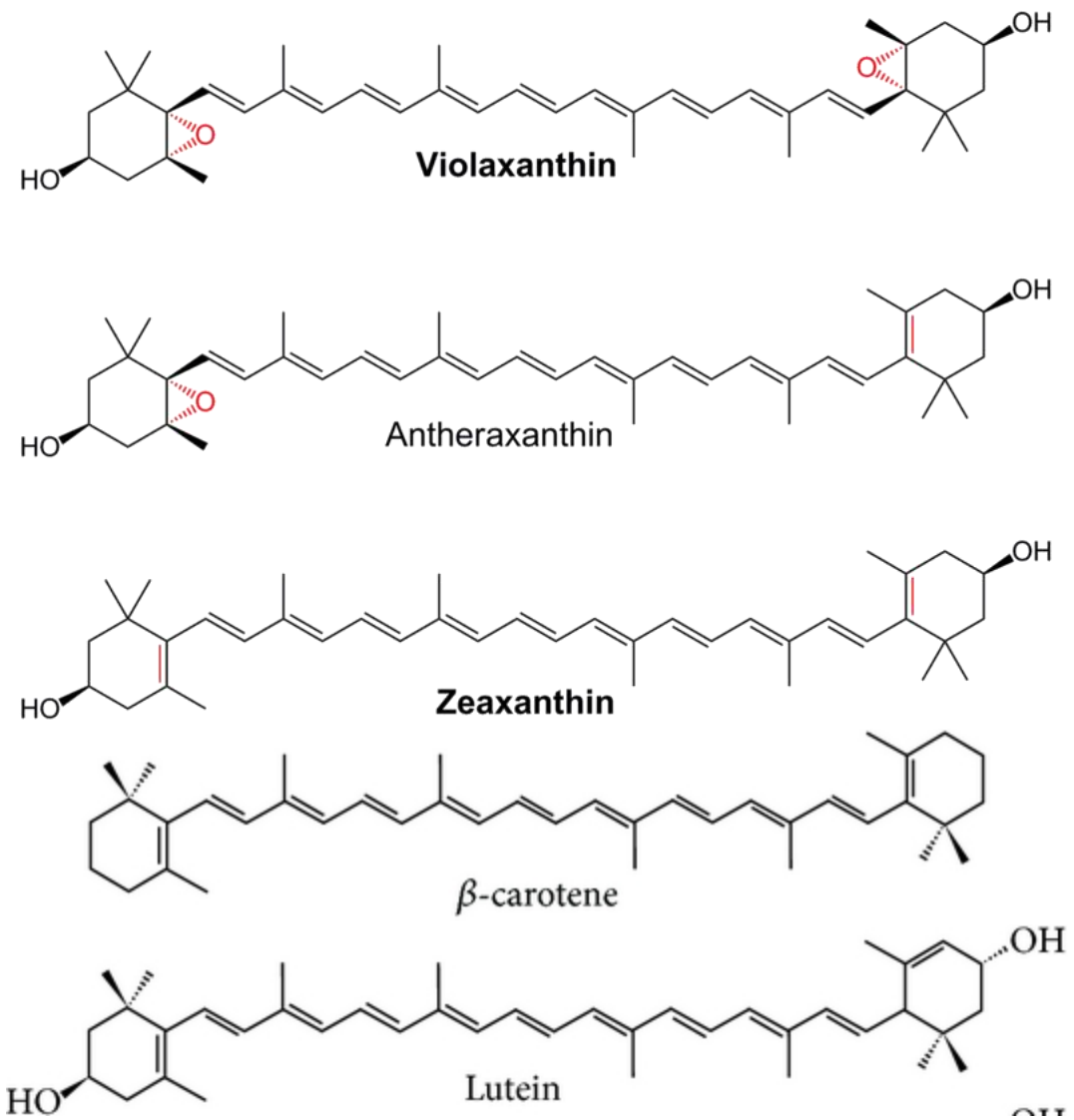


*Figure 1.12 - Structure of some important carotenoids in* Chlamydomonas *spp. Image by Yikrazuul, released into the public domain.*

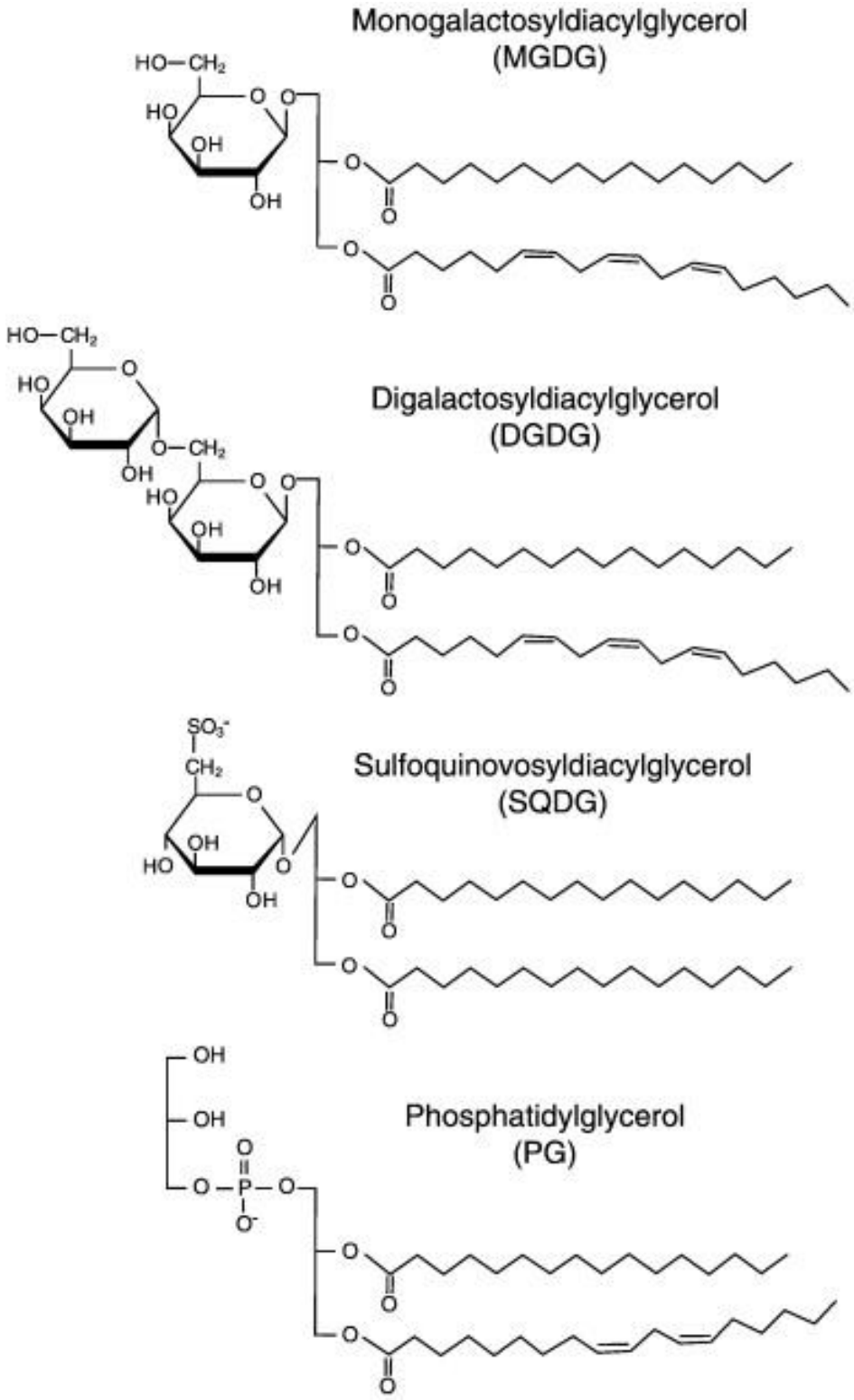


*Figure 1.13 - Structure of the four primarily thylakoid membrane lipids found in* Chlamydomonas reinhardtii *(from Mizusawa and Wada, 2012).*

# CHAPTER TWO

# MATERIALS AND METHODS

## 2.1 Algae Cultivation and Oxidative Stress Exposures

### 2.1.1 Algae Growth and Cultivation

Wild type *C. reinhardtii* (WT CC-125) as well as the photosynthetic mutants CC-1355 (*cbn1*) and CC-4107 (*npq2 lor1*) were obtained from the Chlamydomonas Resource Center (University of Minnesota). The *psaF* mutant line was obtained from a mutagenic screen (Farah et al. 1995), while the *psaF cbn1* was produced by crossing the 3bf strain of Farah et al. (1995) with CC-1355 (Hippler et al. 2000). Both were obtained courtesy of Dr. J-D Rochaix. The two environmentally-isolated *Chlamydomonas* species, *Chlamydomonas* DJX-H (DJX-H) and *Chlamydomonas* DJX-J (DJX-J), were isolated from a decommissioned pit mine in northern Saskatchewan. Cultures of *Chlamydomonas* cells were maintained on Tris-Acetate-Phosphate nutrient medium (TAP) supplemented with arginine and 1.5% agar (Harris 1989). For experiments, cells were transferred to TAP liquid media in sterilized Erlenmeyer flasks, and placed on an orbital shaker at 120 rpm under uniform light conditions of 100 μmol photons $m^{-2}s^{-1}$.

### 2.1.2 Ex Situ Oxidative Stress Exposures

To examine the effects of high light and singlet oxygen on algal cells, cultures were grown in liquid media and then subdivided into control, high light (HL), rose bengal (RB) and high light rose bengal (HLRB) groups by placing 10 mL of the culture into 15 mL clear conical centrifuge tubes. Control cultures were exposed to uniform light conditions of 100 μmol photons $m^{-2}s^{-1}$. RB cultures had rose bengal added to the culture media to a final concentration of 4 μM, and then were exposed to control light conditions. HL cultures were exposed to 750 μmol photons $m^{-2}\,s^{-1}$. HLRB cultures had rose bengal at a final concentration of 4 μM, and exposed to 750 μmol photons $m^{-2}\,s^{-1}$. In each case the cells left under the treatment conditions for 2 h, with gentle agitation. When the treatment was complete, the cells were centrifuged at 2000 g for 5 min and resuspended in 10 mL of TAP. This was repeated three times to remove rose bengal. All cultures were treated in the same way to avoid handling artifacts. Following the final wash, the samples were resuspended in 1.5 mL of TAP and taken to the Canadian Light Source for measurement.

## 2.2 Fourier Transform Infrared Spectromicroscopy

### 2.2.1 Sample Preparation and Equipment

Measurements on individual algal cells were carried out at the Canadian Light Source synchrotron facility (Saskatoon, SK) on the Mid-Infrared beamline (MidIR, 01B1-01) using a Bruker IFS 66v/S interferometer coupled to a Hyperion 2000 FT-IR microscope in synchrotron-light transmission mode. Synchrotron light sources – as compared to benchtop globar light sources – have superior brightness and much better signal:noise ratios, allowing for the collection of clear data from smaller apertures and samples (Carr 2001). For imaging, cells were prepared as per Goff et al. (Goff et al. 2009). Cells in TAP media were centrifuged, and 2 μL of the cell pellet was resuspended in heavy water ($D_2O$) containing 0.1% agarose. $D_2O$ was used to shift solvent absorption away from the amide absorbance region, to allow examination of protein secondary structure. The 0.1% agarose was added to the solution to immobilize *Chlamydomonas* cells with minimal impact on either the cells or their spectra. Cells in the heavy water solution were loaded into a sample holder designed for the study of living cells (Figure 2.1). The solution containing the algal cells was placed between two 1 mm $BaF_2$ optical windows separated by a 15 μm spacer.

### 2.2.2 Measurement of Individual Cells

The brightness and coherence of synchrotron infrared light allows for the use of smaller apertures with a resultant useful signal to noise ratio. However, live cells still exhibit some degree of motility under these measurement conditions, particularly during long-term time-resolved measurements. Drift or movement even at a rate of 1 μm/10 min can result in significant, non-reproducible differences in absorption, particularly given the heterogeneous composition of an individual cell. To ensure the selection and isolation of individual living cells, confocal apertures were set to 2-5 μm greater than the diameter of individual cells, which is near the diffraction limit for IR wavelengths in the fingerprint region. Cell size along the long axis for *C. reinhardtii* and DJX-J cells averaged 7-9 μm, and the larger DJX-H cells 12-15 μm. This allowed cells that exhibited minor degrees of motion, despite the presence of agarose in the media to remain within the IR measurement spot. The top apertures were adjustable, square, glass apertures, and set to 35 μm. The bottom apertures were set-diameter circles (Figure 2.2). In comparison to using top and bottom round apertures, this combination allowed for a wider field of view while scanning for new cells and appeared to reduce baseline variation. In comparison to using adjustable square apertures

on the top and bottom, the bottom round aperture allowed for better exclusion of media in the measurement spot around the oval to round cells, and improved repeatability between days and samples. Background measurements (1024 scans, resolution of 4 $cm^{-1}$) were taken of the media, in an area distant from any cells. Once an individual cell was isolated, 512 scans were taken (4000-800 $cm^{-1}$) at a resolution of 4 $cm^{-1}$.

## 2.3 Data Analysis

### 2.3.1 OPUS

The raw data obtained from the IR scans of individual cells, or cell-free media were analyzed using OPUS 7.2 spectroscopy software (Bruker, United States). Several spectral ranges in the mid-IR range are dominated by solvent components (Figure 2.3). These include 3200-3700 $cm^{-1}$ ($\nu H_2O$, $\nu$HOD), 2200-2700 $cm^{-1}$ ($\nu D_2O$), and 1240-1150 $cm^{-1}$ ($\delta D_2O$). The signals from these regions generally saturate the detector making them unsuitable for sample analysis. The formation of a HOD peak occurs around 1455 $cm^{-1}$, though the precise position varies with the relative concentration of H and D present in the mixture (Max and Chapados 2002). In addition, the detector sees a general intensity decrease in the low wavenumber region as the optical cut-off of $BaF_2$ is reached, combined with the inherent diffraction limitation of the apertures. In the live cell imaging studies performed in this work, no usable data was obtained below 900 $cm^{-1}$. In addition, depending on beam intensity, alignment, and sample holder factors, the spectral region below 1100 $cm^{-1}$ could exhibit any combination of strong baseline variation, poor signal to noise ratio, and limited intensity. The region below the heavy water saturation peak around 1212 $cm^{-1}$ was the first to show poor signal to noise ratio if measurement conditions were suboptimal.

Based on the complex biochemical makeup of the living cells and my interest in studying the effects of high light and singlet oxygen on the cells' lipids and proteins, two distinct spectral regions were used for data analysis: the fingerprint region at 1800-900 $cm^{-1}$ and the CH stretching region at 3050-2800 $cm^{-1}$. The fingerprint region was primarily examined in the 1800-1240 $cm^{-1}$ region due to the limiting factors discussed above. Spectra were min-max normalized to the amide I peak centred around 1650 $cm^{-1}$ (Figure 2.4). The lowest absorbance unit point in the local baseline between 1800-1600 $cm^{-1}$ was set to zero while the maximum absorption was set to '2' and a linear multiplicative scalar was applied. The CH region was further offset corrected to set

the local baseline at 3040-3010 $cm^{-1}$ to '0' (Figure 2.5). No further baseline correction was done. When second derivative spectra were generated, seven smoothing points were used.

### 2.3.2 Principal Component Analysis

Principal component analysis (PCA), an unsupervised statistical approach that extracts and displays important variability, was performed using The Unscrambler X (CAMO Software, Olso, Norway). Min-max normalized spectra were imported from OPUS, and the 1800-1240 and 3050-2800 $cm^{-1}$ regions were analyzed separately. Data preprocessing for the 1800-1240 $cm^{-1}$ region consisted of the application of an extended multiplicative scattering correction (EMSC) to correct for additive, multiplicative, and wavelength-depended spectral effects. This corrected for factors such as differences in path length (different thicknesses in the 15 μm sample space between sample holder loadings), scattering caused by slight differences in the angle of the paired windows inside the sample holder, interference patterns from alignment of the optical windows, condenser and microscope apertures, Mie scattering, and similar factors. EMSC-corrected spectra were visually compared to offset-corrected spectra to ascertain that the spectral changes were relatively minor. Initial analysis of PCA of the CH stretching region showed that while the spectra of different treatments separated out nearly perfectly in PCA space, the loadings were representative of baseline slopes and associated overall intensity differences, rather than changes in the shape and position of peaks. To allow for more meaningful comparisons in the CH stretching region, the EMSC pre-treatment was followed by the generation of second derivative spectra (Savitzky-Golay, 7 smoothing points) which were used for PCA analysis.

Once a PCA was generated, loadings and correlational loadings were examined to see which spectral ranges influenced each principal component axis. Figure 2.6 shows a two-dimensional PCA (A), as well as the loadings and correlational loadings that describe the PC-1 axis (Figure 2.6 B, C) and PC-2 axis (Figure 2.6 D, E). For demonstration purposes, Figures 2.7 and 2.8 display the spectra of individual cells that sit at the extreme ends and middle of PC-1 (Figure 2.7) and PC-2 (Figure 2.8). Important wavenumber regions defined by the correlational loadings in Figure 2.6 are overlain. The correlational loadings for PC-1 from Figure 2.6 (C) are represented in Figure 2.7 by the horizontal purple lines. The correlational loadings for PC-2 from Figure 2.6 E are represented by the horizontal purple lines in Figure 2.8. Looking at Figure 2.7 spectra plotted along the right-hand side of the PC-1 axis tend to have: broader amide I peaks; broader amide II

peaks of lower intensity; broader, more intense 1450 $cm^{-1}$ peaks; and significant reshaping of the 1398 $cm^{-1}$ peak due to changes in the relative contribution of the 1398 $cm^{-1}$ and 1378 $cm^{-1}$ second derivative components. This PC-1 axis, which accounts for 52% of variation between these spectra, is dominated by protein absorbance and by itself can be used to separate the spectra of cells exposed to a combination of high light and rose bengal from all other treatments. The same approach is employed in Figure 2.8 for the spectra of the same three cells relating to PC-2. PC-2 covers regions associated with chlorophyll and ring structures, protein side chains, and the complex fingerprint region. Spectra of cells exposed to rose bengal (RB or HLRB) are cleanly separated from the spectra of control cells and high light cells on this axis alone. The combination of the PC-1 and PC-2 axes leads to much greater separation of spectra than either axis alone.

Data analysis in the following chapters presents PCAs in either two- or three-dimensional space, depending on the significance of each loading and how well it describes the overall variation present in the spectra. In the case of two-dimensional PCAs, this was primarily PC-1 and PC-2. For three dimensional PCAs, this was primarily PC-1, PC-2, and PC-3. In some instances, one of these loadings captured residual baseline variation or described intracultural variability. In these cases, the next numerical PC containing significant correlational loadings was used. These figures overlay PC correlational loadings on treatment averages rather than individual cells, as in Figures 2.7 and 2.8.

### 2.3.3 Baseline Correction Considerations

Artifacts induced by standard OPUS baseline correction algorithms are highlighted in Figure 2.9 and Figure 2.10. These effects are most pronounced over longer spectral regions, as shown in Figure 2.9. Uncorrected averages of *C. reinhardtii* cells obtained on different days are shown in Figure 2.9 A. Figure 2.9 B shows the impact of OPUS's standard rubber band baseline correction. Differences have been induced in the amide I:II ratio, baseline through the fingerprint region (1450-1260 $cm^{-1}$), and the 1080:1040 $cm^{-1}$ ratio. Uncorrected baseline in this region – particularly between 1800-1240 $cm^{-1}$ – is often consistent between days and does not require aggressive correction. Baseline considerations are more complex through 3050-2800 $cm^{-1}$ (Figure 2.10), both in terms of complexity of underlying baseline variation and the impact of available algorithms. Each of these corrections results in final spectra that are dramatically different from the raw spectra and – more importantly – from each other. The application of baseline corrections alters not only

baseline, but also overall peak height, width, position, and ratios. Figure 2.11 demonstrates the nullification of these artifacts in the νCH region via usage of second derivatives. This allows for visualization of peak position and the shape of the original spectra, based on the relative positions of the second derivative peaks, as well as a feature that might have been missed in the original spectra – the presence of a variable contribution around 2888 $cm^{-1}$ between $\nu CH_{2as}$ and $\nu CH_{3s}$.

Underlying scattering artifacts can be corrected for through the use of extended multiplicative scattering correction (EMSC) in Unscrambler that removes additive and multiplicative scattering underlying spectra. The effects of its use are shown in Figure 2.11. Figure 2.11 highlights the spectra of two outlier cells in PCA space (A) and their spectra (B), and the loadings that describe PC-1 and PC-2 (C) without EMSC correction. The loadings for PC-1 and PC-2 (C) appear to be influenced to some degree by underlying baseline variation and scattering. After EMSC correction (Figure 2.11 E-G), the baseline difference in one outlier spectrum through the fingerprint region – which appears to be related to some sort of offset – has been removed. The spectrum from the other outlier cell, which exhibited different height and shape of the 1740 $cm^{-1}$ peak, as well as a different shape through the fingerprint region, was not brought into line and remained an outlier (Figure 2.11 D, E), despite the EMSC correction. Two-dimensional PCA supports these conclusions (Figure 2.11 F). Importantly, the loading associated with the PCA after EMSC (Figure 2.11 F) are more clearly related to spectral features, rather than being dominated by baseline drift. The use of EMSC and baseline correction or second derivatives is not without the generation of artifacts, but the mathematical manipulation of the data is minimized. As such, the final data analysis relied on PCA of EMSC-corrected spectra. No OPUS baseline corrections were used. The 1800-1240 $cm^{-1}$ and 3050-2800 $cm^{-1}$ regions were analyzed separately, and analysis of the CH stretching region also relied on the analysis of second derivative data.

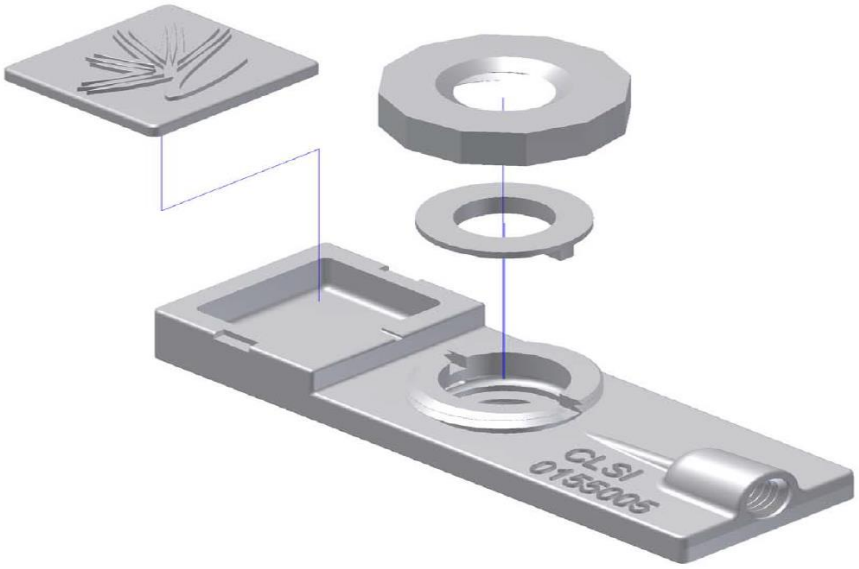


*Figure 2.1 - Sample holder used in infrared measurements of individual living cells. Not shown: gaskets and windows.*

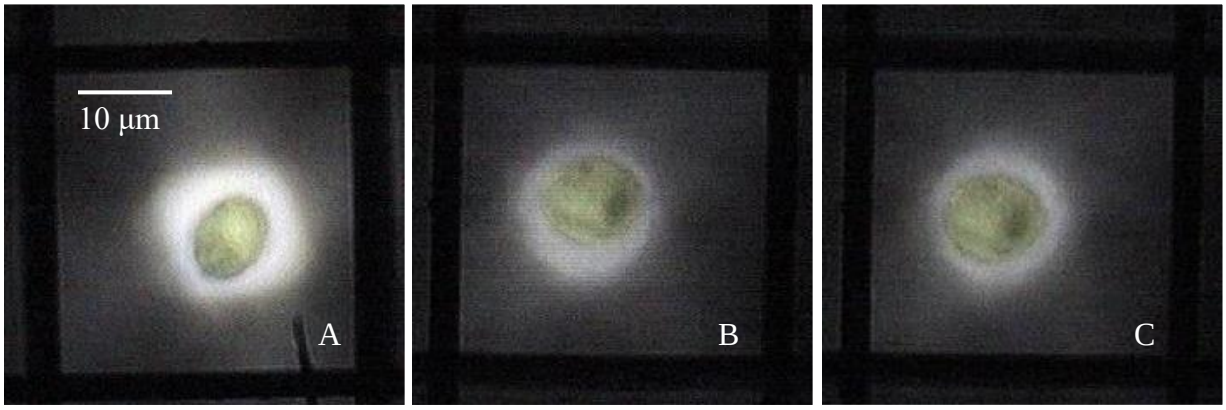


*Figure 2.2 - Aperture alignment for measurement of individual living cells. One cell of the C. reinhardtii CC-4107 cell line (A). The same cell of* C. reinhardtii *wild type is present in (B) and (C), before and after 50 minutes of measurement, showing the small degree of cellular motion still observed. The bottom aperture is the numerical set 0.6 numerical aperture. The top square glass apertures are set at 35x35 μm.*

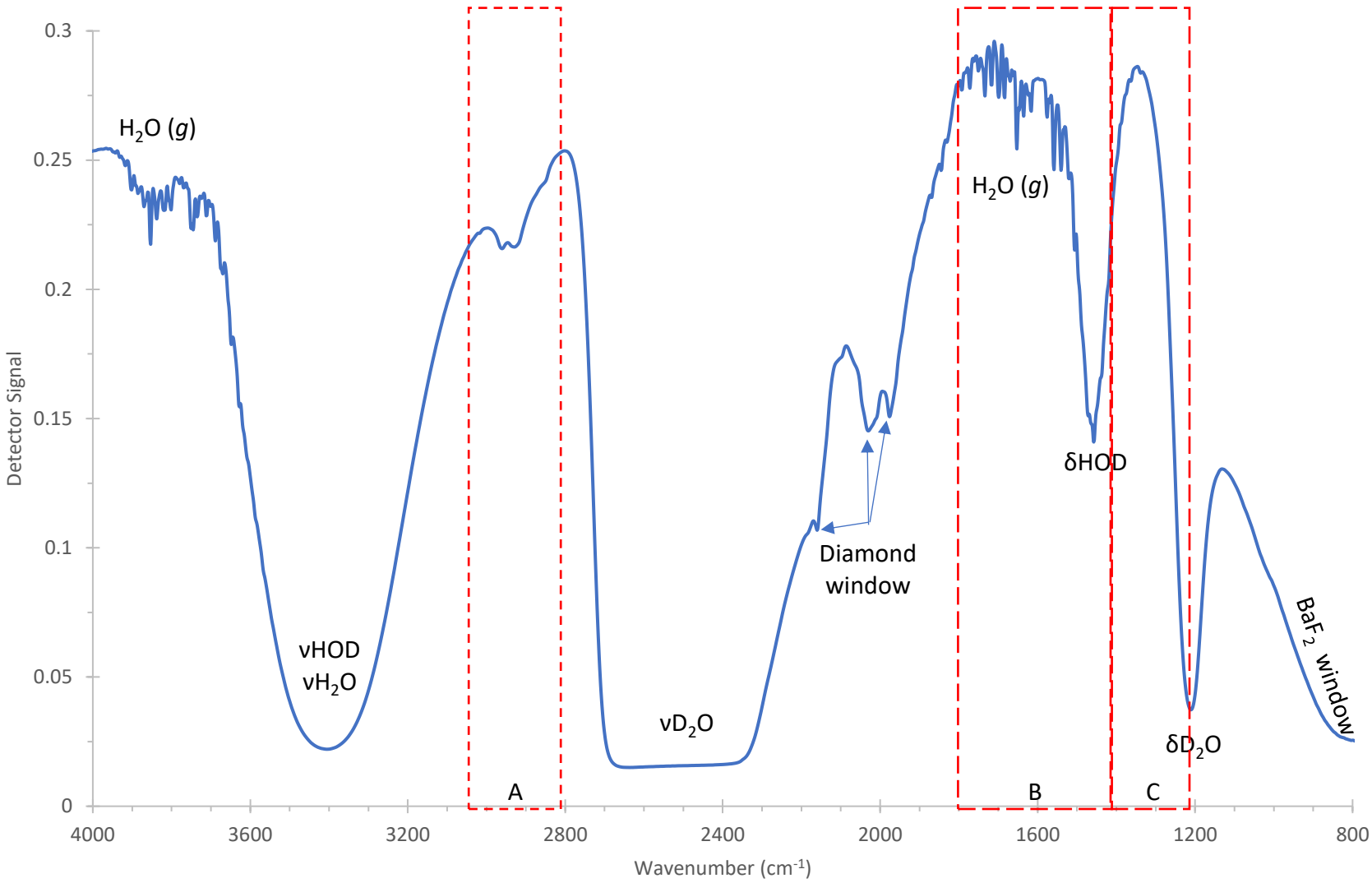


*Figure 2.3 – Reference single channel trace, highlighting regions of absorption of water-heavy water mixtures, atmospheric water vapour, the diamond window, and the intensity cut-off of the two 1mm $BaF_2$ windows. A) vCH region, B) Carbonyls and amides, C) Fingerprint region.*

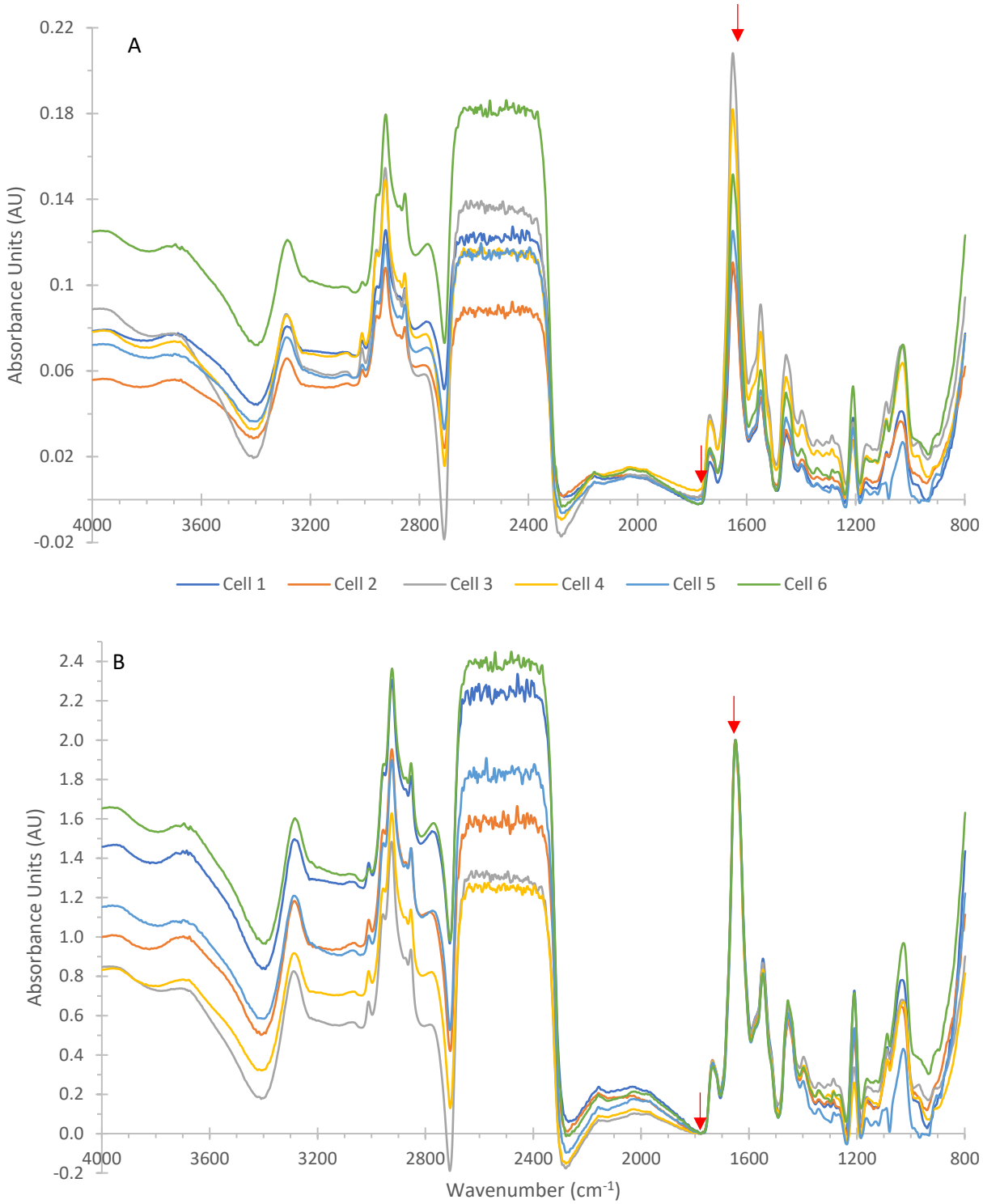


*Figure 2.4 – Full spectra of six individual cells of the CC-4107 cell line. Before (A) and after (B) min-max normalization to the amide I peak (1800-1600 $cm^{-1}$). Red lines arrows highlight the wavenumbers at which the minimum and maximum values are found.*

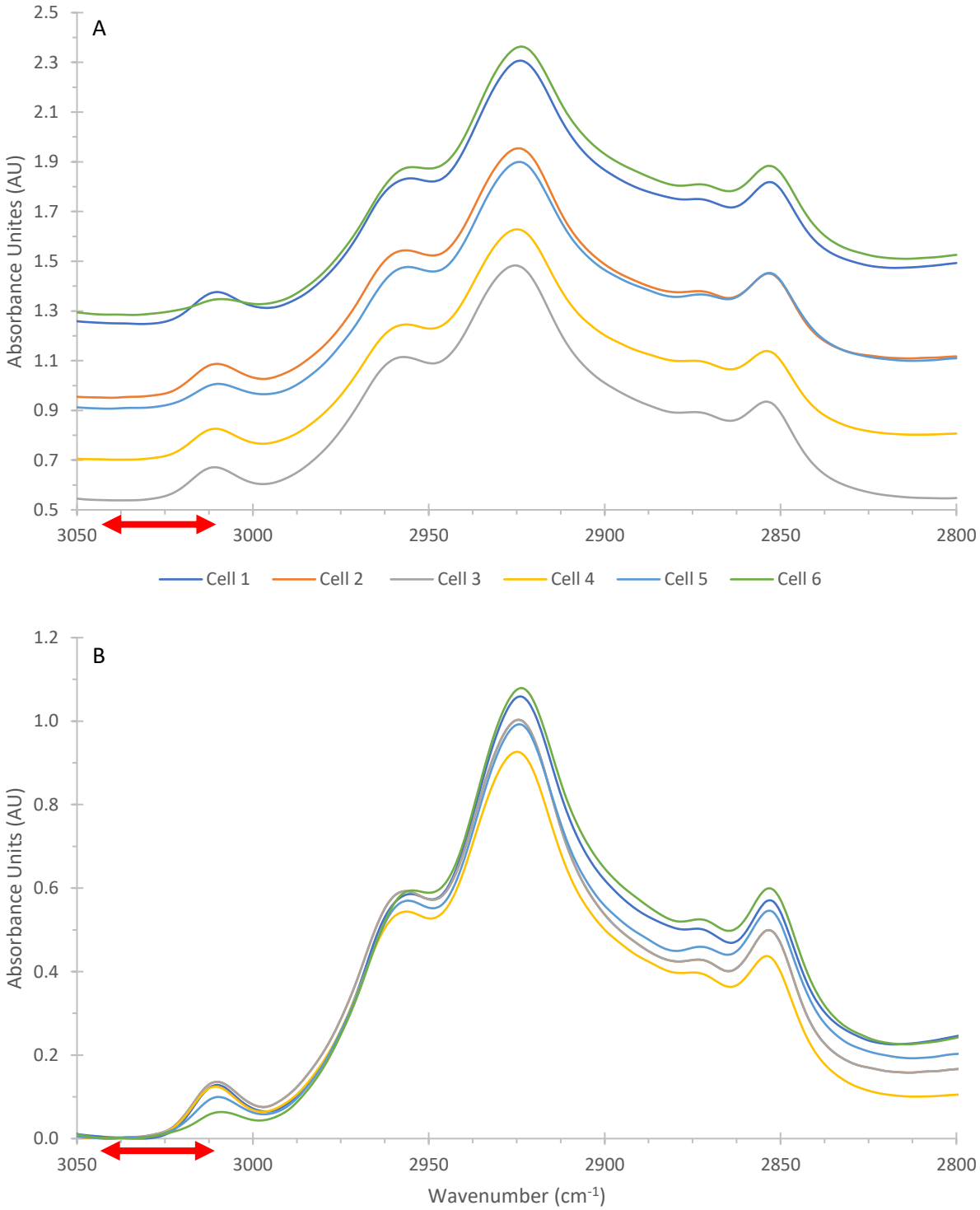


*Figure 2.5 - CH region (3050-2800 $cm^{-1}$) of individual CC-4107 cells. Spectra have been min-max normalized to the amide I peak. Before (A) and after (B) offset correction to the local baseline at 3040-3010 $cm^{-1}$. The local baseline range is highlighted by the double-headed red arrow.*

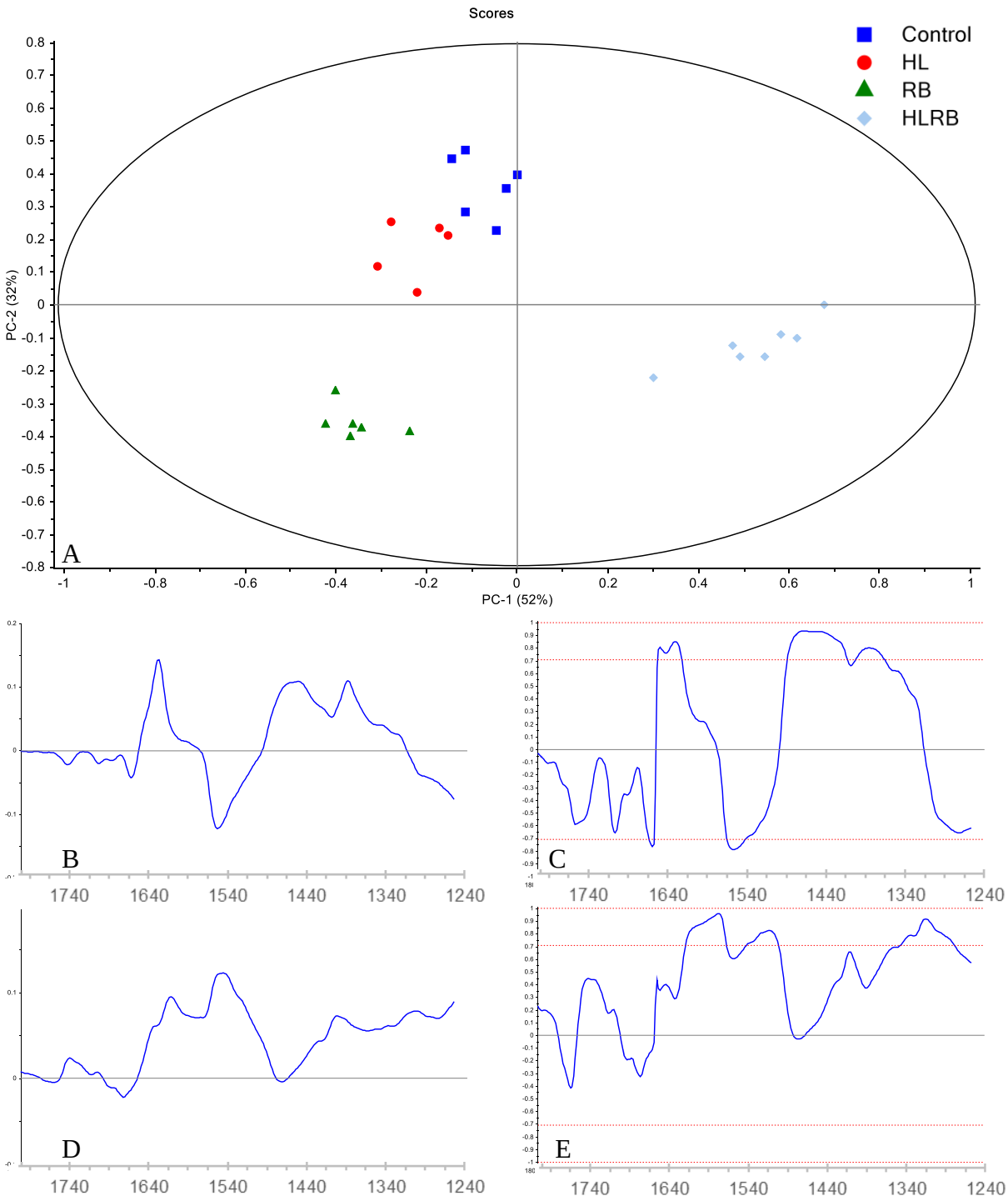


*Figure 2.6 - PCA, loadings, and correlational loadings for the spectra of individual cells of the* Chlamydomonas reinhardtii *line CC-4107 in the 1800-1240 cm$^{-1}$ region. A) Two-dimensional PCA. B and C) loadings and correlational loadings for PC-1. C) and D) loadings and correlational loadings for PC-2.*

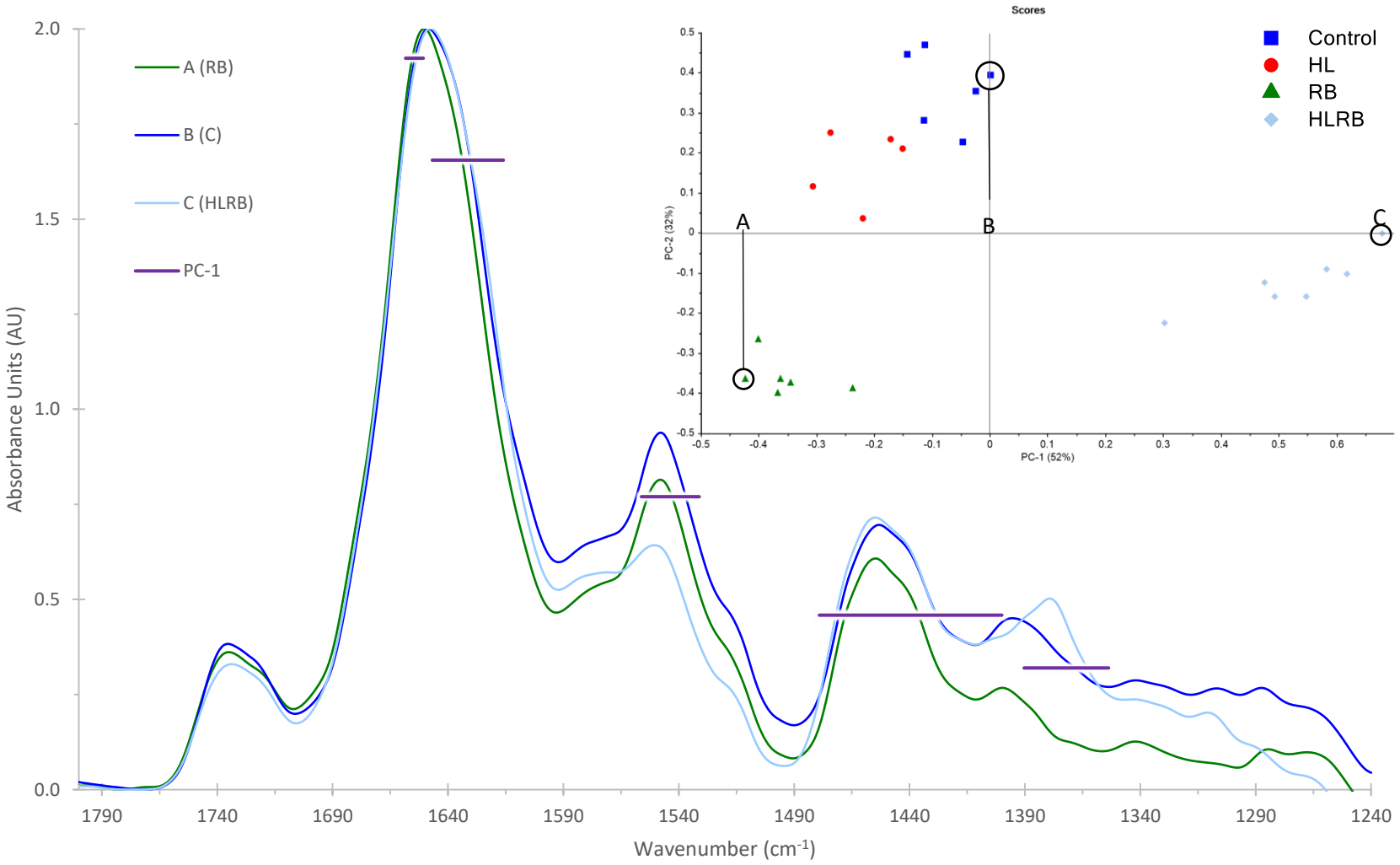


*Figure 2.7 - Spectra of three individual cells of the* Chlamydomonas reinhardtii *mutant CC-CC-4107: A) Spectra of a cell exposed to rose bengal; B) Spectra of a control cell; C) Spectra of a cell exposed to a combination of high light and rose bengal. Inset image shows the position of each spectrum in a principal component analysis and their relationship to PC-1.*

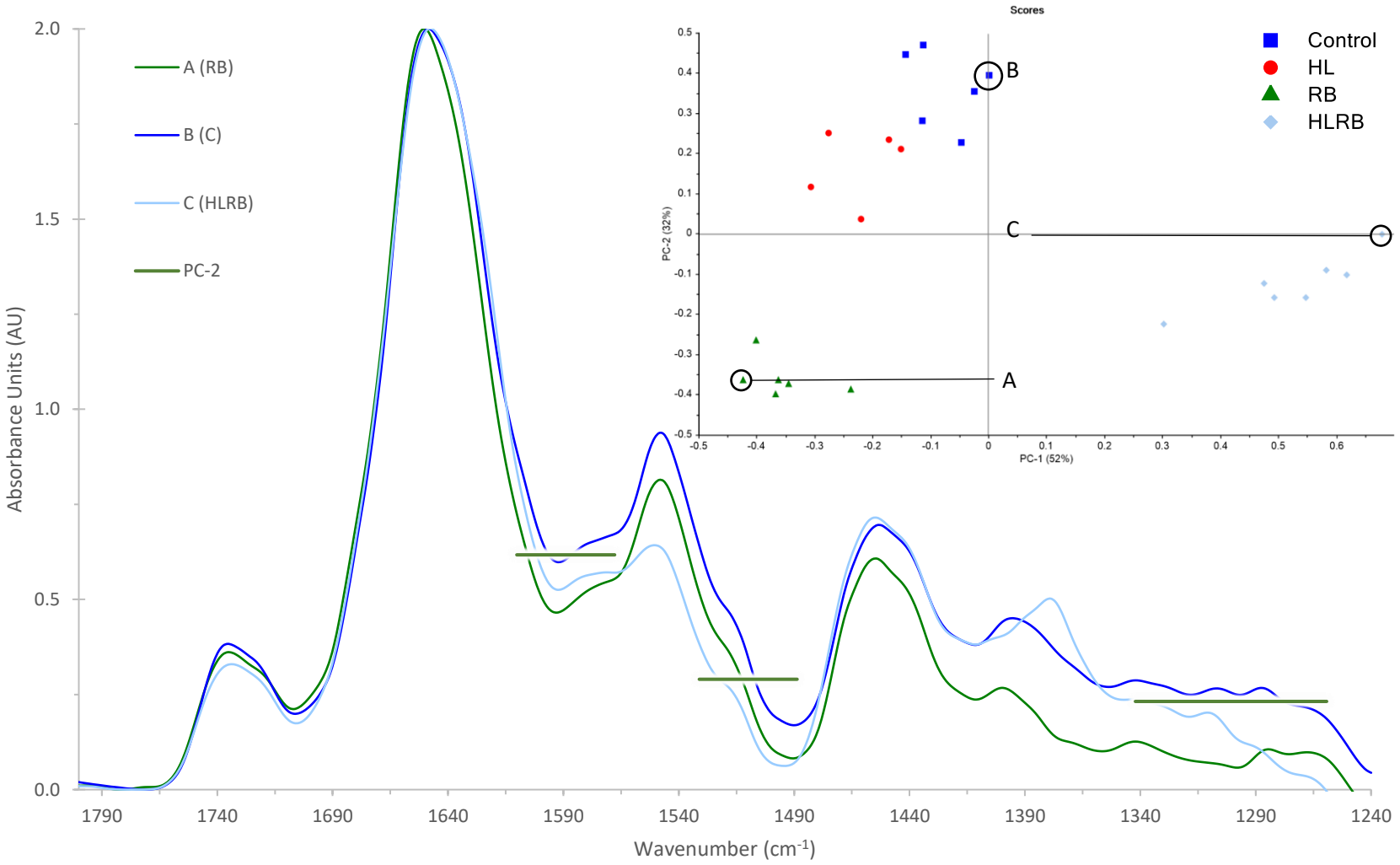


*Figure 2.8 - Spectra of three individual cells of the* Chlamydomonas reinhardtii *mutant CC-CC-4107: A) Spectra of a cell exposed to rose bengal; B) Spectra of a control cell; C) Spectra of a cell exposed to a combination of high light and rose bengal. Inset image shows the position of each spectrum in a principal component analysis and their relationship to PC-2.*

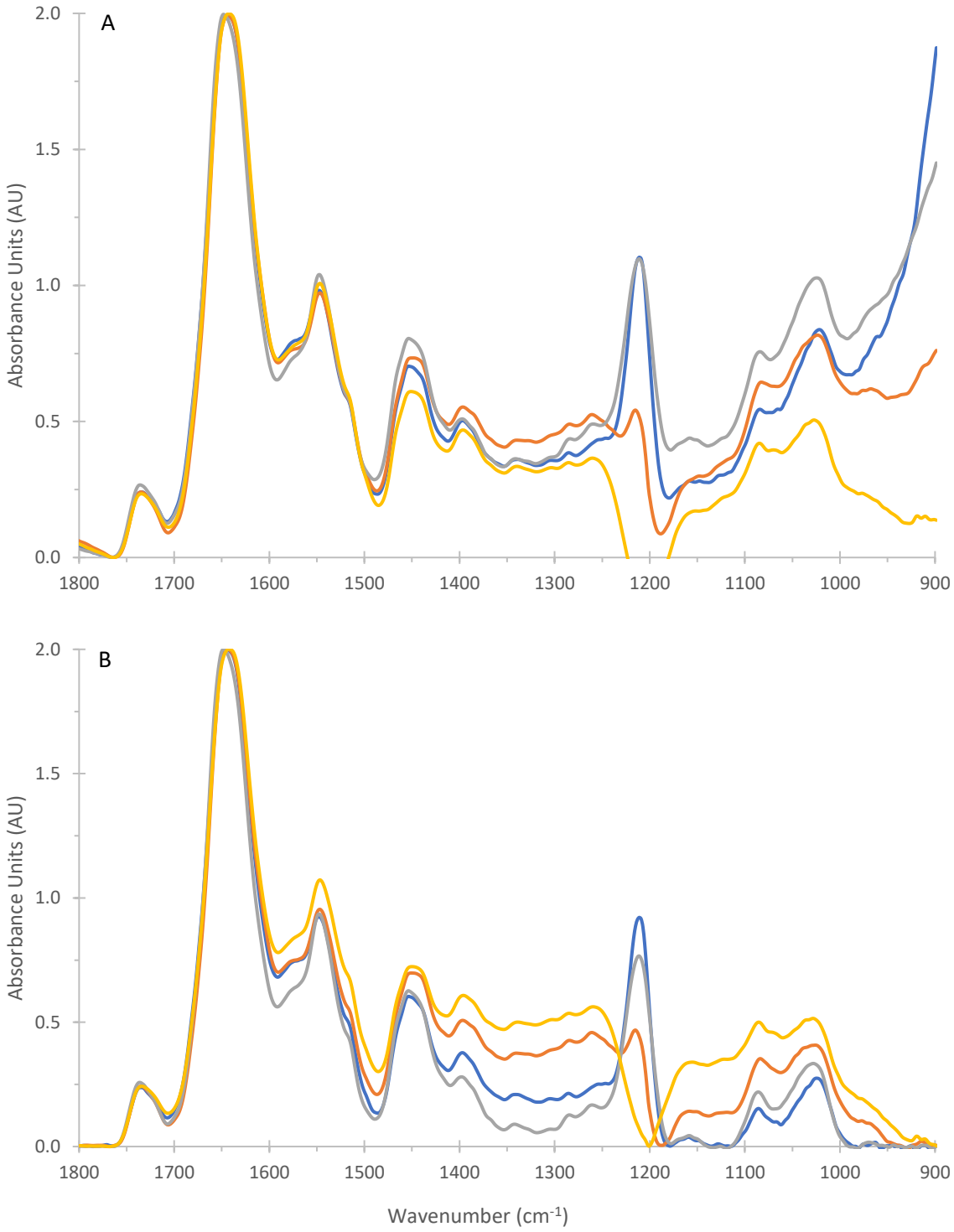


*Figure 2.9 - Demonstration of artifacts induced by baseline correction across the 1800- 900 cm$^{-1}$ region. Each spectrum is the average of 12 control cells of* Chlamydomonas reinhardtii *obtained on different days. A) No baseline corrected. B) Standard OPUS rubber band baseline correction.*

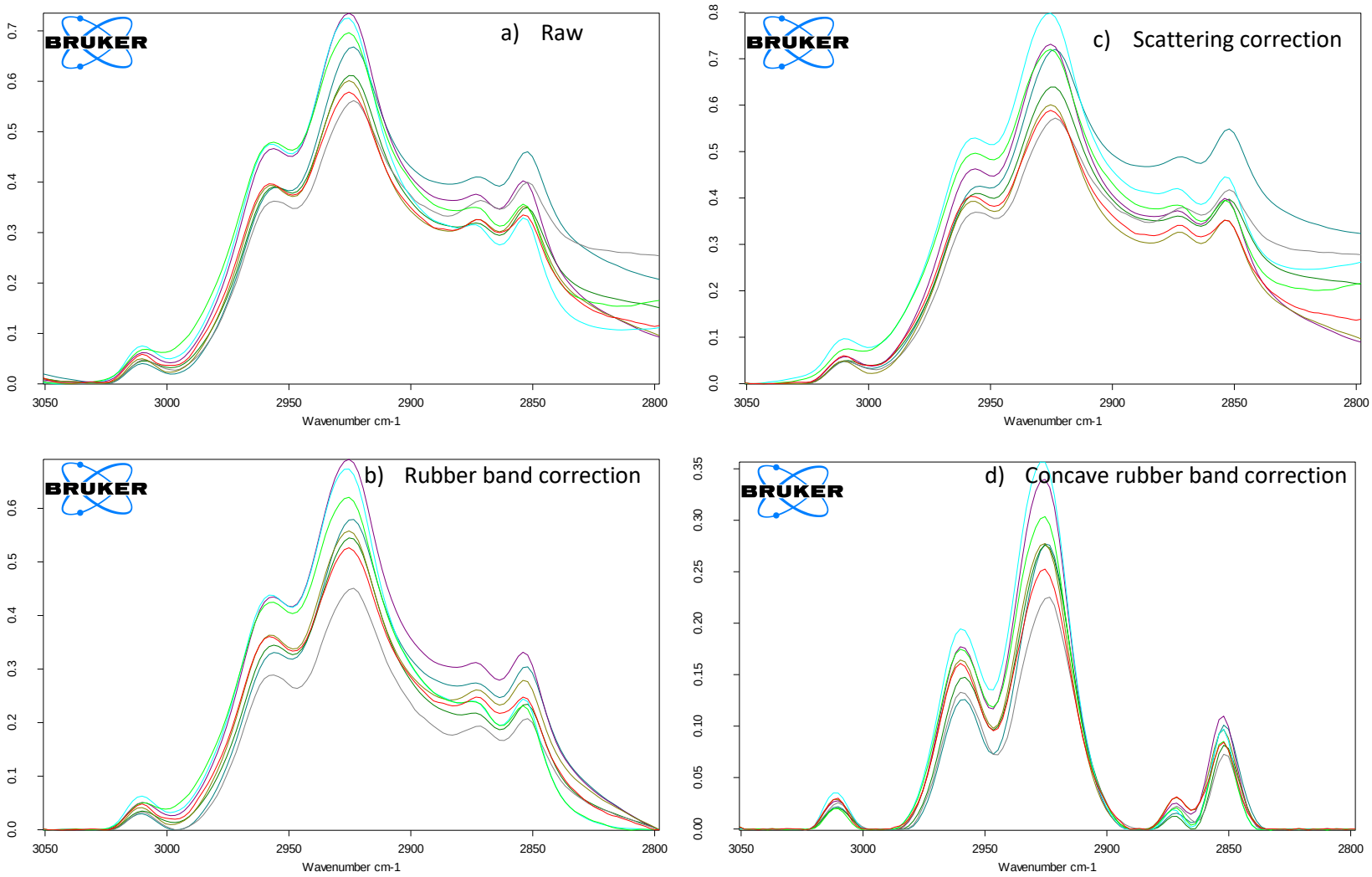


*Figure 2.10 - Artifacts induced by standard baseline correction algorithms across the 3050-2800 $cm^{-1}$ region. A) Raw data. B) OPUS rubber band correction. C) OPUS scattering correction. D) OPUS concave rubber band correction.*

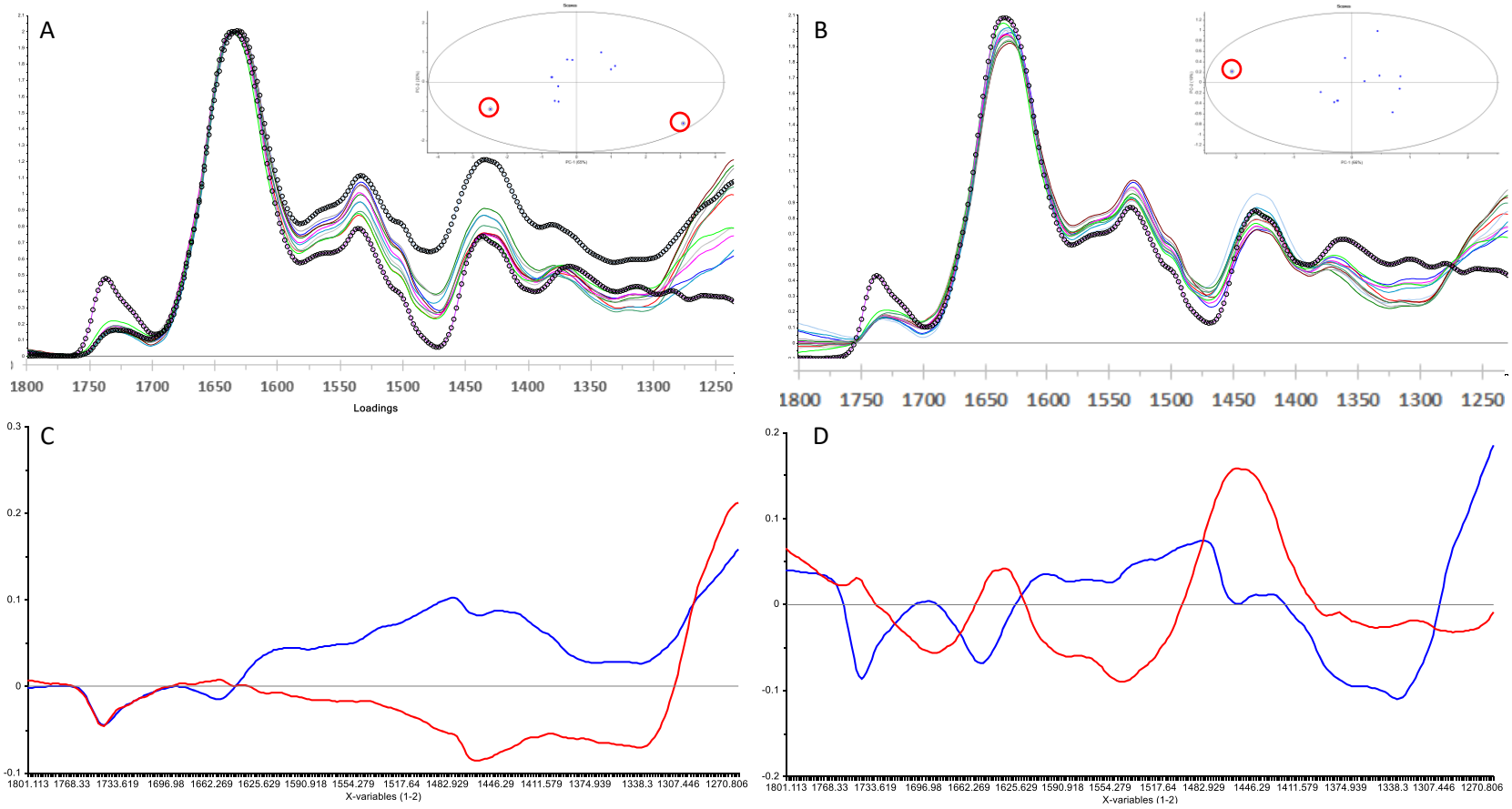


*Figure 2.11 – Principal component analysis and loadings of the spectra of individual cells of DJX-H before (A, C) and after (B, D), extended multiplicative scatter correction. Individual outlier spectra are heavy marked, with their PCA representation circled in red.*

# CHAPTER THREE

# USE OF FOURIER TRANSFORM INFRARED SPECTROMICROSCOPY IN STUDYING INTERCELLULAR, INTERCULTURAL, AND INTERSPECIES VARIATION

## 3.0 Introduction and Goals

The primary purpose of the work presented in this chapter was to understand the extent of intracultural and intercultural spectral variation when comparing individual living cells of *Chlamydomonas* spp. Before moving forward to explore the impact of high light and singlet oxygen on *Chlamydomonas* cells, it was crucial that a thorough understanding was developed not only of the spectra that could be obtained from individual cells, but also the amount of variability that should be expected. The work presented here provided foundational information that was used to optimize my experimental design and data interpretation in the future chapters. Furthermore, the FTIR spectra of three different *Chlamydomonas* species were examined. Since these three species would be used to study responses to high light exposure, I wanted to see what differences could be observed under control growth conditions, considering the limitations of the FTIR system and the inherent variability that may exist within species and even individual batch cultures.

To this end, four primary hypotheses were tested. The first two hypotheses were related to measurement and characterization of variation. Hypothesis 1: that variation between the spectra of clonal cells in the same culture will be minimal, allowing us to assume that the response of individual cells to stressors applied in future work will also be consistent. Hypothesis 2: that the variation observed between the spectra of cells taken from different batch cultures grown under similar conditions will also be small, but greater than the differences observed when comparing spectra taken using cells grown within a single batch culture. If true, spectra obtained from batch grown cells will be similar enough that they can be compared directly across days, or weeks.

Hypotheses three and four were related to the analysis of the different species themselves. Hypothesis 3: the spectra obtained from cells of species from the same genus will show similar but not identical biochemical composition. Thus, the ratios of peaks associated with macromolecules and cellular components will differ across species. To be meaningful, the overall

differences between cells of the three different species must be greater than the differences observed between spectra obtained from cells of the same species (both within individual batches and between batches grown on different days). Hypothesis 4: that the DJX-J and DJX-H species (collectively referred to as the DJX- species) are more similar to each other than to the model organism *C. reinhardtii*. I hypothesize that because DJX-J and -H have coevolved in an isolated aquatic environment in northern Saskatchewan they will be more similar to each other in their biochemical makeup than to *C. reinhardtii*, which was isolated from a soil sample taken from a farmer's field in Massachusetts. A better understanding of inter-species variation could allow this technique to be used as a "bio-prospecting" tool.

## 3.1 Results

### 3.1.1 Variation Between Algal Cells in a Culture (Intercellular/Intracultural Variation)

The study of individual living cells of green algae, rather than of culture smears or bulk measurements, allows for a more complete understanding of the biochemical, physiological, and life-stage variation that exists between individual algal cells in a single batch culture (intracultural variation). Understanding underlying variation is an essential prerequisite to understanding the change induced by stress conditions, such as high light exposure, or the difference between species. It helps provide background for what types of observable variation can be attributable to specific factors. Intracultural variation falls into three basic categories: minor variation between individual cells, spectra exhibiting one or more strongly abnormal peaks, and the presence of distinct subpopulations of cells.

Minor variation was expected to be observed in spectra obtained from individual cells because of differences in their physiology, cell age and growth stage, or metabolism (Figure 3.1, blue spectra). For example, differences in peak ratios, such as the relative intensity of the ~1740 lipid carbonyl, amine I, and amide II peaks each reflected possible differences in the lipid and protein complements of living cells. Because the cell cultures were not synchronized, they could have been at different stages of their cell cycle. Older cells may have had more storage lipids, and dividing cells may have had greater levels of proteins or even different levels of DNA. Because the cells go through a defined cycle, one would expect their spectra to fall within a range (higher lipid to lower lipid, for example). These spectral differences reflect real changes in the cellular

components of healthy, living organisms. The degree of intercellular variation present changed with species. There were also day-to-day differences in the degree of intracultural variation present in a given cell line.

Some spectra did not fall within an otherwise normal range (Figure 3.1, red spectrum). These abnormal spectra were characterized by significant differences in one or more peaks. In Figure 3.1, this could be observed in the 1740 $cm^{-1}$ peak and the lack of a peak in the 1300 - 1240 $cm^{-1}$ region. These so-called abnormal spectra can have a significant impact when spectra are averaged for later analysis. It was not clear what causes these abnormal spectra. They could be caused by abnormalities of the cell. For example, the cell could be undergoing programmed cell death or may have already died. Alternatively, the measurement conditions may have an impact. For example, while I tried to immobilize the cells in agar, small amounts of drift can alter the alignment of the cell in the IR bean, allowing focus to be shifted to just one portion of the cell. One or two of these types of abnormal spectra were typically found when measuring a collection of 10-20 cells from a culture of *Chlamydomonas* spp.

Another interesting finding was that spectra taken from a single batch culture suggested that distinct subpopulations of cells existed within it (Figure 3.2). These spectra were different than those described above as abnormal, as multiple spectra that differed in the same manner were present. Again, there was no clear reason for the existence of a group of different cells within the culture. It is possible that a mutation occurred, with a resulting accumulation of offspring. As haploid organisms, this is could not be routinely dismissed. However, other explanations such as a partial synchronization of the cells, or a group of older cells that happened to remain located close together during sampling, were more likely to explain this phenomenon. Furthermore, the fact that similar subpopulation divisions were found repeatedly in different cell lines suggests the differences were due to underlying biological factors. Unlike the abnormal spectra, the spectra from the subpopulations shown in Figure 3.2 appeared more similar across most of the peaks being studied. Thus, at a high level, the differences might be assigned to differences in physiology, metabolism, or health. It was important when performing experiments in which control cultures exhibited subpopulations of cells, to account for that factor when examining the spectra of cells exposed to various treatments. One cannot *a priori* expect both subpopulations to respond to the treatment in the same manner.

The impact of inherent variation on the averaging of spectra was demonstrated in Figure 3.3. In Figure 3.3A were a set of spectra from five cell. One cell (cell E, blue) was missing a peak at 1080 $cm^{-1}$. When averaging these spectra, the resultant averages including and excluding this cell were determined to examine the impact of that single cell's spectrum. Figure 3.3 B allowed comparison of averaged spectra when cell E was omitted. There were minimal differences apparent even in the 1080 $cm^{-1}$ region. A similar pattern emerged in another set of cells, highlighted in Figure 3.3C and D. In this case, the averages compared were those that contained or excluded three cells that differed from typical spectra. In Figure 3.3C, cell F appeared to have a baseline offset present in the fingerprint region (1500-1240 $cm^{-1}$), while cell G exhibited a stronger ~1740 $cm^{-1}$ lipid carbonyl peak, and cell I had an abnormal 1080:1040 $cm^{-1}$ ratio. The averages generated using all ten cells versus the seven standard cells were almost identical (Figure 3.3 D), even through the regions of higher variability. This reliability in the averaging procedure was important to note, particularly when dealing with limited sample sizes. These findings suggested that the retention of spectra exhibiting one or two minorly anomalous peaks would not significantly skew results. One or two outlier spectra were typically found in a measurement sample of 10-20 cells from a culture of *Chlamydomonas* spp.

While the robust nature of spectral averaging seen in Figures 3.2 and 3.3 was useful because it protects the larger dataset from perturbations caused by one outlier, the averaging procedure may obscure factors of concern, such as the presence of subpopulations of cells, as demonstrated in Figure 3.2. In Figure 3.2, averaging obscured the presence of two subpopulations of cells, and the average obtained from the spectra of all cells differed from those obtained from the two populations. Figure 3.2A shows the spectra of individual cells, colour coded into subpopulations a (blue) and b (red). Figure 3.2B shows the spectra obtained by averaging all cell (green), subpopulation a (blue), or subpopulation b (red). The differences between these averages were most apparent in the relative intensities of the amide I and amide II protein peaks, the relative intensities of the 1080 and 1040 $cm^{-1}$ peaks, and differences in the shape and intensity of the 1398 $cm^{-1}$ peak. These indicated the presence of groups of cells exhibiting differences in their biochemical makeup. In experiments where control cultures exhibit the presence of cellular subpopulations, analysis of the spectra of non-control cells must account for potential differences in cellular response to stressors. Blind averaging or bulk measures would result in spectra that are not representative of any of the cells present in the sample, as well as obscuring a potential basis

for differences in response to stressors. This would have negated the advantage of using the synchrotron-based FTIR spectromicroscopy and would in effect have provided the same type of result as using a smear of cells on an IR window.

For future work in this thesis, significant outliers were removed from data sets before analysis. The presence of subpopulations of cells within a culture was found several times. This was dealt with by removing the spectra of the smaller subpopulation from the analytical data pool. In the data sets analyzed for this thesis, the smaller subpopulation of cells was always the one that differed from the most from the 'typical' spectra observed on other days. In addition, it is to be noted that the average spectra present in this thesis were primarily generated from the spectra of six to nine individual cells. Averages were never generated from fewer than five cells or more than eleven. This number is limited by the time constraints inherent with synchrotron work. Synchrotron shifts are eight hours long and allotted in six-month blocks. Previous work (Goff et al. 2010) has shown that when cells of *C. reinhardtii* are kept in the sample holder used in this work for longer periods of time, their secondary fermentative metabolism is activated, and ethanol is evolved at a concentrations that are visible in the resultant spectra. Reducing the length of time each culture spends in the sample holder prevents the switch to fermentative metabolism, and keeps the time available for hydrogen-deuterium exchange constant. In addition, as this chapter will show, it was essential that all stress measurements be carried out on cells from the same bulk culture on the same day, which limited the number of cells that could be measured. A balance had to be struck between the number of spectra obtained for each culture on a given day, and the number of days during which each species was examined.

### 3.1.2 Variation Between Algal Cultures of the Same Species (Intercultural Variation)

In addition to spectral differences between individual clonal cells within the same culture, variation was observed in the spectra of cells from different batch cultures. This intercultural variation – variation between the same species or cell line based on culture variables – was likely due to a change in the cellular biochemical composition related to a variety of culture growth factors. These included culture age, health, density, and growth stage. While we used cultures in mid-log growth phase, some cultures grew faster or slower than others.

Intercultural variation in three species of *Chlamydomonas* is shown in Figure 3.4 (*C. reinhardtii*), Figure 3.5 (DJX-H), and Figure 3.6 (DJX-J). Internally, all three species exhibited

some degree of variation in the ratios of major peaks, as well as in the shape and position of the amide I protein peak. In the 1800-900 $cm^{-1}$ region (Figures 3.4-6 A), *C. reinhardtii* (Figure 3.5) appeared to exhibit the least intercultural variation. Most of the difference, particularly in the 1400-1240 $cm^{-1}$ and < 1185 $cm^{-1}$ regions appeared to be due to baseline offset. In this region, spectra of DJX-H cells (Figure 3.5A) exhibited the greatest degree of intercultural variation, particularly in the intensity and shape of the strong, unassigned 1260 $cm^{-1}$ peak that was not found in either of the other species. Intercultural variation in DJX-J (Figure 3.6 A) appeared to be intermediate. The scale of the intercultural variation was largely on the same level as that of the intracultural variation. These differences also related to the ease of growing the three species. DJX-H cells grew the slowest under the standard conditions we used.

Intercultural variation in the CH stretching region (3050-2800 $cm^{-1}$, Figures 3.5-7 B) appeared to be primarily due to baseline variation. This was visible in the absolute difference in intensity at 2800 $cm^{-1}$ as well as in the shape of the line that could be drawn to connect the offset normalization point at 3040-3010 $cm^{-1}$ and the 2835-2800 $cm^{-1}$ region devoid of spectral features. In addition, some differences were present in peak positions and resolution. As per Chapter 2 (section 2.3.3), this could be addressed through the use of second derivatives in the analysis of this region.

Understanding the degree of intracultural – and particularly intercultural - variation present in spectral measurements was key for experimental designs involving cross-comparisons. This was demonstrated in Figure 3.7, which showed the spectra of individual cells of DJX-H collected on two different days. On both day 1 and day 2, spectra were collected from control cells, as well as from cells of the same culture exposed to high light (HL), rose bengal (RB), or a combination of high light and rose bengal (HLRB). Each point on the loading plot represents the spectrum of an individual cell in the 1800-1240 $cm^{-1}$ region. The same projections and loadings are displayed in both Figures 3.7A and B, and in panels C and D, with only the labels changed. Figures 3.7A and B shows the complete, clean separation of spectra obtained on two separate days from two different cultures. Figures 3.7C and D show the same plots when spectra are labelled via treatment (dark blue, C; red, HL; green, RB; light blue, HLRB). (These treatments will be described in detail later in the thesis.) A diagonal line has been added for reference for day to day separation. This figure raised two primary concerns regarding experimental design and cross-comparison of

experimental results. First was the possible conflation of intercultural variation with differences induced by exposures to compounds of interest. Second was variation in the response of cultures to a stressor (in this case RB). The first concern, conflation of intercultural variation and the effects of the oxidative stressors, could be demonstrated by theoretical comparison of the spectra of control cells from day 1 (C1) with the spectra of HL cells from day 2 (HL2), and vice versa (C2 vs HL1). In PCA space, there was clean separation between C1 and HL2 spectra, as there was between C2 and HL1 spectra. This suggested that exposure to HL induced significant and observable spectral differences. Comparison of the plotting of C1 and HL1 spectra, as well as C2 and HL2 spectra, contradicted this suggestion. There was significant overlap in PCA space of C and HL spectra obtained on the same day, indicating that in these cells, HL did not have a significant effect on the spectra. The separation between C1/HL2 and C2/HL1 spectra was driven by intercultural variation – differences under control conditions – something that would have been lost with weaker experimental design.

The second concern, variation in the response of cultures to a compound or stressor of interest, again required strong experimental design to correctly parse. The spatial PCA relationship between the spectra of control cells and RB-treated cells varied on day 1 (where the spectra of cells exposed to RB and HLRB overlap) and day 2 (where the spectra of cells exposed to RB overlap with those of control cells and HL cells). Cross-comparison would simultaneously obscure these differences in response and attribute intercultural differences to induced spectral change.

To address these concerns, experimental design for this thesis required obtaining all infrared spectra to be compared from the same culture grown on the same day. Measurements of oxidative stress were designed so that C, HL, RB, and HLRB spectra were obtained from the same batch culture. This prevented conflation of intercultural differences with those induced by treatment. In addition, patterns of change in response to stressors were compared between days. For example, there was no comparison of differences in the absolute height of the ~1740 $cm^{-1}$ lipid carbonyl peak in the spectra of HLRB cells obtained on different days. Instead, observations were made of how the intensity of the ~1740 $cm^{-1}$ peak changed in the spectra of HLRB cells when compared to the spectra of C cells obtained on the same day. These same observations were made across multiple days to ensure that a specific observed response to a stressor was consistent. In the case of the response of DJX-H cells to RB exposure, as shown in Figure 3.7C, experimental data

obtained on other days exhibited significant overlap in the spectra from RB and HLRB treatments. This aligned with the response seen on day 1 and indicated that it was the lack of response seen on day 2 that was abnormal.

### 3.1.3 Differences Between Closely Related Species of *Chlamydomonas* (Interspecies Variation)

#### 3.1.3.1 Fingerprint region

Visual examination of the 1800-1240 $cm^{-1}$ region of these three species of *Chlamydomonas* spp. could identify differences in peak composition (Figure 3.8). From this, we could infer that the three algal species contained different relative amounts of compound classes such as lipids and proteins. Differences in the shapes of these peaks also allowed the observation that there were interspecies differences in the lipid cohort and protein secondary structures. These differences are expected to reflect the different evolutionary paths that the three species have taken to adapt to survive in their natural environment. For example, the ~1740 $cm^{-1}$ lipid carbonyl band differed in both shape and intensity between *C. reinhardtii* (blue) and, DJX-H and DJX-J (red, green). Both DJX-H and DJX-J exhibited a lower overall intensity of the ~1740 $cm^{-1}$ peak in comparison to the amide I peak. In addition, their second derivative components showed relatively weaker contributions from the 1740 $cm^{-1}$ component when compared to the 1720 $cm^{-1}$ component, and poorer resolution of the 1700 $cm^{-1}$ carbonyl component. These three components were assigned to esters, carboxylates, and unassigned, respectively (Movasaghi et al. 2008). These spectral differences could be interpreted in terms of the overall amounts of lipids present in the cell (lipid abundance), as well as differences in the relative amounts of various types and classes of lipids (lipid cohort).

Spectral differences were also present when comparing the amide I and amide II protein peaks between the three species. DJX-H and -J had broader, more symmetrical amide I peaks with a lower peak position (1642 $cm^{-1}$) compared to *C. reinhardtii* (1644 $cm^{-1}$). Second derivative components of the amide I peak were indicative of the secondary structure of the proteins being measured (Barth 2007; Barth and Zscherp 2002; Miller et al. 2013). Examination of the second derivative spectra of these three species reveals differences in the shape and position of the amide I peak to be due to a relative enrichment of β-sheets (1633 $cm^{-1}$) in comparison to α-helixes (1652 $cm^{-1}$) in DJX-H and DJX-J. This was most pronounced in the spectra of DJX-H cells. In addition,

DJX-H and DJX-J showed a lower relative contribution from the 1608 $cm^{-1}$ component that is associated with chlorophylls and derived compounds. These differences were not as pronounced in the spectra as differences in the ~1740 $cm^{-1}$ peak or the strong, broad, 1260 $cm^{-1}$ peak. They were, however, highly consistent, and far more pronounced in the second derivative spectra. Visual examination of second derivatives of the amide I peak allowed for easy discrimination of unlabelled DJX-H spectra from the spectra of cells of DJX-J or *C. reinhardtii*. The consistency of this difference, combined with the reliability of the second derivative, and the fact that this region of the spectra was consistently important on PCA loadings makes me confident that these differences were real and significant. Changes in the shape of the amide II peak were subtler and appeared to be related to slight increases in the width of the 1547 $cm^{-1}$ and 1515 $cm^{-1}$ components, which when compared to *C. reinhardtii* are broader in DJX-J and narrower in DJX-H.

Other differences were present in the fingerprint region below the amide II peak in spectra obtained from cells of the three species. This region is increasingly complicated, with numerous overlapping absorbance peaks. The shape of the ~1450 peak was slightly different in all three species due to the relative contributions from its three components in the second derivative (1467 $cm^{-1}$, 1456 $cm^{-1}$, and 1440-1438 $cm^{-1}$), which were associated with $\delta CH_2$ and $\delta CH_3$ of lipids and proteins (Movasaghi et al. 2008), δHOD absorption (Max and Chapados 2002), and HOD exchange off proteins associated with the amide II peak (Barth 2007). The spectra of DJX-H cells showed an overall greater intensity in the 1450 $cm^{-1}$ peak, as well a stronger relative contribution from the second derivative 1456 $cm^{-1}$ component. Differences in peak shapes and intensities were present in the 1398 $cm^{-1}$ and 1340 $cm^{-1}$ peaks, but they were relatively subtle. These peaks each had two variable second derivative components with a number of possible assignments (Table 2.1).

The most immediately observable difference in the spectra obtained from the *Chlamydomonas* spp. cells was the presence of a strong, broad peak centred around 1260 $cm^{-1}$ in the spectra of DJX-H cells. This peak started around 1310 $cm^{-1}$ and ran through the analytical cut off at 1240 $cm^{-1}$. This is a region associated both with $PO_4^-$ and the amide III protein peak (Movasaghi et al. 2008). As such, it has potential overlapping assignments with proteins, phospholipids, nuclear and chloroplastic DNA and RNA, and phosphorylated storage products or photosynthetic proteins (Irihimovitch and Yehudai-Resheff 2008; Zer and Ohad 2003). One strong

possibility is polyphosphate compounds, which in their pure form absorb primarily through this region and below (Khoshmanesh, Cook, and Wood 2012). No firm assignment can be made based on my observations and available data.

Using principal component analysis (PCA), it was possible to differentiate between these three species of *Chlamydomonas* (Figure 3.8 B). The PCA loadings reflected differences in protein secondary structure and peaks in the fingerprint region. The overall separation between the spectra of different species was dominated by PC-1 (67%) which was driven by the presence of the strong, broad peak centred around 1260 $cm^{-1}$ in the spectra of cells of DJX-H (red). This difference was so strong that it nearly obscured the other differences between species. Data analysis after exclusion of this peak (using 1800-1310 $cm^{-1}$, Figure 3.9) allowed for better separation of *C. reinhardtii* (blue) from DJX-H (red) and DJX-J (green). In this PCA (Figure 3.9 B inset), the spectra separated neatly along PC-2, which was driven by differences in the 1740 $cm^{-1}$ lipid peak (the DJX- species have more similar lipid cohorts to each other, and lower lipid abundance), as well as the relative enrichment of β-sheets in the DJX- species, and differences in the width of the 1398 $cm^{-1}$ peak.

#### 3.1.3.2 CH stretching region

Visual examination of the high wavenumber CH stretching region (3050-2800 $cm^{-1}$, Figure 3.10) revealed a variety of differences between *C. reinhardtii* and the DJX- species, visible in the original spectra and second derivative spectra. These were reflected in the distribution of their second derivative spectra in PCA space (Figure 3.10B, inset). These spectra were normalized to the amide I peak before being offset corrected at 3040-3010 $cm^{-1}$. The overall higher intensity of the $CH_2$ and $CH_3$ peaks in *C. reinhardtii* was consistent with this species' correspondingly stronger 1740 $cm^{-1}$ peak (Figure 3.9), suggesting overall greater lipid abundance with respect to proteins. The spectra of *C. reinhardtii* cells (blue) was reflective of a higher degree of lipid unsaturation, based on the greater intensity of the 3010 $cm^{-1}$ peak. Absorbance in this regions resulted from olefinic unsaturation (Hayati et al. 2005). For an overview review of peak assignments, refer to Table 1.2. This observation was inconsistent with lipid assays of these three *Chlamydomonas* spp., which showed that *C. reinhardtii* lipids show the lowest relative degree of unsaturation (unpublished data). This may be partially attributed to the fact that the DJX- species exhibited overall lower spectral intensity in the CH stretching region. It is important to recall that all spectra

were normalized to the amide I protein peak rather than the 1740 $cm^{-1}$ lipid carbonyl, so this normalization may have skewed observation of the overall degree of lipid unsaturation. In addition, when compared to *C. reinhardtii*, the spectra of the DJX- species exhibited higher CH peak positions and greater peak widths. The differences, specifically in $\nu CH_{2s}$ peak position (2851 $cm^{-1}$ in *C. reinhardtii*, 2853 $cm^{-1}$ in the DJX- species) and peak widths, indicated increased membrane disorder in the DJX- species (Derenne et al. 2013). The DJX- species also showed different absorptions around the unassigned CH second derivative component at 2995 $cm^{-1}$. This may have been due to interaction of the upshifted $\nu CH_{3s}$ peak and another unidentified contribution at 2885 $cm^{-1}$.

Principal component analysis of the CH stretching region (Figure 3.10 B) confirmed that the spectra of DJX-H (red) and DJX-J (green) cells could be differentiated from the spectra of *C. reinhardtii* cells based on intensity, width and position of the CH peaks.

## 3.2 Discussion

Beginning this portion of the thesis, my goal was twofold:

1) Understand the extent of intracultural and intercultural spectral variation of individual living cells of *Chlamydomonas* spp., and how that will influence experimental design and interpretation. (Hypotheses 1 and 2.)

2) Characterize differences in the spectra of three species of *Chlamydomonas*: *reinhardtii*, DJX-J, and DJX-J. (Hypothesis 3 and 4.)

Despite the use of haploid, clonal cultures grown under uniform environmental conditions, a significant degree of spectral variation was observed to be present at every level of analysis. Because of this inherent level of difference between cells, the use of blind averaging, bulk measurements, or culture smears had the potential to result in significantly skewed data. I have shown that averaging of spectra obtained from individual cells is reliable and an ideal tool for situations in which the degree of variability is known and oversight has occurred (Figure 3.3). In the presence of extreme outliers (Figure 3.1) or the presence of subpopulations of cells (Figure 3.2), averaging can potentially result in spectral output that differs significantly. Measurement of individual cells allowed for greater understanding of the types and degrees of variation present in a sample and informs and guides experimental design. This was particularly important when

considering how individual cells might react to a specific stressor. Significant differences in infrared spectra were directly related to differences in the biochemical makeup of the cells. It was important to be aware of these underlying differences not only because of their influence on averages but also because they may signal abnormalities within a single culture, or because altered physiology may influence cellular responses to experimental conditions.

Intercultural differences, or differences between cultures of the same species obtained on different days, did show observable spectral variation (Figures 3.4-3.6). The impact that this had on cross-comparisons depended on the extent of the differences being measured. In the case of the relatively subtle effects of oxidative stress (Figure 3.7) direct comparison of spectra between days inherently conflated innate, intercultural variation with induced variation. Without full treatment regimes that were obtained on the same day, it was impossible to decouple these observations. Based on my observations, I was able to develop clear protocols for my future work in comparing the impact of a variety of oxidative stressors. This required obtaining spectra from control and treated cells isolated from the same batch culture, on the same day. Analysis involved observations of patterns of change induced by stressors when compared to control cells. Repeatable observation of these patterns of change were required before they were definitively associated with a response to a stressor.

Examination of the spectra of the individual control cells from Day 1 and Day 2 represented in Figure 3.7 showed differences in lipid cohort, relative abundance, and protein secondary structure The biochemical makeup of unicellular green algae such as *C. reinhardtii* can change rapidly in response to factors such as nutrient limitation, stage of the cell cycle, or growth phase (Bölling and Fiehn 2005; Cross and Umen 2015; Holman et al. 2000, 2003), and FTIR has been used to observe and identify these metabolomic differences (Chen et al. 2012; Dean et al. 2010; Holman et al. 2000). Complicating my observations was the fact that the biochemical makeup of cells is responsive to many environmental and developmental changes. FTIR measures the absorbance of infrared radiation by functional groups, thus it informs regarding classes of chemicals within the cell but cannot directly identify specific compounds. Its main advantage is the ability to observe individual, living cells. In addition, it appeared that spectral regions that are responsive to intercultural variation were the same ones impacted by exposure to stressors. Specifically, it appeared that the lipid and protein cohorts were both highly variable between

cultures and highly responsive to oxidative stress. Cellular carbohydrates, as indicators of photosynthetic activity, were also highly variable in response to a number of cellular factors, but their primary absorptions occur in the region below 1200 $cm^{-1}$ and as such were not used in this infrared analysis.

In the case of comparison between *Chlamydomonas* spp. (Figures 3.4-3.6; 3.8-3.10), the differences observed between species were stronger than those seen between cultures of the same species. Principal component analysis of the spectra of these three species confirmed many of the visual observations. It allowed the separation of the spectra of all three species in the 1800-1240 $cm^{-1}$ region, and separation of the DJX- species from *C. reinhardtii* in the CH stretching region. Spectra of the DJX- species indicated that they had very similar relative amounts of lipids (relative intensity of the 1740 $cm^{-1}$ peak, relative intensity of the $CH_2$ peaks), lipid cohorts (shape of the 1740 $cm^{-1}$ peak, shape and position of CH peaks, relative degree of unsaturation), and membrane disorder (shape and position of the $\nu CH_2$ peaks). The overall secondary structure of their proteins were also similar. In comparison to *C. reinhardtii*, they exhibited a relative enrichment of β-sheet structures, a difference even more pronounced in the spectra of DJX-H cells. In comparison, *C. reinhardtii* spectra indicated relatively higher lipid abundance, with greater unsaturation, and less membrane disorder. Increased levels of lipid unsaturation are generally associated with increased membrane disorder and altered fluidity. This discrepancy with regards to unsaturation and membrane disorder may be related to the relatively higher lipid abundance in *C. reinhardtii*. That is that *C. reinhardtii* cells may have an absolutely higher number of unsaturated bonds present due to higher lipid abundances, but their percent degree of unsaturation is still lower than that of DJX-H and DJX-J cells. Differences in the position and width of the $CH_2$ and $CH_3$ peaks are related to membrane disorder on the basis of CH chain diversity and packing peaks (Derenne et al. 2013; Kiwi and Nadtochenko 2004; Lewis and McElhaney 2006, 2013). Compared to the DJX- species, the amide I peak in spectra from *C. reinhardtii* was narrower with a higher peak position, due to the relative enrichment of α-helixes. Despite these similarities, initial PCA of the 1800-1240 $cm^{-1}$ region grouped *C. reinhardtii* and DJX-J together, separately from DJX-H. This was based on the characteristic broad, strong peak centred around 1260 $cm^{-1}$ that is found only in spectra from DJX-H cells. This peak is unassigned. It, and the greater enrichment of β-sheets allow one to definitively differentiate the spectra of DJX-H cells from those of DJX-J. The removal of this 1260 $cm^{-1}$ peak from consideration by PCA analysis allowed clean separation of spectra of cells

from the DJX- species when compared to those of *C. reinhardtii* (Figure 3.9). In the absence of the 1260 $cm^{-1}$ peak, PC-2 allowed separation of the environmental sister species from the spectra of *C. reinhardtii* on the basis of relative lipid abundances (lower in DJX- species; DJX-H, red; DJX-J, blue) and the relative contribution of the β-sheet component to the amide I peak (higher in the spectra of DJX- species).

## 3.3 Summary and Conclusions

Fourier transform of infrared spectromicroscopy of individual living cells is a powerful tool when used carefully. The capacity of FTIR to differentiate between cell types, species of cells, or cells exposed to varying environmental conditions, based on their biochemical makeup, is useful only if proper experimental design is grounded in the understanding of the inherent differences present in your measurement populations. Variation between cells and between cultures was greater than hypothesized. The use of single-cell spectral analysis allowed me to fully capture the various types of variation present. This allowed for the development of improved measurement protocols and the identification of experimental design limitations. Specifically, the preclusion of the comparison of control and exposure spectra obtained on different days for systems in which relatively subtle effects are observed or anticipated.

The spectra obtained from the DJX-H and -J cells were more similar to each other than to *C. reinhardtii*, the model lab species. This fits with my expectations that two species that co-evolved under the same environmental conditions, would have developed similar biochemical makeups to thrive in that niche. More specifically, these environmental species – when compared to *C. reinhardtii* – showed differences in membrane disorder and protein structure. These are changes that may reflect different physiological adjustments to their environment, highlighting the capacity to use FTIR spectromicroscopy to examine how cells respond to environmental changes. However, despite their coevolution, DJX-H and -J cells are not identical. The spectra obtained from these two species exhibit reliable spectral differences, such as the strong, broad 1260 $cm^{-1}$ peak that is only measured in DJX-H cells.

Overall, this study showed benefits and challenges to the study of individual living cells. My results highlighted the importance of understanding inherent and induced variation when developing an experimental design. The degree of inherent variation found with and between cultures, when compared to the intensity of changes induced by experimental conditions, is an

essential factor for designing experiments. Study of individual living cells of three species was able to differentiate between them and suggested possible environmental or physiological reasons for some of the observed changes.

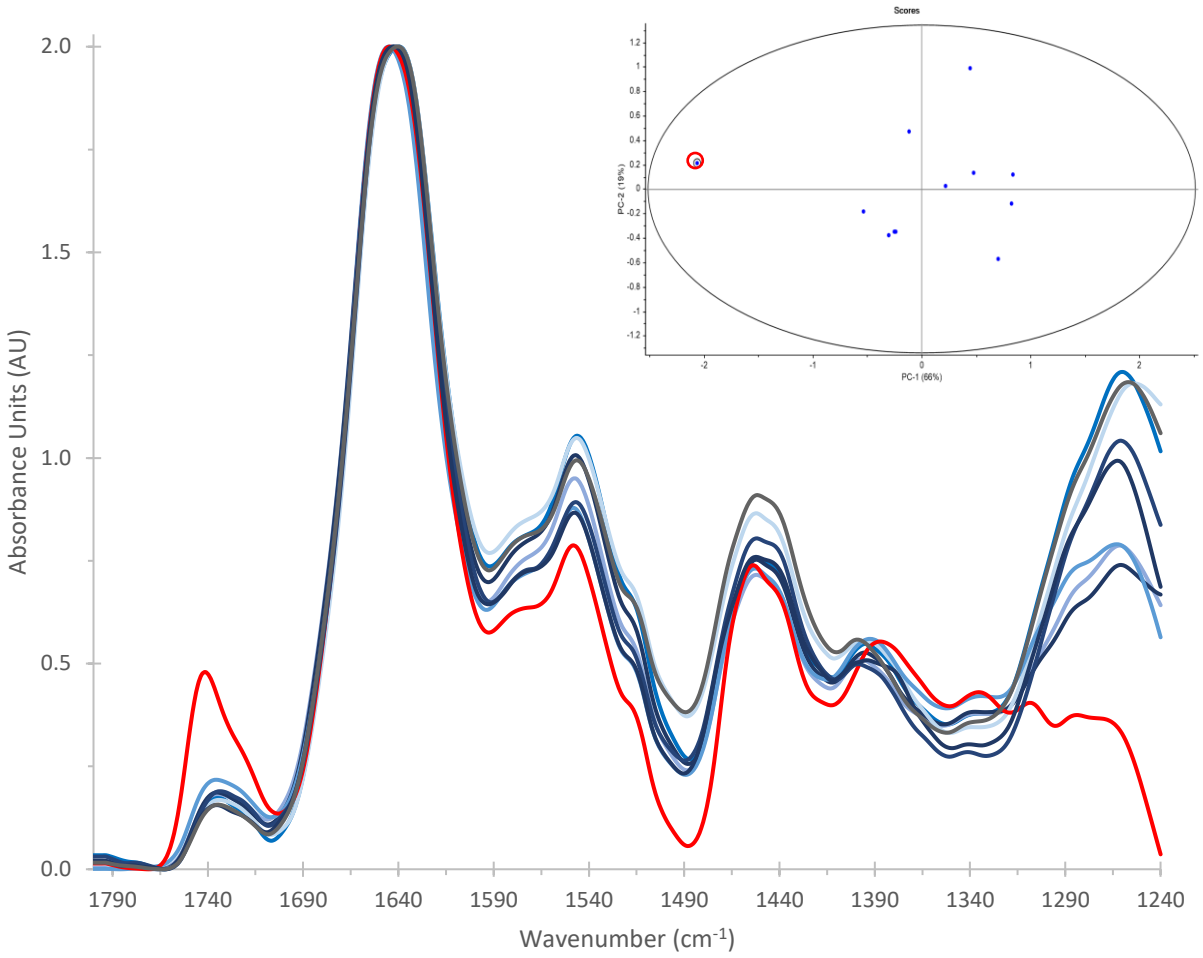


*Figure 3.1 - Spectra of individual living cells of* Chlamydomonas *DJX-H obtained from a single culture. Spectra in blue exhibit inherent intercultural variation in line with the minor, continuous variation expected from cells exhibiting slight differences in physiology, metabolism, and biochemical composition. The red spectrum is an outlier identified by strong, discrete differences. These are most obvious in the ~1740 $cm^{-1}$ lipid carbonyl, 1398 $cm^{-1}$, 1308 $cm^{-1}$, and 1260 $cm^{-1}$ peaks. Inset: PCA confirming outlier status.*

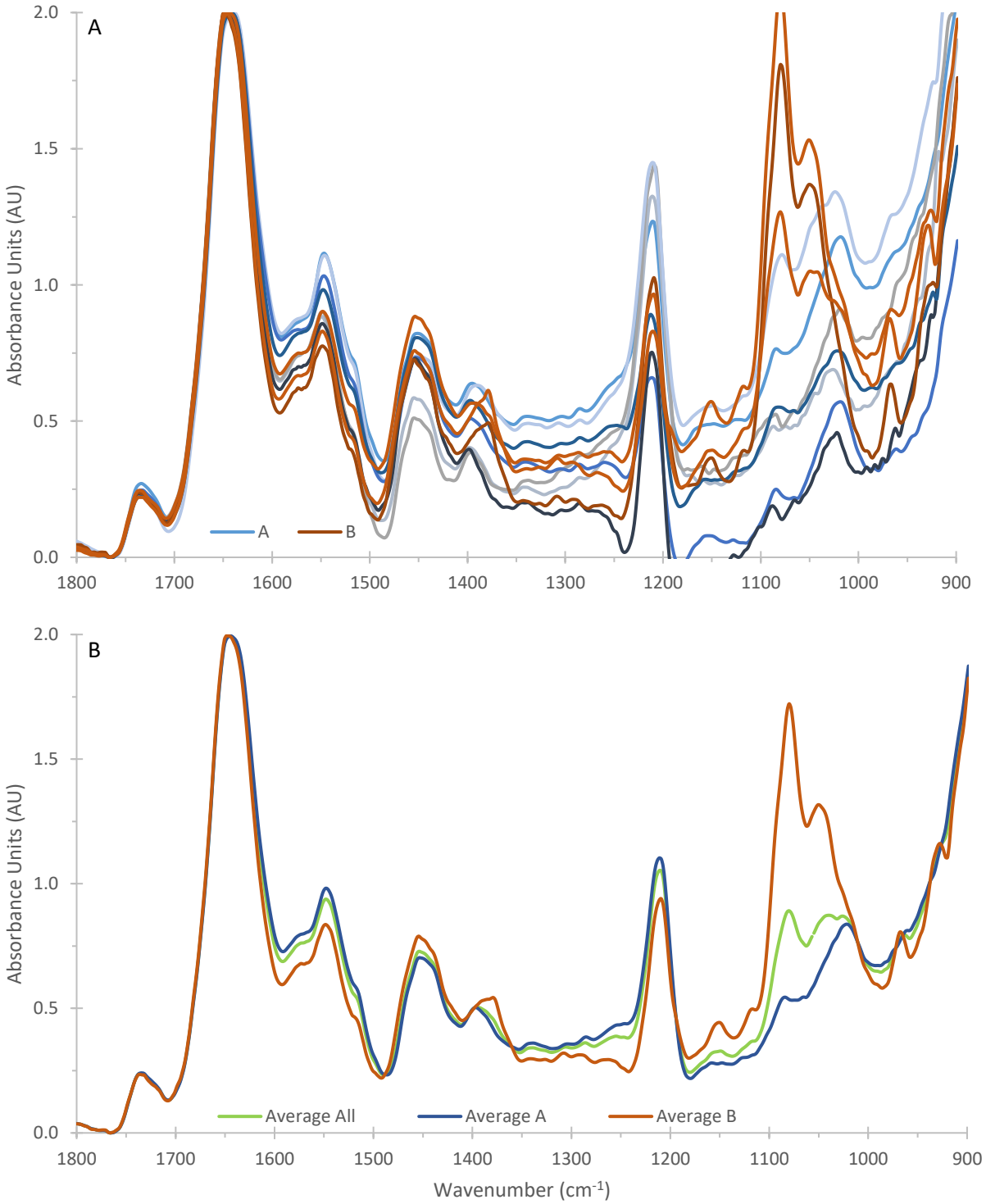


*Figure 3.2 – A) Identification of two subpopulations of cells within a culture of* Chlamydomonas *DJX-J. Subpopulation 'b' is differentiated by the strength and position of 1398 $cm^{-1}$, as well as the strength of 1308 $cm^{-1}$, 1080 $cm^{-1}$, 1040 $cm^{-1}$, and 1020 $cm^{-1}$. B) Influence of the presence of two subpopulations of cells on the average procedure.*

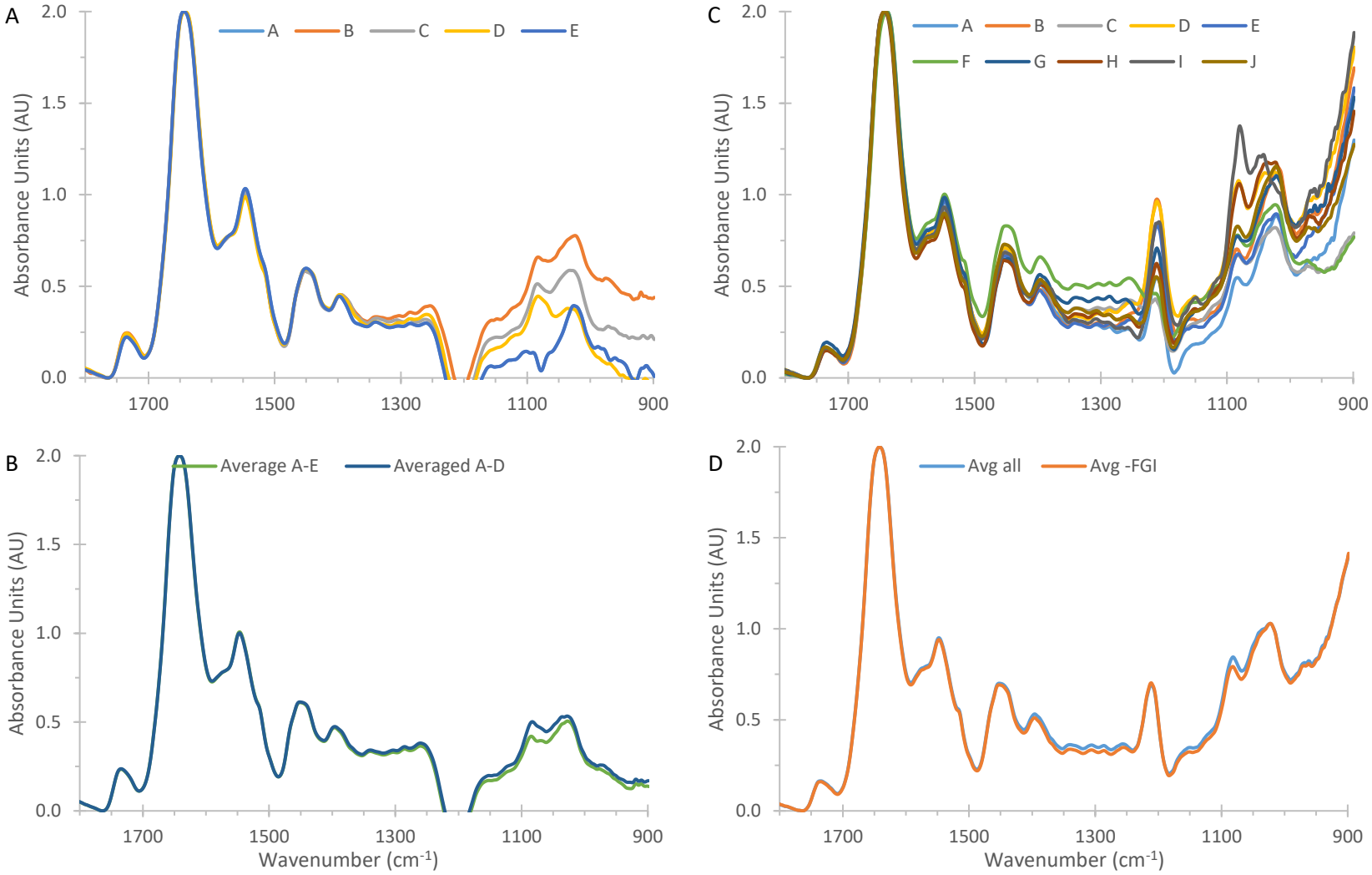


*Figure 3.3 - Influence of one abnormal spectra on an average generated from four cells (left, A, B). Influence of three out of ten spectra having one abnormal peak on the average generated (right, C, D).*

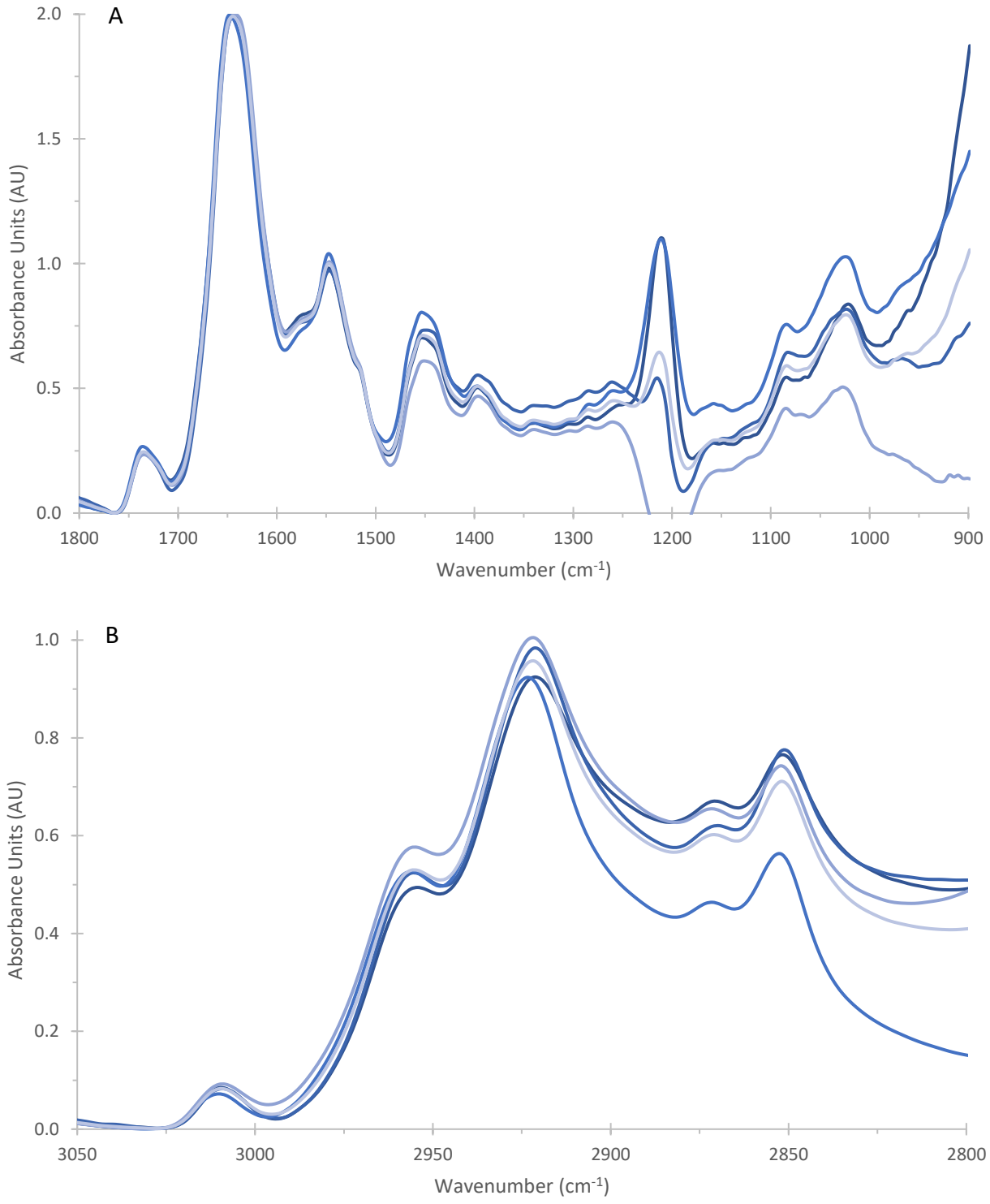


*Figure 3.4 - Day to day variation in cultures of* Chlamydomonas reinhardtii. *Each trace represents the average spectra of a separate culture. A) Fingerprint region, 1800-950 $cm^{-1}$. B) CH stretching region, 3050-2800 $cm^{-1}$.*

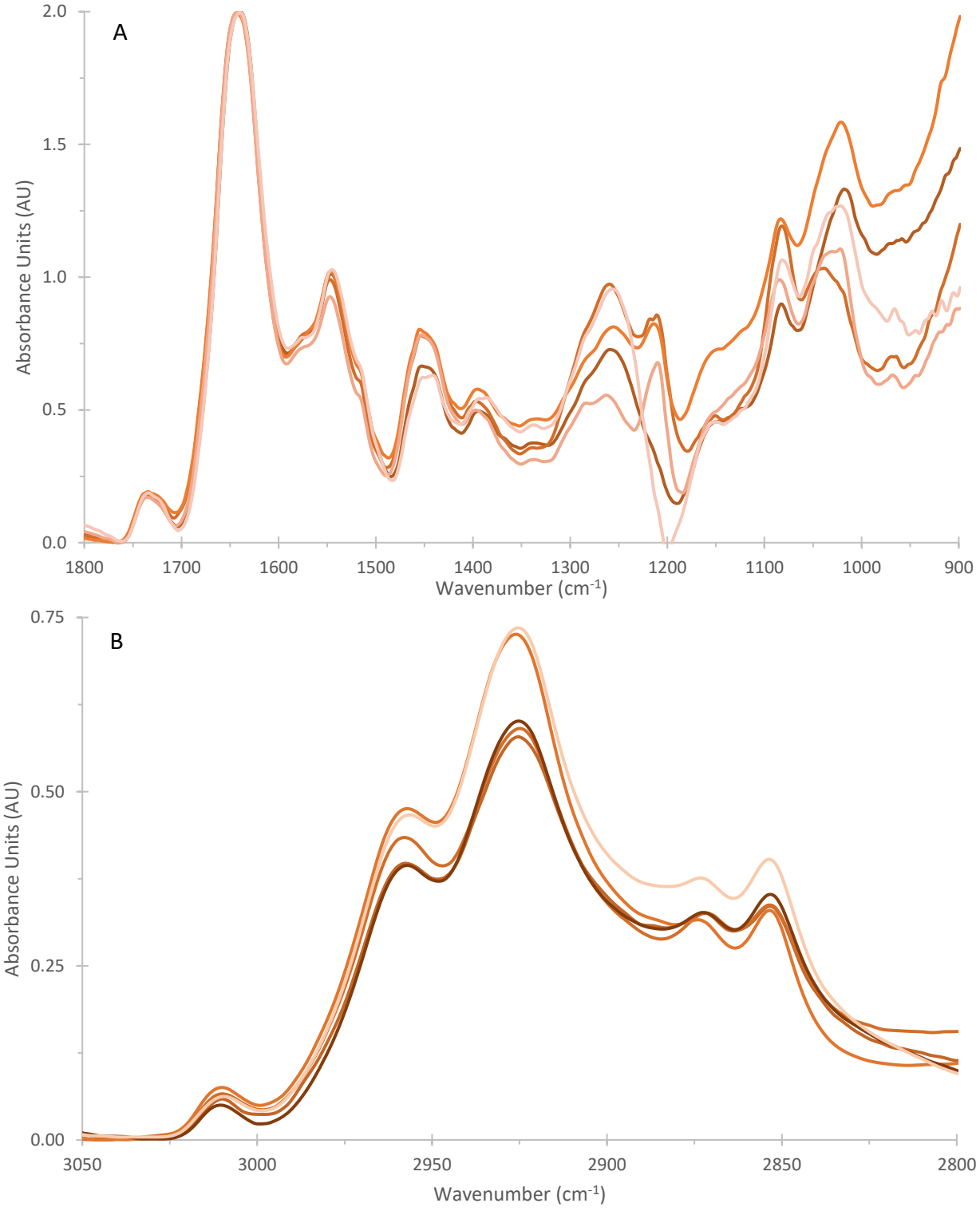


*Figure 3.5 - Day to day variation in cultures of* Chlamydomonas *DJX-H. Each trace represents the average spectra of a separate culture. A) 1800-950 cm$^{-1}$. B) CH stretching region, 3050-2800 cm$^{-1}$.*

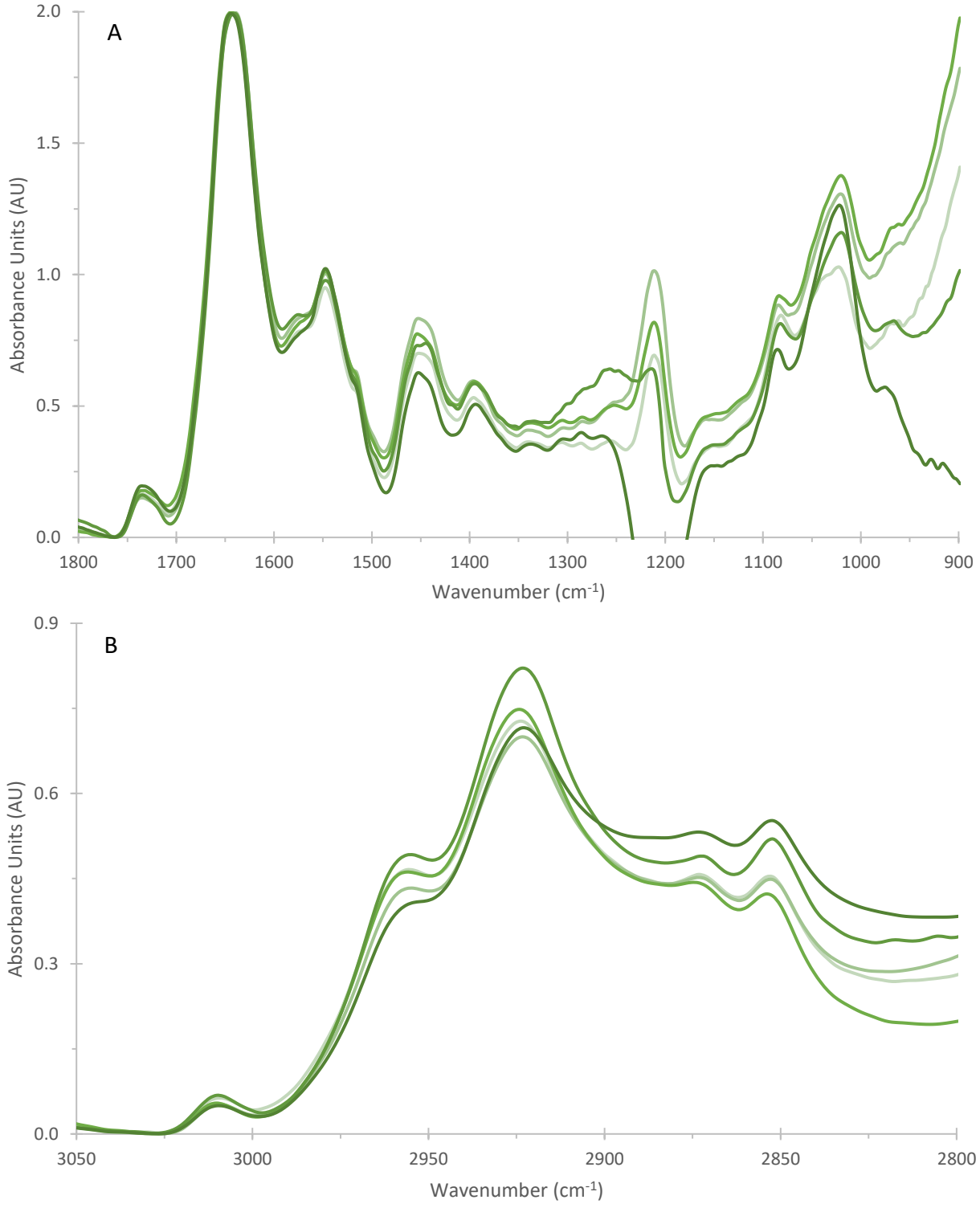


*Figure 3.6 - Day to day variation in cultures of* Chlamydomonas *DJX-J. Each trace represents the average spectra of a separate culture. A) 1800-950 cm$^{-1}$. B) CH stretching region, 3050-2800 cm$^{-1}$.*

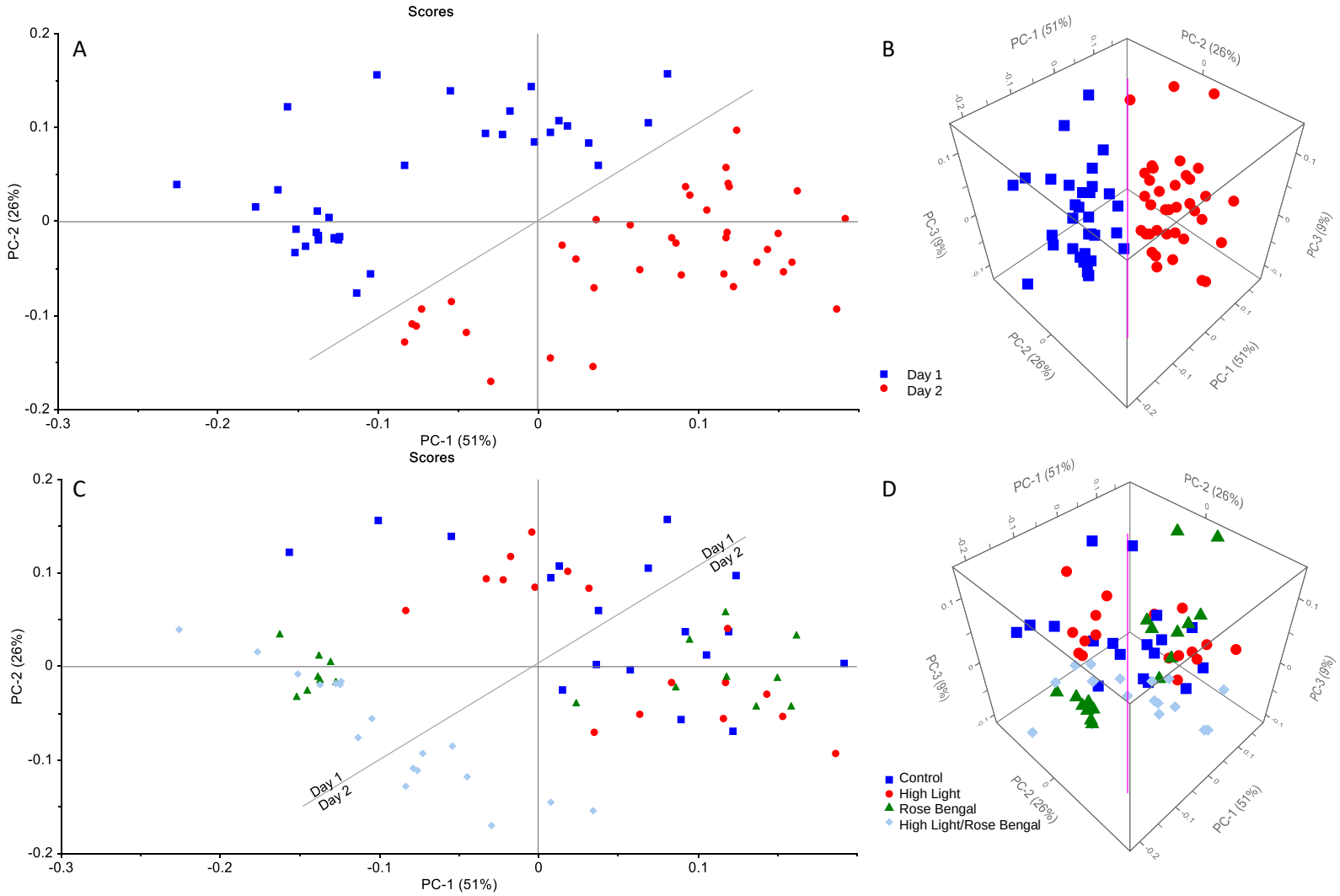


*Figure 3.7 - Demonstration of spectral separation in PCA space by day/culture rather than treatment regime for* Chlamydomonas *DJX-H. AB: Blue is day one, red is day two. CD: Colour scheme is adjusted. Blue: control; red: high light exposure; green: rose bengal exposure; light blue: combination of high light and rose bengal exposure. Diagonal line added for reference.*

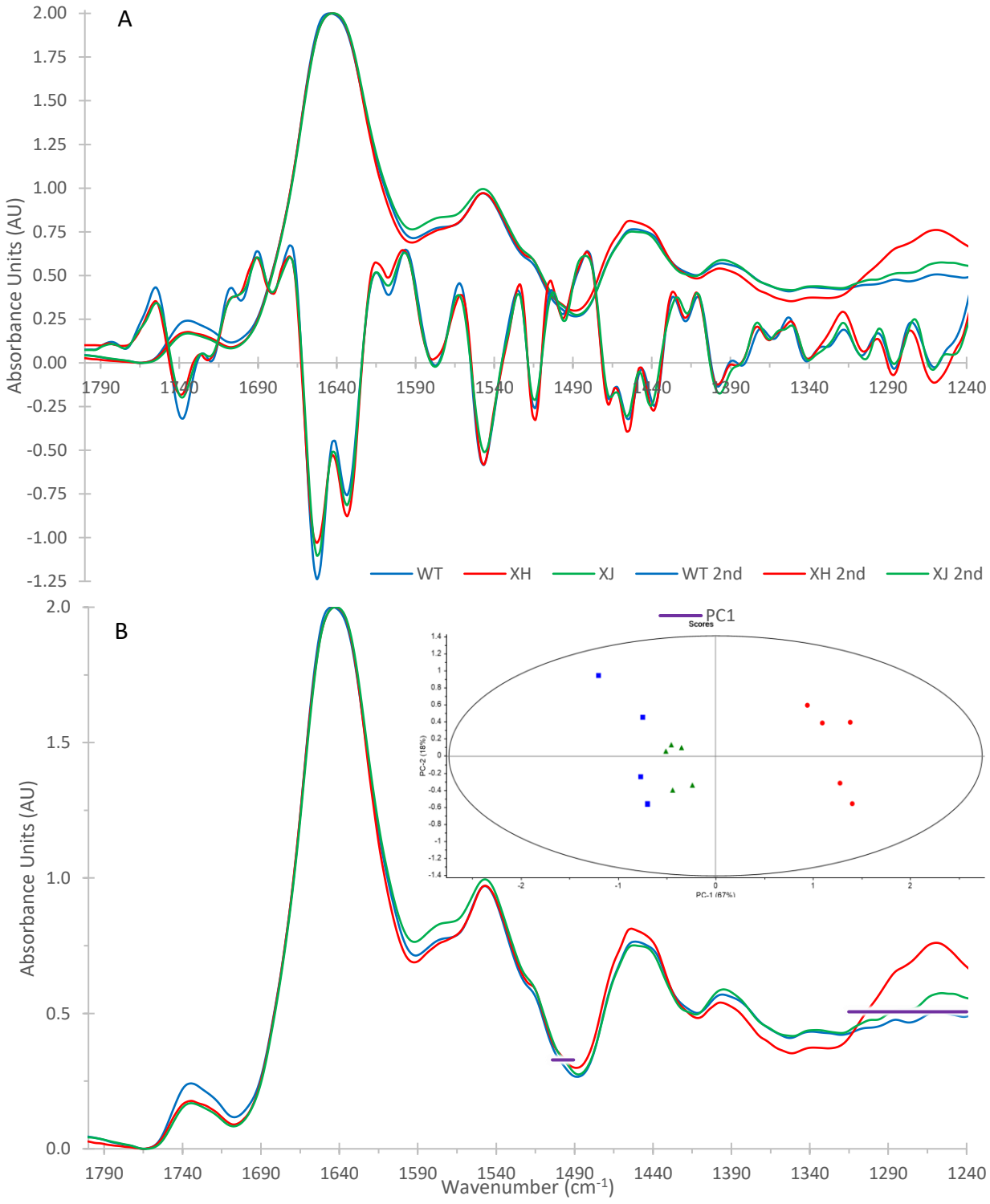


*Figure 3.8 - FTIR measurements of the 1800-1240 cm$^{-1}$ region in* Chlamydomonas reinhardtii *(blue),* Chlamydomonas *DJX-H (red) and* Chlamydomonas *DJX-J (green). Spectra are the averages of the individual spectra used in principal component analysis, and have been normalized to the amide I peak. A) Average spectra and scaled 2$^{nd}$ derivatives; B) Average spectra overlain with the loadings generating inset image (PC1-3: 67%, 18%, 5%).*

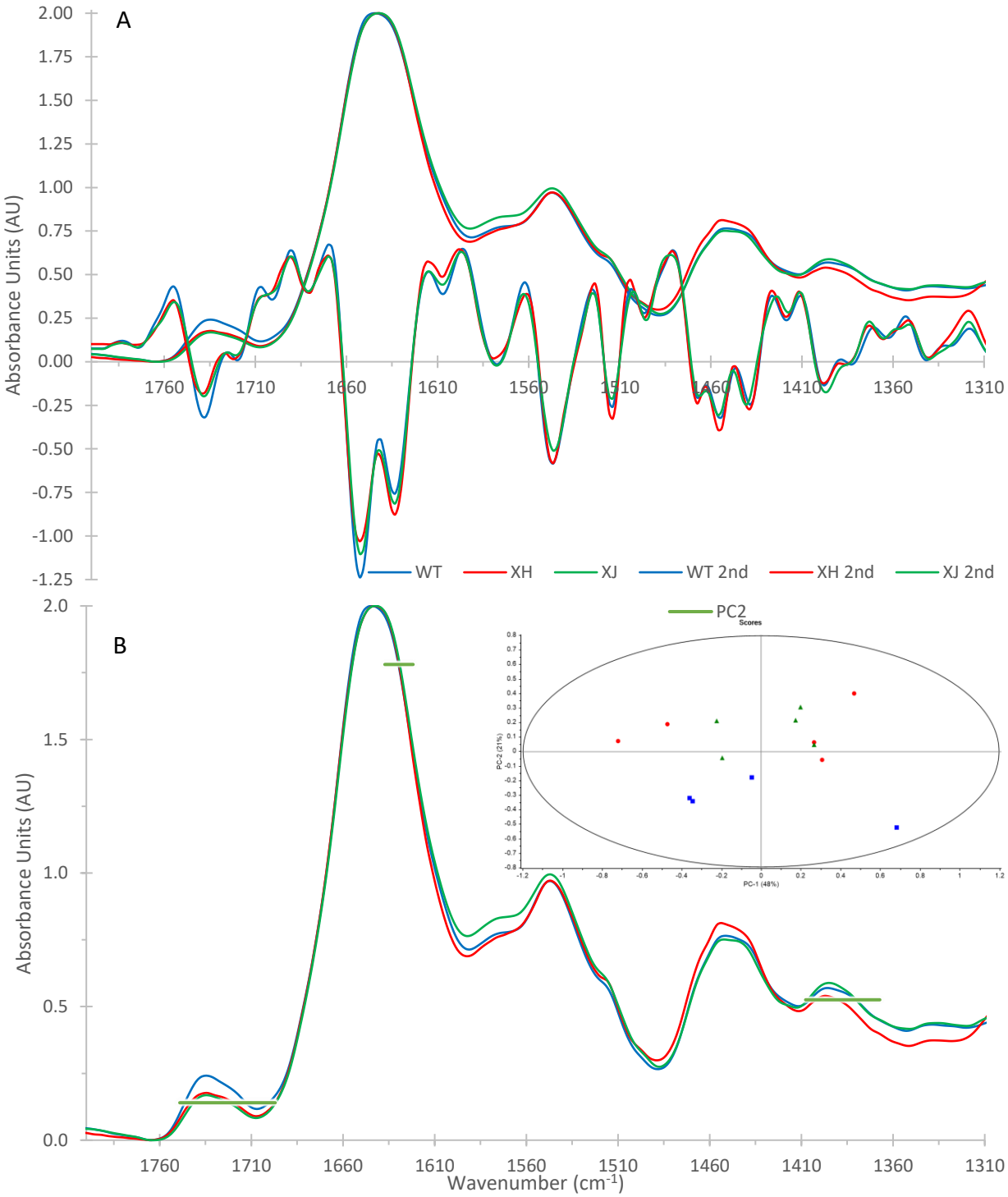


*Figure 3.9 - FTIR measurements of the 1800-1310 cm$^{-1}$ region in* Chlamydomonas reinhardtii *(blue),* Chlamydomonas *DJX-H (red) and* Chlamydomonas *DJX-J (green). Spectra are the averages of the individual spectra used in principal component analysis and have been normalized to the amide I peak. A) Average spectra and scaled 2$^{nd}$ derivatives; B) Average spectra overlain with the loadings generating inset image (PC1-2: 48%, 21%).*

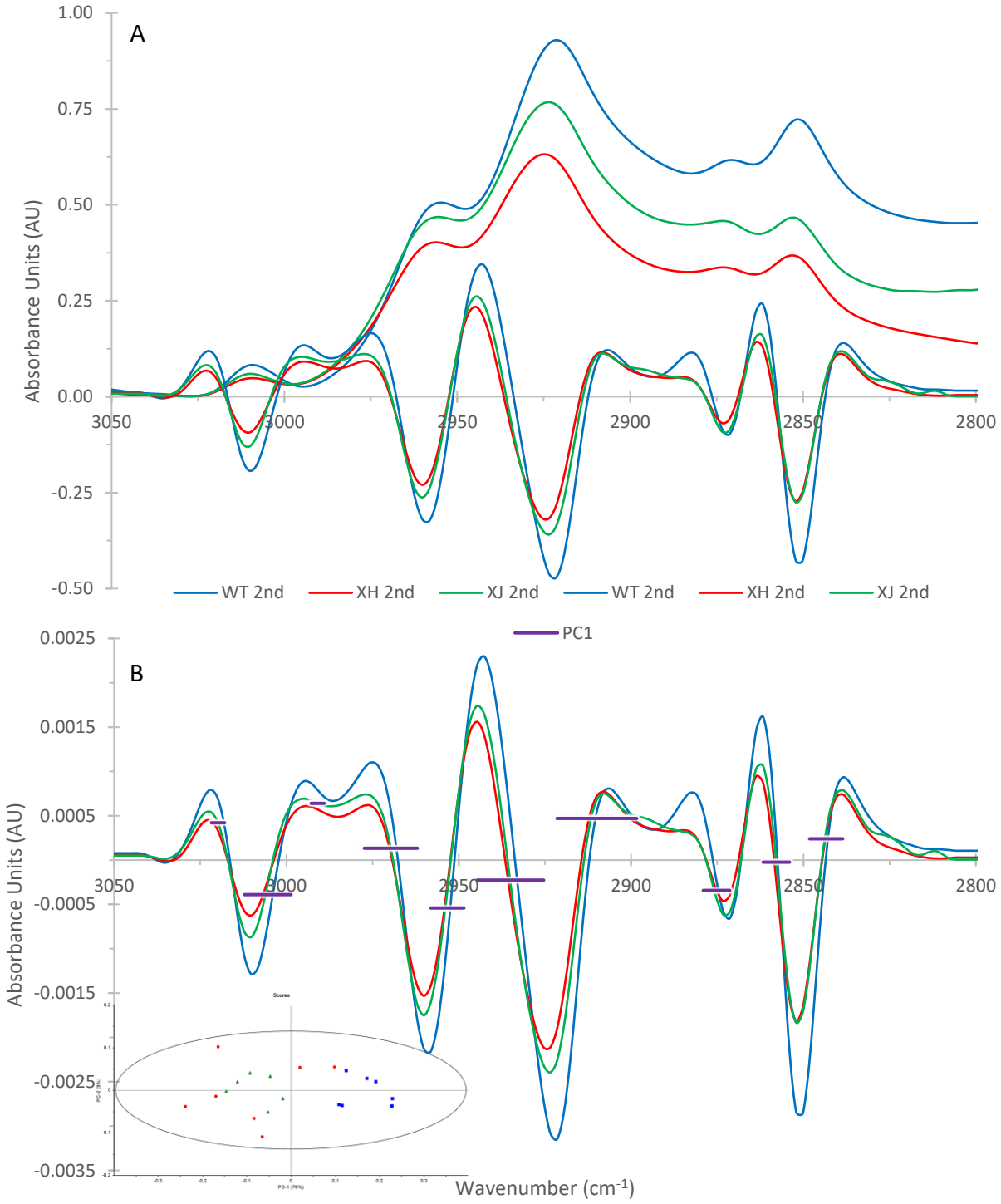


*Figure 3.10 - FTIR measurements of the 3050-2800 cm$^{-1}$ region in* Chlamydomonas reinhardtii *(blue),* Chlamydomonas *DJX-H (red) and* Chlamydomonas *DJX-J (green). Spectra are the averages of the individual spectra used in principal component analysis and have been normalized to the amide I peak, then offset corrected 3050 – 3000 cm$^{-1}$. A) Average spectra and scaled 2$^{nd}$ derivatives; B) Average of 2$^{nd}$ derivative spectra overlain with the loadings generating inset image. (PC1-3: 57%, 18%, 7%).*

# CHAPTER FOUR

# EFFECT OF OXIDATIVE STRESSORS ON THREE SPECIES OF *CHLAMYDOMONAS*

## 4.0 Introduction and Goals

As mentioned in the introduction, singlet oxygen is the major reactive oxygen species (ROS) responsible for photooxidative damage in plants (Triantaphylides et al. 2008). It is generated in the chloroplast under high light conditions, along with a variety of other ROS. Rose bengal is a photosensitizer that produces singlet oxygen when it is exposed to white light. Singlet oxygen, regardless of exogenous or endogenous origin, is highly reactive and not subject to enzymatic scavenging (Edreva 2005). Cellular adaptations to mediate its effects include physical quenching via carotenoid or tocopherol interaction and chemical quenching via oxidative reactions (Edreva 2005; Triantaphylides and Havaux 2009), Singlet oxygen-mediated damage occurs primarily in lipids, proteins, and DNA. The most common target of $^1O_2$ reactions are compounds that contain unsaturated (C=C) bonds. Lipids found in the thylakoid membranes in algae such as *C. reinhardtii* are highly unsaturated, and thus provide many targets for oxidative damage. The energetic expense of lipid oxidation is less for the cell than that of protein oxidation (Edreva 2005; Girotti and Kriska 2004; Moller et al. 2007; Rokitskaya et al. 2014) (for further details, see Chapter 1, section 1.1.3, Biological Consequences of Singlet Oxygen). As such it can be hypothesized that in living cells experiencing oxidative stress, indications of damage to lipids may precede those of damage to proteins and coincide with indicators of controlled changes to protein structure.

There is much work still to be done to better understand the physiology and metabolism of the *Chlamydomonas* DJX-H and -J species. However, all three are unicellular, green algae of similar size, and belong to the same genus. As shown in Chapter 3, there are intriguing differences in the IR spectra obtained from cells of these species, including in regions of the spectra related to lipids and proteins. It is unknown how these differences will influence the cellular response to high light or rose bengal-induced stress. The experiments performed in this chapter will help explain whether the DJX- species are damaged to a greater level, and perhaps via a different set of biochemical components.

The work presented in this chapter serves two primary purposes: to establish the utility of Fourier-transform infrared spectromicroscopy (FTIR) in studying the response of individual living cells to physiological stressors, and to elucidate the response of whole-cell response of living cells to stress caused by singlet oxygen, high light, or the combination of both. To this end, the three species of *Chlamydomonas* examined in Chapter 3, were exposed to one of three stress conditions. High light (HL) induces acclimation responses and cellular damage due to the production of reactive oxygen species. One of the primary types of ROS produced by photosynthetic cells upon exposure to high light is singlet oxygen. To examine the impact of singlet oxygen exposure, in the absence of high light, cells were exposed to the singlet oxygen generating dye rose bengal (RB). To ensure that a cellular response could be observed cells were treated with the combination of high light and rose bengal (HLRB). In this situation, not only should the cells experience stress from internally produced singlet oxygen, but also be exposed to high levels of RB-produced singlet oxygen. When exposed to higher intensities of light, rose bengal produces greater amounts of singlet oxygen. This combined HLRB treatment is intended to severely damage the cells.

Several distinct hypotheses were developed describe the expected cellular responses. Firstly, and most importantly, that it would be possible to observe biochemical responses to HL and singlet oxygen exposure in individual cells. Based on the current models of oxidative stress associated with HL or RB exposure, and familiarity with IR spectra of these cells, we predict that peaks associated with lipids and proteins will show the strongest and most relevant responses to oxidative stress. Furthermore, we predict that cellular changes observed in response to exposure to high light stress (primarily from endogenously produced singlet oxygen) will be very similar to that of exogenous singlet oxygen (produced from the photosensitizer rose bengal). It is predicted that the species-specific response to HL and RB will differ between *C. reinhardtii*, DJX-H, and DJX-J because the DJX- species have evolved under a different set of environmental conditions. From Chapter 3, we also know that even under control conditions, there are sufficient biochemical differences between the three species to differentiate them based on their FTIR spectra. Finally, we anticipate that exposure to a combination of endogenous and exogenous oxidative stressors will result in a greater degree of cellular response. Indeed, this treatment can be considered our "sledgehammer". It is not designed to be environmentally relevant, it is designed to severely damage the cells. We intended for this treatment to exceed the capacity of cellular mechanisms that neutralize oxidative damage and result in gross cellular damage or even cell death.

# 4.1 Results

## 4.1.1 *Chlamydomonas reinhardtii*

### 4.1.1.1 Fingerprint Region (1800-1240 $cm^{-1}$)

Significant differences were observed in the infrared spectra of *C. reinhardtii* cells exposed to HL (red), RB (green), or HLRB (light blue), when compared to untreated, control cells, and it was possible to differentiate between them using their spectra and principal component analysis (PCA, Figure 4.1). These exposures resulted in differences in the infrared spectra that indicate changes to the cellular biochemical makeup that were associated with physiological responses to the treatments or due simply to photo-induced reactions. All three exposures resulted in a relative increase in the strength of the ~1740 $cm^{-1}$ lipid carbonyl peak, when normalized to the amide I peak (Figure 4.1). Changes in the relative contributions of the second derivative components at 1740 $cm^{-1}$ and 1718 $cm^{-1}$ were most pronounced in the spectra of cells exposed to HLRB (Figure 4.1, light blue), which showed a relative enrichment of the 1718 $cm^{-1}$ component as well as an upshift to 1724 $cm^{-1}$. There was a decrease in the unassigned 1700 $cm^{-1}$ carbonyl component in all exposures. These differences in the lipid-associated carbonyl peak and its components in the spectra of HLRB cells were consistent with changes one expects to see during the oxidation of lipids. Decreases in the 1744 $cm^{-1}$ second derivative component, combined with an increase in the lower wavenumber side of this peak was consistent with breakdown of lipid components and the formation of products of lipid oxidative breakdown, including ketones, aldehydes, hydroperoxides, and endoperoxides (Ismail et al. 1993; Kiwi and Nadtochenko 2004; Santos et al. 2013; Voort et al. 1994). Kiwi et al (2004) further go on to show that in time-resolved studies of ongoing lipid peroxidation, the first change expected is decreased intensity of the 1744 $cm^{-1}$ followed by increased absorption at 1726 $cm^{-1}$ resulting in upshifting and broadening of the peak.

Multiple changes also occurred in absorbance peaks associated with proteins and their secondary structure as shown through the amide I, amide II, and amide II' peaks (Figure 4.1). Exposure to HL resulted in narrowing and upshifting of the amide I peak, whereas HLRB exposure resulted in a slight broadening and downshifting. Examination of the second derivative spectra shows these shifts are related to differences in protein secondary structure. In comparison to spectra from control cells, the spectra of cells exposed to HL (Figure 4.1, red) the α-helix to β-sheet ratio (1653 $cm^{-1}$ to 1633 $cm^{-1}$) changes in favour of the α-helix components, whereas in the

spectra of cells exposure to HLRB (light blue) this ratio changes in the favour of the β-sheet component. In the spectra of RB cells (green) this ratio showed a slight change in favour of the α-helical component (Figure 4.1). The relative increase in β-sheet contributions seen in the second derivative spectra of HLRB cells, combined with downshifting and increased peak width, was consistent with the formation of intermolecular β-sheets formed through denaturation of α-helical proteins (Berterame et al. 2016; Dong, Randolph, and Carpenter 2000; Shivu et al. 2013). All treatments caused an increase in the 1680 $cm^{-1}$ turn/loop/aggregate second derivative absorption.

The spectra of cells following the treatments indicate changes in the protein peaks that are consistent with increased heavy water influx into the cells. Specifically, overall decreased strength of the amide II peak and increased strength of the amide II' peak were noted (Figure 4.1). The absorption of the amide II peak is primarily due to out-of-phase coupling of ρNH and νCN, with minor contributions from ρCO, νCC, and νNC. Exposure of proteins to heavy water (deuterium oxide, $D_2O$) results in time-dependent exchange of hydrogen and deuterium from the NH group, resulting in a mixture of ρNH and ρND vibrations (Barth 2007). The IR absorption of ρND occurs at significantly lower wavenumbers than does ρNH (ρND mixes with other absorption peaks in the 1070-900 $cm^{-1}$ region), which decouples the vibrations from νCN and results in peak splitting. The absorption of decoupled νCN occurs around 1460 $cm^{-1}$, and the resultant peak is known as the amide II' (Barth 2007). The extent of H-D exchange increases with increased exposure of proteins to heavy water. Therefore, the relative intensities of the amide II and amide II' peaks can be used as an indicator of the extent of exposure of the cellular proteins to heavy water. As viewed in FTIR spectra of living cells suspended in heavy water, increased rates of H-D exchange indicate greater amounts of heavy water penetrating the cell. In addition, partially deuterated water (HOD) formed by H-D exchange from proteins, cellular water, and other compounds, has a δHOD absorption around 1450 $cm^{-1}$. This overlaps with the amide II' peak. In the absence of altered membrane permeability, this H-D exchange still takes place, albeit at a much lower rate. This was controlled for by limiting and standardizing the length of time that a given algal culture was suspended in $D_2O$. In the spectra of cells exposed to rose bengal (RB, HLRB), indicators of increased H-D exchange were greater, and spectra also showed downshifting of the second derivative positions of the β-sheets (both RB and HLRB) and α-helix (HLRB only) (Barth 2007). Spectra of cells exposed to rose bengal (RB, HLRB, Figure 4.1 - green and light blue) also showed

altered shaping of the amide II 1575 $cm^{-1}$ and 1545 $cm^{-1}$ second derivative components. This evidence suggests increased penetration of $D_2O$ into the cells.

Other consistent spectral differences were observed in cells following oxidative stress treatments, but they cannot be firmly assigned to specific chemical changes inside the cells, at this time. For example, in addition to overall differences in the strength of the 1450 $cm^{-1}$ peak, exposure of cells to high light and/or rose bengal resulted in reshaping of this peak as observed in the relative intensities of its second derivative components (Figure 4.1 - RB and HLRB: relative increase in both 1467 and 1437 $cm^{-1}$, HL: relative increase in 1467 $cm^{-1}$ and decrease in 1437 $cm^{-1}$). A relative decrease in intensity of the 1457 $cm^{-1}$ component as was observed in oxidized lipids (Kiwi and Nadtochenko 2004), but the overlapping assignments of this peak and its component are difficult to untangle. Several differences of varying intensity were present in the fingerprint region below 1400 $cm^{-1}$, including minor changes in the shape of the 1398 $cm^{-1}$ peak (related to the relative intensities of the 1398 $cm^{-1}$ and 1380 $cm^{-1}$ second derivative components), 1308 $cm^{-1}$ (increased in intensity in the second derivative spectra of HL, RB), and 1285 $cm^{-1}$ (decreased intensity in all exposures), but again without additional information these changes cannot be definitively prescribed to specific cellular components.

The use of principal component analysis of infrared spectra supported the importance of the above spectral differences in separating out the response of cells to the different oxidative stress exposures (Figure 4.1B). Each of the treatments caused changes in the chemical makeup of the cells, which allowed the resulting spectra to be differentiated in PC space. The loadings reflect increased HD exchange, changes in protein secondary structure, lipid oxidation, and differences in the 1398 $cm^{-1}$, 1308 $cm^{-1}$, and 1285 $cm^{-1}$ peaks. The spectra of cells exposed to rose bengal (RB, HLRB) were separated from all other spectra primarily on the basis of the increase in H-D exchange, suggesting altered membrane permeability (Figure 4.1B - inset - PC-1, 54%). The spectra of cells exposed to HL or RB could be separated from the spectra of control cells on the basis of PC-2 (23%), which described changes in protein secondary structure and altered intensity and width of the 1740 $cm^{-1}$ peak. PC-2 also had some utility in differentiating the spectra of HLRB cells from those of RB cells, but its power was increased when combined with the information from PC-3 (14%) which was driven by the formation of oxidative by-products around 1700 $cm^{-1}$ and the changes in the shape of amide II second derivative component at 1575 $cm^{-1}$.

#### 4.1.1.2 CH Stretching Region (3050-2800 $cm^{-1}$)

In the fingerprint region, the different exposures (HL, RB, HLRB) resulted in spectral changes that were distinct and unique to each treatment (Figure 4.1). However, the major changes induced in the high wavenumber CH region of the spectra (2800-3050 $cm^{-1}$) were due to changes in peak intensity (Figure 4.2A). In the second derivative spectra used for analysis (Figure 4.2B), differences in peak intensity were still found. The nature of second derivatives means that these differences were due to the peak widths as well as intensity differences in the untransformed spectra (Figure 4.2A). One of the most important differences observed in the spectra of this region was the change in the degree of unsaturation in the spectra of HLRB-treated cells, indicated by the relative intensity of the unsaturated lipid peak at 3010 $cm^{-1}$. The spectra of cells exposed to HLRB show a decrease in the intensity of this peak in comparison to the $CH_{2as}$ at 2921 $cm^{-1}$. This was consistent with exposure to singlet oxygen as the C=C double bonds in unsaturated lipids are a common target (Girotti and Kriska 2004; Triantaphylides et al. 2008). The $CH_2$ and $CH_3$ peaks exhibited a minor degree of peak broadening in cells from the treatment groups, an effect that was most obvious in the spectra of HLRB cells (Figure 4.2A). In cells exposed to rose bengal (Figure 4.2 - RB, HLRB) the position of the $CH_{2as}$ and $CH_{2s}$ peaks were upshifted by one wavenumber (2921 $cm^{-1}$ to 2922 $cm^{-1}$ and 2852 $cm^{-1}$ to 2853 $cm^{-1}$ respectively). Changes in the width of the CH peaks, combined with increased peak position of the $CH_2$ peaks, is often used as an indicator of increased membrane disorder (Derenne et al. 2013; Kiwi and Nadtochenko 2004; Lewis and McElhaney 2006, 2013), and is also seen as a result of lipid oxidation (Kiwi and Nadtochenko 2004).

The combination of PCs 1-3 described broadening and upshifting in the CH peaks and a decrease in the intensity of the 3010 $cm^{-1}$ (Figure 4.2B). As expected by visual examination of the spectra, there was tight clustering of all the treatment regimes in PCA space, with tighter overlap of the spectra of C and HL-treated cells, and of the spectra of RB and HLRB cells.

### 4.1.2 *Chlamydomona*s DJX-H

#### 4.1.2.1 Fingerprint Region (1800-1240 $cm^{-1}$)

Visual examination of the spectra of cells of *Chlamydomonas* DJX-H under the treatments used in this study identified a different pattern of responses than those seen in *C. reinhardtii* (Figure 4.3). Exposure to high light alone (red) resulted in limited spectral responses. Spectral

differences induced by exposure to rose bengal (RB, HLRB; green and light blue) were similar in pattern but different in magnitude when compared to spectra from *C. reinhardtii* cells exposed to those treatments.

An increase in the relative intensity of the ~1740 $cm^{-1}$ lipid carbonyl peak was observed in the spectra of cells exposed to rose bengal (RB, HLRB). The second derivative of this peak in the spectra of HLRB cells showed relative enrichment of the 1720 $cm^{-1}$ component, along with increased peak width of this component. On days with indicators of greater degrees of oxidative stress, this increased peak width resolved to two contributions in the second derivative, one at 1724 $cm^{-1}$ and one at 1711 $cm^{-1}$. This set of changes in the spectra of HLRB cells was indicative of oxidative damage to lipids and the formation and decomposition of lipid hydroperoxides (Ismail et al. 1993; Kiwi and Nadtochenko 2004; Santos et al. 2013). These changes were more pronounced in the HLRB spectra from *Chlamydomonas* DJX-H cells than they were in the spectra of HLRB *C. reinhardtii* cells.

Changes to the cells resulted in observed differences in the protein-associated peaks amide I, amide II, and amide II' in response to exposure to rose bengal (RB, HLRB). These three absorbance regions are associated with protein secondary structure and increased hydrogen-deuterium exchange. Two of these second derivative changes – differences in the ratio of α-helixes to β-sheets, and the strength of the 1608 $cm^{-1}$ – were inconsistent between measurements obtained from different bulk cultures measured on different days. The spectra of cells exposed to RB always showed a minor relative enrichment in α-helixes compared to control spectra. The spectra of cells exposed to HLRB, however, variably showed enrichment of α-helixes or β-sheets. The spectra of cells exposed to rose bengal (RB, HLRB) consistently showed an increase in the intensity of the ~1680 $cm^{-1}$ peak assigned to turns, as well as increased width of this peak and downshifting of its position. This was most pronounced in the spectra of HLRB cells (light blue). Despite inconsistencies in the α-helix to β-sheet ratio change, exposure to HLRB resulted in an increased overall width of the amide I peak, partially due to an increase in the 1680 $cm^{-1}$ component, and partially due to consistent increases in width of the α-helix and β-sheet components, combined with their position downshifting by ~5 $cm^{-1}$ (Figure 4.3A, light blue line). The second derivative spectra of cells exposed to RB showed similar increases in the width of these two components, with less downshifting present in the β-sheet component and no position change in the α-helix

component. Increased width and downshifting of the β-sheet component is consistent with the formation of intermolecular β-sheets formed via protein denaturation (Berterame et al. 2016; Dong et al. 2000; Shivu et al. 2013). Increased width of the α-helix component could be due to increased presence of the random and loop structures (Kong and Yu 2007).

In addition to spectral changes associated with differences in protein secondary structure, there was evidence of increased hydrogen-deuterium exchange in rose bengal-exposed cells (Figure 4.3A: RB, green; HLRB, light blue). The reciprocal intensity changes of the amide II and amide II' peaks (~1545 $cm^{-1}$, ~1440 $cm^{-1}$) indicated that the ρNH and νCN vibrations of the amide II peak had decoupled due to H-D exchange off of the ρNH group (ρNH → ρND). Given that rate of H-D exchange is directly related to how much heavy water the proteins are exposed to, this observed difference in the spectra of RB and HLRB spectra indicated that the proteins inside these cells had been exposed to greater amounts of $D_2O$. As the only source of $D_2O$ present was the $D_2O$/agarose mixture the cells were suspended in, changes in the relative intensity of the amide II and amide II' peaks were interpreted as indicates of increased membrane permeability. The spectra of *C. reinhardtii* cells exposed to rose bengal (Figure 4.1: RB, green; HLRB, light blue) showed a slight increase in H-D exchange. In comparison, the spectra of DJX-H rose bengal cells showed a much greater increase in H-D exchange. This was most pronounced in the spectra of DJX-H cells are HLRB exposure, where the amide II peak was nearly entirely gone.

In addition, visual examination of the spectra found several other consistent patterns of change associated with oxidative stress exposure. Given the complexity of peak assignments, specific chemical changes associated with these spectral differences are not assigned. The spectra of all cells exposed to the treatments used in this study showed changes in the shape of the 1575 $cm^{-1}$ second derivative component and changes in the ratios of the second derivative components of the 1450 $cm^{-1}$ peak (Figure 4.3A). All exhibited a relative decrease in intensity of the central 1456 $cm^{-1}$ component. The spectra of cells exposed to rose bengal (RB, HLRB; green, light blue) also showed significant flattening of the ~1398 $cm^{-1}$ peak associated in the second derivative with the relative decrease of the 1398 $cm^{-1}$ component. They also exhibited strong increases and downshifting in the 1340 $cm^{-1}$ peak and loss of the broad peak centred around 1260 $cm^{-1}$. The spectra of HLRB cells showed a loss of the underlying 1285 $cm^{-1}$ peak.

Use of principal component analysis supports many of the visual observations of spectral differences (Figure 4.3). PC-1 (59%) cleanly separated the spectra of cells exposed to rose bengal (RB, HLRB) from those that had not been (C, HL) based on the loss of the amide II and 1260 $cm^{-1}$ peaks. The spectra of cells exposed to rose bengal (RB, HLRB) could be separated from each other based on a mix of PC-2 (14%) and PC-3 (13%), which described the shape and intensity of the 1450 $cm^{-1}$ peak, differences in protein secondary structure, and the formation and decomposition of lipid hydroperoxides. Interestingly, changes in the 1398 $cm^{-1}$ and 1340 $cm^{-1}$ peaks, which could be visually used as an indicator of rose bengal exposure, did not influence these loadings (Figure 4.3B).

#### 4.1.2.2 CH Stretching Region (3050-2800 $cm^{-1}$)

The exposure of DJX-H cells to the treatments used in this study resulted in increased width of the $CH_2$ and $CH_3$ peaks, and a resultant decreased peak resolution (Figure 4.4). Interpretation of overall changes in intensity were again confounded by the nature of second derivatives. The trends to increased peak widths and decreased peak resolution were strongest in the spectra of cells exposed to HLRB (light blue). The spectra of these cells also showed the almost complete loss of the unsaturated lipid peak at 3010 $cm^{-1}$. The spectra of cells exposed to rose bengal (Figure 4.4 - RB, green; HLRB, light blue) also showed the evolution of an unknown CH peak around 2885 $cm^{-1}$ (Figure 4.4, arrow) and upshifting of the $CH_{2as}$ peak position. These differences were also more pronounced in the spectra of cells exposed to HLRB.

Principal component analysis of this region (Figure 4.4B inset) showed separation of the spectra of these cells on the basis of the width and resolution of the $CH_2$ and $CH_3$ peaks, $CH_2$ peak position, decreased lipid unsaturation, and the evolution of an unknown CH-containing compound. The combination of these first three factors was suggestive of changes in membrane lipid diversity, including the breaking of CH bonds and alteration of chain length, leading to altered membrane fluidity.

A potential assignment for the unknown CH absorption around 2885-2880 $cm^{-1}$ is the $CH_{3s}$ group of short-chain alkanes such as ethane and pentane. Lipid peroxidation is known to generate these compounds, and their increased concentration has been used to monitor the progress of lipid oxidation (Hamilton et al. 1997). The $CH_{2as}$ and $CH_{3as}$ absorptions for these compounds are found on the high wavenumber side of the commonly observed CH peaks in algal systems. The presence

of this unassigned peak is primarily observed in conjunction with strong increases in the 1720-1700 $cm^{-1}$ region, a spectral component assigned to lipid oxidative breakdown products.

### 4.1.3 *Chlamydomonas* DJX-J

#### 4.1.3.1 Fingerprint Region (1800-1240 $cm^{-1}$)

Visual examination of the spectra of cells of *Chlamydomonas* DJX-J (Figure 4.5) indicated that its response to high light and/or rose bengal was more similar to that of DJX-H (Figure 4.3) than that of *C. reinhardtii* (Figure 4.1). The spectra of cells exposed to high light alone (HL, red) showed no significant response in comparison to the spectra of control cells (C, dark blue). The spectra of cells exposed to rose bengal (RB, green; HLRB, light blue) showed similar changes that differed in magnitude.

The spectra of cells exposed to rose bengal showed an overall increase in the relative intensity of the ~1740 $cm^{-1}$ lipid carbonyl peak and decreased resolution in respect to the amide I (Figure 4.5). The second derivative spectra showed this to be due to increased absorptions in the 1725-1700 $cm^{-1}$ region associated with the formation and decomposition of the by-products of lipid oxidation (ketones, aldehydes, lipid hydroperoxides, lipid endoperoxides, etc.) (Ismail et al. 1993; Kiwi and Nadtochenko 2004; Santos et al. 2013). The decrease in the 1740 $cm^{-1}$ component and increased absorption in the 1726-1700 $cm^{-1}$ components was greater in the spectra of HLRB cells (light blue). This pattern of change has also been seen during peroxidation of the membranes of *Escherichia coli* (Nadtochenko et al. 2005).

Differences in the amide I protein peak in response to rose bengal exposure (RB, HLRB) were more consistent with those seen in the spectra of HLRB *C. reinhardtii* cells (Figure 4.1) than those seen in HLRB *Chlamydomonas* DJX-H (Figure 4.3). The spectra of cells exposed to rose bengal showed a relative increase in the intensity of the ~1680 $cm^{-1}$ second derivative component and decrease in the α-helical components when compared to that assigned to β-sheets. In addition, all three of these components exhibited increased peak width and downshifting in position. These types of changes are consistent with the formation of intermolecular β-sheets from unwound α-helixes as well as potentially the formation of other protein intermediates. There was also an increase in the width of the 1575 $cm^{-1}$ second derivative component of the amide II and reshaping of the 1545 $cm^{-1}$ second derivative component. These differences were more pronounced in the spectra of HLRB cells than in RB cells.

Changes in the relative intensity of the amide II and amide II' peaks, indicative of increased H-D exchange and therefore altered membrane permeability, were strongest in the spectra of DJX-J cells exposed to rose bengal (RB, green; HLRB, light blue). Virtually no change was seen in the spectra of DJX-J HL-exposed cells, while those exposed to rose bengal (RB, HLRB) exhibited a near total loss of this peak. This change was even more pronounced in the spectra of HLRB cells. This pattern was similar to that seen in the spectra of DJX-H cells, where exposure to rose bengal also caused a strong increase in membrane permeability and $D_2O$ influx. The spectra of *C. reinhardtii* cells indicated that exposure to any of the stressors (HL, and particularly RB, HLRB) increased membrane permeability, though to a lesser degree than was seen in the DJX- species. In addition, the amide II' peak widens in the spectra of cells exposed to rose bengal due to the relative loss in intensity of the central 1455 $cm^{-1}$ component of the triplet found in the second derivative.

A variety of changes found in the fingerprint region below 1400 $cm^{-1}$ were consistent with those seen in the spectra of DJX-H cells but were similarly unlinked to specific biochemical responses. In the spectra of rose bengal exposed cells (RB, HLRB) there was reshaping of the 1398 $cm^{-1}$ peak, with a relative decrease in the 1398 $cm^{-1}$ second derivative component. In addition, the 1340 $cm^{-1}$ peak showed increased intensity, and the 1285 $cm^{-1}$ peak decreased in the spectra of HLRB cells. As discussed above, there are multiple overlapping peak assignments for these features, but it is worth noting that a previous study of membrane peroxidation in *E. coli* observed increases around 1400 $cm^{-1}$ associated with the formation of aldehydes during the breakdown of hydroperoxides of lipid endoperoxides (Nadtochenko et al. 2005), and the subsequent decrease of this peak as reactions progress (Kiwi and Nadtochenko 2004).

The use of PCA confirmed these observations (Figure 4.5B inset). Spectra separated along PC-1, with significant overlap between C and HL spectra (dark blue squares, red circles), and RB and HLRB spectra (green triangles, light blue diamonds) plotting along the negative axis. Spectra of RB cells plotted closer to C/HL cells than did HLRB spectra. The other principal component, PC-2, was primarily influenced by residual baseline differences in the 1300-1240 $cm^{-1}$ region. PC-1 described increased hydrogen-deuterium exchange, increased formation of lipid oxidative products, upshifting of the amide I peak, and changes in the shape and intensity of the 1398 $cm^{-1}$ and 1340 $cm^{-1}$ peaks. This suggested that there is one pattern of spectral change seen in oxidatively stressed cells of DJX-J, with observed differences being related to the degree of stress. This is in

contrast to the spectra of oxidatively stress *C. reinhardtii*, which appeared to exhibit distinct patterns of spectral change based on the source of stress exposures.

#### 4.1.3.2 CH Stretching Region (3050-2800 $cm^{-1}$)

In the CH stretching region (Figure 4.6), patterns of response observed were similar to those observed in the fingerprint region. The spectra of cells exposed to HL (red) were indistinguishable from those of control cells (dark blue). The spectra of cells exposed to rose bengal (RB, green; HLRB, light blue) showed similar responses, though the differences observed were greater in the spectra of HLRB cells. Exposure to rose bengal resulted in indicators of broken CH chains and increased membrane disorder (broadening and upshifting of CH peaks), decreased degrees of lipid unsaturation (ratio of 3010 $cm^{-1}$ to $CH_{2as}$), and the evolution of short-chain alkanes (increased contribution around 2885 $cm^{-1}$). These changes were more pronounced in the spectra of HLRB cells than RB cells. Most interestingly, the peak associated with unsaturated lipids at 3010 $cm^{-1}$ was almost entirely lost in cells exposed to the combined HLRB exposure, whereas it showed increased peak width in the spectra of RB cells.

Principal component analysis of the second derivative spectra of this region (Figure 4.6 B inset) confirmed these observations. The spectra from HL cells (red circles) and C cells (dark blue squares) showed significant overlap. The spectra of cells exposed to rose bengal (RB, green triangles; HLRB, light blue diamonds) could be separated from HL and C spectra and each other by a combination of changes in peak widths, positions, and the intensities of the unsaturated lipid peak and 2885 $cm^{-1}$ contribution.

## 4.2 Discussion

Through these experiments, we were able to observe and examine the effects of high light and rose bengal treatments on individual living cells of green algae. We were also able to observe species-specific differences in how the cellular biochemical makeup changed following these treatments. As hypothesized, the observed damage accrued in response to high light exposure differed between *C. reinhardtii* and the DJX- species. The impact of HL exposure on DJX-H and -J cells was limited. It was not clear if this was due to a greater degree of high-light tolerance or if the high-light induced changes were not IR-visible in the same way. It is also possible that the DJX-H and -J cells were damaged in a similar manner as *C. reinhardtii* cells, but that repair mechanisms acted at a timescale that prevented their observations. Critically, we were able to

obtain better resolution than predicted for the change in cellular biochemical makeup between HL and RB exposure: contrary to my hypothesis, all three species exhibited starkly different responses to endogenously-produced singlet oxygen (HL) than they did to exogenously-produced singlet oxygen (RB).

Overall analysis of the two spectral regions of *C. reinhardtii* suggests that cells exhibit a distinct response to each of the treatments to which they were exposed. The presence of rose bengal – alone or in combination with high light - appears to alter membrane fluidity and permeability in a way that is not seen with exposure to high light alone. Of the individual treatments, the impact of HL-exposure was more localized within the cell, whereas the spectra of rose bengal-exposed cells (RB, HLRB) indicated disruption of the plasma membrane. The slight change seen in peak position in the $CH_2$ peaks in all treatments is suggestive of increases in membrane disorder, but its co-occurrence with increased hydrogen-deuterium exchange in cells exposed to rose bengal that suggests significant physiological alterations to the cellular membranes.

When changes in lipids are interpreted from differences in the ~1740 $cm^{-1}$ lipid carbonyl peak, the similarity in the response of RB and HLRB-treated cells is unexpected. Exposure to HL and RB show very similar types of change in lipid composition as read from this peak. It is only in the spectra of HLRB cells that there are indicators of higher degrees of oxidative damage and the formation of lipid peroxides, and only in these cells is there a high degree of loss of unsaturation in lipids. This suggests that while there may be a similar degree of lipid oxidative damage mediated by RB and HL exposure, it is not localized in the same place. Generation of singlet oxygen by high light occurs primarily in the thylakoid membranes, whereas singlet oxygen generated by rose bengal occurs initially at the plasma membrane. It may be taken up by the cell or enter the cell through the generation of membrane damage and then impact the entire cell. The thylakoid membranes of the chloroplast are composed of highly unsaturated lipids and contain high concentrations of carotenoids, chlorophylls, and proteins. The more general distribution of rose bengal and its damage suggests some of the observed lipid changes occur within the plasma membrane resulting in the altered membrane permeability and increased H-D exchange. This is exacerbated in the HLRB exposures, which see increased generation of singlet oxygen from both the chloroplasts and rose bengal itself, which produces singlet oxygen in catalytic light-dependent manner.

Cells of photosynthetic organisms such as *C. reinhardtii* are capable of physiological acclimation to adverse growth conditions such as exposure to excess light, which cause oxidative damage. The suite of responses act in the short, medium, and long-term. Short-term mechanisms such as light avoidance, state-transitions, and non-photochemical quenching act to diminish the amount of light being absorbed by the cell and used for photosynthesis. The direct effect here is less light being absorbed means less singlet oxygen production and hence less damage. For example, in the process of state-transitions, cells detect an energy imbalance in photosynthesis and as a result, light-harvesting proteins associated with PSII are phosphorylated. In the phosphorylated state, the proteins migrate from PSII to PSI. This could show up in our experimental data as an altered phosphate absorbance peak. However, work on another project has determined that DJX-H and -J have lost the capacity to phosphorylate LHC proteins (Miskiewicz and Wilson - unpublished data), thus such a peak would only appear the spectra obtained from *C. reinhardtii* cells.

On the medium-term, cells have programmed cellular mechanisms that diminish rates of photosynthesis, decreasing singlet oxygen production, while using up excess energy - primarily ATP. The most thoroughly studied example is the process of PSII photoinhibition. During this highly regulated process, the proteins of the PSII reaction centre core are phosphorylated and degraded. Replacement protein subunits are then translated, and the reaction centre reassembled. While seen as an energetically expensive process, remember that when cells are under high-light stress, they have too much energy available. It is reasonable to postulate that some of the changes in protein secondary structure in cells exposed to HL are associated with (these above-described changes in protein pools and phosphorylation). This is further supported by the patterns of change in protein secondary structure seen in cells exposed to HLRB, which are consistent with protein denaturation. The overwhelming of the cell's adaptive mechanisms would lead to some degree of protein denaturation; this observation is consistent with the observation of the formation of lipid hydroperoxides and their decomposition products observed in these same cells. Changes in other peaks in the fingerprint region were not attributable to specific physiological differences but were associated with specific stressor responses. Most interesting amongst these is the decreased absorption of the 1285 $cm^{-1}$ peak in response to any degree of oxidative stress.

Long-term acclimation responses are also observed in algal cells exposed to excess light. These include an increased capacity for non-photochemical quenching, reduced light-harvesting protein abundance, and faster growth rates, and the accumulation of repair enzymes (Leisinger et al. 2001; Wilson and Huner 2000). These processes require altered gene expression. A long-term acclimation of this type would be initiated quickly, but generally require times that exceed the period used in this study to be complete. In fact, due to their high stability and the photooxidative risk inherent with the release of chlorophyll or its degradation products from light-harvesting complexes, decreasing the size of the LHC seems to require cell growth and reproduction.

The environmental species *Chlamydomonas* DJX-H exhibits different patterns of response to oxidative stressors when compared to the differences induced in *C. reinhardtii*, which exhibits a distinct physiological response to each of the oxidative stressors tested. In comparison, the spectra of DJX-H cells exhibit virtually no response to HL exposure beyond minor changes in the CH stretching region. In addition, spectral response to RB and HLRB are similar, though the HLRB response is amplified in intensity.

The lack of changes in the spectra obtained from DJX-H cells following HL exposure does not necessarily indicate that this species has a greater tolerance for high light exposure than *C. reinhardtii*. The spectral changes seen in *C. reinhardtii* HL cells may indicate an acclimation response to mediate current or future damage mediated by high light exposure. Supporting this is the fact that the environmental DJX- species are known to lack the ability to undergo state transitions in response to high light exposures. The DJX- species accumulate fewer spectral changes in response to HL exposure. This may indicate the lack of a physiological response to this level of high light exposure. In this case, this may be a result of decreased damage – the threshold that triggers high light stress may not have been reached in these experiments. It is also possible that the protein repair or disposal mechanisms are more rapid in DJX- species. Finally, it may also be that the HL changes seen in *C. reinhardtii* are at least partly associated with acclimation changes, such as state transitions that are not present in the DJX- species.

The changes to protein secondary structure are somewhat inconsistent in the spectra of DJX-H cells. Exposure to rose bengal (RB, HLRB) does consistently show broadening and downshifting of the second derivative components at 1680 $cm^{-1}$, α-helixes, β-sheets, and the amide II 1575 $cm^{-1}$. In addition, some of these changes may be attributable to H-D exchange. Decreased

absorption of the amide II peak coupled with increased intensity of the 1450 $cm^{-1}$ amide II' peak indicates disrupted plasma membrane functionality and increased influx of heavy water into the cell during rose bengal exposures (RB, HLRB). The degree of membrane disruption induced by RB exposure appears to be similar between DJX-H and *C. reinhardtii* cells. In contrast, exposure to HLRB appears to have a much greater impact on cells of DJX-H than on cells of *C. reinhardtii*. Spectra of DJX-H cells following HLRB treatment show a more pronounced decrease in absorption of the 1740 $cm^{-1}$ second derivative component, coupled with a greater increase in the 1720-1700 $cm^{-1}$ region assigned to breakdown products of oxidized lipids, lipid hydroperoxides, and lipid endoperoxides. This is combined with the near-total loss of unsaturated lipids measured by the 3010 $cm^{-1}$ olefinic peak, decreased resolution of the CH peaks, and the evolution of an unidentified peak that could potentially be assigned to short-chain alkenes generated via lipid oxidation

Overall, the environmental species DJX-H appears to exhibit a muted or suppressed response to high light exposure, and stronger response to rose bengal exposure, including some novel but repeatable spectral changes. It is interesting to note that the amplified lipid response to rose bengal exposure is similar to some of the differences found between these species under control conditions (Chapter 3). Compared to *C. reinhardtii*, cells of DJX-H have more disordered membranes (broader $CH_2$ and $CH_3$ peaks with higher peak positions), as well as lower overall lipid abundances (relatively lower intensity of 1740 $cm^{-1}$), and a lower degree of absolute lipid unsaturation (relatively lower intensity of 3010 $cm^{-1}$). The combination of these factors could result in a greater degree of penetration of rose bengal into the cell. Following this, the decreased relative abundance of sacrificial unsaturated lipids, combined with lack of cellular response to reduced high light damage, could result in cascading oxidative stress signalling and mount a greater challenge to cellular responses. In addition, the degree of lipid oxidation found in the spectra of cells exposed to rose bengal, and particularly the high light rose bengal combination, appears to result in the evolution of detectable levels of short-chain alkanes.

The presence of an unidentified CH peak around 2880-2885 $cm^{-1}$ is sometimes found in systems exhibiting high degrees of lipid oxidation. These systems exhibit increased absorption in the 1720-1700 $cm^{-1}$ region, which includes absorptions from the breakdown products of lipid oxidations (ketones, aldehydes, lipid hydroperoxides, lipid endoperoxides, etc.); time course of

lipid damage: decrease at 1744, increase at 1726, with upshifting and broadening of the peak (Ismail et al. 1993; Kiwi and Nadtochenko 2004; Santos et al. 2013). The evolution of ethane and pentane can be used monitor lipid autoxidation (Hamilton et al. 1997); these short-chain alkanes tend to have strong absorptions around 2960, 2930, and 2880 $cm^{-1}$, in addition to another strong absorption around 1465 $cm^{-1}$.

Cells of *Chlamydomonas* DJX-J exhibit responses to oxidative stressors that more closely resemble those of its environmental sister species *Chlamydomonas* DJX-H than the laboratory strain *C. reinhardtii*. Cellular responses to high light exposure are entirely absent in DJX-J, whereas DJX-H cells show minor changes, predominantly in CH lipid peaks. The spectra of *C. reinhardtii* HL cells indicates distinct changes in protein secondary structures. As with DJX-H, when compared to *C. reinhardtii*, there is no direct indication of whether this is indicative of greater tolerance to high-light exposure or of impaired adaptive or acclimation responses.

Cells of DJX-J and DJX-J share several responses to rose bengal exposure (RB, HLRB) not seen in *C. reinhardtii*. These are the relative decreased of the 1398 $cm^{-1}$ second derivative component of the 1398 $cm^{-1}$ peak, increased intensity of the 1340 $cm^{-1}$ peak, and the evolution of a compound or compounds that exhibit CH absorption around 2885 $cm^{-1}$, potentially short-chain alkanes produced from oxidative lipid damage. In contrast, changes seen in protein secondary structures of DJX-J cells exposed to rose bengal were most similar to those seen in the spectra of *C. reinhardtii* HLRB cells, when it is posited protein damage has occurred.

In all species, there were distinct spectral differences in RB vs HL cells. The localization of singlet oxygen production heavily influenced cellular response: HL exposure results in singlet oxygen generation by the photosystems in the chloroplasts, whereas rose bengal is most distributed throughout the cell. Rose bengal appears to target all membrane lipids and alter membrane transport. *C. reinhardtii* appears to acclimate to high light exposure in a way not seen in DJX-H or DJX-J; these strains are in turn more sensitive to HLRB exposure. This combination exposure to high light and rose bengal elicited a stronger response than either high light or rose bengal alone. In *C. reinhardtii* this response was distinct from that of either HL or RB. In DJX-H and DJX-J it was essentially an amplified version of RB exposure.

It is interesting to note that the spectra of DJX-H and DJX-J cells indicate that even under control conditions, their membranes are more disordered and have less unsaturated than those of

*C. reinhardtii*, and these differences are amplified by oxidative stress exposures. These differences are likely related to evolutionary history, as the environmental species can grow successfully under a much broader range of low temperatures (down to 4°C) as opposed to *C. reinhardtii* (lower growth limit of 16°C).

## 4.3 Summary and Conclusions

The experiments described in this chapter successfully demonstrated the utility of synchrotron FTIR to study the subtle effects of oxidative stress at the level of the individual cell. The power of the system allowed us to successfully differentiate between biochemical impacts induced by different sources of singlet oxygen. I was able to clearly observe changes related to oxidative modification of protein and lipid bonds. There was also a series of characteristic or diagnostic changes in peaks with multiple overlapping assignments, not to mention the impact of H-D exchange on protein bond energies.

One of the most important observations in this work is the variety of distinct responses observed in different species in response to different sources of singlet oxygen. When generated by rose bengal, singlet oxygen appears to have a significant impact on the plasma membrane structure and function. This treatment leads to movement of $D_2O$ into the cell, in a light-dependent manner. This was observed to a greater extent in the DJX- species, suggesting that their plasma membranes are more sensitive to oxidative damage originating outside of the cell, than *C. reinhardtii*. Thus, it appeared that the type of treatment was more important to the degree of damage that accumulated in DJX-H and DJX-J cells whereas the spectral changes of *C. reinhardtii* cells appeared to be a function of both type and degree of oxidative stress.

The apparent tolerance of DJX-H and -J cells to HL exposure is intriguing. We know that they have evolved in a different type of environment than *C. reinhardtii* cells, but it is unclear why they would be more tolerant of high-light exposure. We know that the DJX-H and -J cells do not have the capacity to perform state-transitions, a short-term defence mechanism, but other defence mechanisms remain to be elucidated. On-going research is investigating the process of photoinhibition and the PSII damage-repair cycle in DJX-H and -J cells, work that was spurred on by this study.

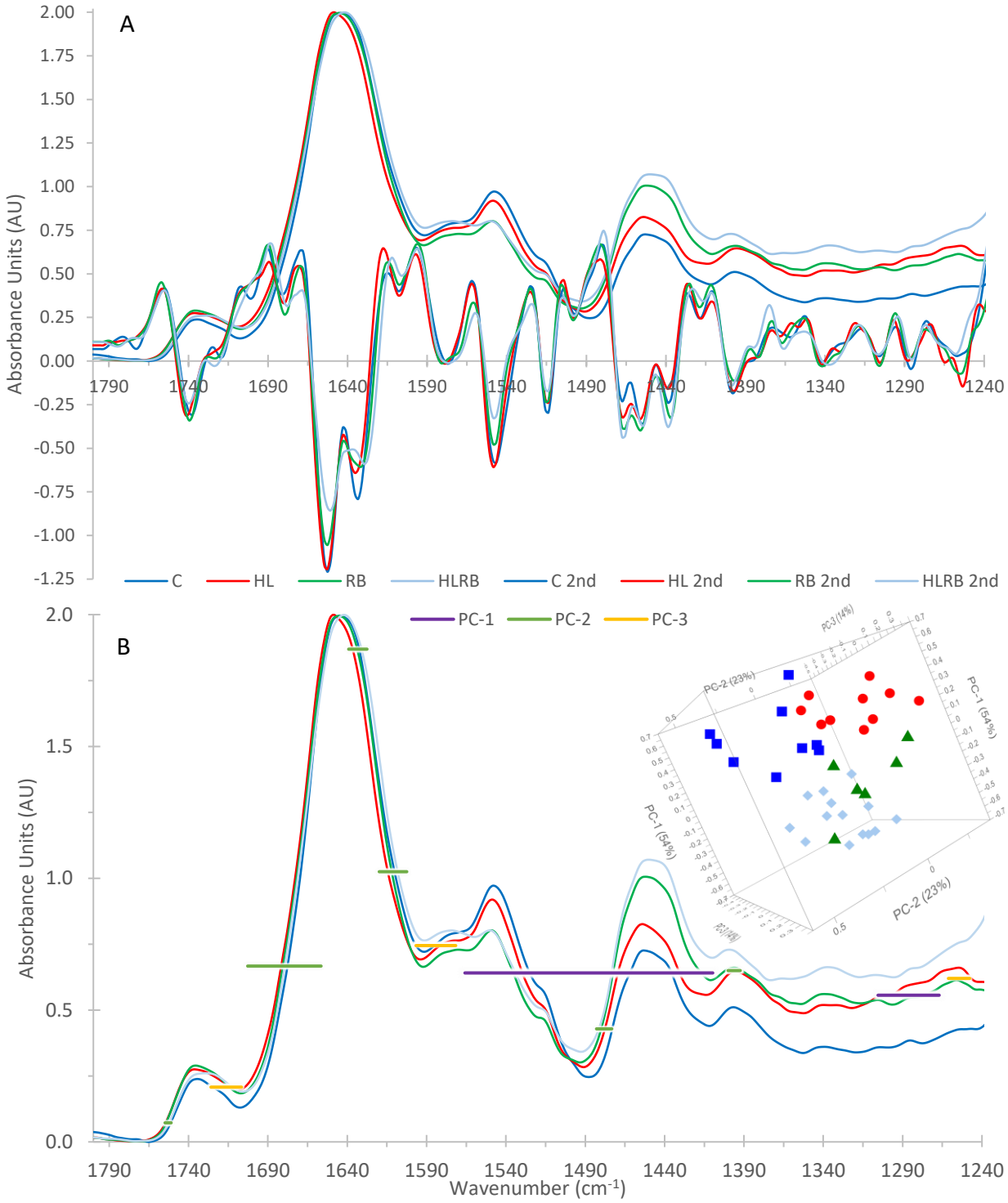


*Figure 4.1 – FTIR measurements of the 1800-1240 cm$^{-1}$ region in* Chlamydomonas reinhardtii *(WT) under control (C), high light (HL), rose bengal (RB), high light (HL) and high light + rose bengal (HLRB) conditions. Spectra are the averages of the individual spectra used in principal component analysis, and have been normalized to the amide I peak. A) Average spectra and scaled 2$^{nd}$ derivatives; B) Average spectra overlain with the loadings generating inset image (PC1-3: 54%, 23%, 14%).*

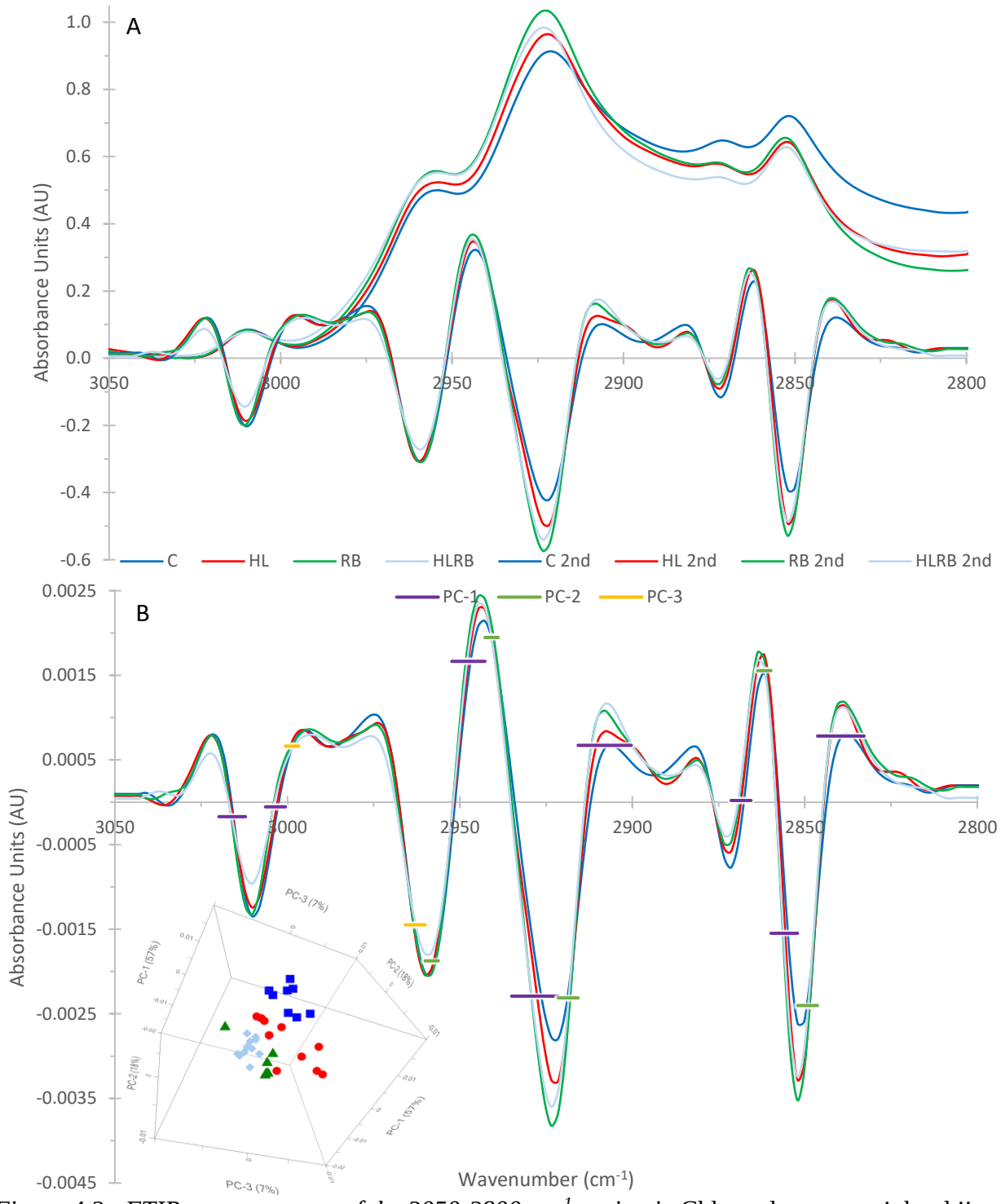


*Figure 4.2 - FTIR measurements of the 3050-2800 cm$^{-1}$ region in* Chlamydomonas reinhardtii *(WT) under control (C), high light (HL), rose bengal (RB), high light (HL) and high light + rose bengal (HLRB) conditions. Spectra are the averages of the individual spectra used in principal component analysis, and have been normalized to the amide I peak, then offset corrected 3050 – 3000 cm$^{-1}$. A) Average spectra and scaled 2$^{nd}$ derivatives; B) Average of 2$^{nd}$ derivative spectra overlain with the loadings generating inset image. (PC1-3: 57%, 18%, 7%).*

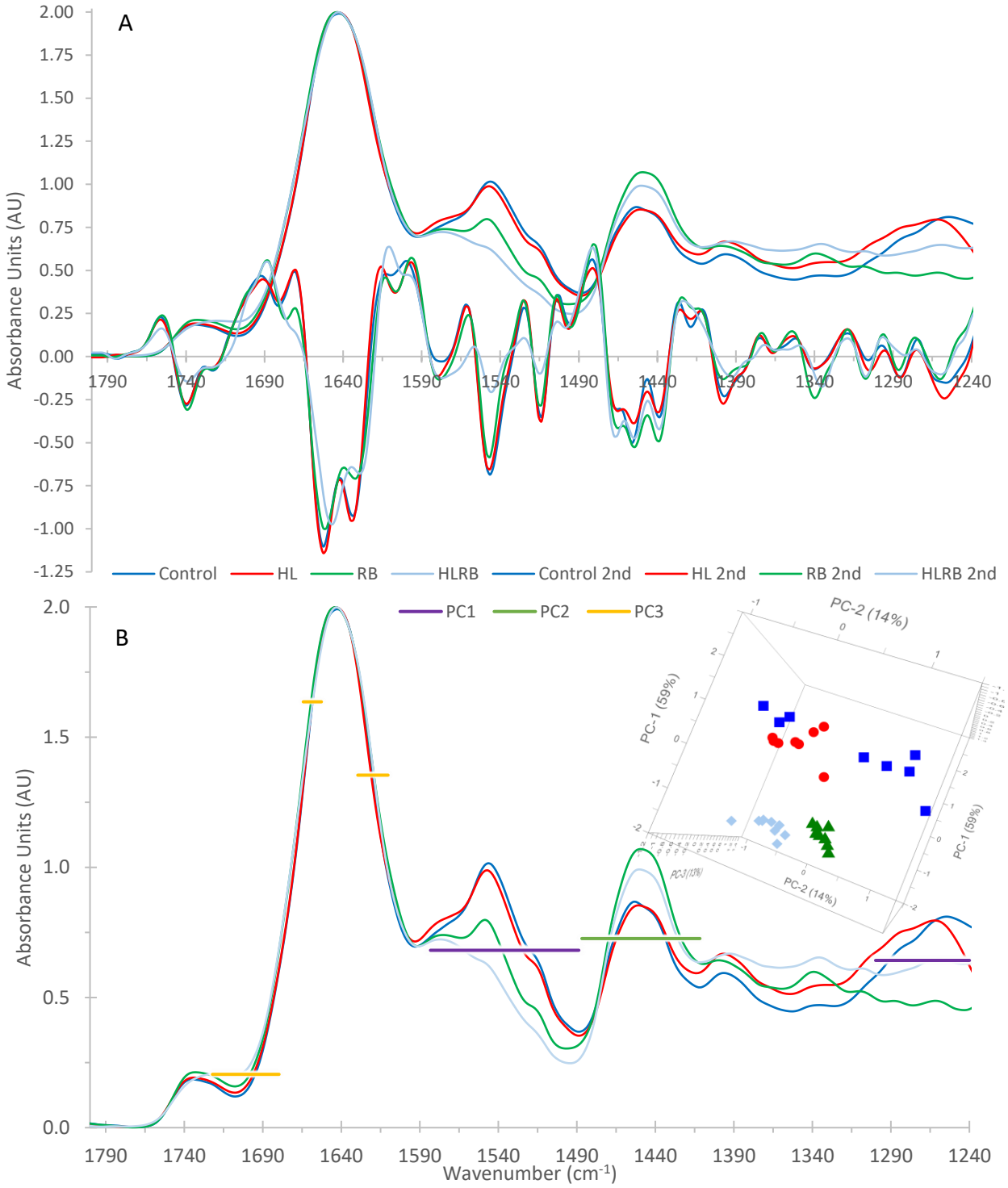


*Figure 4.3 - FTIR measurements of the 1800-1240 cm$^{-1}$ region in* Chlamydomonas *DJX-H under control (C), high light (HL), rose bengal (RB), high light (HL) and high light + rose bengal (HLRB) conditions. Spectra are the averages of the individual spectra used in principal component analysis, and have been normalized to the amide I peak. A) Average spectra and scaled 2$^{nd}$ derivatives; B) Average of 2$^{nd}$ derivative spectra overlain with the loadings generating inset image (PC1-3: 59%, 14%, 13%).*

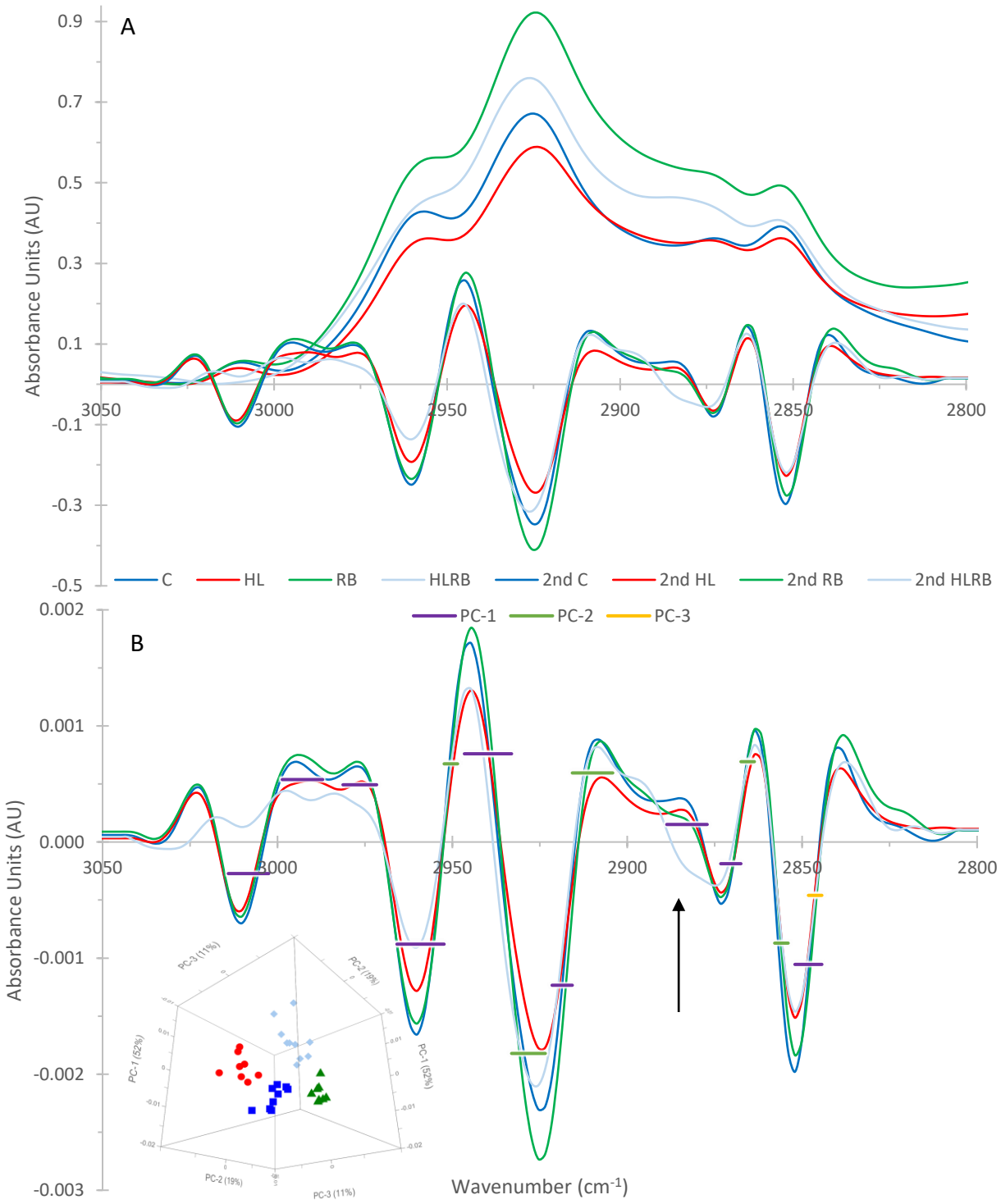


*Figure 4.4 - FTIR measurements of the 3050-2800 cm$^{-1}$ region in* Chlamydomonas *DJX-H under control (C), high light (HL), rose bengal (RB), high light (HL) and high light + rose bengal (HLRB) conditions. Spectra are the averages of the individual spectra used in principal component analysis, and have been normalized to the amide I peak, then offset corrected 3050 – 3000 cm$^{-1}$. A) Average spectra and scaled 2$^{nd}$ derivatives; B) Average of 2$^{nd}$ derivative spectra overlain with the loadings generating inset image (PC1-3: 52%, 19%, 11%).*

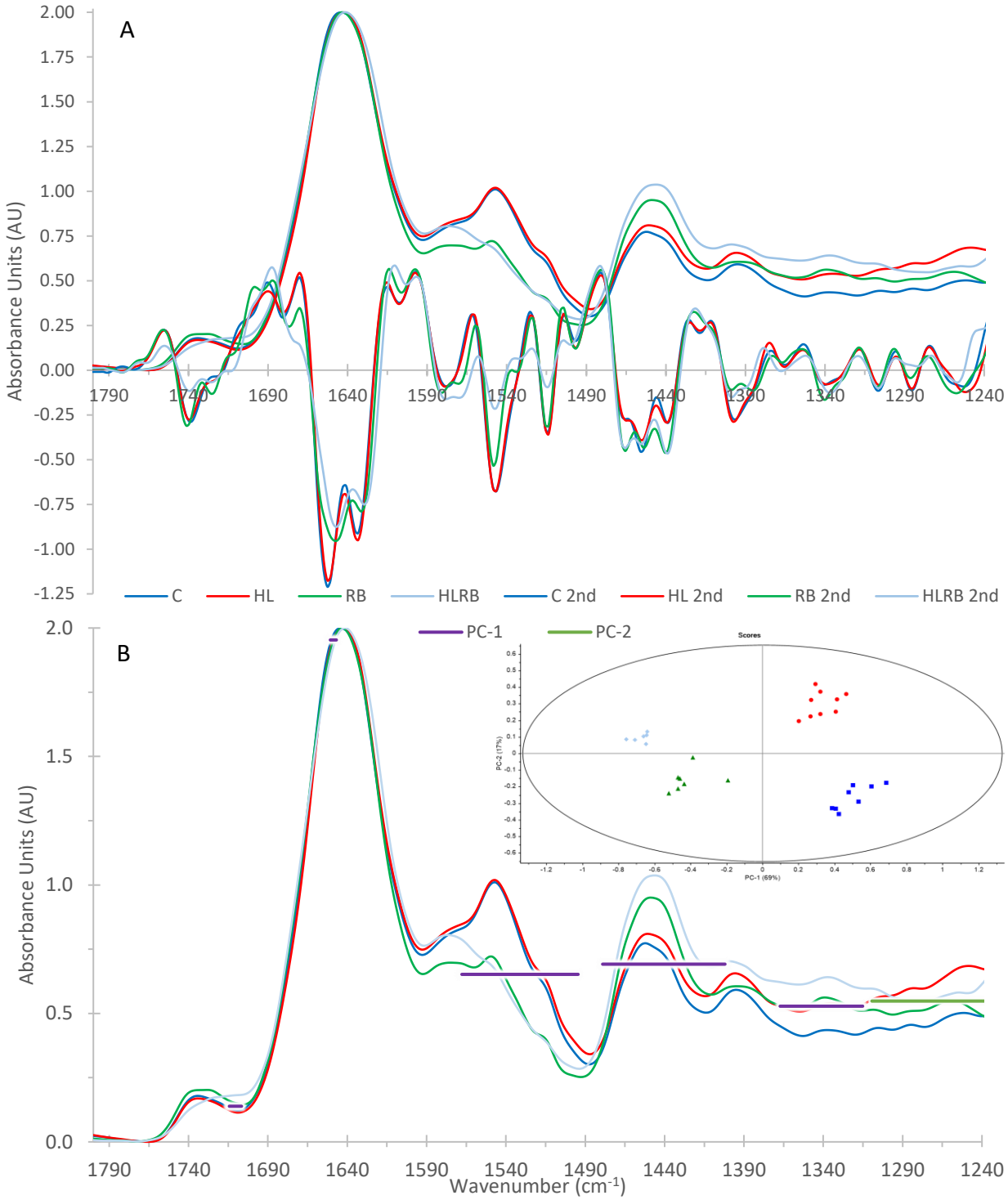


*Figure 4.5 - FTIR measurements of the 1800-1240 cm$^{-1}$ region in* Chlamydomonas *DJX-J under control (C), high light (HL), rose bengal (RB), high light (HL) and high light + rose bengal (HLRB) conditions. Spectra are the averages of the individual spectra used in principal component analysis, and have been normalized to the amide I peak. A) Average spectra and scaled 2$^{nd}$ derivatives; B) Average of 2$^{nd}$ derivative spectra overlain with the loadings generating inset image (PC1-2: 89%, 17%; PC-2 is included for graphing purposes only).*

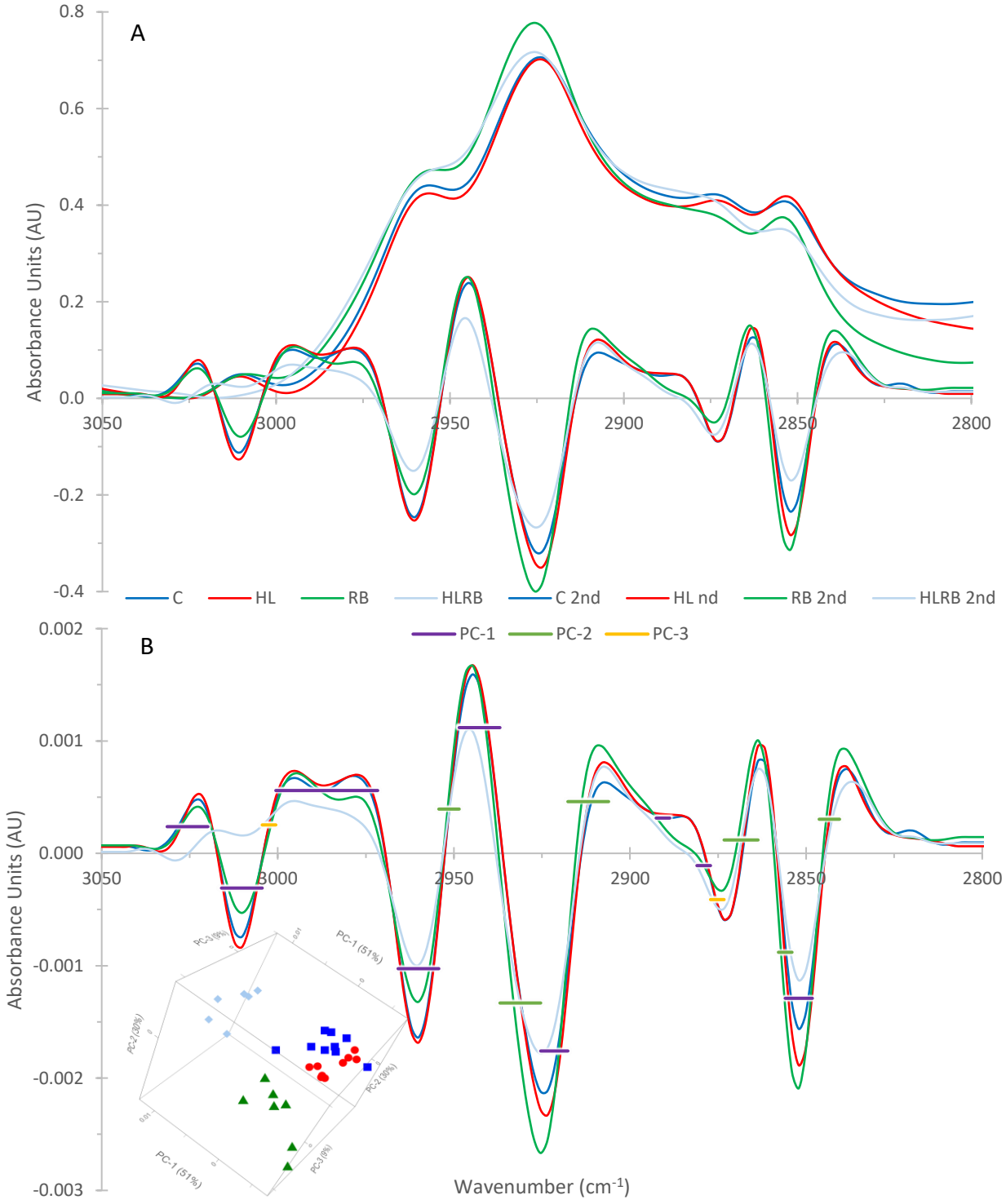


*Figure 4.6 - FTIR measurements of the 3050-2800 cm$^{-1}$ region in* Chlamydomonas *DJX-J under control (C), high light (HL), rose bengal (RB), high light (HL) and high light + rose bengal (HLRB) conditions. Spectra are the averages of the individual spectra used in principal component analysis, and have been normalized to the amide I peak, then offset corrected 3050 – 3000 cm$^{-1}$. A) Average spectra and scaled 2$^{nd}$ derivatives; B) Average of 2$^{nd}$ derivative spectra overlain with the loadings generating inset image (PC1-3: 51%, 30%, 9%).*

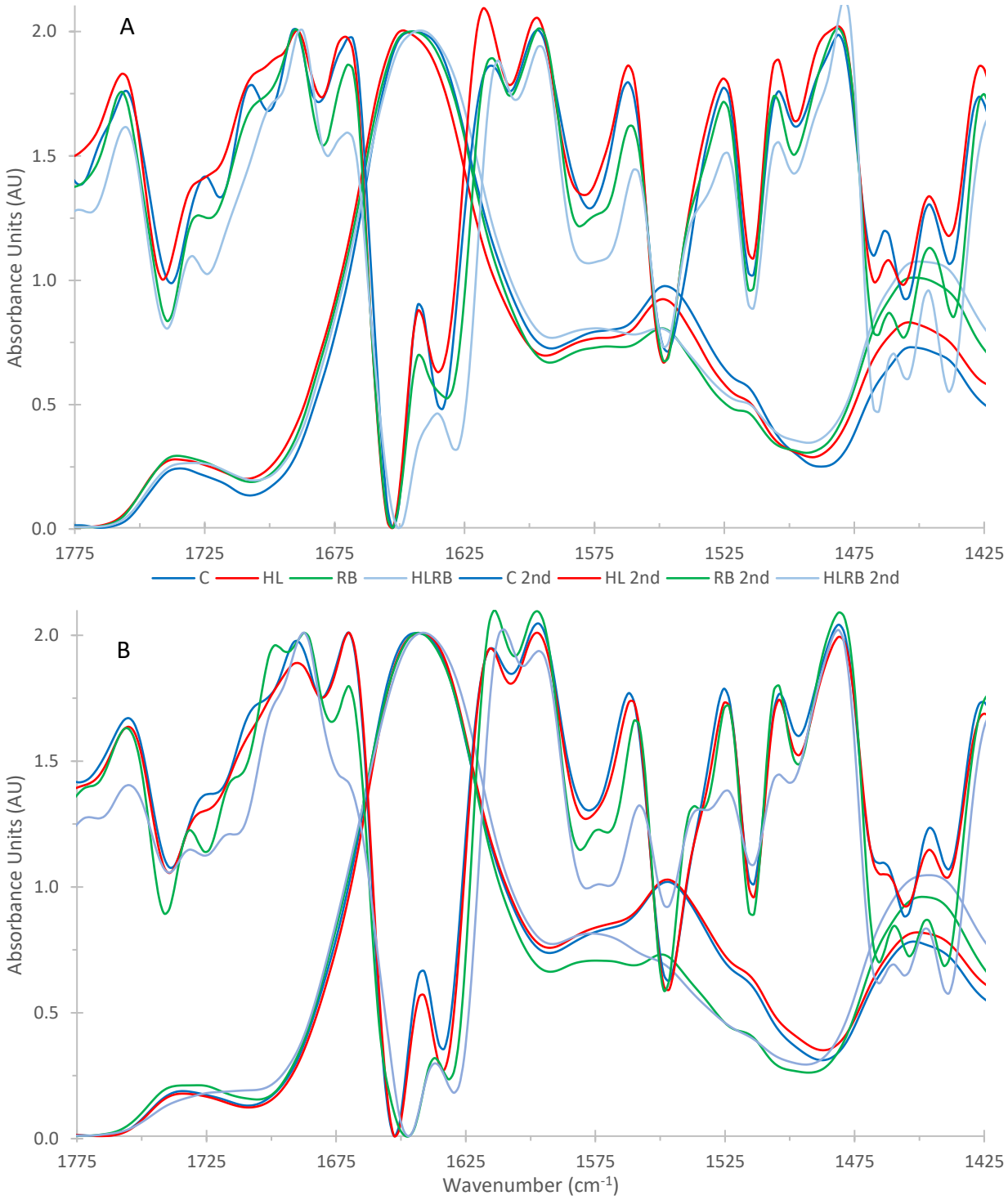


*Figure 4.7 - Overlay of second derivative spectra normalized to the α-helical component for A)* Chlamydomonas reinhardtii*; and B)* Chlamydomonas *DJX-J.*

# CHAPTER FIVE

# SPECTRAL CHARACTERIZATION OF DIFFERENCES INDUCED BY PHOTOSYNTHETIC MUTATIONS

## 5.0 Introduction and Goals

The experiments described in chapter 4, highlighted that using single-cell synchrotron FTIR microscopy, we could identify spectral changes that occur in *C. reinhardtii* cells that were exposed to high light and/or rose bengal (Figures 4.1-4.2). The main changes observed were in lipids and protein structure. It was interesting to note that the two *Chlamydomonas* species isolated from northern Saskatchewan (DJX-H and DJX-J) showed little impact from HL exposure, but accumulated greater damage due to RB treatment (Figures 4.3-4.6). To better elucidate the impacts of high light and rose bengal on *Chlamydomonas* cells, we decided to make use of four photosynthetic mutants of *C. reinhardtii*. My goal was to examine the impact of the disruption of specific photosynthetic mechanisms on the infrared spectra when compared to the infrared spectra of wild type (WT) cells. Because the mutations have been characterized, these cell types will allow me to gain further insight into the damage mechanisms resulting from high light and rose bengal exposure. This will better inform us of how these two stresses affect the cells at a physiological and biochemical level. As a starting point I obtained and examined spectra from the mutant cell lines using the synchrotron-based FTIR spectromicroscopy setup used in the previous two chapters. I wanted to see if I could identify differences in the spectra from these cells under control conditions and attribute any differences to predicted physiological and biochemical changes caused by the mutations they carry. The four mutant strains used in this study were selected to probe specific aspects of high-light tolerance and singlet oxygen production:

1) CC-4107 is a cell line derived from a cell wall mutant (*cw15*) and carries defects in the gene encoding Zeaxanthin Epoxidase (*npq2*), and *lor1*, the gene encoding the enzyme needed to convert lycopene into α-carotene. As a result the CC-4107 cells constitutively accumulate zeaxanthin at the expense of violaxanthin and antheraxanthin, while lacking α-carotene, loroxanthin, and lutein (Niyogi 1997; Polle 2001). Due to these differences, the CC-4107 cells accumulate different ratios of LHCI and LHCII polypeptides, and a greater capacity for oxygen evolution under very high light levels (Polle 2001). Normally, cells accumulate violaxanthin which acts as a light absorbing pigment to

support photosynthesis. Under high light conditions, violaxanthin is converted to zeaxanthin by the enzyme violaxanthin de-epoxidase as a short-term acclimation response to protect the photosynthetic apparatus. Under these conditions, zeaxanthin acts as an energy quencher through the thermal dissipation of excess light energy (non-photochemical quenching – NPQ – zeaxanthin dominant) (Baroli et al. 2003). CC-4107 also carried the *lor1* mutation which blocks lutein and other accessory pigments; the primary impact appears to be reduced size of the PSII antenna and reduced photosynthetic efficiency under low and normal light conditions (Polle 2001). The cell line this mutant is derived from is the CC-425/CC-400. The cell wall mutant CC-400 is known to have a rudimentary cell wall, retaining the innermost and outermost layers, W1 and W7 (Harris 2009); the remaining layers are synthesized and excreted into the media without assembly (Voigt, Munzner, and Vogeler 1991). I hypothesize that spectra of the CC-4107 mutant will exhibit the most distinct differences when compared to WT cells, in part as it retains only a partial cell wall. Because of this difference, I expect that there will be differences in the ratios of protein secondary structures, an increase in the ratio of lipids to proteins, and observable differences in the lipid cohort relating to the increased importance of the plasma membrane in maintaining cellular integrity. The altered xanthophyll cycle of CC-4107 cells means that under control conditions some aspects of their spectra may be similar to the spectra of WT cells exposed to/adapted to high light.

2) The *psaF* mutant cells lack the PSAF subunit of Photosystem I. As a result, the cells exhibit diminished rates of plastocyanin docking at PSI and hence a slower rate of electron transfer to PSI (Farah et al. 1995). This strain grows photoautotrophically under low to moderate light levels but dies when exposed to greater than 750 μmol photons $m^2$ $s^{-1}$ (Berry, Brzezowski, and Wilson 2011; Hippler et al. 2000). Under high light conditions, the *psaF* mutation results in a buildup of electrons along the electron transport chain (ETC), which can lead to the production of superoxide if electrons are donated to $O_2$. In addition, excited PSI will remain as $P700^+$ for longer periods of time potentially leading to PSI photoinhibition. As a result, the cells die due to photooxidative damage (Farah et al. 1995). The *psaF* strain used in this study was backcrossed several times to a wild type strain. Thus it has a normal cell wall and minimal other genetic

differences. I predict there will be no observable differences between the spectra of WT and *psaF* cells under control conditions, due to the relatively minor nature of the *psaF* mutation and unaltered photosynthetic rates under low-moderate light conditions

3) The CC-1355 strain has a mutation (*cbn1-48*) in the gene encoding Chlorophyll a Oxidase, and as a result lacks chlorophyll b (Chl *b*) (Tanaka et al. 1998). Chl *b* is a key cofactor of LHC polypeptides but is not found in the reaction centre core complex proteins, which includes the special pair of chlorophyll molecules. There is a variety of literature available on a variety of *C. reinhardtii* Chl *b* mutants. It is often hard to compare these different strains, as some are leaky mutants that produce a small amount of Chl *b* (Eichenberger, Boschetti, and Michel 1986; Michel, Tellenbach, and Boschetti 1983; Park and Hoober 1997; Polle et al. 2000; Tanaka et al. 1998). The closest analogue to *cbn1-48* appears to be the *pg-113* mutant described by Eichenberger et al. (1986). This mutant contains only trace amounts of Chl *b*. As Chl *a* is the core pigments of PSI and PSII, these complexes are still assembled, while LHC proteins are in much lower abundance (Eichenberger et al. 1986; Michel et al. 1983; Park and Hoober 1997; Polle et al. 2000; Tanaka et al. 1998). Data from CC-1335 shows this to also be true (Miskiewicz and Wilson, unpublished results). The decreased LHC antenna accumulation also means a reduced level of carotenoids, such as neoxanthin, violaxanthin, and β-carotene in the thylakoid membranes (Eichenberger et al. 1986; Tanaka et al. 1998). Mutant cells lacking Chl *b* exhibit altered thylakoid stacking due to the diminished levels of LHC proteins (Michel et al. 1983), which may, in part, explain why they have been found to exhibit altered C16:C18 ratios, as well as decreased levels of polyunsaturated fatty acids. The *pg-113* strain accumulated more 16:1 and 18:1 fatty acids, and concomitantly less 16:3 and 16:4, and less 18:3; overall levels of C16 were also decreased (Eichenberger et al. 1986). Thus, I expect to see altered protein structural ratios in the *cbn1-48* strain's FTIR spectra, due to the loss of the alpha-helical LHC proteins, and a change in the lipid compliment.

4) A *psaF cbn1* double mutant was obtained from a cross between the *psaF* and CC-1355 strains. This strain was used in a proof of concept experiment that demonstrated the reduced light absorption caused by Chl *b* deficiency was able to suppress the high-light-

lethal phenotype of the *psaF* deficient strain (Hippler et al. 2000). Given that no significant spectral differences are hypothesized in cells of the *psaF* line, I predict that the spectra obtained from the double mutant will be very similar to those of CC-1355.

## 5.1 Results

Synchrotron FTIR spectromicroscopy was used to obtain infrared spectra from individual living cells of *C. reinhardtii* to allow the comparison of spectral differences between wild type cells and the four mutant strains described above. The spectra were analyzed and inspected as described in Chapters 3 and 4, however the complicated 1800-1240 $cm^{-1}$ fingerprint region (Figures 5.1-2) was found to better differentiate these cell lines than the five primary peaks of the CH stretching region (Figures 5.3-4; 3010 $cm^{-1}$, $CH_{2as}$, $CH_{3as}$, $CH_{2s}$, and $CH_{3s}$) in which the majority contributor to spectra is lipids.

### 5.1.1 Fingerprint Region

Visual examination of the averaged spectra of individual cells under control conditions (Figure 5.1) allowed identification of a number of spectral differences associated with the biochemical make up of the cells, caused by the photosynthetic mutations in the cells being studied. The ~1740 $cm^{-1}$ lipid carbonyl peak appeared to differ in both shape and intensity between cell lines. The shape of the ~1740 $cm^{-1}$ was most similar in WT (dark blue) and CC-4107 (red), with CC-1355 (light blue), *psaF* (green), and *psaF cbn1* (maroon) exhibiting a relative change in the contributions from the 1740 $cm^{-1}$ and 1718 $cm^{-1}$ components, and poorer separation from the amide I peak due to a general increase in absorption in the 1720-1700 $cm^{-1}$ region. With regards to signal strength, CC-4107 cells (red) had a greater overall intensity of the ~1740 $cm^{-1}$ peak (normalized to the amide I peak), with WT and *psaF* exhibiting similar median strength (dark blue, green), and cells of CC-1355 and *psaF cbn1* exhibiting the relatively weakest peak (light blue, maroon). An additional carbonyl second derivative component was located around 1700 $cm^{-1}$. Due to its position and the relative abundance of proteins and lipids in cells, it was generally found within the amide I peak envelope rather than the ~1740 cm lipid carbonyl peak. This second derivative component, when compared to the spectra of WT cells, was weaker in the *psaF cbn1* and CC-4107 lines (maroon, red) and stronger in the spectra of cells of the *psaF* and CC-1355 lines (green, light blue).

Spectral differences were also visible in the protein amide I and amide II peaks. In the spectra of CC-4107 cells (red), the amide I peak maxima occurred at a higher wavenumber, and the peak itself was narrower and less symmetrical. Compared to the secondary structure of WT cells, the second derivative from CC-4107 spectra showed a relative enrichment in α-helix conformations (1655 $cm^{-1}$), a decrease in β-sheet conformations (1629 $cm^{-1}$, likely contains overlapping cellular water contribution around 1635 $cm^{-1}$) as well as increased contributions from the 1680 $cm^{-1}$ and 1608 $cm^{-1}$ components (Barth 2007; Berterame et al. 2016; Miller et al. 2013; Movasaghi et al. 2008). The 1680 $cm^{-1}$ absorption was attributable to unordered and random turns and coils (Barth 2007; Berterame et al. 2016; Miller et al. 2013; Movasaghi et al. 2008), as well as to hydrogen-bonding absorptions of (C=O) in the protein backbone (Dovbeshko et al. 2000). In comparison, the amide I peak was relatively consistent in the spectra of WT, *psaF*, and CC-1355 cells (dark blue, green, and light blue), though examination of the second derivative showed some differences associated with the relatively minor component at 1608 $cm^{-1}$. Cells of the Chl *b*-less CC-1355 line exhibited a reduced contribution of the 1608 $cm^{-1}$ component likely associated with C=C bonds in chlorophylls and chlorophyll-derived pigments (Holt and Jacobs 1955). This change was also present in the spectra of the Chl *b*/*psaF* double mutant *psaF cbn1* (maroon). When compared to WT, *psaF*, or CC-1355, the spectra of these *psaF cbn1* cells exhibited further differences in the amide I peak consistent with changes in protein secondary structure. Spectra of cells of the double mutant *psaF cbn1* exhibited a lower amide I peak position and broader, more symmetrical peak shape due to the relative enrichment of the β-sheet component. The amide I peak was found around 1648 $cm^{-1}$ in the spectra of CC-4107 cells, around 1642 $cm^{-1}$ in the spectra of *psaF cbn1* cells, and 1645/1646 $cm^{-1}$ in all other cell lines.

Spectral differences were also found in the shape of the amide II peak of the different cell lines, leading to differences in the ratio of in the amide I:amide II peaks. However, there was some degree of variation in the ratio in spectra of controls cells of the same cell line obtained on different days. Differences in the peak shape appeared to be more replicable than those of absolute height. Compared to WT cells (dark blue), the amide II peak is narrower in cells of CC-4107 (red), and wider in cell lines lacking Chl *b* (CC-1355, light blue, *psaF cbn1*, maroon). These differences were related to changes in the shape and relative intensity of the 1545 $cm^{-1}$ and 1580 $cm^{-1}$ second derivative components.

The spectra in the fingerprint region below 1500 $cm^{-1}$ contained a series of peaks with overlapping assignments to a variety of functional groups. The peak centred around 1450 $cm^{-1}$ had three second derivative components associated with it, around 1467, 1455, and 1437 $cm^{-1}$. These were likely associated with:

1) A combination of $\delta CH_2$ and $\delta CH_3$ of lipids, phospholipids, and proteins (Movasaghi et al. 2008);

2) The amide II' peak formed through decoupling of amide II's ρNH and νCN vibrations due to H-D exchange off the ρNH group (Barth 2007);

3) δHOD itself had a broad absorption around 1446 $cm^{-1}$, though this peak position shifts several wavenumbers to either side depending on the relative concentration of $H_2O$ and $D_2O$ (Max and Chapados 2002).

As such, differences in the shape, intensity, and position of the 1450 $cm^{-1}$ peak and its second derivative components can be said to describe differences in some combination of protein and/or lipid absorptions. Its diagnostic use was limited except when an overall increase in intensity was paired with decreased intensity of the 1545 $cm^{-1}$ peak. This combination indicated the conversion of the amide II peak to amide II' due to increased hydrogen-deuterium exchange. The spectra of WT cells differed from the spectra of all mutant cells in the degree of separation of the 1467 $cm^{-1}$ and 1455 $cm^{-1}$ second derivative components. In the second derivative spectra of wild type cells, these two components were clearly resolved in comparison to poorer resolution in the photosynthetic mutant lines.

Differences between the spectra of cell lines were also present in the shape of the 1398 $cm^{-1}$ peak as revealed by the relative contribution of the second derivative components at 1398 $cm^{-1}$ and 1380 $cm^{-1}$. Compared to WT spectra, cells of *psaF* and CC-1355 showed a relative decrease in the 1398 $cm^{-1}$ components, and cells of CC-4107 showed a relative increase. The peak at 1338 $cm^{-1}$ also exhibited spectral differences between cell lines. In spectra from WT, CC-4107, and *psaF* cells, it had two distinct contributions at 1346 $cm^{-1}$ and 1330 $cm^{-1}$, with the second contribution reduced in cells of CC-4107. In cells lines lacking Chl *b* (CC-1355, *psaF cbn1*) the peak was downshifted to 1335 $cm^{-1}$ and the second derivative contained only one broad

component. These two contributions can be associated with split $CH_2$ wagging, or $\omega CH_2$ and $\delta CH$ of polysaccharides with ring components (Movasaghi et al. 2008).

One of the most immediately striking spectral differences between the spectra obtained from these cell lines was the presence of an extremely strong, broad peak in the *psaF* cell line underlying the spectra from 1315-1240 $cm^{-1}$ and centred around 1260 $cm^{-1}$. This is a region associated both with $PO_4^-$ and the amide III protein peak (Movasaghi et al. 2008). Given the relatively minor predicted physiological differences between WT and *psaF* cells, this peak remains unassigned. Other unassigned peaks in this region also showed spectral differences between cell lines. The peak at 1308 $cm^{-1}$, sometimes assigned to amide III and sometimes to unknown compounds (Movasaghi et al. 2008), was stronger and better defined in cells of the CC-4107 line and those lacking Chl *b* (CC-1355, *psaF cbn1*) than it was in cells of WT or *psaF*. Spectral differences were also found in the 1285 $cm^{-1}$ peak. Absorptions in this region are sometimes assigned to the amide III peak, specific proteins, or general NH deformation (Movasaghi et al. 2008). Of interest in plant and algal cells is an alternate assignment to tetrapyrrole compounds, such as those in chlorophyll and cytochromes (Derenne et al. 2013). Looking at the second derivative of this component, to negate the influence of the strong, broad 1260 $cm^{-1}$ peak, this component was stronger in the spectra of CC-4107 cells and was weaker amongst cells of lines lacking Chl *b* (CC-1355, *psaF cbn1*). This suggests that its absorption may be partly related to photosynthetic or carotenoid compounds.

Principal component analysis of this region (1800-1240 $cm^{-1}$) confirmed that it was possible to separate the spectra of these photosynthetic mutant cell lines (Figure 5.2). PC-1 (purple horizontal line) described 37% of total variability and was driven by differences in the relative abundance of lipids (intensity of ~1740 $cm^{-1}$ lipid carbonyl) and protein secondary structure (shape and position of the amide I and II peaks). This was useful in separating the spectra of CC-4107 cells (red circles: increased relative abundance of lipids, increased abundance of α-helixes, narrow amide II) and the spectra of the *psaF cbn1* double mutant (maroon triangles: decreased relative abundance of lipids, increased relative abundance of β-sheets, broad amide II peak) from the spectra of WT, *psaF*, and CC-1355 cells (dark blue squares, green triangles, light blue diamonds) which were located around the origin of PC-1. PC-2 (green horizontal line, 24%) primarily describes the strong, broad 1260 $cm^{-1}$ peak found only in the spectra of cells of the *psaF* mutant.

The origin of this peak is unknown. In PCA space, the spectra of *psaF* cells (green triangles) plotted along the positive end of the PC-2 axis and all other spectra plot along the negative end. PC-3 (21%, yellow horizontal line) referred to several peaks in the complex fingerprint region at 1360-1260 $cm^{-1}$ and was consistent with the changes in this region seen in the Chl *b* mutants (CC-1355, light blue diamonds; *psaF cbn1*, maroon triangles), namely broadening and downshifting of the 1340 $cm^{-1}$ peak, increased intensity of the 1308 $cm^{-1}$ peak, and decreased intensity of the 1285 $cm^{-1}$ peak.

### 5.1.2 CH Stretching Region

When examining the high wavenumber CH region (3050-2800 $cm^{-1}$), a lesser degree of spectral variation was observed (Figure 5.3). This was reflected in the degree to which the cell lines were separated in PC space (Figure 5.4). The spectra presented in Figure 5.3 were normalized to the amide I peak, then offset corrected at 3040-3010 $cm^{-1}$. Due to underlying baseline variation, which could not be adequately corrected, the second derivative was used for PCA. Visual examination of the spectra showed the same basic peaks present amongst all cell lines, as expected. The 3010 $cm^{-1}$ peak is associated with the C-H stretching vibration of unsaturated lipids. Both its absolute intensity and its intensity relative to $CH_{2as}$ was greatest in cells of CC-4107 (red). The spectra from WT and *psaF* cell lines (dark blue, green) exhibited similar intensities in this region, while spectra from cell lines lacking Chl *b* (CC-1355, light blue; *psaF cbn1*, maroon) exhibit reduced intensity in the 3010 $cm^{-1}$ peak. The peak was narrowest and best resolved from the $CH_{3as}$ in WT and CC-4107 cell lines, with the others showing broader 3010 $cm^{-1}$ that were more poorly resolved. Positions of the $CH_2$ and $CH_3$ peaks exhibited slight differences between cell lines. The spectra obtained from all mutant cell lines exhibited a higher peak position for $CH_{3as}$, $CH_{2as}$, and $CH_{3s}$. Only cells of the CC-4107 line exhibited a higher peak position for $CH_{2s}$, which was the most reliable indicator of changes in the degree of membrane disorder (Lewis and McElhaney 2013). In the second derivative spectra of cells lacking Chl *b* there was an additional unassigned contribution present at 2885 $cm^{-1}$ (Figure 5.3, blue arrow), similar to that in the spectra of the cells of DJX-H and DJX-J that were exposed to exogenous oxidative stress (as described in Chapter 4).

Principal component analysis (Figure 5.4) did a good job of separating the spectra from WT and CC-4107 cells, but overlap remained between *psaF*, CC-1355, and *psaF cbn1* spectra. PC-1 and PC-2 described the peak widths and positions. PC-1 (64%, purple horizontal line) helped

separate the spectra of WT and CC-4107 from the other cells, which had stronger unsaturated lipid peaks (3010 $cm^{-1}$) and narrower $CH_2$ and $CH_3$ peaks when compared to the spectra of *psaF*, CC-1355, and *psaF cbn1*. The position at which the $CH_2$ and $CH_3$ peaks were found was described by PC-2 (21%, horizontal green line). This was most successful in separating the spectra of WT and CC-4107 cells (dark blue squares, red circles). CH peak positions were consistently upshifted in the spectra of CC-4107 cells. This loading was less useful in differentiating the spectra of *psaF*, CC-1355, and *psaF cbn1* highlighting the similarity of the cell types. These three mutant lines exhibited more day to day variation in peak position and generally occupied an intermediate distance along this axis in PC space.

## 5.2 Discussion

Beginning this portion of the thesis, my goal was to characterize the spectra of a set of *C. reinhardtii* photosynthetic mutants. Each of the mutant cell types has distinct biochemical and physiological differences due to the genetic lesion(s). Not only did I want to see how similar the cells were to each other, but I wanted to know if I could distinguish between them using the live cell-imaging synchrotron FTIR spectromicroscopy system. I felt this was important because the effects of oxidative stress caused by high-light exposure and/or rose bengal treatment can be quite subtle. Being able to distinguish between the cell types would give me greater confidence when I interpret the impact these stresses have on the cells in Chapter 6. I also wanted to know if the biochemical differences predicted to exist between the cell types based on existing knowledge of each of the mutations, would be observable with the system I am using. While the differences were subtle, consistent differences were observable.

Spectra of cells of the CC-4107 differed the most strikingly from the spectra of all other cell lines, indicating high degrees of physiological and metabolic differences (Figures 5.1, 5.3, red line). In principal component space, they were clearly separated from all other spectra in both the 1800-1240 $cm^{-1}$ fingerprint region and CH stretching region (Figures 5.2, 5.4, red circles). These cells exhibited dramatic differences in the relative abundance of lipids and composition of lipid cohort, as well as in the overall secondary structure of cellular protein pools. Cells of the CC-4107 line carry three mutations that may impact infrared spectra. Two of these mutations, *npq2-5* and *lor1*, result in altered accumulations of carotenoids and xanthophylls (Niyogi 1997). The *npq2* mutation disrupts the enzyme zeaxanthin epoxidase and results in accumulation of zeaxanthin at

the expense of antheraxanthin and violaxanthin (Niyogi 1997). The *lor1* mutation disrupts lutein and loroxanthin synthesis (Baroli and Niyogi 2000). The third mutation, *cw15*, results in a partial cell wall deficiency in which cells lack cell wall layers W2-6 while retaining W1 and W7 (Harris 2009). As the cell wall of *C. reinhardtii* is primarily composed of glycoproteins, this could potentially impact protein-related absorption peaks. To lesser extent, this would also impact peaks associated with carbohydrates. Previous FTIR work on the *C. reinhardtii* cell wall mutant CC-400, which carries only the *cw15* mutation, indicated that this mutation alone has a minimal impact on the shape, position, and relative intensities of these peaks, though there was a slight increase in the strength of the ~1740 $cm^{-1}$ lipid carbonyl in relation to the amide I protein peak (Goff et al. 2013). Because the *C. reinhardtii* cell wall is composed primarily of glycoproteins, this may have an effect on the protein-related absorbance bands - for example, amide I and II. The *cw15* defect may also lead to altered CH absorbance as fewer carbohydrates would be present in the cell wall. However, neither of these cases appear to be supported by the spectra (Figs 5.1 and 5.3). When compared to the spectra of WT cells, spectra of CC-4107 cells had much stronger absorptions in the ~1740 $cm^{-1}$ lipid carbonyl peak and the 3010 $cm^{-1}$ unsaturated lipid peak, indicating relatively higher levels of total lipids with a greater degree of unsaturation. In addition, the $CH_2$ and $CH_3$ peaks had higher positions, including the crucial $CH_{2s}$ peak position used as an indicator of membrane disorder. The mutations carried by the CC-4107 cell line do not directly impact lipid production, but previous work (Goff 2012) indicated that the cohort of lipids and phospholipids present is more diverse and are often modified in response to changes in cell wall structure. This may be due to their increased role in cellular homeostasis. Again, the relative strength increase may be due to normalization to the amide I band, and the decrease in total proteins present when the cell wall is not present.

Spectra of CC-4107 cells also show differences in protein secondary structure in relation to the spectra of WT cells or the cell wall mutant CC-400 (Goff et al. 2013). The clearest differences were visible in the amide I peak and its second derivative, where we saw an upshift and narrowing of the amide I peak, due to a relative enrichment of α-helixes and loss of β-sheets, as well as increase absorption of the 1680 $cm^{-1}$ (turns and globular proteins) and 1608 $cm^{-1}$ (chlorophyll/pigment) components. The amide II peak similarly narrowed. These differences could be attributed to the partial loss of the glycoprotein cell wall. It is interesting to note, however, that exposure to high light in cells of the WT and *psaF* lines resulted in upshifting and narrowing

of the amide I peak so that it more closely resembles that of CC-4107. In WT cells, alteration of the xanthophyll pool to favour zeaxanthin occurs in response to high-light stress and triggers physiological adaptations associated with nonphotochemical quenching. As such, I suggest that mutation-induced alteration of the xanthophyll pool results in similar physiological responses to those observed by high-light induced alteration of the xanthophyll pool, as measured by FTIR spectroscopy. In addition, the unassigned peaks at 1308 $cm^{-1}$ and 1285 $cm^{-1}$ were sharper and better resolved than in the spectra of WT cells. As hypothesized, the spectra of CC-4107 cells exhibited changes in protein secondary structure, lipid cohort and membrane organization, and the protein secondary structure was indeed more similar to that of high light-adapted WT cells than WT cells under control conditions.

Of the four photosynthetic mutant lines described in this work, *psaF* was predicted to have the least resultant physiological changes under control conditions. The PsaF protein makes up a small portion of the total protein present within an individual cell, and its loss does not impact the assembly of any other protein complexes. Under normal light conditions, its metabolism and physiology are near identical to that of WT cells. This predicted structural and physiological similarity is largely borne out by the very similar spectra obtains from *psaF* and WT cells. Importantly and unexpectedly, the spectra of *psaF* cells could be clearly separated from the spectra of all other cells lines based on the strong, broad absorption centred around 1260 $cm^{-1}$ (Figure 5.1, green trace), and described by PC-2 (Figure 5.2, green horizontal line). This difference is not explainable with my data, but the 1310-1240 $cm^{-1}$ region is commonly associated with amide III peaks of proteins, as well as a variety of phosphate groups including those associated with phospholipids and DNA (Movasaghi et al. 2008). A similar unassigned peak was present in cells of the DJX-H line (Figure 3.5, 3.8). In DJX-H cells this absorbance peak decreased dramatically in response to rose bengal (RB, HLRB) exposure (Figure 4.3). It will be interesting to see if the *psaF* strain similarly loses this peak when its spectra are examined in Chapter 6.

Neither of the potential assignments for this peak are consistent with what we know of the physiology or metabolism of the *psaF* line, suggesting that there may be unknown knock-on differences induced by the loss of the PSAFG protein subunit, or possibly something hidden in the genetic background of this strain, because of the absence of this peak in spectra from the *psaF cbn1* cells. In the case of the *psaF* cell line, virtually no spectral differences were predicted

between WT and *psaF* cells under control conditions. The presence of a strong, broad peak around 1260 $cm^{-1}$ raises a number of questions as to its infrared assignment and physiological source. Additional minor differences in lipid-associated peaks (changes in relative contributions of the second derivative components of the ~1740 $cm^{-1}$ lipid carbonyl, decreased resolution of the 3010 $cm^{-1}$ unsaturated lipid peak) and protein second derivatives (1680 $cm^{-1}$, 1580 $cm^{-1}$), as well as the 1398 $cm^{-1}$ peak are more within the range of minor metabolic differences induced by high light exposure in WT cells (Figure 4.1, 4.2) could suggest that minor degrees of oxidative stress may be present under control light conditions.

The spectra of cells carrying mutations that result in a loss of Chl *b* (CC-1355, *psaF cbn1*) show a specific set of differences when compared to other cell lines. They share a series of changes related to lipid profiles, including a relative decrease in the intensity of the ~1740 $cm^{-1}$ lipid carbonyl peak and changes in the relative contributions of its second derivative components Figures 5.1, 5.2), decreased unsaturation, and increased width of the CH peaks (Figures 5.3, 5.4) suggesting changes in overall lipid abundance, diversity, and membrane structure. Not only do these cells lack Chl *b*, but as a result they also are unable to accumulate many of the LHC proteins associated with PSI and PSII, and those that they do are often in lower abundance (Eichenberger et al. 1986; Michel et al. 1983; Park and Hoober 1997; Polle et al. 2000; Tanaka et al. 1998). Thus, one might expect significant changes in the protein absorbance peaks, and perhaps in the lipid absorbance regions because of the significant interactions that the LHC proteins would have with the thylakoid membrane lipids. They are also expected to have a slightly altered lipid cohort, specifically the enrichment of mono-unsaturated 16:1 and 18:1 fatty acids at the expense of polyunsaturated fatty acids 16:3, 16:4, and 18:3 (Eichenberger et al. 1986). These predicted differences in lipid cohort are present in the spectra and PCA loadings, but changes associated with protein peaks were subtler. Strikingly, spectra of cells of the double mutant *psaF cbn1* completely lack the strong, broad contribution around 1260 $cm^{-1}$. Both CC-1355 and *psaF cbn1* cell lines show evidence of a CH contribution at 2885 $cm^{-1}$ under control conditions that is consistent with that seen in the spectra of DJX-H and DJX-J cells after rose bengal treatment (Figures 4.4, 4.6). As hypothesized, the spectra of the Chl *b* mutants were very similar to each other when compared to the spectra of WT cells, despite the presence of unexpected spectral differences between WT and *psaF* cells

While the nature and underlying mechanisms of some of the changes observed in the spectra of these photosynthetic mutants are unknown – particularly those in previously unassigned peaks – we can observe some differences which correspond to the predicted biochemical differences. Amongst these, it is reasonable to suggest the second derivative component at 1608 $cm^{-1}$ is associated with chlorophyll due to its decreased intensity in the Chl *b* mutants. Other work has assigned an absorption in this region to C==C and C==N in chlorophyll *a*, chlorophyll *b*, as well as pigments and compounds derived from them (Ballschmiter and Katz 1972; Holt and Jacobs 1955; Weigl and Livingston 1953). Similarly, there is suggestion that the absorption at 1285 $cm^{-1}$, which overlaps with possible assignments for amide III peaks, is at least partly due to the absorption of tetrapyrroles such as chlorophyll (Derenne et al. 2013).

## 5.3 Summary and Conclusions

In this chapter, we have differentiated between a set of four photosynthetic mutant cells of *C. reinhardtii* based on FTIR spectra of individual cells. Using principal component analysis, I could confirm the significance of spectral differences present upon visual analysis of the spectra.

As I found in the previous chapters, the strongest spectral differences, as well as those that were the most straightforward to interpret, were mostly associated with the lipid and protein peaks. This is reflective of differences in relative abundances of different types of proteins present and their secondary structure, as well as lipid cohort, unsaturation, and membrane ordering. Many of these changes could be directly correlated to what is known about the physiological and metabolic impacts of the photosynthetic mutations being studied. One key example of this was the decreased intensity of the 3010 $cm^{-1}$ olefinic lipid peak in the Chl *b* cell lines known to have decreased degrees of lipid unsaturation. Another, subtler example was the relative strength of the 1608 $cm^{-1}$ second derivative component. In the spectra of mutants lacking Chl *b* it decreased, suggesting/confirming that in the spectra of *Chlamydomonas* spp. it is primarily associated with absorption from chlorophyll and related compounds, rather than a downshifted protein secondary structure.

Spectra of the CC-4107 mutant line showed the largest spectral differences when compared to wild type cells or to other photosynthetic mutations. Spectra of the *psaF* mutant suggested that the physiology and metabolism of these cells were altered in ways exceeding those anticipated by

what is known about its genetic background. Finally, the loss of Chl *b* appears to be the stronger driving factor of spectral differentiation when compared with the loss of the *psaF* mutant.

Knowing these details about the spectra of the four photosynthetic mutants, and my ability to distinguish between the spectra of their control cells, I can go forward, exposing them to high light and/or rose bengal, and look for specific effects of these stresses on the biochemical makeup of the individual cells.

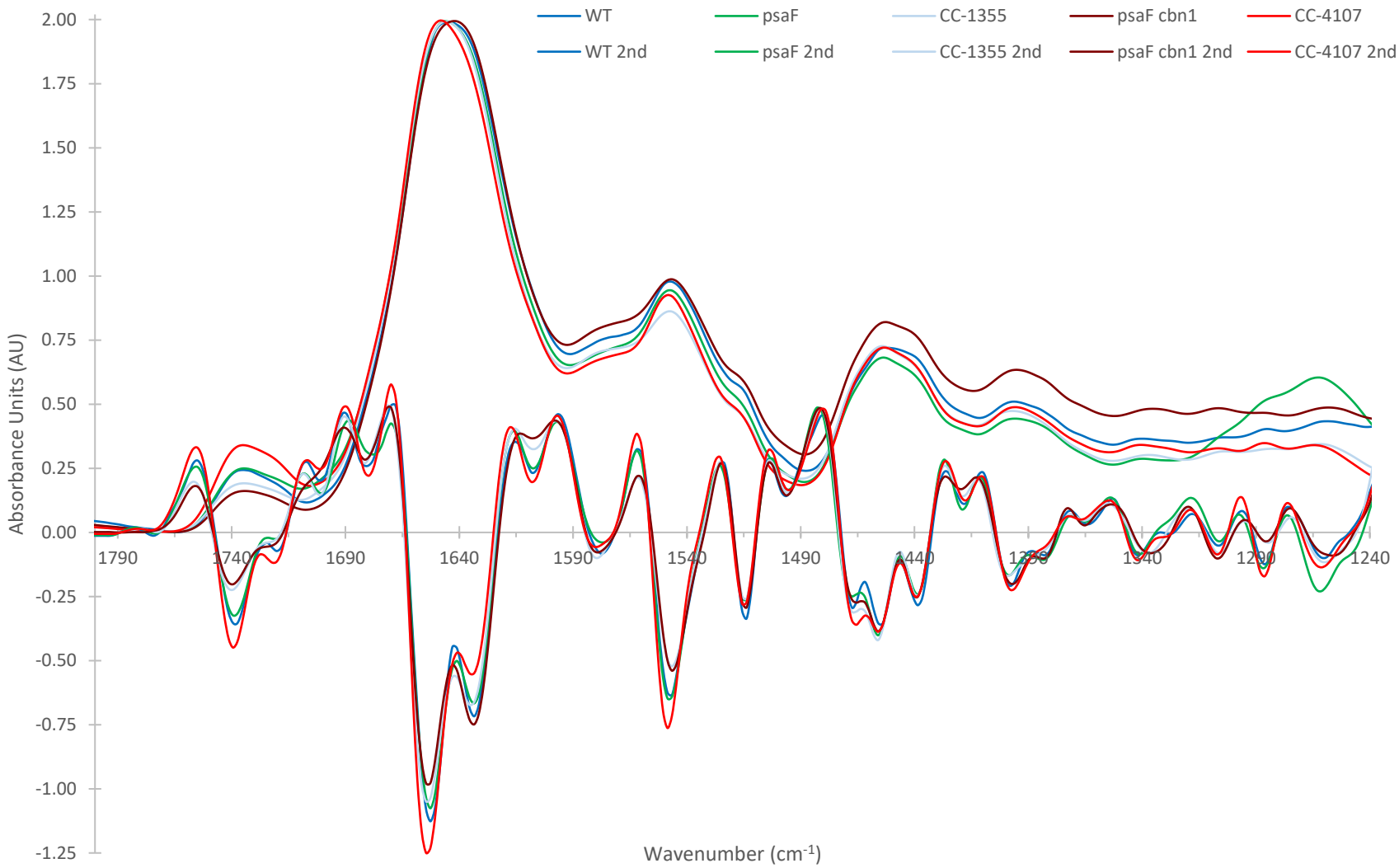


*Figure 5.1 - FTIR measurements of the 1800-1240 cm$^{-1}$ region in* Chlamydomonas reinhardtii *(WT) and four of its photosynthetic mutants: a zeaxanthin hyperaccumulator (CC-4107), a mutant lacking the psaF subunit (*psaF*), a mutant lacking chlorophyll B (CC-1355), and a double mutant lacking both the psaF subunit and chlorophyll B (*psaF cbn1*). Spectra are normalized to amide I and are the average of five to six days.*

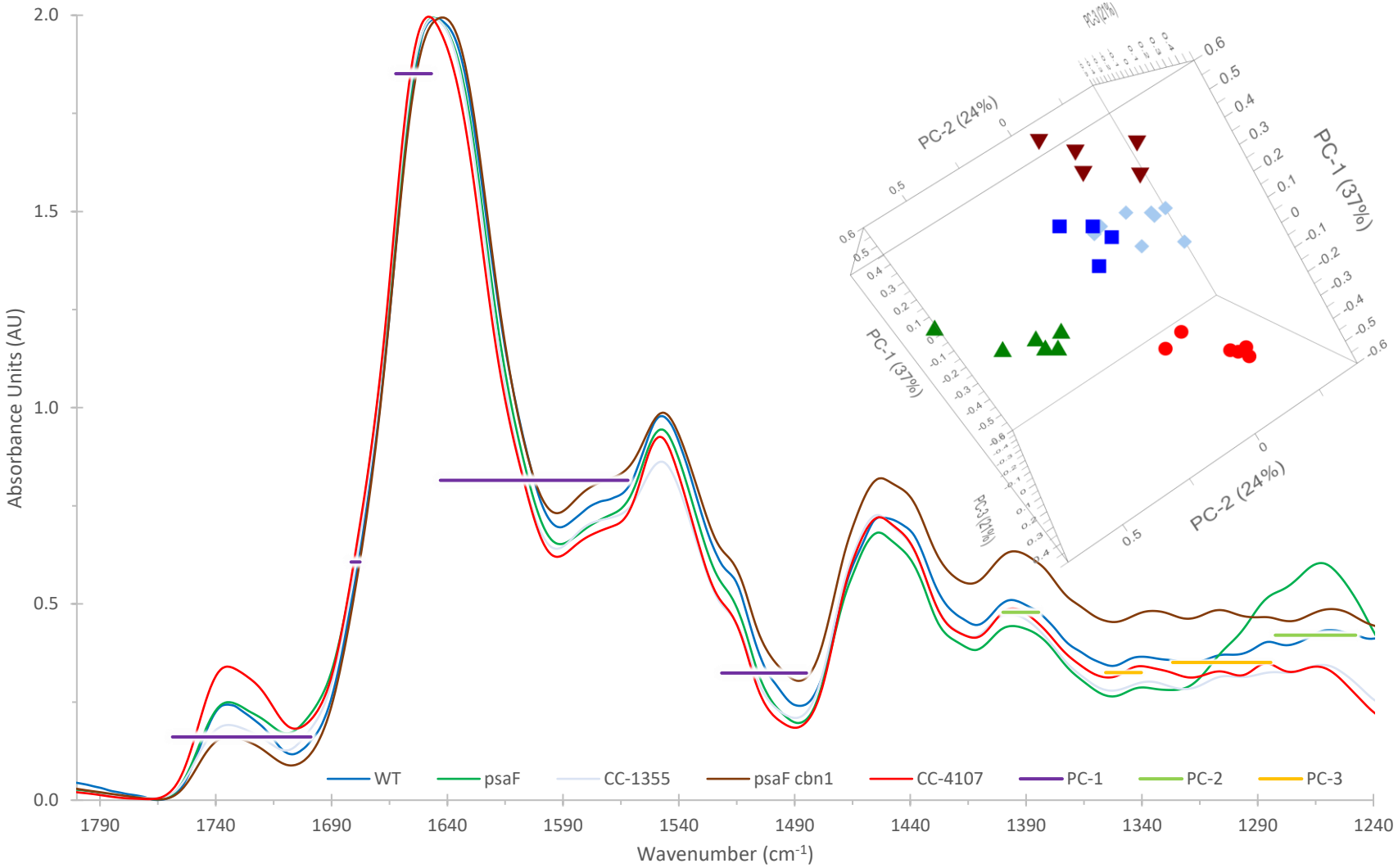


*Figure 5.2 – FTIR measurements and principal component analysis of the 1800-1240 cm$^{-1}$ region in* Chlamydomonas reinhardtii *(WT) and four of its photosynthetic mutants: a zeaxanthin hyperaccumulator (CC-4107), a mutant lacking the psaF subunit (*psaF*), a mutant lacking chlorophyll B (CC-1355), and a double mutant lacking both the psaF subunit and chlorophyll B (*psaF cbn1*). Spectra are normalized to amide I and are the average of five to six days. (PC1-3: 37%, 24%, 21%.)*

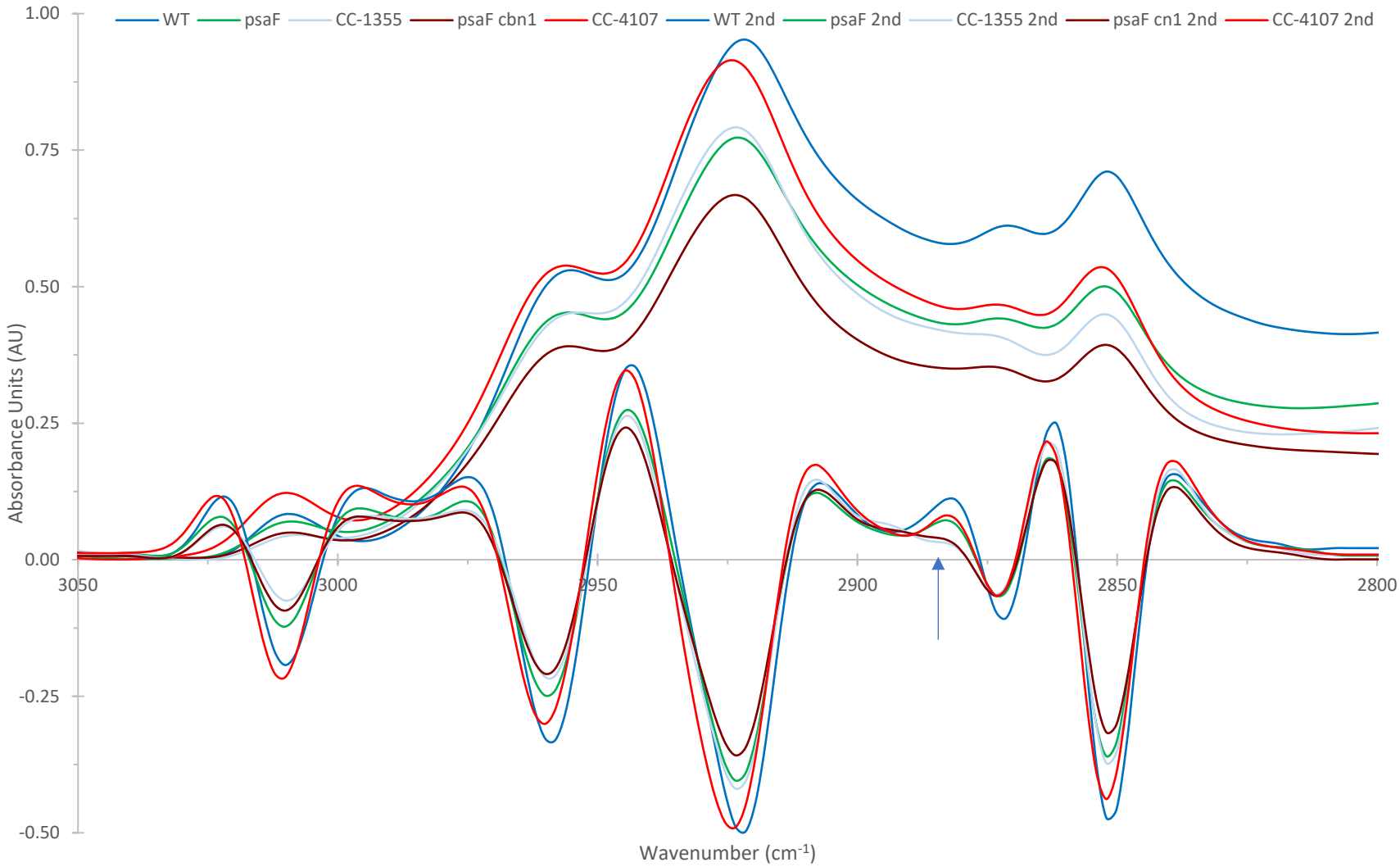


*Figure 5.3 - FTIR measurements of the 3050-2800 $cm^{-1}$ region in* Chlamydomonas reinhardtii *(WT) and four of its photosynthetic mutants: a zeaxanthin hyperaccumulator (CC-4107), a mutant lacking the psaF subunit (*psaF*), a mutant lacking chlorophyll B (CC-1355), and a double mutant lacking both the PsaF subunit and chlorophyll B (*psaF cbn1*). Spectra are normalized to amide I and offset corrected 3040-3010 $cm^{-1}$ and are the average of five to six days. Arrow indicates unknown contribution at 2885 $cm^{-1}$.*

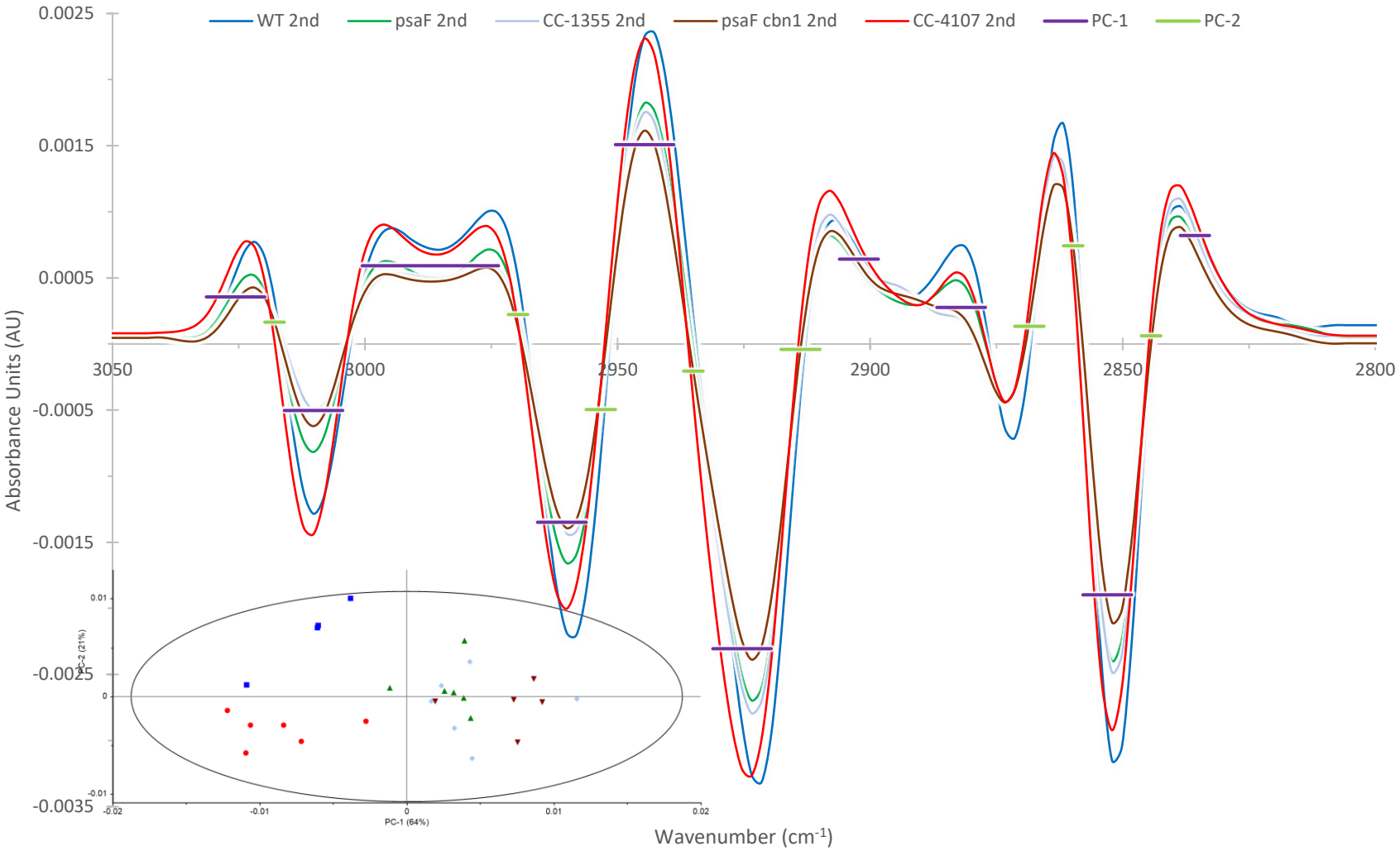


*Figure 5.4 - FTIR measurements and principal component analysis of the 3050-2800 cm$^{-1}$ region in* Chlamydomonas reinhardtii *(WT) and four of its photosynthetic mutants: a zeaxanthin hyperaccumulator (CC-4107), a mutant lacking the PsaF subunit (*psaF*), a mutant lacking chlorophyll B (CC-1355), and a double mutant lacking both the PsaF subunit and chlorophyll B (*psaF cbn1*). Spectra are normalized to amide I and offset corrected 3040-3010 cm$^{-1}$ and are the average of five to six days. (PC1-2: 64%, 21%.)*

*Table 5.1 – Overview of major differences in the infrared spectra of cells of photosynthetic mutants relative to the spectra of wild type cells of* Chlamydomonas reinhardtii. *CC-4107 is cell was deficient (lacks W2-6), accumulates zeaxanthin, and lacks lutein and other xanthophylls.* psaF *lacks the PSAF subunit. CC-1355 lacks chlorophyll* b *and may have an altered lipid profile. The double mutant (*psaF cbn1*) carries the differences associated with the loss of chlorophyll* b *and the lack of the PSAF subunit.*

| | | Change compared to WT cells | | | |
|---|---|---|---|---|---|
| | | CC-4107 | *psaF* | CC-1355 | *psaF cbn1* |
| 3010 | Height | + | | - | - |
| | Shape | | Δ | Δ | Δ |
| CH | Width | | + | + | + |
| | $CH_{2as}$ position | up | up | up | up |
| | $CH_{2s}$ position | up | | | |
| | 2885 | | | + | + |
| 1740 | Intensity | ++ | | - | - |
| | Shape | | Δ | Δ | Δ |
| AI | Position | up | | | down |
| | Width | -- | | | + |
| | α-helix:β-Sheet | ↑ α-helix | | | ↑ β-sheet |
| | 1608 | + | | - | - |
| AII | Height | - | - | - | |
| | Shape | Δ | | Δ | Δ |
| 1450 | Height | | - | | + |
| | 1467 | + | - | - | - |
| | 1455 | Δ | Δ | Δ | Δ |
| | 1437 | - | - | - | - |
| 1398 | Shape (1398/1380) | Δ | Δ | Δ | Δ |
| 1338 | Shape | | | Δ | Δ |
| | Position | | up | down | down |
| | 1308 | + | | + | + |
| | 1285 | + | | - | - |
| | 1260 | | +++ | | |

# CHAPTER SIX

# EFFECTS OF OXIDATIVE STRESSORS ON PHOTOSYNTHETIC MUTANTS OF *CHLAMYDOMONAS REINHARDTII*

## 6.0 Introduction and Goals

As I have continued to build on and refine my FTIR spectromicroscopy measurements of green algal cells, a number of questions remain when considering how the biochemical makeup of cells changes following exposure to high light and/or rose bengal. Using a combination of high light and rose bengal exposures I assessed how the chemical components of cells are damaged by singlet oxygen and examined both the mechanism of action and the cells' sensitivity to the singlet oxygen inducing conditions (Chapter 4). When comparing the responses of different species of *Chlamydomonas*, I saw that *C. reinhardtii* and the *Chlamydomonas* DJX- species exhibited significantly different responses to individual stressors. For example, spectra of the DJX- species showed limited response to the high-light treatment, while in spectra obtained from *C. reinhardtii* cells changes in lipid and protein profiles could be observed. When looking at the spectra of DJX- species in response to rose bengal (RB, HLRB), it was clear that their plasma membranes were more sensitive to singlet oxygen produced by RB than were those of *C. reinhardtii* cells.

Moving beyond the large-scale observations of lipid and protein changes in response to high light and/or rose bengal, the differential changes could be difficult to interpret both due to the complexity of the systems I am studying, but also because there are no true benchmarks that can be used to study living green algal cells. In Chapter 5, I set out to see if it was possible to distinguish between a set of photosynthetic mutants of the model alga, *C. reinhardtii*, as well as to ascertain what spectral differences were present that might influence their spectral response to high light and/or rose bengal. Based on the accumulated knowledge using *C. reinhardtii* as a model system for the study of photosynthesis, and previous characterizations of these four mutant cell lines, it should be possible to more easily assign changes in the cellular biochemical makeup, as measured using FTIR spectromicroscopy. Thus, in this chapter I will compare the CC-4107 (*npq2 lor1*), *psaF*, CC-1355, and *psaF cbn1-48* (cross of the *psaF* and CC-1355 lines) cells following treatments with high light, rose bengal, and a combination of the two stressors.

Based on previous research, I expect that CC-4107 cells will be less sensitive to high light (and potentially rose bengal, and therefore HLRB), because it constitutively accumulates greater amounts of zeaxanthins, giving it a correspondingly higher capacity to dissipate excess light energy via nonphotochemical quenching. The zeaxanthin that CC-4107 cells accumulate is also a potent antioxidant, which can interact with singlet oxygen in a manner that is not damaging to the cell.

I know that the *psaF* strain is more sensitive to high light as that is how the mutant strain was selected (Farah et al. 1995; Hippler et al. 2000). It appears to be high light sensitive due to photooxidative damage caused by PSI overexcitation (Berry et al. 2011), suggesting that the high light sensitivity arises due to damage in the chloroplast. It is thus not clear if rose bengal will have a greater effect on the *psaF* cells than the wild type cells. The CC-1355 mutant is disrupted in the chlorophyll *a* oxidase gene and thus does not produce chlorophyll *b*. As a result, it does not accumulate a full set of light harvesting proteins (Miskiewicz and Wilson 2017). The resulting diminished absorptive cross-section of PSII and PSI means that fewer photons are absorbed and by extension, the cells would "perceive" the irradiance to be lower than it is. Thus, I expect that CC-1355 cells will be less affected by high-light exposure than the control cells. However, as mentioned for the *psaF* cells, it is not clear what exposure to rose bengal will do. A side effect of a lack of light harvesting proteins is a diminished abundance of carotenoids, and likely an altered thylakoid lipid composition, as suggested by the measurements discussed in Chapter 5. However, because the light-harvesting proteins, their carotenoids, and the thylakoid membranes are located in the chloroplast, the alterations may have no impact on the cells' sensitivity to rose bengal generated singlet oxygen.

In their research, Hippler et al. (2000) demonstrated that when *psaF* cells were crossed with CC-1355, the lack of chlorophyll b was able to suppress the high-light sensitive phenotype of the *psaF* mutation. Thus, I expect that the double mutant cells will be less sensitive to high-light exposure than the *psaF* cells. It is not clear what impact the two mutations will have when it comes to rose bengal exposure, but I expect that by examining the three cell types (*psaF*, CC-1355, and *psaF cbn1*), I will gain insight into the molecular mechanisms of rose bengal induced damage.

Four photosynthetic mutants of wild type *Chlamydomonas reinhardtii* were utilized to examine the impact of the disruption of specific photosynthetic mechanisms on cellular damage

caused by exposure to high light, the singlet oxygen generator rose bengal, or a combination of these two treatments. The expected effects on the four mutant strains were:

1) The combination of mutations in CC-4107 effectively results in cells that are preadapted to high light exposure. One study demonstrated that CC-4107 is less sensitive to $^1O_2^*$ generated by rose bengal (Baroli et al. 2003). As such, cells of the CC-4107 should exhibit a decreased sensitivity to high light exposure or rose bengal, with less observable impact on its biochemical makeup following either the HL, RB, or HLRB treatments. The altered xanthophyll cycle of CC-4107 cells means that under control conditions the spectra may be similar to the spectra of WT cells exposed to/adapted to high light.

2) The *psaF* mutant cells lack the PSAF subunit of Photosystem I. As a result, it is thought that the cells are killed by the accumulation of reactive oxygen species generated by PSI charge recombination events (Berry et al. 2011; Rochaix, Fischer, and Hippler 2000). As such, the *psaF* strain should be affected to a greater degree by high-light exposure than are wild type cells. I predict there will be no observable differences between the spectra of WT and *psaF* cells under control conditions, due to the relatively minor nature of the *psaF* mutation and unaltered metabolic rate under low-moderate light conditions. The mechanism for this difference does not suggest that exposure to RB will result in a response differentiable from that of WT cells.

3) The CC-1355 strain has a mutation (*cbn1-48*) in the gene encoding Chlorophyll *a* Oxidase, and as a result lacks Chl *b* (Tanaka et al. 1998). Knock on effects of the *cbn1-48* mutation, such as diminished LHC content, lower levels of protective carotenoids, and altered lipid content make it difficult to predict what impact the high light and/or rose bengal treatments will have on the biochemical makeup of these cells. There may also be potential effects observed from the resultant decrease in photosynthetic efficiency and rates of photosynthesis and metabolism.

4) *psaF cbn1*: The result of a cross between the *psaF* and CC-1355 strains, I expect that the double mutant will be more tolerant to high light than the *psaF* strain, however, the impact that the *cbn1* mutation has on the overall damage accrued in this strain is hard to predict.

Thus, even though we started with the idea that these mutants should give specific responses that will be predictable because we have a good understanding of how the cellular physiology is altered in these strains, we can already see – based on the measurements made in Chapter 5, and a more thorough investigation of the impacts that these mutations could have on the cells – that even simple-seeming systems lead to significant complications when looking at the biochemical makeup of living cells using FTIR absorbance spectromicroscopy.

## 6.1 Results

### 6.1.1 Wild Type

The response of wild type *C. reinhardtii* cells to HL, RB, and HLRB treatments was covered in depth in Chapter 4. A very brief overview is provided here (Figures 6.1, 6.2) to enable the comparison of mutant and wild type response to high light and rose bengal. All three treatments had an impact on the composition of the cellular lipid cohort and induced changes in membrane disorder. These changes were more pronounced in the spectra of rose bengal treated cells (RB, HLRB), which also show indications of altered membrane permeability. This suggested that high-light exposure resulted in thylakoid-localized lipid damage, while exogenous rose bengal caused broader cellular damage to lipids. The spectra of cells exposed to HLRB showed evidence of the formation of lipid oxidation by-products. Characteristic changes in protein secondary structure were seen in the spectra of HL cells, suggesting that HL exposure altered their folding pattern. This could be due to damage, or cellular response mechanisms that involve protein refolding. Changes in protein secondary structure observed in the spectra of HLRB exposed cells were consistent with H-D exchange and the formation of protein aggregates, both suggestive of significant oxidative damage.

### 6.1.2 CC-4107

Cells of the CC-4107 line exposed to HLRB consistently presented with two subpopulations that could be clearly differentiated based on spectral differences. One smaller population showed virtually no spectral changes induced by HLRB exposure. These spectra were very similar to those of HL or RB cells, showing minimal differences in comparison to control cells. The subpopulation of unaffected cells was removed from analysis.

#### 6.1.2.1 Fingerprint region

The spectra of CC-4107 cells exposed to the stresses used in this study (Figure 6.3) exhibited patterns of change that shared some similarities to those seen in WT cells (Figure 6.1). The spectra of CC-4107 cells under control conditions (Figure 6.3, dark blue) shared a number of similarities with the spectra of WT cells exposed to high light (Figure 6.1, red), particularly in the amide I peak, indicating similarities in protein secondary structure. The overall response of the CC-4107 cell line to high light and/or rose bengal appeared muted in comparison to that of the WT cell line. This was particularly true when comparing the spectra of CC-4107 C and HL exposure cells. The overall relative intensity of the ~1740 $cm^{-1}$ lipid carbonyl peak decreased slightly in the spectra of HLRB treated cells, due to a relative decrease of the 1740 $cm^{-1}$ component, associated with early stages of oxidative lipid damage. There was a slight decrease in the relative intensity of this component in the spectra of CC-4107 RB-treated cells as well. Overall changes in the intensity and shape of this peak were less than is seen in WT. WT HLRB cells also showed greater reshaping of the ~1740 $cm^{-1}$ lipid carbonyl than seen in CC-4107 HLRB. In WT HLRB spectra there was a greater relative decrease of the 1740 $cm^{-1}$ component and broad increase in the 1720-1700 $cm^{-1}$ region associated with the formation and breakdown of lipid oxidation products.

Patterns of change observed in protein secondary structure in response to RB and HLRB were similar in pattern to those seen in WT cells. Exposure to RB resulted in a change in the α-helix to β-sheet ratio in the favour of α-helixes, while HLRB treatment resulted in a change in this ratio in the favour of β-sheets. Additionally, exposure to HLRB resulted in downshifting of the 1680 $cm^{-1}$, α-helix, and β-sheet components, as well as decreased intensity and downshifting of the 1608 $cm^{-1}$ component. These changes observed are similar to those seen in the WT cell line, though they lack the increased peak widths seen in the components in WT HLRB spectra. The amide II protein peak yielded further evidence of protein changes in response to rose bengal exposure (RB, HLRB) in the form of hydrogen-deuterium exchange resulting from altered membrane permeability. The observed change in the intensity of the amide II peak in response to RB exposure was stronger in the spectra of WT RB cells than of CC-4107 RB cells. The observed change in the intensity of the amide II peak in response to HLRB exposure was of similar intensity in the spectra of WT HLRB cells and CC-4107 HLRB cells. Despite this, cells of the CC-4107 cell line did not show the reshaping of the second derivative components seen in the spectra of WT

HLRB cells. Differences in the shape of the 1450 $cm^{-1}$ peak and the relative contributions of its second derivative components were minimal.

The spectra of RB and HL treated CC-4107 cells showed no consistently repeatable changes in the 1400-1240 $cm^{-1}$ region. Repeatable spectral changes seen in HLRB cells included modification of the 1398 $cm^{-1}$ peak and decreased intensity of the 1285 $cm^{-1}$ tetrapyrrole and amide III peak. In the presented spectra there was a strong increase in the intensity of the 1378 $cm^{-1}$ component, accompanied by increased intensity at 1310 $cm^{-1}$. This change, however, was not consistent between days.

Examination of the principal component analysis of these spectra confirmed the importance of many of these observations. The combination of PC-1 (52%) and PC-2 (32%) described differences associated with protein secondary structure, altered membrane permeability, and some unassigned indicator peaks in the fingerprint region. They could be used to cleanly separate the spectra of HLRB and RB cells from the non-rose bengal treatments and from each other. There were indications of increased H-D exchange in both sets of exposures, though the degree was much greater in that of HLRB cells. Differences in protein secondary structure suggested by amide I second derivatives were subtle but mirrored those seen in WT cells. The internal α-helix to β-sheet ratio changed in the favour of the α-helical component in RB spectra, and in the favour of the β-sheet component in HLRB spectra.

#### 6.1.2.2 CH stretching region

Examination of the CH stretching region of CC-4107 cells indicated that the oxidative stressors in question resulted in some degree of change to lipid structure and function (Figure 6.4). There was a decrease in the degree of unsaturation in lipids exposed to HL, RB, and HLRB measured by the intensity of the 3010 $cm^{-1}$ peak. This was most pronounced in the spectra of HLRB-treated cells. In addition, the spectra of HLRB-treated cells exhibited upshifted positions and increased width for $CH_{2as}$ and $CH_{2s}$ peaks. This combination resulted in decreased resolution of the CH peaks and was indicative of changes in CH chain diversity and increased membrane disorder. This combination of factors suggested minor changes in lipid cohorts in response to either HL or RB, but more serious changes induced by the HLRB treatment. In comparison to WT exposures, all exhibited lesser differences in peak positions and widths, but greater changes in the unsaturated lipid peak.

The relatively minor degree of change observed in this region was confirmed by PCA analysis. The combination of PC-1 and PC-2 described changes in $CH_2$ peak position and the degree of unsaturation. On this basis, there was minor separation of HL and RB exposures from C spectra, and clean separation of HLRB spectra from all others.

### 6.1.3 *psaF*

#### 6.1.3.1 Fingerprint region

The spectra of *psaF* cells exposed to the stressors used in this study exhibited distinct patterns of change (Figure 6.5) when compared to the spectra obtained from WT cells (Figure 6.1), though significant overlap was present in the spectra differences induced by exposure to high light (Figure 6.5 HL, red; HLRB, light blue). The overall intensity of the 1740 $cm^{-1}$ lipid carbonyl peak increased in intensity and changed in shape in response to all treatments. There was increased absorption in the 1720-1740 $cm^{-1}$ region associated with the formation of lipid oxidative breakdown products. As with the spectra of WT cells, these differences were more pronounced in the spectra of cells treated with rose bengal (RB, green; HLRB, light blue), and of greatest significance in the spectra of cells exposed to HLRB. The second derivative spectra of HLRB-treated cells showed upshifting and increased width of the 1720 $cm^{-1}$ component, in addition to decreased intensity of the 1740 $cm^{-1}$ component. The spectra showed evidence of changes in protein secondary structure in all exposures, similar to the protein secondary structure changes observed in spectra from HL or RB-treated WT cells. In all treatments, the internal ratio of the α-helix/β-sheet components changed in the favour of α-helixes. Second derivative spectra of HLRB cells resulted in three additional spectral differences: increased intensity and downshifting of the 1680 $cm^{-1}$ component, broadening and downshifting of the β sheet component, and decreased intensity of the 1608 $cm^{-1}$ chlorophyll component. The presence of rose bengal (RB, HLRB) resulted in increased width of the 1575 $cm^{-1}$ second derivative components, similar to what was observed in the spectra of WT and *Chlamydomonas* DJX-J cells. Additionally, exposure to high light (HL, HLRB) resulted in spectral indicators of altered membrane permeability in the form of increased hydrogen-deuterium exchange. This was in contrast to the WT and DJX- species, which showed these indicators as a result of rose bengal exposure (RB, HLRB).

Second derivative spectra of the 1450 $cm^{-1}$ peaks showed similar changes. The relative intensity of the 1567 $cm^{-1}$ component increased in high light exposures (HL, HLRB), while the

intensity of the 1437 $cm^{-1}$ component increased in the spectra of HLRB cells. In all exposures, the shape of the 1398 $cm^{-1}$ peak changed due to a relative decrease in intensity of the 1398 $cm^{-1}$ component, similar to the pattern observed in DJX-species in response to rose bengal exposure, though muted in intensity. The strong, broad peak underlying the 1260 $cm^{-1}$ region, whose only homologous presence in the similar 1260 $cm^{-1}$ peak seen in the spectra of *Chlamydomonas* DJX-H cells, did not exhibit repeatable changes between exposure days. This was in contrast to the similar peak in DJX-H which disappeared from spectra of cells exposed to RB or HLRB. Examination of the second derivative spectra of HLRB-treated *psaF* cells showed decreased absorption in the 1285 $cm^{-1}$ tetrapyrrole peak.

Examination of principal component loadings, as well as the plotting of the spectra of individual living cells in PCA space, confirmed the importance of many of these observations described above (Figure 6.5 B). PC-1 described the narrowing of the protein peaks amide I and amide II, as well as changes in the 1398 $cm^{-1}$ and 1260 $cm^{-1}$ peaks, and could be used to neatly separate the spectra of C cells from the spectra of HL, RB, and HLRB cells. The spectra of HL, RB, and HLRB cells overlapped along PC-1 but separated along PC-2, which describes the intensity of the amide II and 1450 $cm^{-1}$ amide II' peak. Spectra of cells exposed to high light (HL, HLRB) were therefore confirmed to exhibit indicators of altered membrane permeability via differences in this ratio. Spectra of cells exposed to RB showed a minor decrease in the intensity of the amide II peak with a concurrent and unexplained decrease in 1450 $cm^{-1}$ intensity. PC-3, which described the evolution of lipid oxidation products, was useful in differentiating between cells exposed to high light alone (HL) versus high light and rose bengal (HLRB). Cells exposed to HLRB tended to show an increased presence of the byproducts of lipid oxidation. The spectra of all cells exposed to stress treatments (HL, RB, HLRB) showed a greater deal of variation in this measurement region than did the spectra of control cells.

#### 6.1.3.2 CH stretching region

Examination of the CH stretching region at 3050-2800 $cm^{-1}$ indicated that exposure to stress conditions used in this study altered hydrocarbon chains and the overall lipid cohorts (Figure 6.6). This was indicated by increased peak width and upshifting of $CH_2$ peak positions and decreased intensity of the 3010 $cm^{-1}$ unsaturated peak, suggesting an increased variety of CH chains and greater membrane disorder, as well as decreased lipid unsaturation. The degree of these changes

was similar in the spectra of HL-treated cells (red) and RB-treated cells (green), and greatest in the spectra of HLRB-treated cells (light blue). In comparison to the spectra of WT cells, the degree of upshifting, increased peak width, and decreased unsaturation seen in the spectra of *psaF* cells in response to treatment were more pronounced. This was especially true with respect to changes in the intensity of the 3010 $cm^{-1}$ peak which was almost eliminated after HLRB treatment. In the spectra of WT cells, even HLRB-treated WT cells, there was only a minor decrease in the intensity of the 3010 $cm^{-1}$ unsaturated lipid peak (Figure 6.2). The overall extent of changes in the CH stretching region were greater in the spectra of *psaF* cells than in the spectra of WT cells. It was interesting to note that the spectra of *psaF* cells under control conditions already indicated greater membrane disorder, CH chain variety, and lower degrees of unsaturation than seen in the spectra of WT cells under control conditions.

Examination of principal component loadings, as well as the plotting of the spectra of individual living cells in PCA space, confirmed these observations (Figure 6.6 B). The combination of PCs 1-3 allowed neat separation of all treatment regimes based on a combination of peak widths, positions, and the intensity of the unsaturated lipid peak at 3010 $cm^{-1}$. As in the low wavenumber fingerprint region, there was more variation present in the spectra of cells exposed to HL or RB than in the HLRB treatment or under control conditions.

### 6.1.4 CC-1355

#### 6.1.4.1 Fingerprint region

Loss of Chl *b*, combined with altered lipid and pigment profiles, was found to alter the response of cells of the CC-1355 line to oxidative stress (Figure 6.7). When compared to WT, there was a decrease in susceptibility to high-light exposure (HL) and increased evidence of oxidative lipid and protein damage following HLRB exposures. Minimal changes were seen in the spectra of RB cells, but those that were present were similar in scope to those seen in WT RB spectra.

Changes observed in the ~1740 $cm^{-1}$ lipid peak in response to treatment with high light and/or rose bengal are similar in pattern to those observed in WT cells. There was an overall increase in the intensity of the ~1740 $cm^{-1}$ peak in all three exposures (HL, red; RB, green; HLRB, light blue). In the spectra of cells exposed to rose bengal (RB, HLRB), there was a relative increase in absorption in the 1720-1700 $cm^{-1}$ region associated with lipid oxidation. This was most

pronounced in the spectra of cells exposed to HLRB treatment. In the second derivative spectra, both RB and HLRB treatments showed a relative decrease in intensity of the 1700 $cm^{-1}$ component. In the spectra of WT cells, this loss of the 1700 $cm^{-1}$ component was seen in the spectra of HL, RB, and HLRB cells. For the CC-1355 cell line, HLRB spectra showed further evidence of the formation of the by-products of lipid oxidation in the relative decrease in intensity of the 1740 $cm^{-1}$ component, and the broadening of the 1720 $cm^{-1}$ component.

Changes in protein secondary structure observed in CC-1355 cells exposed to rose bengal (RB, HLRB) were similar to those seen in the spectra of WT RB and HLRB cells, though the HLRB patterns of change were amplified in the spectra of CC-1355 HLRB cells. The characteristic narrowing and upshifting of the amide I peak seen in WT HL cells was absent in CC-1355 HL spectra, indicating that the high-light stress response observed in the spectra of WT cells may not have been triggered. Similarly, the muted response to HL in the spectra of CC-1355 cells, the protein peaks in the spectra of CC-1355 cells exposed to rose bengal alone (RB) showed minimal evidence of modification. When compared to the spectra of WT RB-treated cells, there was minimal evidence of altered membrane permeability, as indicated by H-D exchange. There was a low level of amide II – amide II' conversion, and the position of the amide I β-sheet component did not downshift. In contrast, changes in protein secondary structure in response to HLRB exposure in the CC-1355 line were greater compared to those seen in the spectra of WT HLRB cells. There was an increase in the intensity of the 1680 $cm^{-1}$ component. The internal second derivative ratio of α-helixes:β-sheets changed strongly in favour of β-sheets, and the 1608 $cm^{-1}$ chlorophyll component decreased. In addition, there was downshifting in the peak position of all four second derivative components, and broad increases in the width of the 1680 $cm^{-1}$, α-helix, and β-sheet components. HLRB spectra also exhibited the near-total conversion of the 1545 $cm^{-1}$ amide II component to the amide II' peak. The combination of these changes in the protein-associated peaks in HLRB cells indicated a high degree of altered membrane permeability as well as the conversion of native protein structures to denatured forms and intermolecular β-sheets. This combination indicated HLRB exposure in the CC-1355 cell line resulted in large-scale changes in membrane function and protein structure, to an extent greater than that seen in WT HLRB cells.

Changes were seen in the fingerprint region, including in the shape of the 1450 $cm^{-1}$ peak. Exposure of CC-1355 cells to any of the treatments treatment resulted in a relative increase in the

intensity of the 1467 and 1437 $cm^{-1}$ components and broadening of the peak, though these changes were most pronounced in HLRB spectra. There were other minor, unassigned changes observed in the 1400-1240 region of varying reproducibility but these were repeatable primarily in the spectra of HLRB cells, which show decreased 1398 $cm^{-1}$ intensity, downshifting of the 1340 $cm^{-1}$ component, and decreased intensity of the 1285 $cm^{-1}$ peak.

#### 6.1.4.2 CH stretching region

Examination of the CH stretching region (Figure 6.8) showed that the HLRB treatment (light blue) caused changes in lipid composition and membrane disorder, while minimal differences were observed in the spectra of CC-1355 cells following the RB or HL treatments (green, red). Exposure to HLRB resulted in the near-total loss of the 3010 $cm^{-1}$ peak, an indicator of the decreased presence of unsaturated lipids. Evidence of alterations in CH chains and membrane disorder were present in the spectra of cells exposed to rose bengal (RB, green; HLRB, light blue) in the observed upshift in $CH_{2as}$ and $CH_{2s}$ peak positions. These changes were more pronounced in the spectra of HLRB cells, which also showed increased peak widths, decreased peak resolution, and increased absorption at 2885 $cm^{-1}$, possibly due to the evolution of short-chain alkanes via lipid oxidation (arrow).

The use of principal component analysis confirmed these observations (Figure 6.8 B inset). Spectra of C cells (dark blue squares) overlapped in PCA space with spectra of HL cells (red circles). They were separated from the spectra of RB cells (green triangle) and HLRB cells (light blue diamonds) on the basis of peak position; spectra of HLRB cells were further separated by a combination of peak width and decreased intensity of the 3010 $cm^{-1}$ peak. The increase in the 2885 $cm^{-1}$ component, though sufficient to visually differentiate HLRB spectra from other treatments, did not influence the loadings.

### 6.1.5 *psaF cbn1*

#### 6.1.5.1 Fingerprint region

When examining the impact of the stress conditions used in this study on the *psaF cbn1* double mutant, changes observed in the fingerprint region in response to oxidative stress (Figure 6.9) were minimal in the spectra of HL and RB treated cells (red, green), but more pronounced in the spectra of HLRB cells (light blue). The overall responses observed were more similar to those seen in the spectra of CC-1355 cells (Figure 6.7), rather than *psaF* or WT cells (Figures 6.1 and

6.5). Changes in the ~1740 $cm^{-1}$ lipid carbonyl peak associated with lipid oxidation were observed in the spectra of cells exposed to rose bengal alone, and to a greater extent in the spectra of HLRB-treated cells. These changes included decreased intensity of the 1740 $cm^{-1}$ second derivative components, broadening of the 1720 $cm^{-1}$ component, and a general increase in intensity in the 1720-1700 $cm^{-1}$ region associated with products of lipid oxidation. The degree to which this region increased in spectra from HLRB-treated *psaF cbn1* cells exceeded that observed in any other cell line of *C. reinhardtii* and paralleled that seen in *Chlamydomonas* DJX- species.

Minor differences were observed in protein secondary structure in response to both HL and RB treatments. The changes seen in the spectra of HLRB cells mirrored those seen in cells of WT, *psaF*, and CC-1355 treated with HLRB. In *psaF cbn1* HLRB cells, there was broadening of the 1680 $cm^{-1}$, α-helix, and β-sheet components, as well as downshifting of these components and the 1608 $cm^{-1}$ components. There were also changes in the relative intensity and relative contributions of these four components. There was a relative increase in absorption from 1680 $cm^{-1}$, a decrease in the α-helix component, an increase in the β-sheet components, and a decrease in the 1608 $cm^{-1}$ chlorophyll components. The downshifting and increased bandwidth of the β-sheet component was suggestive of the formation of intermolecular β-sheets and globular proteins, including the denaturation of α-helical proteins into intermolecular β-sheets, (Berterame et al. 2016; Dong et al. 2000; Shivu et al. 2013) rather than more controlled remodelling and repair processes induced by other stressors. Differences in the spectra of HLRB *psaF cbn1* cells in the amide II peak and its second derivatives also most closely mirrored those seen in HLRB CC-1355 cells: a relative decrease in intensity, indicating increased hydrogen-deuterium transfer and thus, altered membrane permeability. Broadening of the 1575 $cm^{-1}$ component, and a relative decrease in intensity of the 1515 $cm^{-1}$ ring component were also evident. Similar changes were seen following the HLRB treatment in other cell lines, but the magnitude and pattern observed in the spectra from *psaF cbn1* cells most closely resemble those from CC-1355.

Differences observed in the shape of the 1450 $cm^{-1}$ peak observed in the spectra from *psaF cbn1* cells in response to the treatments used in this study mirrored those seen in the other cell lines. There was a relative increase in the intensity of the 1467 $cm^{-1}$ and 1437 $cm^{-1}$ components and therefore increased peak width following all treatments. Changes were also present in the shape and intensity of the 1398 $cm^{-1}$ peak, but these were not consistent between days. This

uncertainty was magnified by the fact that the 1382 $cm^{-1}$ second derivative component was abnormally high in the spectra of control cells in Figure 6.9. Despite this, the spectra of HL and RB treated cells consistently showed narrowing of the 1398 $cm^{-1}$ peak due to a relative decrease in the intensity of the 1382 $cm^{-1}$ component. In contrast, when examining spectra from HLRB-treated cells there was a consistent flattening of this peak due to decreased absorption by the 1398 $cm^{-1}$ component. Despite some inconsistencies between days, the spectra of cells exposed to rose bengal (RB, HLRB) exhibit increased absorption by the 1340 $cm^{-1}$ peak. In addition, in the spectra of HLRB cells, there was a decreased in the 1287 $cm^{-1}$ peak associated with tetrapyrrole and amide III absorptions. These changes in the region below 1400 $cm^{-1}$ were similar to those seen in the spectra of the DJX- species after exposure to rose bengal (RB, HLRB).

Examination of principal component analysis of these spectra (Figure 6.9B) confirmed the broader observations made. Overall, exposure to HL resulted in a minimal number of spectral changes. Spectra of RB cells (green triangles) were only slightly separated from C and HL (dark blue squares, red circles) along PC-1, which was dominated by changes in the lipid peroxide region, protein secondary structure, and indicators of increased membrane permeability. Additional contributions to this loading occurred in the poorly-characterized fingerprint region. Spectra of HLRB cells were much more cleanly separated along this loading, indicating greater degrees of lipid and protein modification and altered membrane transport.

#### 6.1.5.2 CH stretching region

Examination of spectra and second derivative spectra of *psaF cbn1* cells exposed to the treatments used in this study revealed extensive changes to lipids in HLRB-treated cells (Figure 6.10). Their spectra showed decreased unsaturation (decreased intensity of the 3010 $cm^{-1}$ peak), and alteration in membrane fluidity and CH chain variety (upshifted $CH_2$ peak positions, plus increased peak width and decreased resolution between peaks) as well as the evolution of short-chain alkanes often found in the generation and breakdown of oxidized lipids (increased 2885 $cm^{-1}$).

Principal component analysis of the second derivate spectra (Figure 6.10) showed an interesting pattern. Spectra of HLRB cells separated cleanly on the basis of peak position, width, and lipid unsaturation, while there was much overlap between C, HL, and RB spectra. It was interesting to note that spectra from the HL-treated cells were primarily found in quadrant IV

(negative PC-1, negative PC-2) while RB spectra were primarily located in quadrant II (positive PC-1, positive PC-2) and the spectra of C cells exhibited sufficient variability to occupy quadrants I, II, and IV, overlapping with the spectra of both HL and RB treated cells. This suggested that under control conditions, significant variation in lipid composition was present, and that some of this inherent variation in the region was reduced by exposure to specific oxidative stressors.

## 6.2 Discussion

### 6.2.1 CC-4107

As predicted, cells of the CC-4107 line were protected from the effects of all three treatments used in this study. Further, under control conditions, the spectra of CC-4107 was in fact very similar to the high light phenotype observed in WT HL cells. In addition, a minimal number of changes were observed in the spectra of either HL or RB cells, suggesting that the mutations present in the CC-4107 cells conferred a degree of protection to high-light mediated damage. This also confirmed the observations by Baroli et. al (2003) suggesting that the mutation confers some degree of protection to RB exposure. Of special note with the CC-4107 cells was the significantly reduced lipid damage. Not only was there less lipid oxidation, but there was also much less evidence for membrane leakage, as measured by the extent of hydrogen-deuterium exchange on amide II intensity. Interestingly, despite resistance to membrane leakage, the spectra of RB-exposed CC-4107 cells (RB, HLRB) showed an increased loss of unsaturated lipid bonds. This was more pronounced in the spectra of HLRB cells.

As intended, the HLRB exposures still caused significant damage in the CC-4107 cells, although less than in the WT cells. For example, there were changes in the absorbance peaks associated with protein structure. The spectra of HLRB-treated CC-4107 cells still exhibited hydrogen-deuterium exchange. However, spectra from HLRB-treated WT cells were indicative of both increased H-D exchange and the formation of protein aggregates.

### 6.2.2 *psaF*

As predicted, the loss of the PSAF protein resulted in increased sensitivity to high-light stress. Unlike the WT or CC-4107 cells, high light had a bigger impact on the cellular lipids and proteins than did rose bengal exposure. When examining the PCA of these cells following the three treatments, the spectra from HL and HLRB-treated cells clustered together, distinctly separate from the control or RB-treated cells. This highlights the impact that the loss of the PSAF protein

has on the cells, and explains the type of damage that accumulates and leads to the death of these cells when light intensity is high.

Changes observed in the protein secondary structure in *psaF* cells in all exposures were similar to those seen in WT HL cells, where the internal α helix:β-sheet ratio changes in favour of the α-helical component. Despite this, exposure to HLRB in both cell lines resulted in increased intensity and downshifting of the 1680 $cm^{-1}$ component, downshifting and broadening of the β-sheet component, and decreased intensity and downshifting of the 1608 $cm^{-1}$ chlorophyll component. The influence of these stressors on the shape and intensity of the amide II peak also differed between cell lines. In both, the presence of rose bengal resulted in broadening of the 1575 $cm^{-1}$ second derivative component.

Changes in membrane permeability followed a similar pattern to that seen in proteins. The spectra of *psaF* cells exposed to HL showed increased rates of H-D exchange as compared to those of WT HL cells. The examination of the CH stretching region for both lines gave further indication of the damage that accumulated in the *psaF* cells. Despite the decreased influence of RB on membrane permeability in the *psaF* cell line, the CH region showed that cells exposed to rose bengal (RB, HLRB) experienced greater loss of lipid unsaturation than was seen in WT cells exposed to rose bengal.

Overall, high light was a stronger driving force for cellular damage in *psaF* cells than is rose bengal. This was true for both the protein and lipid components of the cells. As mentioned previously, it appears that the *psaF* cells are under high-light stress even when grown under control light conditions.

### 6.2.3 CC-1355

As predicted, the loss of Chl *b* in the CC-1355 cell line appeared to reduce the impact of high-light exposure alone. The characteristic changes in the amide I protein peak seen in response to high-light exposure in WT cells was absent in the spectra of CC-1355 cells exposed to high light. Based on this expectation, we provide added evidence that the changes observed in the amide I region of the spectra of WT and *psaF* cells are related to HL damage. Additional spectroscopic support for this concept comes from the observation that the amide I peaks of WT HL cells most closely resembled the amide I peaks of CC-4107 C and HL spectra.

It was unknown what impact the loss of Chl *b* and associated compounds would have on the susceptibility of this line to singlet oxygen stress mediated by rose bengal. Minor differences were observed in the intensity of the 1740 $cm^{-1}$ lipid-associated peak in the spectra of both HL and RB cells, but these were not correlated in any significant differences in the CH stretching region. This, combined with the minor increase in H-D exchange in spectra of RB-treated CC-1355 cells, suggests that this cell line also exhibits reduced sensitivity to RB exposure. The reason for this is not clear at this time. However, when CC-1355 cells were exposed to HLRB, there was significant damage to proteins and lipids. I observed the loss of unsaturated lipids, the evolution of by-products of lipid oxidative damage (ketones, hydroperoxides, short-chain alkanes, and more), increased cellular permeability, and the formation of protein aggregates. These differences were far greater than observed in WT cells, suggesting reduced cellular capacity to neutralize the synergistic action of high light and rose bengal. It is possible that the altered lipid profile of CC-1355 cells, specifically the diminished levels of unsaturated lipids, may lead to this sensitivity. The loss of the unsaturated lipids could mean that the cells essentially lost a singlet oxygen absorbing "sponge" used sacrificially to absorb damage. It is interesting to note here that the *Chlamydomonas* DJX- species were similarly more sensitive to HLRB treatment. Overlapping change included the combination of high degrees of altered membrane permeability, loss of unsaturated lipids, large-scale formation of lipid oxidation products, and significant broadening of the second derivative components of the amide I peak. Perhaps they also were lacking compounds in their membranes that could accumulate greater degrees of damage before the selective permeability of the plasma membrane failed and allowed an influx of heavy water.

### 6.2.4 *psaF cbn1*

As predicted, from the knowledge that the cbn1 mutation counters the high-light lethal phenotype of the *psaF* strain, I did not see a specific high-light impact on the spectra of *psaF cbn1* cells. The increased sensitivity to high-light stress observed in the *psaF* cells was neutralized by the loss of Chl *b* and the other associated effects of the *cbn1* mutation. The protective effect held when comparing the WT, *psaF*, and *psaF cbn1* cells under control conditions as well, where the spectral differences induced by the loss of the *psaF* subunit were not found in the spectra of the *psaF cbn1* cells. The spectra of *psaF cbn1* cells spectra under control conditions most closely resembled those of the CC-1355 line, suggesting that the loss of Chl *b* appeared to influence the biochemical make up of the cells to a greater degree than did the loss of the *psaF* subunit. No firm

predictions were made regarding the effect of the double mutants on rose bengal response, but the response of the double mutant to RB was similar to that of the line's response to HL, in that it was muted in comparison to that of WT and similar to that of CC-1355. The characteristic narrowing of the amide I peak and altered α-helix:β-sheet seen in HL exposures in WT and *psaF* cells lines were absent. The impact of exposure to rose bengal alone (RB) on membrane permeability was reduced when compared to that of WT cells. Exposure to HLRB resulted in similar patterns of change to those seen in the spectra of CC-1355 HLRB cells. This was particularly true in the 1720-1700 $cm^{-1}$ region associated with lipid oxidative damage and the 2885 $cm^{-1}$ theorized to be related to the oxidatively-mediated generation of short-chain alkanes. This is understandable when considered in the context of a missing singlet oxygen "sponge" in these cells in the form of photoprotective carotenoids, due to the *cbn1* mutation. The combination of these factors suggested that while cells of the *psaF cbn1* line were less susceptible to damage from high light or rose bengal alone, the combination of these factors resulted in extreme damage to the plasma membrane and increased the severity of knock-on effects.

## 6.3 Summary and Conclusions

Many of the predicted impacts of photosynthetic mutations were born out via analysis of FTIR data of individual living cells. One broad prediction supported by high light exposure in all mutants is that the characteristic narrowing and upshifting of the amide I peak seen in WT *C. reinhardtii* is associated with acclimative phenotypic changes. Similar changes were seen in the spectra of *psaF* HL cells, while they were not observed in the Chl *b* mutants CC-1355 and *psaF cbn1*. Perhaps most telling was the spectra of the zeaxanthin hyperaccumulation mutation CC-4107. The altered balance of the xanthophyll pool induced by the *npq2* mutation appears to induce biochemical changes associated with the high-light phenotype even under control conditions, when no evidence of cellular stress was observed.

As predicted, the mutations associated with the CC-4107 line appear to be protective of HL and RB, as well as the HLRB combination. Different patterns of change were observed in the lipid peaks and this was associated with a lower degree of change in membrane permeability than was seen in any of the other cell types. In addition, while changes in the 1740 $cm^{-1}$ lipid carbonyl peak indicated some degree of loss of lipids to oxidation, it was not accompanied by the production of lipid oxidation by-products seen in all other cell lines. This set of observations fits nicely with the

concept of a singlet oxygen absorbing "sponge" that arose in discussing the impact of HLRB on *cbn1* and *psaF cbn1* cells. These cells have a greater capacity to detoxify singlet oxygen, perhaps through accumulating greater levels of lipid peroxides and sacrificing the lipid double bonds. The protection provided by the mutations in the CC-4107 cells were not limited to the cells' lipids, changes in the protein peaks were primarily associated with H-D exchange form altered membrane permeability, rather than gross damage or denaturation.

The loss of the *psaF* subunit did appear to increase sensitivity to high light exposure, particularly increasing the degree of alteration of membrane permeability. It is important to note that there was evidence of oxidative stress even under control conditions.

The Chl *b* mutant CC-1355 had a muted response to high light exposure alone, reinforcing the idea that these cells simply absorb less light due to their diminished LHC. The combination of the loss of Chl *b* was even able to mitigate the damaged caused by the *psaF* mutation under high-light exposure The *cbn1* and *psaF cbn1* mutants exhibited near-identical responses to oxidative stress. Both exhibited only minor spectral changes in response to either high light or rose bengal alone, but showed a strong synergistic effect when exposed to the HLRB-treatment. The higher degree of sensitive to HLRB (as compared to WT HLRB) can likely be correlated to the decreased level of unsaturated lipids as well as to other pigments involved in mediating the response (chlorophylls, other pigment compounds). These cells showed high degrees of lipid oxidation, the formation of short-chain alkanes, and protein aggregates in the form of intermolecular beta sheets and other forms. It is these compounds taken together that likely form this singlet oxygen "sponge" which protects the cells from more moderate levels of stress.

Overall, these experiments helped show the utility of FTIR of individual living cells in better elucidating cellular responses to high light and/or singlet oxygen generated by rose bengal. I was able to identify which classes of cellular components were impacted by these stresses and explain why they occurred based on the mutant cell lines used in this study. The use of these photosynthetic mutants also allowed us to better characterize responses induced by exogenous and endogenous oxidative stressors.

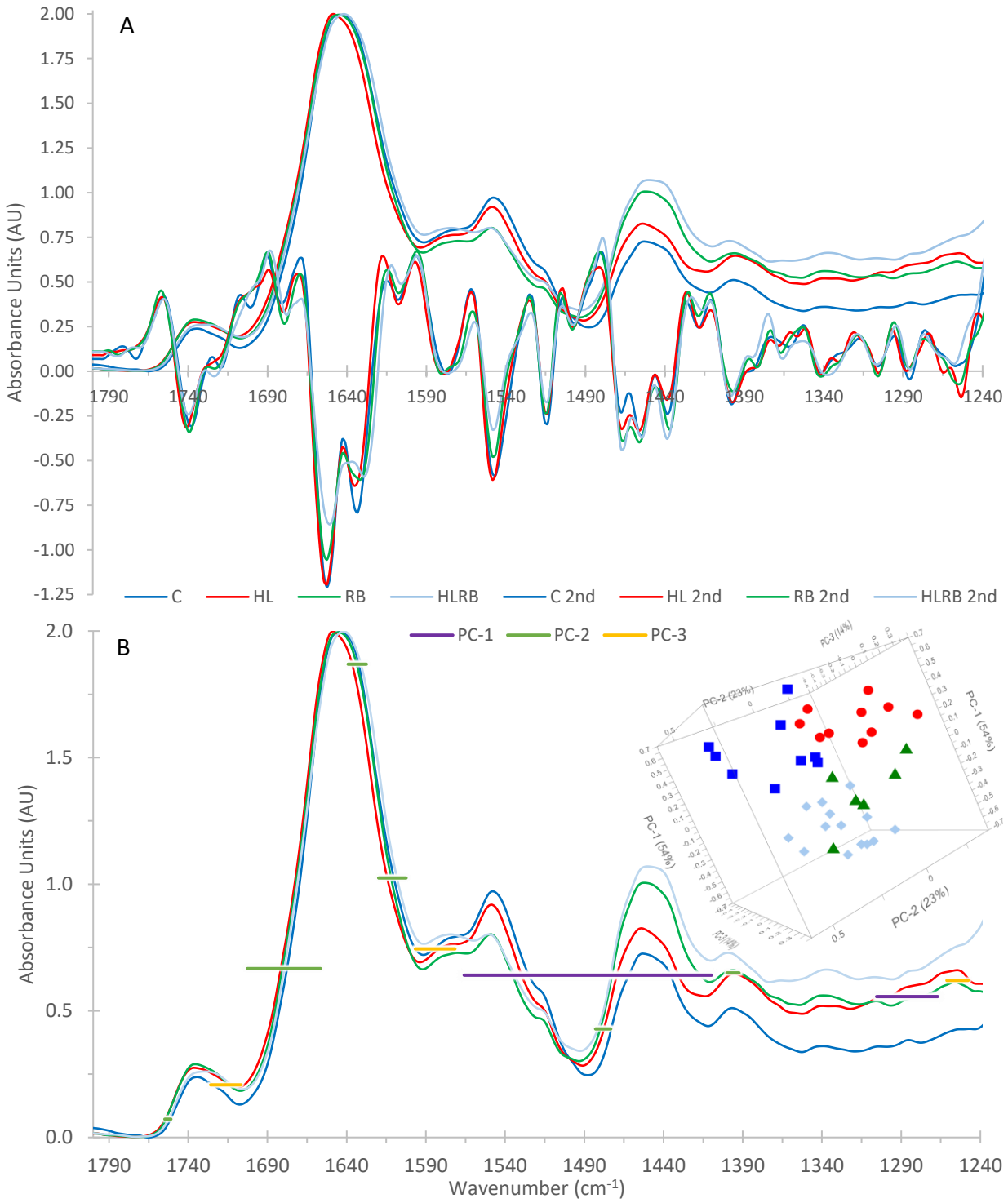


*Figure 6.1 – FTIR measurements of the 1800-1240 cm-1 region in* Chlamydomonas reinhardtii *(WT) under control (C), high light (HL), rose bengal (RB), high light (HL) and high light + rose bengal (HLRB) conditions. Spectra are the averages of the individual spectra used in principal component analysis and have been normalized to the amide I peak. A) Average spectra and scaled 2nd derivatives; B) Average spectra overlain with the loadings generating inset image (PC-1-3: 54%, 23%, 14%).*

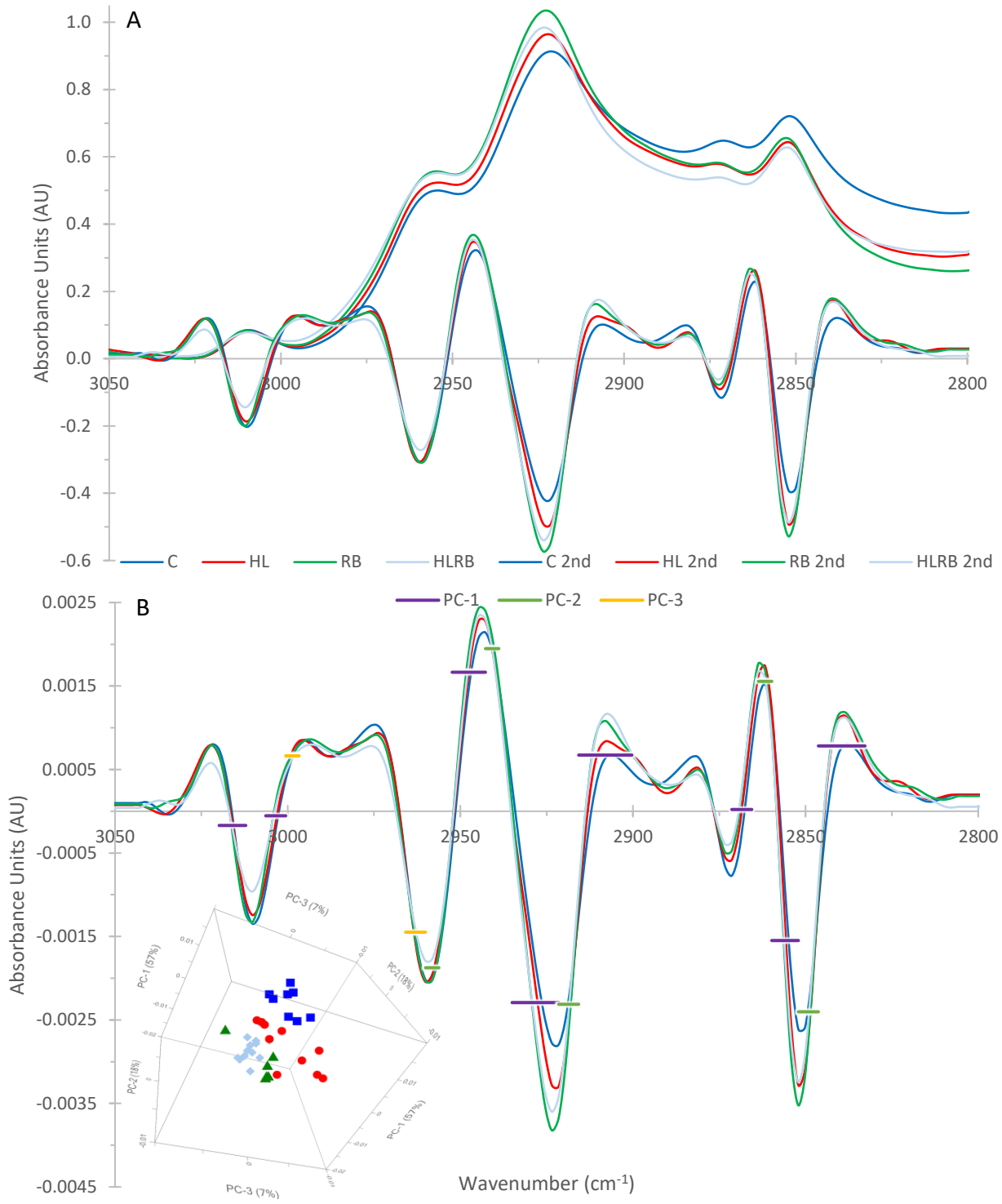


*Figure 6.2 - FTIR measurements of the 3050-2800 cm$^{-1}$ region in* Chlamydomonas reinhardtii *(WT) under control (C), high light (HL), rose bengal (RB), high light (HL) and high light + rose bengal (HLRB) conditions. Spectra are the averages of the individual spectra used in principal component analysis and have been normalized to the amide I peak, then offset corrected 3050 – 3000 cm$^{-1}$. A) Average spectra and scaled 2$^{nd}$ derivatives; B) Average of 2$^{nd}$ derivative spectra overlain with the loadings generating inset image. (PC-1-3: 57%, 18%, 7%).*

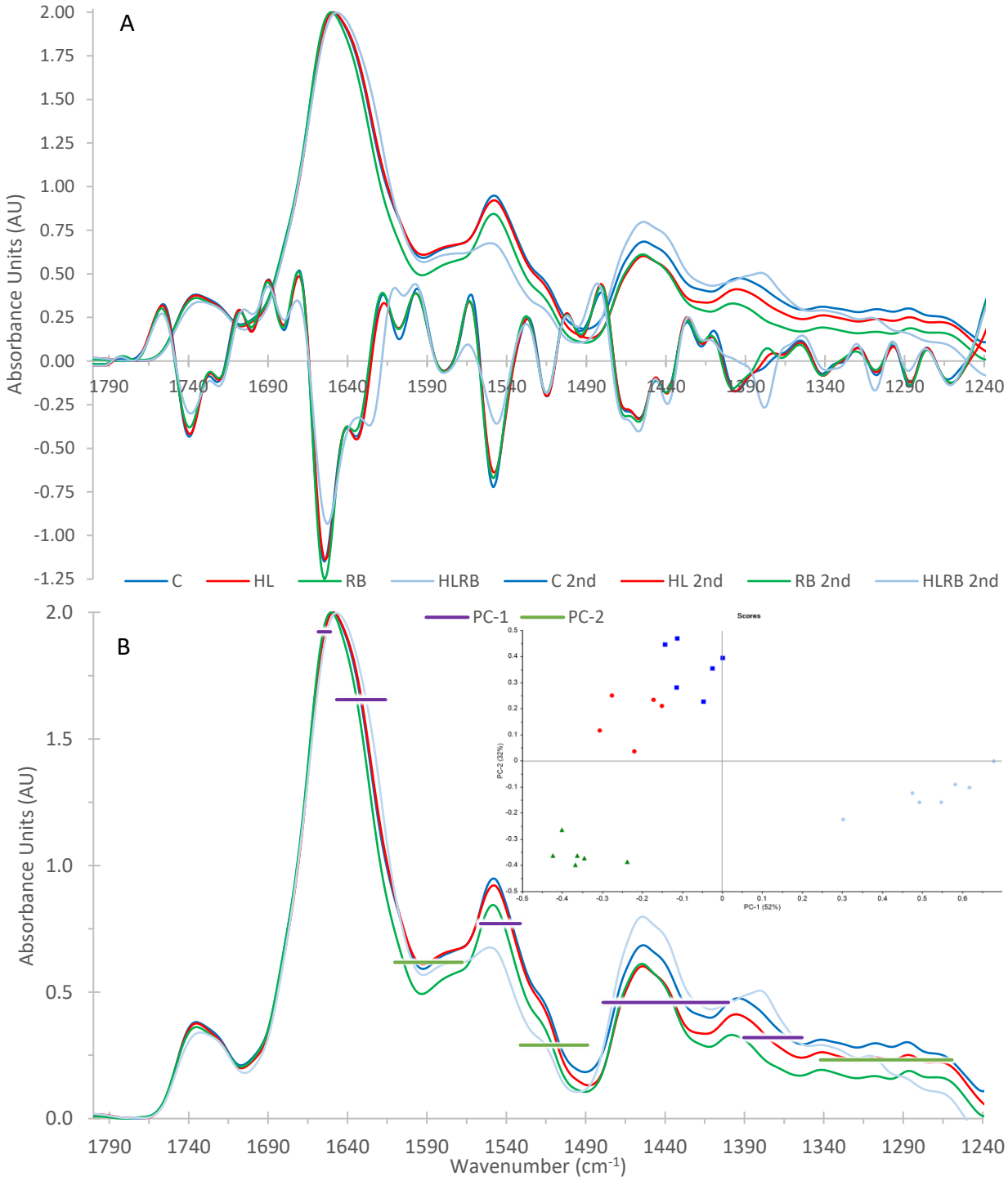


*Figure 6.3 – FTIR measurements of the 1800-1240 cm$^{-1}$ region in a* Chlamydomonas reinhardtii *zeaxanthin hyperaccumulation mutant (CC-4107) under control (C), high light (HL), rose bengal (RB), high light (HL) and high light + rose bengal (HLRB) conditions. Spectra are the averages of the individual spectra used in principal component analysis and have been normalized to the amide I peak. A) Average spectra and scaled 2$^{nd}$ derivatives; B) Average spectra overlain with the loadings generating inset image (PC-1-3: 52%, 32%).*

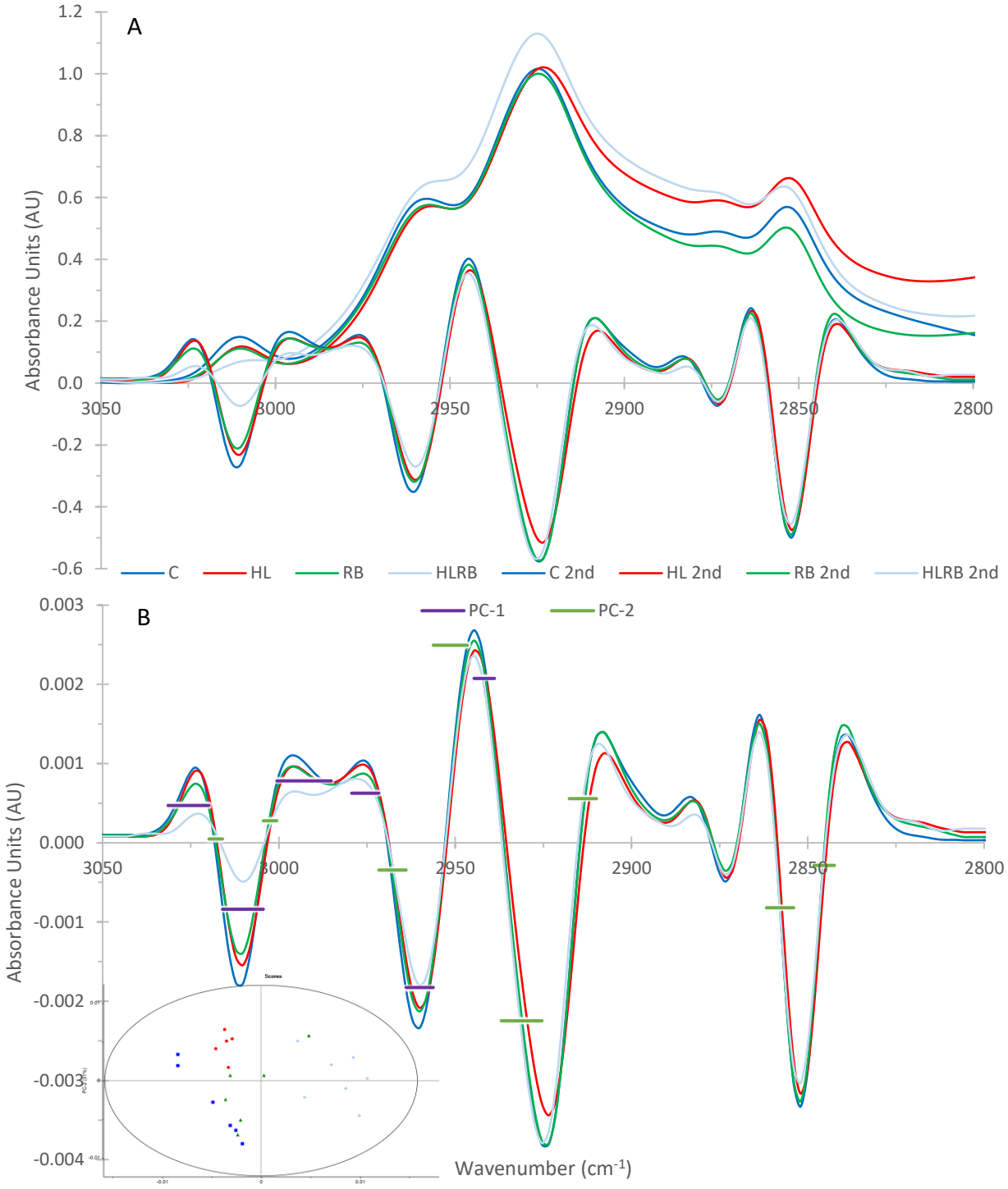


*Figure 6.4 - FTIR measurements of the 3050-2800 cm$^{-1}$ region in a* Chlamydomonas reinhardtii *zeaxanthin hyperaccumulation mutant (CC-4107) under control (C), high light (HL), rose bengal (RB), high light (HL) and high light + rose bengal (HLRB) conditions. Spectra are the averages of the individual spectra used in principal component analysis and have been normalized to the amide I peak, then offset corrected 3050 – 3000 cm$^{-1}$. A) Average spectra and scaled 2$^{nd}$ derivatives; B) Average of 2$^{nd}$ derivative spectra overlain with the loadings generating inset image. (PC-1-3: 51%, 31%).*

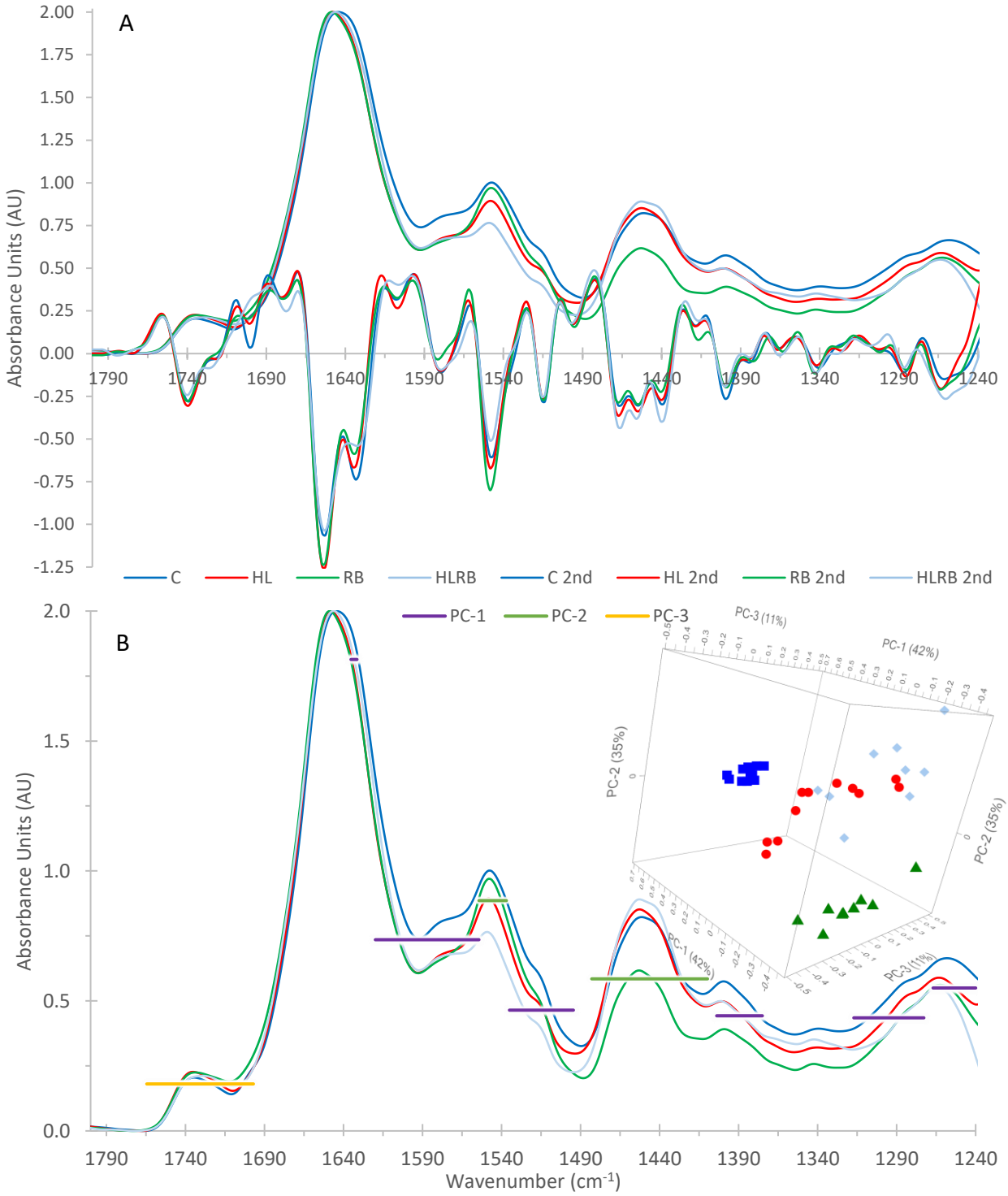


*Figure 6.5 - FTIR measurements of the 1800-1240 cm$^{-1}$ region in a* Chlamydomonas reinhardtii *PSAF mutant* (psaF) *under control (C), high light (HL), rose bengal (RB), high light (HL) and high light + rose bengal (HLRB) conditions. Spectra are the averages of the individual spectra used in principal component analysis and have been normalized to the amide I peak. A) Average spectra and scaled 2$^{nd}$ derivatives; B) Average spectra overlain with the loadings generating inset image (PC-1-3: 52%, 35%, 11%).*

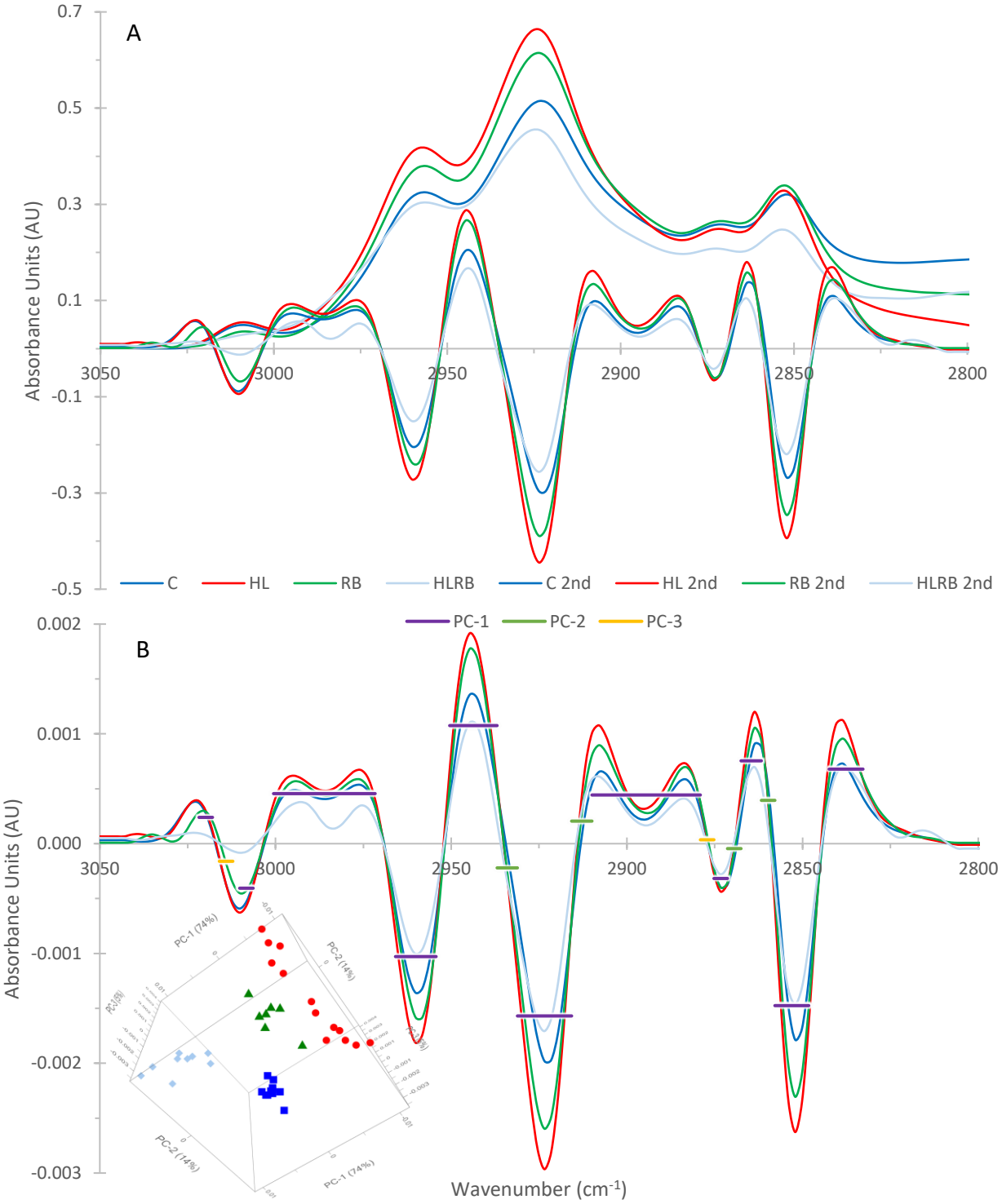


*Figure 6.6 - FTIR measurements of the 3050-2800 cm$^{-1}$ region in a* Chlamydomonas reinhardtii *PSAF mutant* (psaF) *under control (C), high light (HL), rose bengal (RB), high light (HL) and high light + rose bengal (HLRB) conditions. Spectra are the averages of the individual spectra used in principal component analysis and have been normalized to the amide I peak. A) Average spectra and scaled 2$^{nd}$ derivatives; B) Average spectra overlain with the loadings generating inset image (PC-1-3: 74%, 14%, 5%).*

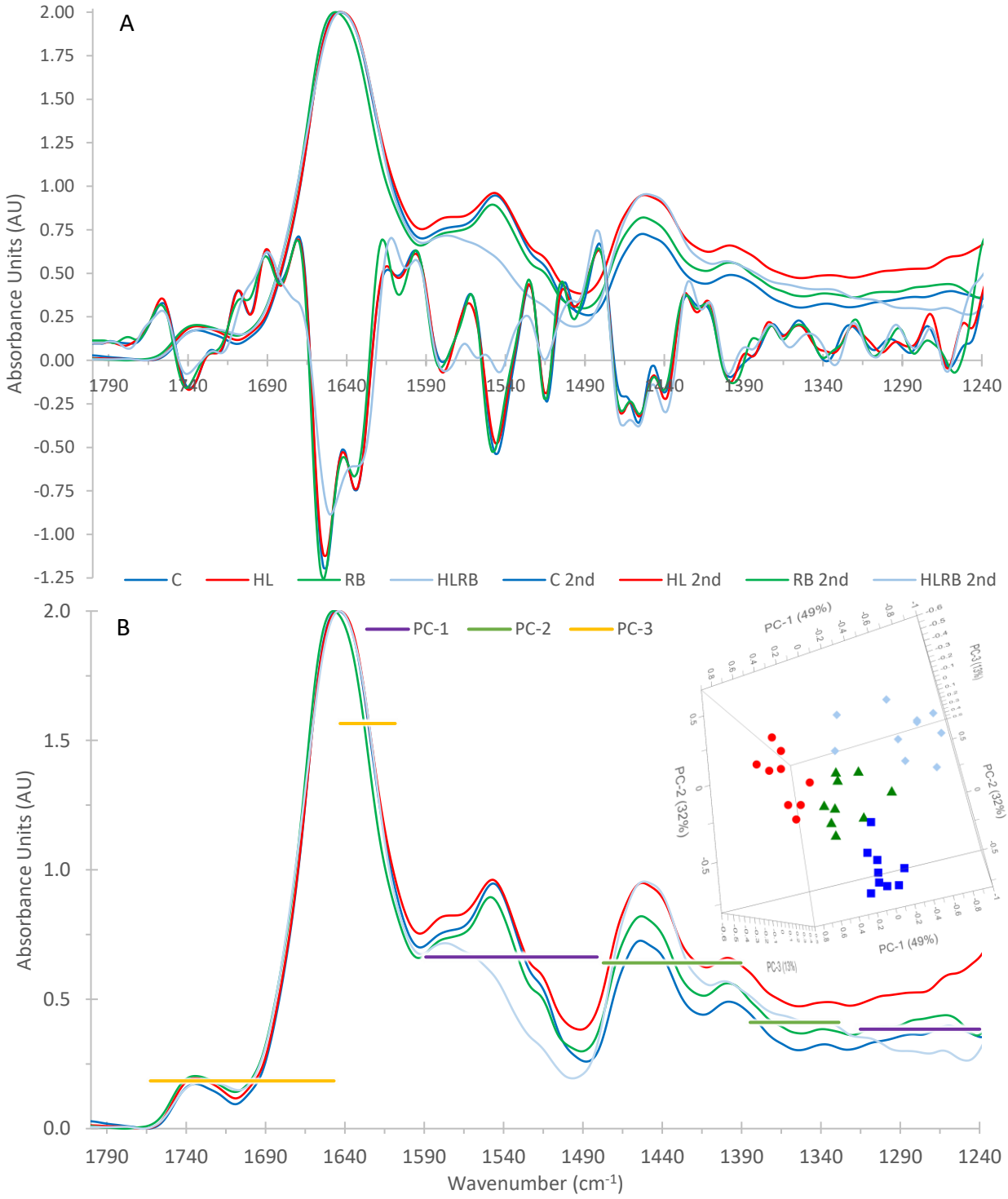


*Figure 6.7 - FTIR measurements of the 1800-1240 cm$^{-1}$ region in a chlorophyll B-deficient* Chlamydomonas reinhardtii *mutant (CC-1355) under control (C), high light (HL), rose bengal (RB), high light (HL) and high light + rose bengal (HLRB) conditions. Spectra are the averages of the individual spectra used in principal component analysis and have been normalized to the amide I peak. A) Average spectra and scaled 2$^{nd}$ derivatives; B) Average spectra overlain with the loadings generating inset image (PC-1-3: 49%, 32%, 13%).*

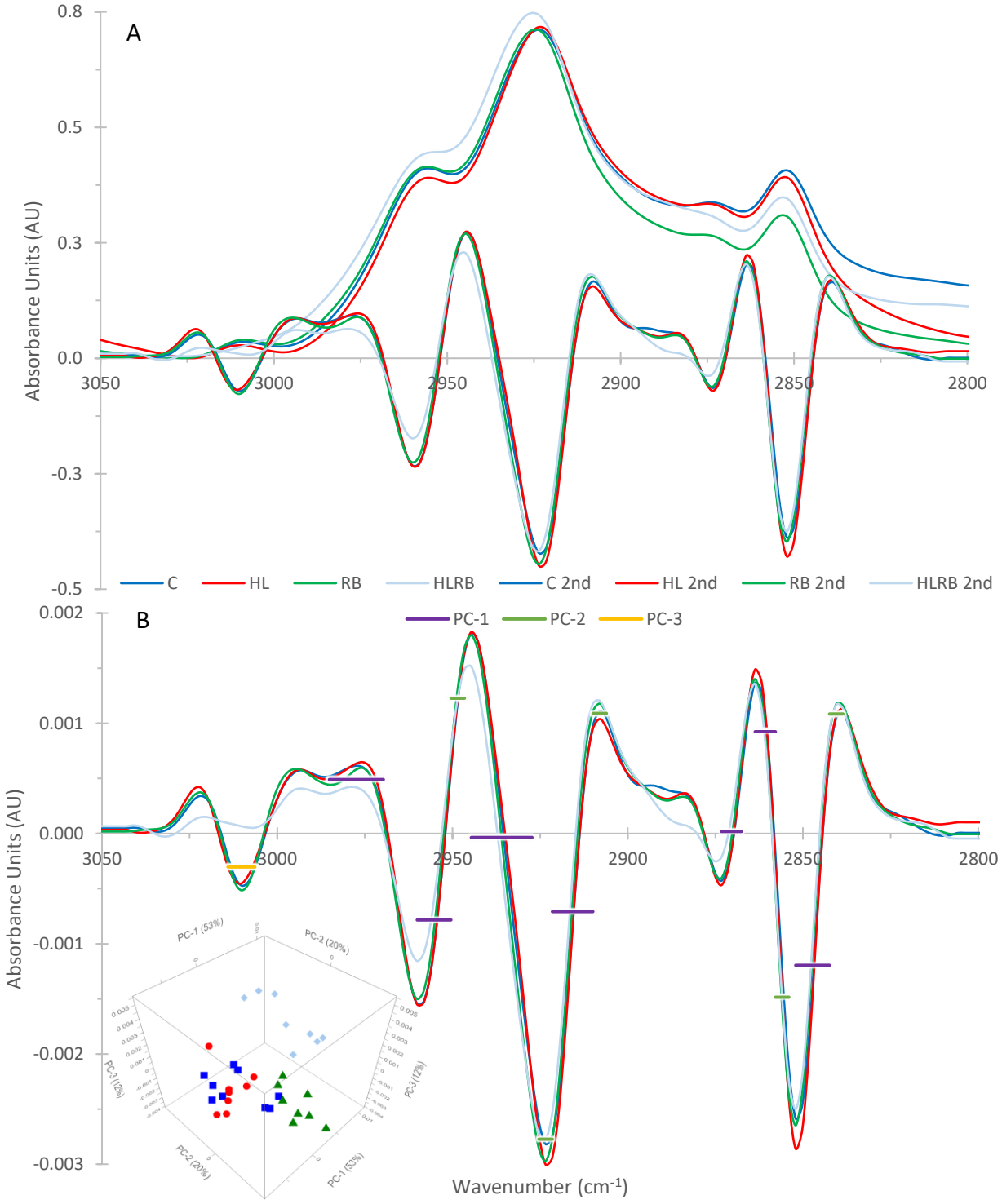


*Figure 6.8 - FTIR measurements of the 1800-1240 cm$^{-1}$ region in a chlorophyll B-deficient* Chlamydomonas reinhardtii *mutant (CC-1355) under control (C), high light (HL), rose bengal (RB), high light (HL) and high light + rose bengal (HLRB) conditions. Spectra are the averages of the individual spectra used in principal component analysis and have been normalized to the amide I peak. A) Average spectra and scaled 2$^{nd}$ derivatives; B) Average spectra overlain with the loadings generating inset image (PC-1-3: 53%, 20%, 12%).*

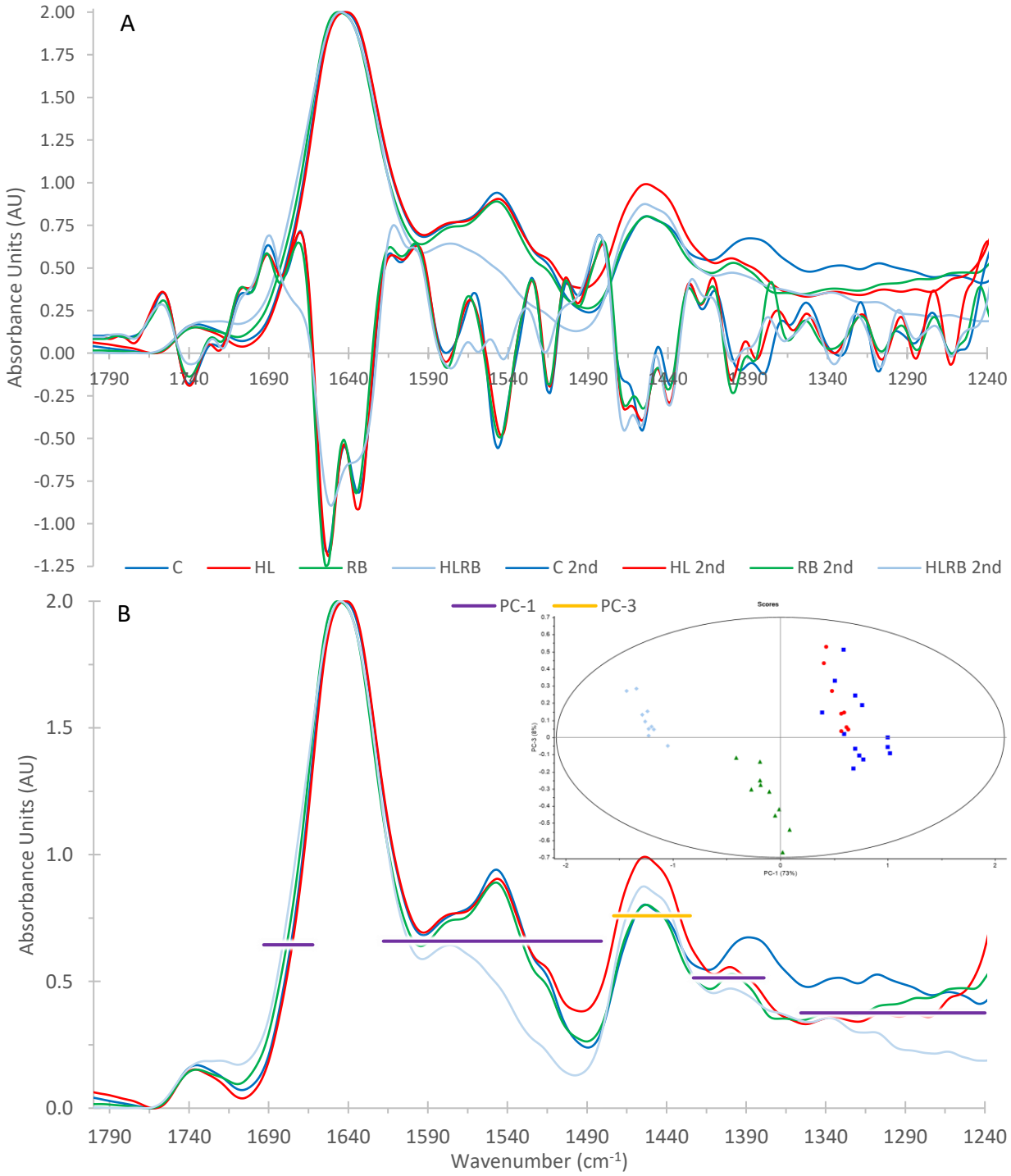


*Figure 6.9 - FTIR measurements of the 1800-1240 cm$^{-1}$ region in a chlorophyll B and PSAF-deficient* Chlamydomonas reinhardtii *mutant (*psaF cbn1*) under control (C), high light (HL), rose bengal (RB), high light (HL) and high light + rose bengal (HLRB) conditions. Spectra are the averages of the individual spectra used in principal component analysis and have been normalized to the amide I peak. A) Average spectra and scaled 2$^{nd}$ derivatives; B) Average spectra overlain with the loadings generating inset image (PC-1, 3: 73%, 8%). PC-2 (12%), which describes variation in the 1398 cm$^{-1}$ peak of control cells, is excluded.*

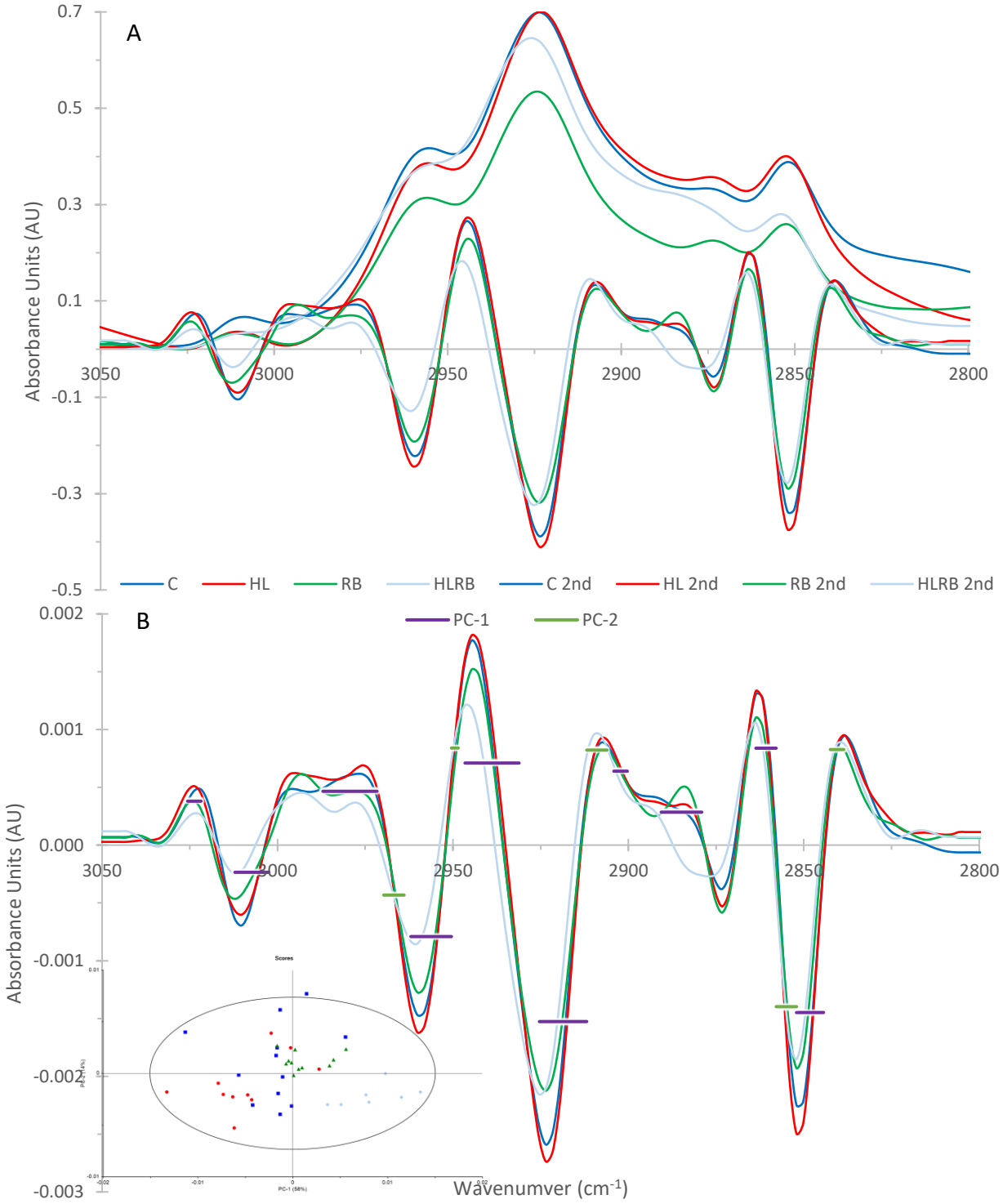


*Figure 6.10- FTIR measurements of the 1800-1240 cm-1 region in a chlorophyll B and PSAF-deficient* Chlamydomonas reinhardtii *mutant (*psaF cbn1*) under control (C), high light (HL), rose bengal (RB), high light (HL) and high light + rose bengal (HLRB) conditions. Spectra are the averages of the individual spectra used in principal component analysis and have been normalized to the amide I peak. A) Average spectra and scaled 2nd derivatives; B) Average spectra overlain with the loadings generating inset image (PC-1-3: 53%, 20%, 12%).*

*Table 6.1 - Overview of notable spectral changes induced by exposure to high light and/or rose bengal in wild type and photosynthetic mutants of Chlamydomonas reinhardtii, relative to spectra of control cells of the same cell line.*

| | | WT | | | CC-4107 | | | *psaF* | | | CC-1355 | | | *psaF cbn1* | | |
|---|---|---|---|---|---|---|---|---|---|---|---|---|---|---|---|---|
| | | HL | RB | HLRB | HL | RB | HLRB | HL | RB | HLRB | HL | RB | HLRB | HL | RB | HLRB |
| 1740 | Intensity | + | + | + | | | - | + | + | + | + | + | + | | | + |
| | 1720-1700 | | | + | | | | | + | + | | | + | | | ++ |
| Amide I | Shift | up | | down | | up | down | up | up | up | | + | | | up | up |
| | Width | - | | + | | - | + | - | - | Δ | | - | | | | + |
| | 1680 | | + | + | | | - | | | + | | | +/up | | | ++/up |
| | α-helix:β-sheet | ↑ α-helix | | ↑ β-sheet | | ↑ α-helix | ↑ β-sheet | ↑ α-helix | ↑ α-helix | ↑ α-helix | | | ↑ β-sheet | ↑ β-sheet | | ↑ β-sheet |
| | α, β position | | - | - | | | -- | | | - | | | -- | | | -- |
| | 1608 | | | - | - | - | -- | + | | - | | + | - | | | - |
| Amide II | Height | - | -- | -- | | - | -- | - | | -- | | - | --- | - | - | --- |
| | Shape | | Δ | Δ | | | Δ | | Δ | Δ | Δ | Δ | Δ | Δ | Δ | Δ |
| 1450 | Height | + | ++ | ++ | | | + | + | - | + | + | + | + | | + | + |
| | 1467 | + | + | + | | + | + | + | | + | + | + | ++ | + | + | + |
| | 1455 | | | | | | + | | | | | | | | | |
| | 1437 | - | + | + | | | + | - | - | + | + | | + | + | | + |
| 1398 | Strength | | | | | | | - | - | - | Δ | Δ | Δ | Δ | Δ | Δ |
| | 1398/1380 | | + | + | + | + | --- | - | - | - | | | | Δ | Δ | Δ |
| 1338 | Shape | | Δ | Δ | | | Δ | Δ | | Δ | Δ | | Δ | Δ | Δ | Δ |
| | position | | | - | | | Δ | | up | up | | down | down | | | |
| | 1308 | + | + | | | | + | | | - | + | + | + | - | - | |
| | 1285 | - | - | - | | | - | | | | Δ | Δ | Δ | + | + | |
| | 1260 | Δ | Δ | Δ | | | | Δ | Δ | Δ | Δ | Δ | Δ | Δ | Δ | Δ |
| | 1240 | | | | | | | - | - | - | + | + | -- | | | --- |
| 3010 | Height | | | - | - | - | -- | - | - | --- | - | | - | - | | --- |
| | Shape | | | Δ | | | | | | | | | | | | |
| CH | Width | | | + | | | | - | - | + | - | - | + | | | + |
| | Position | + | + | + | - | | + | + | + | ++ | - | | + | | | + |
| | 2885 | + | + | + | | | + | | | | + | + | ++ | + | | ++ |

# CHAPTER SEVEN

# FUTURE WORK

## 7.1 Time-Resolved High-Light Response

In addition to the study of individual living cells presented in the body of this thesis, additional time-resolved studies of individual cells exposed to high light were carried out. A single cell was measured repeatedly five times before being exposed *in situ* to high light for 15 minutes. Repeated measurements were then carried out upon the same cell. This allowed the cell to be used as its own control, removing the confounding effect of biochemical differences between cells. These *in situ* exposures to high light were done by removing the diffuser apparatus from the microscope illuminator, and then turning the intensity all the way up. The time scale and intensity of this illumination was necessarily less than that of *ex situ* illumination, but it allowed the observation of the spectral response of individual cells to this stressor. Control cells were measured repeatedly over the same timescale, but without the illumination. These measurements were carried out for all seven cell lines (*C. reinhardtii* and is four photosynthetic mutants, and the *Chlamydomonas* species DJX-H and DJX-J). Two examples of this are shown in Figures 7.1 and 7.2 (wild type *C. reinhardtii* and the *psaF* photosynthetic mutant respectively).

Time-resolved studies of wild type *C. reinhardtii* after *in situ* exposure to high light showed several expected changes based on previous *ex situ* experiments (Figure 7.1). In the 1800-1240 $cm^{-1}$ fingerprint region, the most interesting of these were: narrowing and upshifting of the amide I peak, and H-D exchange observed via the decreased intensity of the amide II and concurrently increased intensity of the 1450 $cm^{-1}$ peak that includes the amide II' peak. This time-dependent H-D exchange was also seen in the time-resolved spectra of control WT cells at a similar rate.

There was a general decrease in overall intensity of the CH stretching region that appeared to be associated with baseline intensity changes in the 1800-1240 $cm^{-1}$ fingerprint region, as well as with altered absorption from the saturated $D_2O$ stretching region at 2800-2000 $cm^{-1}$ (Figure 7.1). Aside from this, there was a visible trend of slight upshifting in the peak positions of the $CH_{2as}$ and $CH_{2s}$ peaks, indicative of either changes in membrane disorder or chain length diversity. There were minor, unstable changes in the degree of resolution between the 3010 $cm^{-1}$ unsaturated lipid

peak and $CH_{3as}$ peak, which suggested evolution and decomposition of intermediate by-products, potentially due to damage and repair. Also shown are visual images taken of the target cell prior to measurements, after 15 minutes of high light exposure, and then again after all FTIR measurements were taken (Fig 7.1). This is to illustrate that the baseline changes seen were unlikely to be due to cellular drift during the measurement process.

As expected based on data presented in Chapter 6, and our knowledge of the *psaF* mutant phenotype, time-resolved studies of a cell of the *C. reinhardtii* photosynthetic mutant *psaF* showed stronger patterns of change in response to *in situ* high-light exposure (Figure 7.2). The amide I protein peak first briefly broadened after high light exposure, before it narrowed and upshifted, suggesting the possibility of increased levels of protein damage and repair. Additionally, H-D exchange – as shown by the reciprocal height changes of the amide II and amide II' peaks – occurred at a much greater rate than was seen in WT cells, suggesting alterations to membrane permeability. This was congruent with changes observed in the CH stretching region, particularly the increased width of the CH peaks shown by decreased resolution between the CH, $CH_2$, and $CH_3$ peaks. In addition, the position of the $CH_{2as}$ and $CH_{2s}$ peaks upshifted more strongly than was seen in the WT time-resolved spectra after *in situ* illumination. The underlying baseline changes associated with the 2800-2000 $cm^{-1}$ saturation $D_2O$ region, were similar to those seen in WT cells.

Overall, this type of experiment offers great potential for understanding the response of individual cells to high-light exposure. It opens up avenues for understanding the how cells dynamically change both during high light exposure, but perhaps more importantly, as they begin to recover and repair damaged components once light levels decline.

## 7.2 Exploring Spectral Features

### 7.2.1 Origin of the 1240 $cm^{-1}$ Peak

The strong, broad peak centred around 1260 – 1240 $cm^{-1}$ in the spectra of DJX-H and *psaF* cells is of unknown origin and great interest. It is absent in the spectra of both DJX-J and *C. reinhardtii* WT cells. This is of particular interest given the nature of the *psaF* mutation – given what is known about its physiology, it was not expected to have any significant spectral differences when compared to WT. Similar predictions were made regarding the similarity of DJX-J and DJX-H spectra. The spectral region of this peak suggests the most likely assignments are to the amide

III peaks or phosphate related. In DJX-H cells there does appear to be some relation to peaks below 1100 $cm^{-1}$. One of the primary assignments of these low wavenumber peaks is to phosphate containing compounds. The loss of this 1260 $cm^{-1}$ peak in the spectra of DJX-H cells exposed to both high light and rose bengal (HLRB) is also of great interest. It is unclear if this change is due to physiological modifications or due to the loss of specific compounds due to the increased H-D exchange and increased membrane permeability. Exposure to HLRB in *psaF* cells, which are less sensitive to combined oxidative stress than DJX-H cells, do not show the same loss of this peaks. The similarity of this peak in *psaF* and DJX-H has led to the assumption that the underlying source of this spectral feature is the same or similar, but this has not been proven.

Given that it is one of the main spectral differences between WT and *psaF* cells (Figure 5.1: WT, dark blue; *psaF*, green), it is possible that this peak in the *psaF* line may be related to what appears to be an underlying level of high-light stress under normal levels of illumination. To investigate this possibility, cultures of both *psaF* and WT could be grown under low light and dark conditions, and the resultant infrared spectra compared. Decreased intensity of the 1240 $cm^{-1}$ peak under low light or dark conditions would suggest that its presence in the *psaF* line was related to changes in the cell triggered by long-term exposure to high light. If these experiments confirmed this hypothesis, similar investigations could be undertaken with DJX-H.

The loss of this peak in cells of DJX-H that have been exposed to rose bengal (Figure 4.3: RB, green; HLRB, light blue) coincides with conditions under which there have been major changes in membrane permeability (as indicated by increased rates of H-D exposure) and changes in protein secondary structure (as indicated by changes in protein second derivatives). Unfortunately, this suggests that differences in this peak could be attributed to amide III response to protein changes, modification of phospholipids, or the loss of phosphate-containing compounds or polyphosphate granules due to increased membrane permeability and leakiness. Analysis of the relative protein phosphorylation of WT, DJX-H, and DJX-J cells have been carried out, and do not correlate to the strength of this peak (Wilson 2016). The possibility that this peak is related to the cellular concentration of phosphate compounds or polyphosphate granules could be investigated via chemical analysis of the concentrations of polyphosphate-containing compounds extracted from cells of DJX-H under control conditions and after exposure to HLRB. Differences in relative concentrations would suggest that changes to this peak were due to the loss of cellular components

after extensive increases in membrane permeability. This would correlate with observations of this peak in the *psaF* cell line. The 1240 $cm^{-1}$ peak in *psaF* cells shows a general decrease in response to the HL, RB, and finally HLRB (Figure 6.5), rather than the total loss seen in DJX-H RB and HLRB. The *psaF* cell line also shows less lipid and protein modification under these experimental conditions than do cells of DJX-H. Concurrently, while H-D exchange is increased in comparison to C in *psaF*, this difference is less pronounced than in DJX-H cells exposed to rose bengal.

The combination of these two experiments (low light and dark spectra of *psaF* cells, and phosphorous analysis of DJX-H cells before and after HLRB exposure) would bring significant clarity to the origin of this peak.

### 7.2.2 Cellular Subpopulations Based on the absorbance peak at 1398 $cm^{-1}$

As discussed in greatest detail in Chapter 3 (Figure 3.2), subpopulations of cells were sometimes observed within a culture. These subpopulations were observed in multiple cell lines and could be separated on the basis of repeatable spectral features. Two examples of these average subpopulations are shown in Figure 7.3, and difference spectra calculated from these averages are presented in Figure 7.4. Figure 7.4 also shows the PCA loading generated for the CC-1355 single-cell spectra and is congruent with the difference spectra. The spectra presented are from the CC-1355 and CC-4107 cell lines. While in this case both cell types were exposed to the HLRB treatment, similar subpopulations were found across *C. reinhardtii* cell lines and treatments. Consistent differences are found in peaks at 1477 $cm^{-1}$ (w), 1398 $cm^{-1}$ (sh), 1377 $cm^{-1}$ (m/s), 1308 $cm^{-1}$ (w), 1152 $cm^{-1}$ (m/w), 1118 $cm^{-1}$ (sh), 1080 $cm^{-1}$ (vs), 1051 (s), 1020 (sh), 969 (m), 931 $cm^{-1}$ (m), and 889 $cm^{-1}$ (m). These peaks have overlapping assignments, but can be generalized to proteins and lipids ($\delta CH_2$, $\delta CH_3$, COO-: 1477, 1398, 1377, and 1308 $cm^{-1}$), and phosphorous containing compounds such as phospholipids, DNA, RNA, and phosphosugars (1152, 1118, 1080, 1050, 1020, 969, 931, and 889 $cm^{-1}$) (Movasaghi et al. 2008). Overall analysis and the strength of the changes in the phosphate region suggest that these differences are more likely due to changes in DNA/RNA, phospholipids, or phosphorylation of sugars or proteins. The lack of associated changes in the lipid carbonyl peak at 1740 $cm^{-1}$ or protein secondary structure in the amide I peak suggests it is more likely to be associated with changes in DNA and RNA. This is further supported by the presence of the 969 and 889 $cm^{-1}$ peaks assigned to deoxyribose, the 931 $cm^{-1}$

peak assigned to Z-DNA, and the 1152 $cm^{-1}$ shoulder associated with RNA (Movasaghi et al. 2008; Zhang et al. 2016). There is likely to be contributions from other candidates as well. It should further be noted that difference spectra generated from subpopulations with broad 1398 $cm^{-1}$ peaks downshifted to between 1398 $cm^{-1}$ and 1380 $cm^{-1}$, versus narrow 1398 $cm^{-1}$ peaks downshifted below 1380 $cm^{-1}$, suggest that the higher wavenumber portion of the 1398 $cm^{-1}$ peak is tied to the strength of the 1020 $cm^{-1}$ peak. There are no concurrent changes in the 1240 $cm^{-1}$ phosphate peak, but previous research has suggested that this peak is much less sensitive to changes in DNA and RNA structure and density (Sanchez-Ruiz and Martinez-Carrion 1988; Zhang et al. 2016).

The repeatable presence of these subpopulations of cells, combined with the consistency of the difference spectra between them, suggests that this difference is due to underlying physiological differences. One interesting candidate is the cell cycle. Cells spend the majority of their time in G1, with DNA synthesis and increases in cellular components occurring in S-phase and G2, before cells rapidly undergo mitosis. Many species of *Chlamydomonas* (including *C. reinhardtii*) utilize a modified cell cycle known as multiple fission (Figure 7.5). This is a prolonged $G_1$ phase, followed by rapidly alternating successive S and M phases. Under standard conditions, cells spend approximately 86-97% of their time in $G_1$ phase (Cross and Umen 2015). This would line up with some of the observations made by Holman et al regarding spectral changes during M-phase, as well as observations made by other research groups regarding spectral changes during S-phase (Boydston-White et al. 1999; Holman et al. 2000; Mourant et al. 2003). In the spectra of cells exposed to high levels of oxidative stress, it could also be indicative of damage or altered DNA or changes in RNA transcription.

To investigate this possibility further, one could grow synchronized cultures of *C. reinhardtii*. This is done by entraining the cells into a standard light:dark cycle (Spudich and Sager 1980). While maintaining a strict light:dark cycle would be challenging in the synchrotron Mid-IR hutch, it was demonstrated that addition of the photosynthetic inhibitor dichlorophenyl dimethylurea (DCMU) could mimic a sustained dark period (Spudich and Sager 1980). Removal of DCMU immediately prior to sample loading in the hutch would release the cells, and individual living cells could be followed as they progressed through the cell cycle. We would expect to see significant variation in the peaks described above if they are indeed changing as a result of the cell cycle stage of the cell being measured.

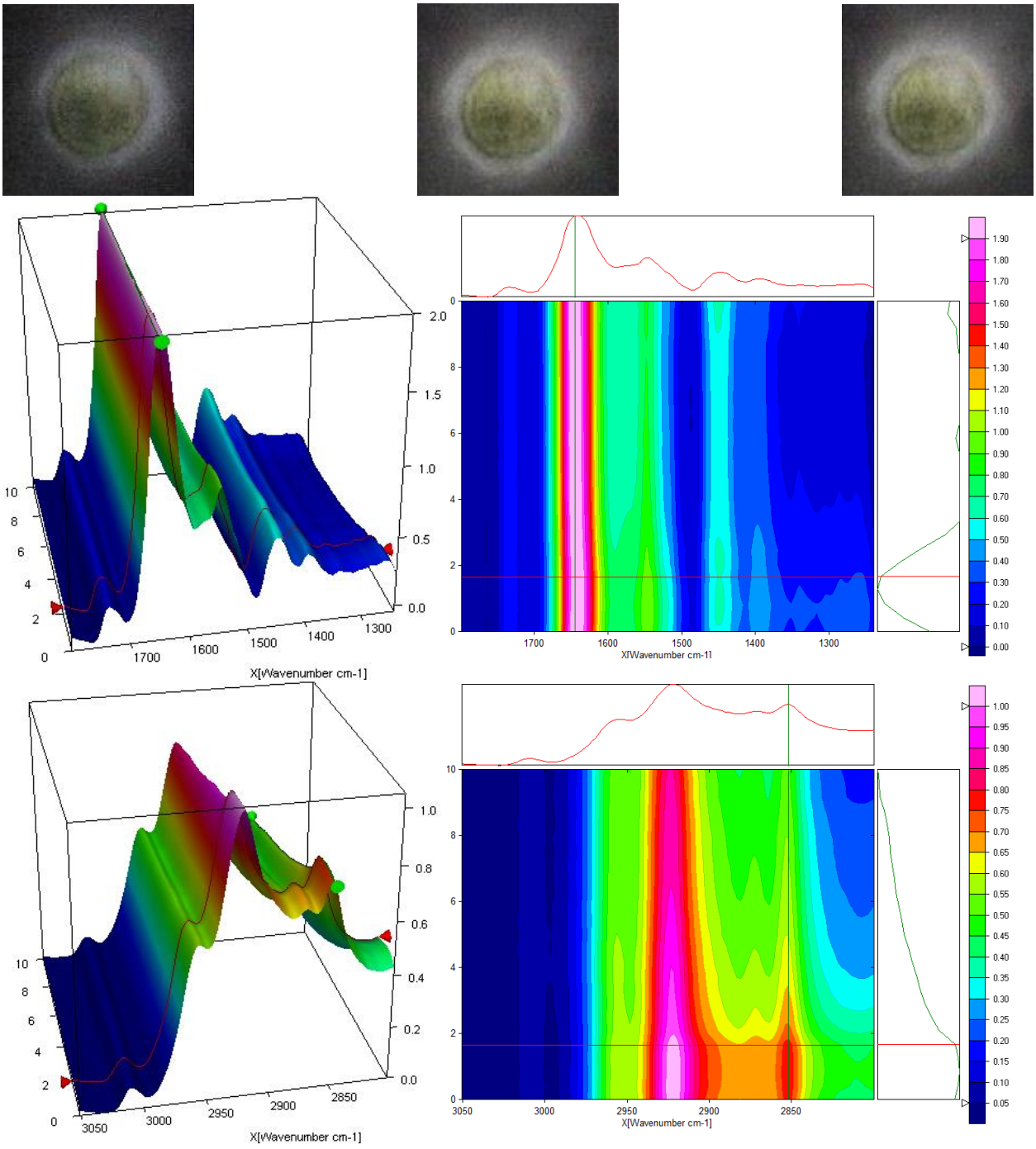


*Figure 7.1 - Time-resolved measurements of a single cell of Chlamydomonas reinhardtii before and after exposure to 15 m of high light. Red horizontal line indicates the time at which high light exposure occurred. Spectra have been min-max normalized to the amide I peak at 1650 cm$^{-1}$ and the local baseline. The CH stretching region was offset corrected to the local baseline at 3040-3010 cm$^{-1}$. The three pictures show the position of the cell before high light, after high light, and after repeated measurements.*

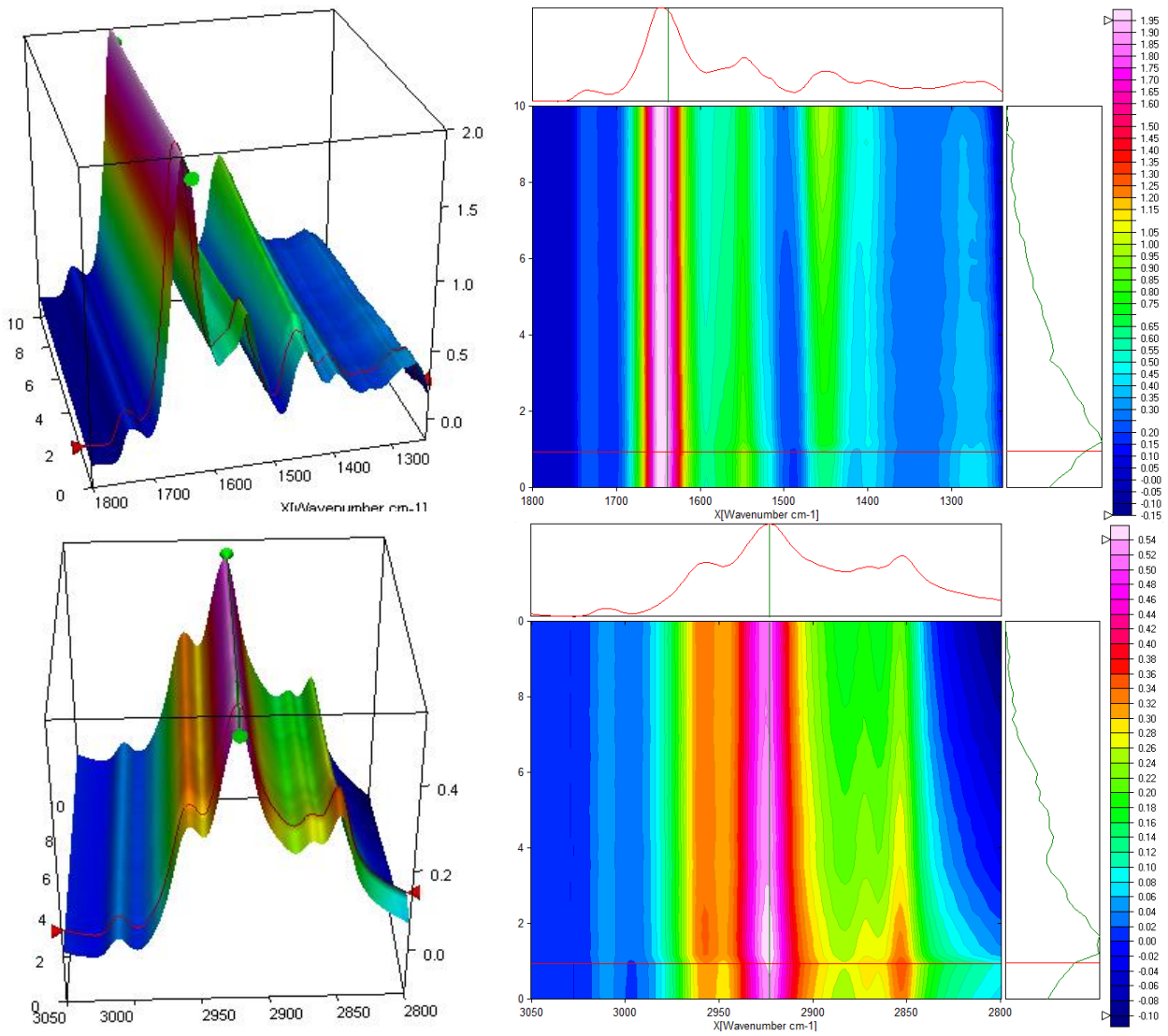


*Figure 7.2 - Time resolved measurements of a single cell of the* Chlamydomonas reinhardtii psaF *mutant before and after exposure to 15 minutes of high light. Red horizontal line indicates the time at which high light exposure occurred. Spectra have been min-max normalized to the amide I peak at 1650 cm$^{-1}$ and the local baseline. The CH stretching region was offset corrected to the local baseline at 3040-3010 cm$^{-1}$.*

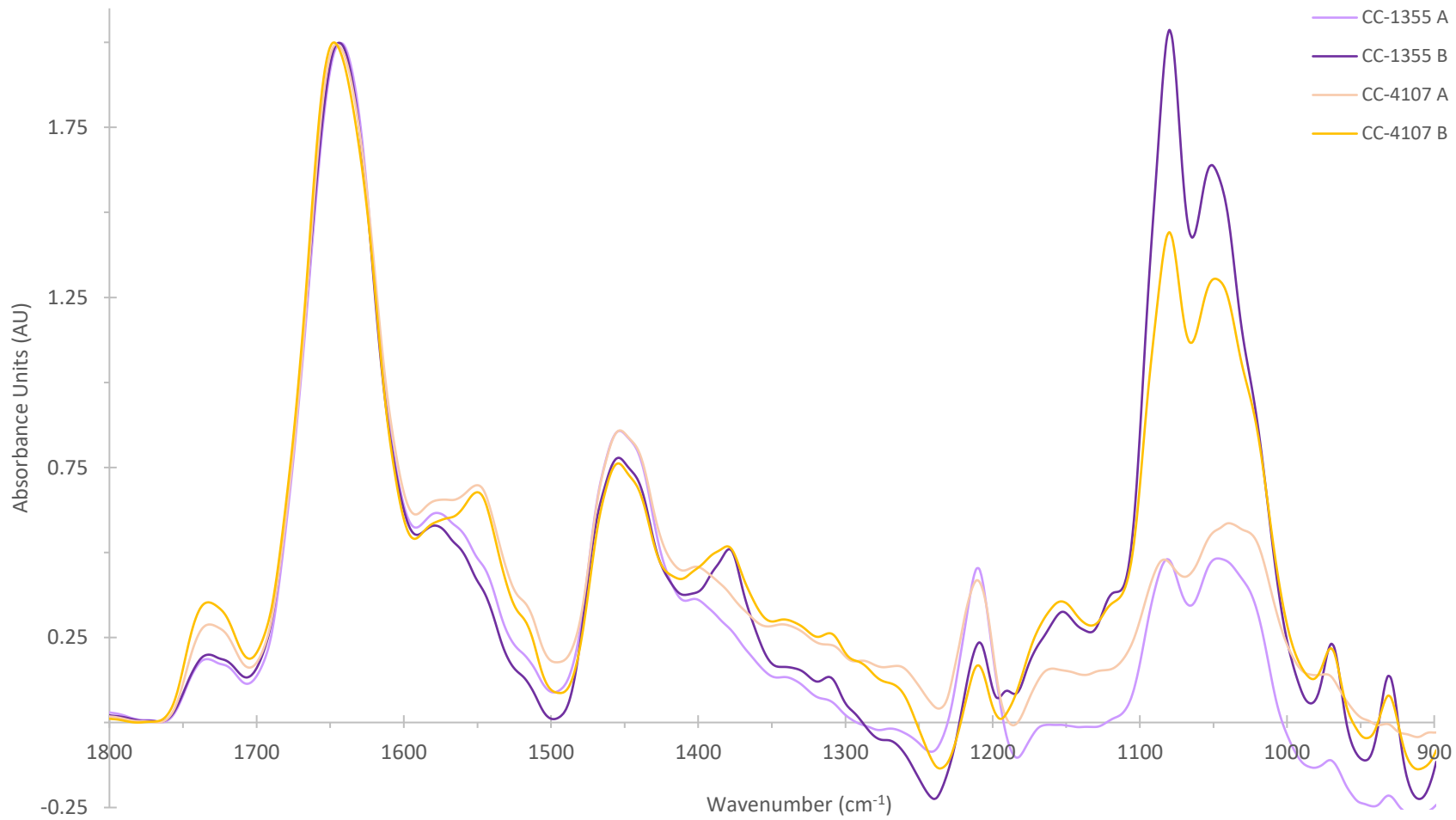


*Figure 7.3 - Average of cellular subpopulations in cells of the CC-1355 cell line (purple) and CC-4107 cell line (orange). Spectra were obtained from cells exposed to high light and rose bengal, but similar subpopulations were obtained from control cultures and other exposures.*

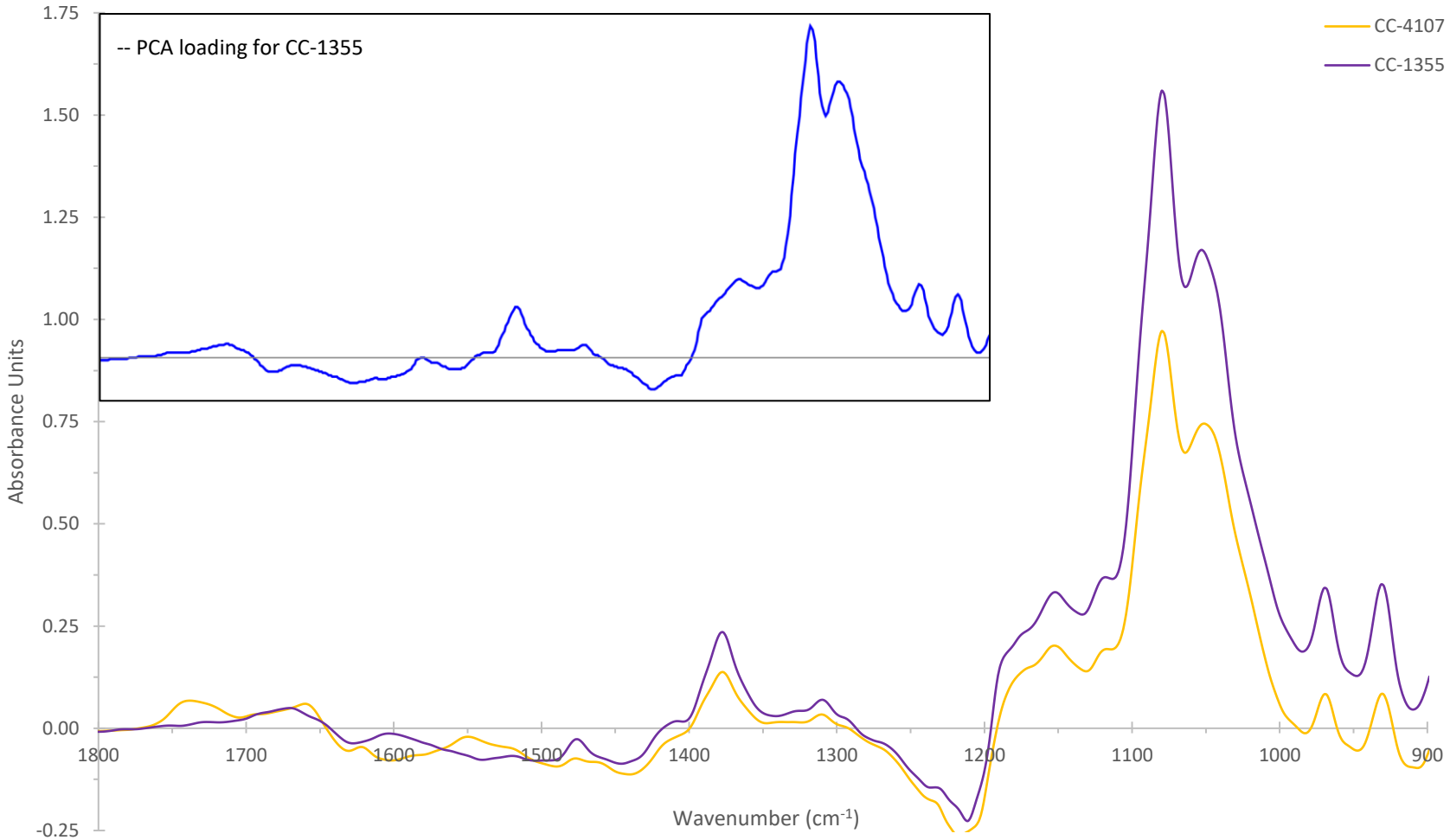


*Figure 7.4 - Difference spectra of the averages from Figure 7.3: CC-1355 (purple) and CC-4107 (orange). Inset in blue is the principal component analysis loading for the spectra from which the purple difference spectrum was obtained. Similar differences in the 1378 $cm^{-1}$ contribution were intermittently observed on other days in other cell lines. Consistent differences were present in 1477 $cm^{-1}$ (w), 1412 $cm^{-1}$ (sh), 1377 $cm^{-1}$ (m), 1308 $cm^{-1}$ (w), 1152 $cm^{-1}$ (m), 1118 $cm^{-1}$ (sh), 1080 $cm^{-1}$ (vs), 1051 (s), 1020 (sh), 969 (m), and 931 $cm^{-1}$ (m).*

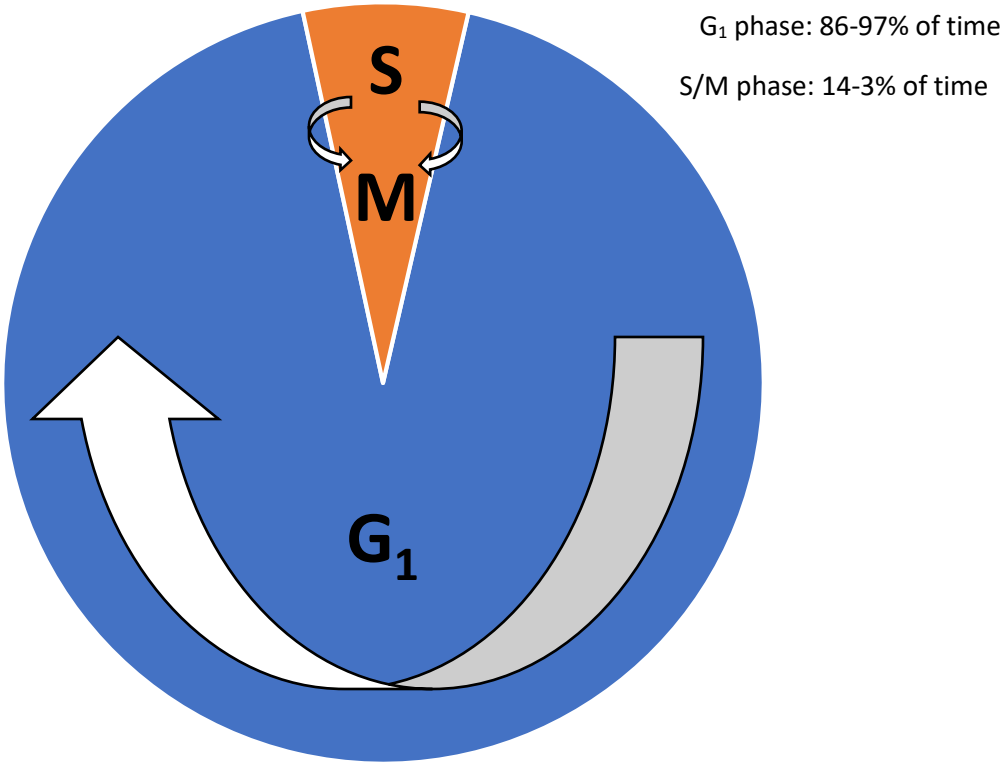


*Figure 7.5 - Cell cycle of* Chlamydomonas reinhardtii.

# CHAPTER EIGHT

# SUMMARY AND CONCLUSIONS

## 8.1 Experimental Design and Differentiating Species and Mutants

The work in this thesis adds to the broader body of research in three primary ways: firstly, in the design and interpretation of FTIR studies of living cells; secondly, understanding the physiological response of individual cells to different oxidative stressors; and thirdly, probing the impacts of photosynthetic mutations on response to oxidative stress. FTIR spectromicroscopy was found to be an extremely powerful system for studying individual living cells and their differences. The power of this system, however, means that extreme caution must be taken when designing and interpreting experiments.

The first, and most foundational, lesson learned herein regarded experimental design. Chapter 3 highlighted the necessity of understanding the extent of the variation present in your experimental system. Though my findings may also be utilized with higher-end lab-based FTIR microscopes, beamtime availability at synchrotron facilities worldwide is limited, with strict scheduling procedures in the place. As such, it is even more important for researchers to conduct initial, exploratory tests. The work presented in this thesis utilizes axenic, monocultured, haploid, clonal, unicellular organisms (*Chlamydomonas* spp.), though culture growth was asynchronous. Given these factors, it can be extrapolated that there is less variation present between individual cells, or between controls on different days, than would be expected in many other test systems. Despite this, significant variation was observed between cells within the same culture, as well as between different cultures grown under near-identical conditions. In short, FTIR spectromicroscopy was able to identify differences in the cellular biochemical makeup resulting from both variation between cultures, as well as variation produced by exposure to experimental stressors. This means the direct comparison of the spectra obtained from cells exposed to various types of experimental treatments obtained on different days would yield results confounded by the overlap in the variation that occurs between days and the variation that occurs as a result of experimental treatment. The nature of synchrotron beamtime scheduling means that it is often more convenient to split controls and exposures across multiple shifts, but it is essential to do

foundational research to understand the extent of and types of variation present in your experimental system that can be discerned by FTIR spectromicroscopy.

This explicit knowledge of the IR spectra of your test system is also essential for another prerequisite for accurate experimental procedure. It allows experimenters to determine when outliers are present in the data that may result in skewed final results. The inclusion of strong outliers in averages can have observable effects on averages. This is particularly pronounced if subpopulations of cells are present. The presence of distinct subpopulations of cells may also raise other questions regarding the system, and its response to experimental stress. Usage of PCA without interpretation of the loadings may lead to differentiation of cell populations on the basis of factors such as baseline variation that have no relation to actual biochemical differences between the individual cells.

The power of FTIR spectromicroscopy to study individual cells was such that it was possible to differentiate between the spectra of different species of *Chlamydomonas* grown under identical conditions, despite an extremely high overall degree of similarity of cellular components. The biochemical and physical/structural similarities between different species of the genus *Chlamydomonas* exceed those even of other Chlorophyceae, which are subdivided primarily by ultrastructure morphology. It also allowed us to discriminate between *Chlamydomonas reinhardtii* cell lines carrying photosynthetic mutations. These differences were primarily associated with cellular lipid and protein cohorts, though an unassigned indicator peak at 1260 $cm^{-1}$ was a characteristic feature in spectra obtained from cells of *Chlamydomonas* DJX-H and the *C. reinhardtii* mutant *psaF* (Figures 3.8 and 5.1, respectively). Some of these differences can be directly correlated to what we know about the physiology and life history of these cells. For example, when compared to wild type *C. reinhardtii*, mutants that lacked Chl *b* (CC-1355 and *psaF cbn1*) are known to have a lipid cohort with less polyunsaturation. This was reflected in the weaker relative intensity of the CH peak at 3010 $cm^{-1}$. Furthermore, the knowledge that these two mutants lacked Chl *b* and therefore had lower overall chlorophyll concentrations helped in assigning the 1608 $cm^{-1}$ second derivative contribution within the amide I envelope to chlorophyll, as well as confirming that the 1285 $cm^{-1}$ peak has at least a strong contribution from tetrapyrrole absorption. Additionally, the *Chlamydomonas* DJX-J and DJX-H species are known to be able to grow down to 4 ℃, in comparison to *C. reinhardtii*, which has a tolerance limit at 16 ℃. This

increased cold tolerance in the DJX- species is expected to be due to greater levels of lipid unsaturation, and variety of lipid molecules in the plasma membrane. This results in greater membrane disorder which was reflected in differences in the high wavenumber CH stretching region of the FTIR spectra. The DJX- species exhibit broader $CH_2$ and $CH_3$ peaks with higher peak positions, indicative of a greater degree of membrane disorder as well as increased variety in hydrocarbon chain length.

We were even able to suggest that one mutant cell line – *psaF* – required further exploration with other techniques. This cell line has lost the *psaF* protein subunit, a difference that under control conditions should have resulted in a normal, wild type phenotype. Instead, it was clearly differentiated from wild type control cells by the presence of the unassigned indicator peak at 1260 $cm^{-1}$ and differences in the lipid cohort, as indicated by the relative strength and shape of the 1740 $cm^{-1}$ lipid carbonyl. These observed differences were not observed in the protein amide I or amide II peaks, suggesting that *psaF* cells carrying this mutations exhibit other physiological differences from wild type cells. This is likely due to unanticipated knock-on physiological effects, but could potentially be the result of an incidental mutation that occurred over the (20,000 to 30,000) generations since the initial isolation of the cell line.

## 8.2 Impact of High Light and/or Rose Bengal on Individual Algal Cells

As discussed in depth in Chapter 1, the primary compound of concern produced via high light stress is endogenously produced singlet oxygen. This is not, however, the only ROS or compound of concern produced. It is possible to position exposure to high light stress as exposure to endogenously produced singlet oxygen, though this is somewhat reductive. This work showed conclusively that it is possible to use FTIR spectromicroscopy to study the impact of high light and/or rose bengal (singlet oxygen, produced endogenously or exogenously) on individual living cells. Furthermore, it was possible to examine the impact of high light and/or rose bengal treatment on cells with known photosynthetic impairments. We could hypothesize about the impact of high light or rose bengal treatments on the cellular biochemical make up, then test that using FTIR spectroscopy. Differences were observed throughout the CH stretching region and 1800-1240 $cm^{-1}$ fingerprint region. The spectral alterations best associated with changes in the cellular biochemical make up were found in peaks related to cellular lipids and proteins. A summary of some of these major changes and their relationship to each other can be found in Tables 8.1 and

8.2. In broad strokes, changes in lipid peaks could be related to altered lipid cohorts. More specifically, the changes resulted from some combination of decreased lipid unsaturation, changes in the diversity of CH chain length, the formation of lipid oxidation by-products such as lipid hydroperoxides and ketones, and the evolution of short-chain alkanes via lipid oxidation. The combination of these factors resulted in altered membrane fluidity and increased membrane permeability. Changes observed in the protein peaks were slightly more broadly interpreted. The degree to which each of these changes occurred varied by system – by treatment and algal line. One consistency was that the evolution of short-chain alkanes (noted by increased absorption at ~2885 $cm^{-1}$) was always associated with specific changes in the lipid carbonyl peak: a relative decrease in the absorption of the 1740 $cm^{-1}$ second derivative component and a strongly increased absorption in the 1720-1700 $cm^{-1}$ region associated with the formation of byproducts of lipid oxidation.

Analysis of the spectra and second derivatives of the amide I peak broadly suggested differences in protein secondary structure. Further analysis of the variety of photosynthetic mutants suggested two broad categories for these changes. The first being acclimative responses mounted in response to high light exposure. These could potentially include mechanisms such as state transitions, photoinhibition, and the xanthophyll cycle. This appeared to be represented by changes in the relative intensity of the second derivative components without significant broadening of these components. In most systems, this involved a change in the α-helix:β-sheet ratio in favour of the α-helix component. The second was associated with systems exhibiting other indicators of high degrees of oxidative stress. In these, there was still a relative change in the ratio of the amide I components. This usually shifted the α-helix to β-sheet ratio in favour of β-sheets. It also showed a relative increase in the intensity of the 1680 $cm^{-1}$ component and broadening of all three second derivative components. This appeared to be associated with the formation of intermolecular β-sheets as well as other molecular intermediates and was indicative of a gross level of protein damage. Overlapping with either of these two observations was the downshifting of the position of the second derivative components by 1-5 $cm^{-1}$. This was associated with H-D exchange due to increased membrane permeability, and was seen in concert with the decrease of the amide II and increase of the amide II". This downshifting was always seen in concert with scenario two (gross protein damage) and also in combination with scenario one (acclimative change or limited damage) in the zeaxanthin hyperaccumulator mutant CC-4107 that also lacked a cell wall. Overall,

H-D exchange was only directly reflective of changes in membrane permeability and therefore increased penetration of deuterium into the cell. Cellular responses to high light and/or oxidative stress were such that strongly increased membrane permeability usually occurred in concert with large-scale protein damage and changes to secondary structure, but H-D exchange was seen in HLRB CC-4107 in the absence of gross damage (Figure 6.3).

The most striking observation was how strongly the type of stress – high light and/or rose bengal, sometimes read as a source of singlet oxygen – influenced cellular response. Singlet oxygen generated by rose bengal had distinctly different impacts on the spectra of individual cells as compared to that generated by high light exposure. In *C. reinhardtii* (WT) exposure to either HL or RB resulted in similar degrees of observed change in lipid-associated peaks. In the spectra of HL-exposed cells, this appeared to be localized to intracellular compartments such as the thylakoid membrane, while the spectra of cells exposed to RB showed evidence of altered membrane permeability suggestive of global damage to cellular lipids and the plasma membrane. In addition, exposure to HL triggered specific and repeatable changes in protein secondary structure not seen in the spectra of cells exposed to RB. The balance of evidence from the photosynthetic mutants supported the supposition that this type of change (type one, as discussed above: narrowing and upshifting of the amide I peak due to the second derivative α:β ratio changing in favour of α-helical structures) was at least partly due to physiological modifications triggered within the cells in response to high light stress, and its resulting high light phenotype. This spectral change in response to high light was present in cells of the *psaF* line, and absent in cell lines lacking Chl *b*. The CC-4107 cell line – which exhibited a high light phenotype under control conditions – was a special case, as the shape and second derivative of the amide I peak under control conditions closely resembled that of WT spectra that had been exposed to high light. In wild type *C. reinhardtii* cells, state transitions alone involve changes to ~80% of LHCs (Ünlü et al. 2014), and light harvesting complex proteins make up a significant portion of total cellular proteins so it is entirely feasible that these differences would be observable in the infrared spectra. In contrast to exposure to HL or RB alone, the combination HLRB exposure resulted in distinctive spectral changes in the protein peaks. Changes in the lipid-associated peaks were often amplified versions of those seen in single exposures, suggesting a greater degree of damage to lipids. In HLRB exposures, different changes were seen in protein secondary structure. The nature of these

changes (type two, as discussed above) indicated gross degrees of protein damage and unfolding, likely due to the rate of damage greatly exceeding the rate of repair and replacement.

As such, it is possible to conclude several main points. Firstly, that singlet oxygen generated by exposure to rose bengal and by exposure to high light resulted in different physiological impacts within the cell. Exposure to rose bengal resulted in global damage to lipids and therefore altered membrane permeability. Exposure to high light resulted in lipid damage localized to intracellular compartments and triggered protein changes associated high light phenotypes. Singlet oxygen generated within the chloroplast was better localized within a cellular compartment that evolved to neutralize its impacts. Secondly, oxidative damage to lipids progressed along a single pathway, while oxidatively-mediated changes to protein secondary structure may have divergent pathways depending upon the degree of damage present.

The environmental sister species *Chlamydomonas* DJX- showed virtually no response to high light, but were more greatly more sensitive to rose bengal exposure. There are two main possibilities for why no response to high light was observed in the DJX- spp. The first is that no high light response was triggered. In this case, it may be that these cells lines are more tolerant to high light stress, and the degree of illumination required to trigger cellular high light response was not reached in this study. Another explanation for an absence of high light response could be a muted or lost acclimative response such as the known loss of state transitions, in which case the cells could be more sensitive to high light. The second possibility is that a high-light response was triggered in these cells, but it was not observed. This could occur if the timescale of cellular response and repair was more rapid, such that any damage or acclimation that accumulated was been undone by the time the FTIR measurements were done. It could further be possible that the protein changes seen in *C. reinhardtii* were specifically associated with state transitions. If so, the DJX- species may possess a different overall suite of high light responses to high light exposure that are not easily observable in the infrared spectra, potentially manifesting as more subtle or complex changes in relatively minor peaks.

The environmental species showed a greater degree of susceptibility to oxidative stress mediated by rose bengal than did WT *C. reinhardtii*. This can be explained in part by the greater disorder of the plasma membranes of these cells, which allowed large amounts of rose bengal into the cells themselves, resulting in a feedback loop of increased membrane permeability caused by

rose bengal allowing more rose bengal into the cell. Visual observation of RB and HLRB cultures showed remnants of rose bengal inside of multiple cells in rose bengal -exposed cultures. Distinct spectral responses to rose bengal (RB, HLRB) were also found in these cells, particularly in the complex fingerprint region below 1400 $cm^{-1}$. In comparison to *C. reinhardtii*, the effects mediated by HLRB were largely the same as those mediated by RB alone, only amplified. Thus it can be concluded that oxidative stress induced by high light or rose bengal again had very different physiological impacts, though the degree of sensitivity to either varies between species.

Work with the *C. reinhardtii* mutants provided a variety of supportive evidence for some of the changes seen in all species. In addition, it supports the hypothesis that changes in protein secondary structure seen under high light conditions are at least partially acclimative. The effects of high light were amplified by the loss of the *psaF* subunit, which caused a backup of electrons in the ETC. The effects of high light were muted by the loss of Chl *b*, even in the *psaF* mutant which exhibited greater baseline sensitivity to high light. The changes to the ETC and light harvesting proteins promoted by the preferential accumulation of zeaxanthin, as well as the increased concentration of carotenoids, protected the CC-4107 cell line from exposure to high light or rose bengal. Even in response to HLRB exposure, spectra of CC-4107 cells exhibited very few indicators of stress (Figure 6.3). Changes in the amide I peak were more associated with controlled remodelling or H-D exchange than with gross damage: the α-helix:β-sheet ratio exhibited minor changes, and there was no broadening of the second derivative components. The relative decrease of the 1608 $cm^{-1}$ component was matched with decreased absorption by the 1285 $cm^{-1}$ component, suggesting this difference was due to changes in or loss of tetrapyrroles such as chlorophyll. Downshifting in the second derivative peak positions did occur, in addition to amide II-amide II' interconversion, suggesting increased membrane permeability and analysis of the lipid peaks appeared to indicate that damaged lipids were removed, repaired, or replaced rapidly, preventing lipid oxidation signalling cascades and the formation of lipid oxidation byproducts.

My twofold research objectives were to investigate the effects of high light and rose bengal exposure on biochemical and metabolic processes of individual living cells of *Chlamydomonas* spp., and to expand the body of literature on the use of FTIR in the study of complex systems exhibiting subtle responses. To this end, I investigated the nature of variation between individual cells and between cultures, elucidated the impacts of high light and/or rose bengal on individual

living cells, and studied how photosynthetic mutations interrupted or potentiated the effect of high light and/or rose bengal on individual living cells. Overall, this work provides an in-depth complete study of individual living cells using FTIR spectromicroscopy. It has allowed greater understanding of the rigours required for experimental design and data analysis. In addition, it has provided insights into the effects of different oxidative stressors on individual living cells, as well as helped to elucidate the role of species-specific differences and photosynthetic mutations on cellular responses.

*Table 8.1 - Overview of major changes observed in lipid-associated infrared peaks, and their relationships to each other.*

| | Change | Peak | | Meaning |
|---|---|---|---|---|
| | ↓ | 3010 $cm^{-1}$ | | Loss of *cis*-unsaturated lipids |
| | ↔ | $CH_2$ peaks | | Increased diversity of lipid chains |
| | ← | $CH_2$ peaks | | Increased membrane disorder |
| * | ↑ | 2890-2880 $cm^{-1}$ | ($2^{nd}$ component) | Formation of short chain alkanes |
| | ↓ | 1740 $cm^{-1}$ | ($2^{nd}$ component) | Oxidative breakdown of lipids |
| * | ↑ | 1720-1700 $cm^{-1}$ | | Formation of the byproducts of lipid oxidation |
| ** | ↓ | Amide II | | H-D exchange, altered membrane permeability |
| ** | ↑ | 1450 $cm^{-1}$ | | H-D exchange, altered membrane permeability |

*, ** Changes appear to be tightly linked



*Table 8.2 - Overview of major changes associated with protein-associated infrared peaks, and their relationships to each other.*

| | Change | Peak | | Meaning |
|---|---|---|---|---|
| | ← | Amide I | | Change in α:β ratio to favour α-helixes in response to high light |
| | →, ↔ | Amide I | | Gross protein damage |
| | ↔ | Amide I | ($2^{nd}$ components) | Gross protein damage, formation of denaturated proteins |
| * | → | Amide I | ($2^{nd}$ components) | H-D exchange |
| * | ↓ | Amide II | | H-D exchange, altered membrane permeability |
| * | ↑ | 1450 $cm^{-1}$ | | H-D exchange, altered membrane permeability |

* Changes appear to be tightly linked

# CHAPTER NINE

# REFERENCES


Allorent, Guillaume et al. 2013. "A Dual Strategy to Cope with High Light in Chlamydomonas Reinhardtii." *Plant Cell* 25(2):545–57.

Alvarez-Ordóñez, A., D. J. M. Mouwen, M. López, and M. Prieto. 2011. "Fourier Transform Infrared Spectroscopy as a Tool to Characterize Molecular Composition and Stress Response in Foodborne Pathogenic Bacteria." *Journal of Microbiological Methods* 84(3):369–78. Retrieved (http://dx.doi.org/10.1016/j.mimet.2011.01.009).

Anjum, Naser A. et al. 2015. "Lipids and Proteins—major Targets of Oxidative Modifications in Abiotic Stressed Plants." *Environmental Science and Pollution Research* 22(6):4099–4121.

Apel, Klaus and Heribert Hirt. 2004. "Reactive Oxygen Species: Metabolism, Oxidative Stress, and Signal Transduction." *Annual Review of Plant Biology* 55(1):373–99. Retrieved (http://www.annualreviews.org/doi/10.1146/annurev.arplant.55.031903.141701).

Asada, K. 2006. "Production and Scavenging of Reactive Oxygen Species in Chloroplasts and Their Functions." *Plant Physiology* 141(2):391–96.

Baker, Matthew J. et al. 2014. "Using Fourier Transform IR Spectroscopy to Analyze Biological Materials." *Nature Protocols* 9(8):1771–91. Retrieved (http://www.nature.com/doifinder/10.1038/nprot.2014.110).

Ballschmiter, K. and J. J. Katz. 1972. "Chlorophyll-Chlorophyll and Chlorophyll-Water Interactions in the Solid State." *BBA - Bioenergetics* 256(2):307–27.

Baroli, I. and K. K. Niyogi. 2000. "Molecular Genetics of Xanthophyll-Dependent Photoprotection in Green Algae and Plants." *Philosophical Transactions of the Royal Society B: Biological Sciences* 355(1402):1385–94. Retrieved (http://rstb.royalsocietypublishing.org/cgi/doi/10.1098/rstb.2000.0700).

Baroli, Irene, An D. Do, Tomoko Yamane, and Krishna K. Niyogi. 2003. "Zeaxanthin Accumulation in the Absence of a Functional Xanthophyll Cycle Protects Chlamydomonas Reinhardtii from Photooxidative Stress." *The Plant Cell* 15(4):992–1008.

Barth, Andreas. 2000. "The Infrared Absorption of Amino Acid Side Chains." *Progress in Biophysics and Molecular Biology* 74(3–5):141–73.

Barth, Andreas. 2007. "Infrared Spectroscopy of Proteins." *Biochimica et Biophysica Acta - Bioenergetics* 1767(9):1073–1101.

Barth, Andreas and Christian Zscherp. 2002. "What Vibrations Tell Us about Proteins." *Quarterly Reviews of Biophysics* 35(4):369–430.

Berry, Lindsay L., Pawel Brzezowski, and Kenneth E. Wilson. 2011. "Inactivation of the STT7 Gene Protects PsaF-Deficient Chlamydomonas Reinhardtii Cells from Oxidative Stress

under High Light." *Physiologia Plantarum* 141(2):188–96.

Berterame, Nadia Maria, Danilo Porro, Diletta Ami, and Paola Branduardi. 2016. "Protein Aggregation and Membrane Lipid Modifications under Lactic Acid Stress in Wild Type and OPI1 Deleted Saccharomyces Cerevisiae Strains." *Microbial Cell Factories* 15(1):39. Retrieved (http://microbialcellfactories.biomedcentral.com/articles/10.1186/s12934-016-0438-2).

Birarda, Giovanni et al. 2010. "Infrared Microspectroscopy of Biochemical Response of Living Cells in Microfabricated Devices." *Vibrational Spectroscopy* 53(1):6–11. Retrieved (http://dx.doi.org/10.1016/j.vibspec.2010.01.016).

Bölling, Christian and Oliver Fiehn. 2005. "Metabolite Profiling of *Chlamydomonas Reinhardti* under Nutrient Deprivation." *Plant Physiology* 139(December):1995–2005. Retrieved (http://www.plantphysiol.org/content/139/4/1995.short).

Boydston-White, S., T. Gopen, S. Houser, J. Bargonetti, and M. Diem. 1999. "Infrared Spectroscopy of Human Tissue. V. Infrared Spectroscopic Studies of Myeloid Leukemia (ML-1) Cells at Different Phases of the Cell Cycle." *Biospectroscopy* 5(4):219–27. Retrieved (http://www.ncbi.nlm.nih.gov/pubmed/10478952).

Brzezowski, Pawel, Kenneth E. Wilson, and Gordon R. Gray. 2012. "The PSBP2 Protein of Chlamydomonas Reinhardtii Is Required for Singlet Oxygen-Dependent Signaling." *Planta* 236(4):1289–1303.

Cai, Shuowei and Bal Ram Singh. 1999. "Identification of β-Turn and Random Coil Amide III Infrared Bands for Secondary Structure Estimation of Proteins." *Biophysical Chemistry* 80:7–20.

Carr, G. L. 2001. "Resolution Limits for Infrared Microspectroscopy Explored with Synchrotron Radiation." *Review of Scientific Instruments* 72(3):1613–19.

Chen, Liang et al. 2012. "Synchrotron Infrared Measurements of Protein Phosphorylation in Living Single PC12 Cells during Neuronal Differentiation." *Analytical Chemistry* 84(9):4118–25.

Chen, X. et al. 2001. "Conformation Transition Kinetics of Regenerated Bombyx Mori Silk Fibroin Membrane Monitored by Time-Resolved FTIR Spectroscopy." *Biophysical Chemistry* 89(1):25–34.

Clède, Sylvain, Clotilde Policar, and Christophe Sandt. 2014. "Fourier Transform Infrared (FT-IR) Spectromicroscopy to Identify Cell Organelles: Correlation with Fluorescence Staining in MCF-7 Breast Cancer Cells." *Applied Spectroscopy* 68(1):113–17.

Coimbra, M. A., A. Barros, D. N. Rutledge, and I. Delgadillo. 1999. "FTIR Spectroscopy as a Tool for the Analysis of Olive Pulp Cell-Wall Polysaccharide Extracts." *Carbohydrate Research* 317(1–4):145–54.

Cross, Frederick R. and James G. Umen. 2015. "The Chlamydomonas Cell Cycle." *Plant Journal* 82(3):370–92.

Davies, M. J. 2004. "Reactive Species Formed on Proteins Exposed to Singlet Oxygen."

*Photochemical & Photobiological Sciences* 3(1):17–25.

Davies, M. J. 2016. "Protein Oxidation and Peroxidation." *Biochemical Journal* 473(7):805–25. Retrieved (http://biochemj.org/cgi/doi/10.1042/BJ20151227).

Davies, Michael J. 2003. "Singlet Oxygen-Mediated Damage to Proteins and Its Consequences." *Biochemical and Biophysical Research Communications* 305(3):761–70.

Dean, A. P., M. C. Martin, and D. C. Sigee. 2007. "Resolution of Codominant Phytoplankton Species in a Eutrophic Lake Using Synchrotron-Based Fourier Transform Infrared Spectroscopy." *Phycologia* 46(2):151–59.

Dean, A. P., D. C. Sigee, B. Estrada, and J. K. Pittman. 2010. "Using FTIR Spectroscopy for Rapid Determination of Lipid Accumulation in Response to Nitrogen Limitation in Freshwater Microalgae." *Bioresource Technology* 101(12):4499–4507.

Dent, R. M., C. M. Haglung, B. L. Chin, M. C. Kobayashi, and K. N. Niyogie. 2005. "Functional Genomics of Eukaryotic Photosynthesis Using Insertional Mutagenesis of Chlamydomonas Reinhardtii." *Plant Physiology* 137(2):545–56. Retrieved (http://www.plantphysiol.org/cgi/doi/10.1104/pp.104.055244).

Derenne, Allison, Thomas Claessens, Caroline Conus, and Erik Goormaghtigh. 2013. "Infrared Spectroscopy of Membrane Lipids." Pp. 1074–81 in *Encyclopedia of Biophysics*. Retrieved (http://link.springer.com/10.1007/978-3-642-16712-6).

Dietz, Karl-Josef, Ron Mittler, and Graham Noctor. 2016. "Recent Progress in Understanding the Role of Reactive Oxygen Species in Plant Cell Signaling." *Plant Physiology* 171(3):1535–39. Retrieved (http://www.plantphysiol.org/lookup/doi/10.1104/pp.16.00938).

Dong, Aichun, Theodore W. Randolph, and John F. Carpenter. 2000. "Entrapping Intermediates of Thermal Aggregation in α-Helical Proteins with Low Concentration of Guanidine Hydrochloride." *Journal of Biological Chemistry* 275(36):27689–93.

Dovbeshko, G. I., N. Y. Gridina, E. B. Kruglova, and O. P. Pashchuk. 2000. "FTIR Spectroscopy Studies of Nucleic Acid Damage." *Talanta* 53:233–46.

Edreva, A. 2005. "Generation and Scavenging of Reactive Oxygen Species in Chloroplasts: A Submolecular Approach." *Agriculture Ecosystems & Environment* 106(2–3):119–33.

Eichenberger, Waldemar, Arminio Boschetti, and Hans Peter Michel. 1986. "Lipid and Pigment Composition of a Chlorophyll B-deficient Mutant of Chlamydomonas Reinhardii." *Physiologia Plantarum* 66(4):589–94.

Farah, Joseph, Fabrice Rappaport, Yves Choquet, Pierre Joliot, and Jean D. Rochaix. 1995. "Isolation of a psaF-Deficient Mutant of Chlamydomonas Reinhardtii: Efficient Interaction of Plastocyanin with the Photosystem I Reaction Center Is Mediated by the PsaF Subunit." *The EMBO Journal* 14(20):4976–84.

Fischer, B. B. et al. 2012. "SINGLET OXYGEN RESISTANT 1 Links Reactive Electrophile Signaling to Singlet Oxygen Acclimation in Chlamydomonas Reinhardtii." *Proceedings of the National Academy of Sciences of the United States of America* 109(20):E1302–11.

Fischer, B. B., A. Krieger-Liszkay, and R. I. L. Eggen. 2004. “Photosensitizers Neutral Red (Type I) and Rose Bengal (Type II) Cause Light-Dependent Toxicity in Chlamydomonas Reinhardtii and Induce the Gpxh Gene via Increased Singlet Oxygen Formation.” *Environmental Science & Technology* 38(23):6307–13.

Fischer, B. B., M. Wiesendanger, and R. I. L. Eggen. 2006. “Growth Condition-Dependent Sensitivity, Photodamage and Stress Response of Chlamydomonas Reinhardtii Exposed to High Light Conditions.” *Plant and Cell Physiology* 47(8):1135–45.

Fischer, Beat B. et al. 2009. “Function and Regulation of the Glutathione Peroxidase Homologous Gene GPXH/GPX5 in Chlamydomonas Reinhardtii.” *Plant Molecular Biology* 71(6):569–83.

Garidel, Patrick and Heidrun Schott. 2006. “Fourier-Transform Midinfrared Spectroscopy for Analysis and Screening of Liquid Protein Formulations Part 2: Details Analysis and Applications.” *BioProcess International* 1:48–55.

Gericke, Arne and Heinrich Hühnerfuss. 1995. “Investigation of Z- and E-Unsaturated Fatty Acids, Fatty Acid Esters, and Fatty Alcohols at the Air/Water Interface by Infrared Spectroscopy.” *Langmuir* 11(1):225–30.

Girotti, A. W. 1985. “Mechanisms of Lipid Peroxidation.” *Journal of Free Radicals in Biology & Medicine* 1(2):87–95.

Girotti, A. W. and T. Kriska. 2004. “Role of Lipid Hydroperoxides in Photo-Oxidative Stress Signaling.” *Antioxidants & Redox Signaling* 6(2):301–10.

Giroud, Christian, Annegret Gerber, and Waldemar Eichenberger. 1988. “Lipids of Chlamydomonas Reinhardtii. Analysis of Molecular Species and Intracellular Site(s) of Biosynthesis.” *Plant Cell Physiology* 29(4):587–95.

Goff, Kira L. 2012. “Toxicity, Morphological Changes, and Dissipation of Oil Sands Naphthenic Acids in Chlamydomonas Reinhardtii.” University of Saskatchewan, Saskatoon, Saskatchewan, Canada.

Goff, Kira L., John V. Headley, John R. Lawrence, and Kenneth E. Wilson. 2013. “Assessment of the Effects of Oil Sands Naphthenic Acids on the Growth and Morphology of Chlamydomonas Reinhardtii Using Microscopic and Spectromicroscopic Techniques.” *Science of the Total Environment* 442:116–22. Retrieved (http://dx.doi.org/10.1016/j.scitotenv.2012.10.034).

Goff, Kira L., Kerry M. Peru, Kenneth E. Wilson, and John V. Headley. 2014. “Evaluation of Biologically Mediated Changes in Oil Sands Naphthenic Acid Composition by Chlamydomonas Reinhardtii Using Negative-Ion Electrospray Orbitrap Mass Spectrometry.” *Journal of Phycology* 50(4).

Goff, Kira L., Luca Quaroni, Tor Pedersen, and Kenneth E. Wilson. 2010. “Measurement of Ethanol Formation in Single Living Cells of Chlamydomonas Reinhardtii Using Synchrotron Fourier Transform Infrared Spectromicroscopy.” Pp. 54–56 in *AIP Conference Proceedings*, vol. 1214, edited by A. Predoi-Cross and B. E. Billinghurst. Banff, Alberta, Canada NV - 1: American Institute of Physics Conference Proceedings.

Goff, Kira L., Luca Quaroni, and Kenneth E. Wilson. 2009. “Measurement of Metabolite Formation in Single Living Cells of Chlamydomonas Reinhardtii Using Synchrotron Fourier-Transform Infrared Spectromicroscopy.” *Analyst* 134(11):2216. Retrieved (http://xlink.rsc.org/?DOI=b915810c).

Green, M. J. and H. A. O. Hill. 1984. “Chemistry of Dioxygen.” *Methods in Enzymology* 105:3–22.

Gruszecki, W. I. et al. 2012. “Spectroscopy of Photosynthetic Pigment-Protein Complex LHCII.” *Acta Physica Polonica A* 121(2):397–400.

Hamilton, R. J., C. Kalu, E. Prisk, F. B. Padley, and H. Pierce. 1997. “Chemistry of Free Radicals in Lipids.” *Food Chemistry* 60(2):193–99.

Harris, E. H. 2009. *The Chlamydomonas Sourcebook*. Second. San Diego: Academic Press.

Harris, Elizabeth H. 1989. “The Chlamydomonas Sourcebook.” P. 780 in, edited by E. H. Harris. San Diego: Academic Press.

Hayati, Ibrahim Nor, Yaakob Bin Che Man, Chin Ping Tan, and Idris Nor Aini. 2005. “Monitoring Peroxide Value in Oxidized Emulsions by Fourier Transform Infrared Spectroscopy.” *European Journal of Lipid Science and Technology* 107(12):886–95.

Heraud, P., B. R. Wood, M. J. Tobin, J. Beardall, and D. McNaughton. 2005. “Mapping of Nutrient-Induced Biochemical Changes in Living Algal Cells Using Synchrotron Infrared Microspectroscopy.” *Fems Microbiology Letters* 249(2):219–25.

Hippler, Michael, Klaus Biehler, Anja Krieger-Liszkay, Jeannette van Dillewjin, and Jean David Rochaix. 2000. “Limitation in Electron Transfer in Photosystem I Donor Side Mutants of Chlamydomonas Reinhardtii.” *Biochemistry* 275(8):5852–59.

Holman, H. N., M. C. Martin, E. A. Blakely, K. Bjornstad, and W. R. McKinney. 2000. “IR Spectroscopic Characteristics of Cell Cycle and Cell Death Probed by Synchrotron Radiation Based Fourier Transform IR Spectromicroscopy.” *Biopolymers* 57(6):329–35.

Holman, H. Y. N., M. C. Martin, and W. R. McKinney. 2003. “Tracking Chemical Changes in a Live Cell: Biomedical Applications of SR-FTIR Spectromicroscopy.” *Spectroscopy-an International Journal* 17(2–3):139–59.

Holmström, Kira M. and Toren Finkel. 2014. “Cellular Mechanisms and Physiological Consequences of Redox-Dependent Signalling.” *Nature Reviews Molecular Cell Biology* 15(6):411–21. Retrieved (http://dx.doi.org/10.1038/nrm3801).

Holt, A. S. and E. E. Jacobs. 1955. “Infra-Red Absorption Spectra of Chlorophylls and Derivatives.” *Plant Physiology* 30(6):553–59.

Hopkinson, John H., Catherine Moustou, Nicola Reynolds, and John E. Newbery. 1987. “Applications of Attenuated Total Reflection in the Infrared Analysis of Carbohydrates and Biological Whole Cell Samples in Aqueous Solution*.” *Analyst* 112(April):501–5.

Horton, P., A. V Ruban, and R. G. Walters. 1996. “Regulation of Light Harvesting in Green Plants.” *Annual Review of Plant Physiology and Plant Molecular Biology* 47:655–84.

Huner, Norman, P. A.Gunna. Öquist, and Sarhan Fathey. 1998. “Energy Balance and Acclimitation To Light and Cold.” *Trends in Plant Science* 3(6):224–30.

Irihimovitch, Vered and Shlomit Yehudai-Resheff. 2008. “Phosphate and Sulfur Limitation Responses in the Chloroplast of Chlamydomonas Reinhardtii.” *FEMS Microbiology Letters* 283(1):1–8.

Ismail, A. A., F. R. van de Voort, G. Emo, and J. Sedman. 1993. “Rapid Quantitative Determination of Free Fatty Acids in Fats and Oils by Fourier Transform Infrared Spectroscopy.” *J.Am.Oil Chem.Soc.* 70(4):335–41.

Jamin, N. et al. 1998. “Chemical Imaging of Nucleic Acids, Proteins and Lipids of a Single Living Cell. Application of Synchrotron Infrared Microspectrometry in Cell Biology.” *Cellular and Molecular Biology* 44(1):9–13.

Jones, Dean P. 2006. “Redefining Oxidative Stress.” *Antioxidants & Redox Signalling* 8:1865–79.

Kacurakova, M. et al. 2000. “FT-IR Study of Plant Cell Wall Model Compounds: Pectic Polysaccharides and Hemicelluloses.” *Carbohydrate Polymers* 43(2):195–203.

Katz, J. J., G. L. Closs, F. C. Pennington, M. R. Thomas, and H. H. Strain. 1963. “Infrared Spectra, Molecular Weights, and Molecular Association of Chlorophylls a and B, Methyl Chlorophyllides, and Pheophytins in Various Solvents.” *Journal of the American Chemical Society* 85(23):3801–9.

Khandal, Dhriti et al. 2009. “Singlet Oxygen-Dependent Translational Control in the Tigrina-d.12 Mutant of Barley.” *Proceedings of the National Academy of Sciences of the United States of America* 106(31):13112–17.

Khoshmanesh, Aazam, Perran L. M. Cook, and Bayden R. Wood. 2012. “Quantitative Determination of Polyphosphate in Sediments Using Attenuated Total Reflectance-Fourier Transform Infrared (ATR-FTIR) Spectroscopy and Partial Least Squares Regression.” *The Analyst* 137(16):3704. Retrieved (http://xlink.rsc.org/?DOI=c2an35289c).

Kiwi, J. and V. Nadtochenko. 2004. “New Evidence for TiO2 Photocatalysis during Bilayer Lipid Peroxidation.” *Journal of Physical Chemistry B* 108(45):17675–84.

Kizil, Ramazan, Joseph Irudayaraj, and Koushik Seetharaman. 2002. “Characterization of Irradiated Starches by Using FT-Raman and FTIR Spectroscopy.” *Journal of Agricultural and Food Chemistry* 50(14):3912–18.

Klasek, Laura and Kentaro Inoue. 2016. *Dual Protein Localization to the Envelope and Thylakoid Membranes Within the Chloroplast*. Elsevier Inc. Retrieved (http://dx.doi.org/10.1016/bs.ircmb.2015.12.008).

Knox, J. P. and A. D. Dodge. 1985. “Singlet Oxygen and Plants.” *Phytochemistry* 24(5):889–96.

Kong, Jilie and Shaoning Yu. 2007. “Fourier Transform Infrared Spectroscopic Analysis of Protein Secondary Structures.” *Acta Biochimica Et Biophysica Sinica* 39(8):549–59.

Krieger-Liszkay, A. 2005. “Singlet Oxygen Production in Photosynthesis.” *Journal of*

*Experimental Botany* 56(411):337–46.

Krieger-Liszkay, A., C. Fufezan, and A. Trebst. 2008. "Singlet Oxygen Production in Photosystem II and Related Protection Mechanism." *Photosynthesis Research* 98(1–3):551–64.

Krimm, By Samuel and Jagdeesh Bandekart. 1986. "Vibrational Spectroscopy and Conformation of Peptides, Polypeptides, and Proteins." *Advances in Protein Chemistry* 48109. Retrieved (https://www.google.com/books?hl=zh-CN&lr=&id=0rke7tuwUysC&oi=fnd&pg=PA181&dq=Vibrational+spectroscopy+and+conformation+of+peptides,+polypeptides,+and+proteins.&ots=uMUdr9akIH&sig=PwhrsMxwz4TUyc9fKZjMdVval4M).

Ledford, H. K., B. L. Chin, and K. K. Niyogi. 2007. "Acclimation to Singlet Oxygen Stress in Chlamydomonas Reinhardtii." *Eukaryotic Cell* 6(6):919–30.

Ledford, H. K. and K. K. Niyogi. 2005. "Singlet Oxygen and Photo-Oxidative Stress Management in Plants and Algae." *Plant Cell and Environment* 28(8):1037–45.

Leisinger, U. et al. 2001. "The Glutathione Peroxidase Homologous Gene from Chlamydomonas Reinhardtii Is Transcriptionally up-Regulated by Singlet Oxygen." *Plant Molecular Biology* 46(4):395–408.

Lewis, RNAH and R. N. McElhaney. 2006. "Vibrational Spectroscopy of Lipids." Pp. 3447–64 in *Handbook of Vibrational Spectroscopy,* vol. 5.

Lewis, Ruthven N. A. H. and Ronald N. McElhaney. 2013. "Membrane Lipid Phase Transitions and Phase Organization Studied by Fourier Transform Infrared Spectroscopy." *Biochimica et Biophysica Acta (BBA) - Biomembranes* 1828(10):2347–58. Retrieved (http://linkinghub.elsevier.com/retrieve/pii/S0005273612003677).

Lewis, S. P., A. T. Lewis, and P. D. Lewis. 2013. "Prediction of Glycoprotein Secondary Structure Using ATR-FTIR." *Vibrational Spectroscopy* 69:21–29. Retrieved (http://dx.doi.org/10.1016/j.vibspec.2013.09.001).

Liu, Jinghua et al. 2013. "Study of Energetic-Particle-Irradiation Induced Biological Effect on Rhizopus Oryzae through Synchrotron-FTIR Micro-Spectroscopy." *Journal of Molecular Structure* 1031:1–8. Retrieved (http://dx.doi.org/10.1016/j.molstruc.2012.07.025).

Machana, Sasipawan, Natthida Weerapreeyakul, Sahapat Barusrux, Kanjana Thumanu, and Waraporn Tanthanuch. 2012. "FTIR Microspectroscopy Discriminates Anticancer Action on Human Leukemic Cells by Extracts of Pinus Kesiya; Cratoxylum Formosum Ssp Pruniflorum and Melphalan." *Talanta* 93:371–82.

Martinez, G. R. et al. 2003. "Oxidative and Alkylating Damage in DNA." *Mutation Research-Reviews in Mutation Research* 544(2–3):115–27.

Di Mascio, P., M. E. Murphy, and H. Sies. 1991. "Antioxidant Defense Systems: The Role of Carotenoids, Tocopherols, and Thiols." *American Journal of Clinical Nutrition* 53(1):S194–200.

Max, Jean-Joseph and Camille Chapados. 2002. "Isotope Effects in Liquid Water by Infrared

Spectroscopy." *The Journal of Chemical Physics* 116(11):4626–42. Retrieved (http://aip.scitation.org/doi/10.1063/1.1448286).

Michel, Hanspeter, Mathias Tellenbach, and Arminio Boschetti. 1983. "A Chlorophyll B-Less Mutant of Chlamydomonas Reinhardii Lacking in the Light-Harvesting Chlorophyll Ab-Protein Complex but Not in Its Apoproteins." *Biochimica et Biophysica Acta - Bioenergetics* 725(3):417–24.

Miller, Lisa M., Megan W. Bourassa, and Randy J. Smith. 2013. "FTIR Spectroscopic Imaging of Protein Aggregation in Living Cells." *Biochimica et Biophysica Acta* 1828(10):2339–46. Retrieved (http://www.ncbi.nlm.nih.gov/pubmed/23357359).

Minagawa, Jun and Ryutaro Tokutsu. 2015. "Dynamic Regulation of Photosynthesis in Chlamydomonas Reinhardtii." *Plant Journal* 82(3):413–28.

Miskiewicz, E. and Kenneth E. Wilson. 2017. "Personal Communication."

Mizusawa, Naoki and Hajime Wada. 2012. "The Role of Lipids in Photosystem II." *Biochimica et Biophysica Acta - Bioenergetics* 1817(1):194–208. Retrieved (http://dx.doi.org/10.1016/j.bbabio.2011.04.008).

Moller, I. M., P. E. Jensen, and A. Hansson. 2007. "Oxidative Modifications to Cellular Components in Plants." Pp. 459–81 in *Annual Review of Plant Biology*, vol. 58, *Annual Review of Plant Biology*. Univ Copenhagen, Dept Agr Sci, DK-1871 Frederiksberg C, Denmark. Univ Copenhagen, Fac Life Sci, Dept Plant Biol, DK-1871 Frederiksberg C, Denmark. Moller, IM (reprint author), Aarhus Univ, Fac Agr Sci, Dept Genet & Biotechnol, DK-8830 Tjele, Denmark. imm@: Annual Reviews.

Mourant, Judith R., Y. R. Yamada, S. Carpenter, L. R. Dominique, and J. P. Freyer. 2003. "FTIR Spectroscopy Demonstrates Biochemical Differences in Mammalian Cell Cultures at Different Growth Stages." *Biophysical Journal* 85(3):1938–47.

Movasaghi, Zanyar, Shazza Rehman, and Dr.Ihtesham ur Rehman. 2008. "Fourier Transform Infrared (FTIR) Spectroscopy of Biological Tissues." *Applied Spectroscopy Reviews* 43(2):134–79. Retrieved (http://www.tandfonline.com/doi/abs/10.1080/05704920701829043).

Nabedryk, E., M. Leonhard, W. Mäntele, and J. Breton. 1990. "Fourier Transform Infrared Difference Spectroscopy Shows No Evidence for an Enolization of Chlorophyll a upon Cation Formation Either in Vitro or during P700 Photooxidation." *Biochemistry* 29(13):3242–47.

Nadtochenko, V. A., A. G. Rincon, S. E. Stanca, and John Kiwi. 2005. "Dynamics of E. Coli Membrane Cell Peroxidation during TiO2 Photocatalysis Studied by ATR-FTIR Spectroscopy and AFM Microscopy." *Journal of Photochemistry and Photobiology A: Chemistry* 169(2):131–37.

Niyogi, K. K. 1997. "Chlamydomonas Xanthophyll Cycle Mutants Identified by Video Imaging of Chlorophyll Fluorescence Quenching." *THE PLANT CELL ONLINE* 9(8):1369–80. Retrieved (http://www.plantcell.org/cgi/doi/10.1105/tpc.9.8.1369).

Noguchi, T., T. Tomo, and Y. Inoue. 1998. "Fourier Transform Infrared Study of the Cation

Radical of P680 in the Photosystem II Reaction Center: Evidence for Charge Delocalization on the Chlorophyll Dimer." *Biochemistry* 37(39):13614–25.

Oleszko, Adam et al. 2015. "Application of FTIR-ATR Spectroscopy to Determine the Extent of Lipid Peroxidation in Plasma during Haemodialysis." *BioMed Research International* 2015:1–9.

Palmucci, M., S. Ratti, and M. Giordano. 2011. "Ecological and Evolutionary Implications of Carbon Allocatiosn in Marine Phytoplankton as a Function of Nitrogen Availability: A Fourier Transform Infrared Spectroscopy Approach." *Journal of Phycology* 47(2):313–23.

Park, H. and J. K. Hoober. 1997. "Chlorophyll Synthesis Modulates Retention of Apoproteins of Light-Harvesting Complex II by the Chloroplast in Chlamydomonas Reinhardtii." *Physiologia Plantarum* 101:135–42.

Polle, J. E., J. R. Benemann, a Tanaka, and a Melis. 2000. "Photosynthetic Apparatus Organization and Function in the Wild Type and a Chlorophyll B-Less Mutant of Chlamydomonas Reinhardtii. Dependence on Carbon Source." *Planta* 211(3):335–44.

Polle, J. E. W. 2001. "Absence of Lutein, Violaxanthin and Neoxanthin Affects the Functional Chlorophyll Antenna Size of Photosystem-II but Not that of Photosystem-I in the Green Alga Chlamydomonas Reinhardtii." *Plant and Cell Physiology* 42(5):482–91. Retrieved (https://academic.oup.com/pcp/article-lookup/doi/10.1093/pcp/pce058).

Rochaix, Jean David, Nicolas Fischer, and Michael Hippler. 2000. "Chloroplast Site-Directed Mutagenesis of Photosystem I in Chlamydomonas: Electron Transfer Reactions and Light Sensitivity." *Biochimie* 82(6–7):635–45.

Rokitskaya, Tatyana I., Elena A. Kotova, Igor I. Agapov, Mikhail M. Moisenovich, and Yuri N. Antonenko. 2014. "Unsaturated Lipids Protect the Integral Membrane Peptide Gramicidin A from Singlet Oxygen." *Febs Letters* 588(9):1590–95.

Sackett, Olivia et al. 2016. "Snapshot Prediction of Carbon Productivity, Carbon and Protein Content in a Southern Ocean Diatom Using FTIR Spectroscopy." *ISME Journal* 10(2):416–26. Retrieved (http://dx.doi.org/10.1038/ismej.2015.123).

Salin, M. L. 1988. "Toxic Oxygen Species and Protective Systems of the Chloroplast." *Physiologia Plantarum* 72(3):681–89.

Sánchez-Alonso, Isabel, Pedro Carmona, and Mercedes Careche. 2012. "Vibrational Spectroscopic Analysis of Hake (Merluccius Merluccius L.) Lipids during Frozen Storage." *Food Chemistry* 132(1):160–67.

Sanchez-Ruiz, Jose M. and Marino Martinez-Carrion. 1988. "A Fourier-Transform Infrared Spectroscopic Study of the Phosphoserine Residues in Hen Egg Phosvitin and Ovalbumin." *Biochemistry* 27(9):3338–42.

Santos, Ana L. et al. 2013. "Effects of UV Radiation on the Lipids and Proteins of Bacteria Studied by Mid-Infrared Spectroscopy." *Environmental Science & Technology* 47:6306–15.

Sherman, Gwendolyn and Shu-Fong Wang. 1967. "Infrared Spectral Observations of Chlorophyll-a and Ethyl Chlorophyllide-a in the Solid State." *Photochemistry and*

*Photobiology* 6:239–45.

Shivu, Bhavana et al. 2013. "Distinct β-Sheet Structure in Protein Aggregates Determined by ATR-FTIR Spectroscopy." *Biochemistry* 52(31):5176–83.

Sies, Helmut. 2016. *Biochemistry of Oxidative Stress Physiopathology and Clinical Aspects*.

Sies, Helmut, Carsten Berndt, and Dean P. Jones. 2017. "Oxidative Stress." *Annual Review of Biochemistry* (86):715–48.

Sigee, D. C., F. Bahram, B. Estrada, R. E. Webster, and A. P. Dean. 2007. "The Influence of Phosphorus Availability on Carbon Allocation and P Quota in Scenedesmus Subspicatus: A Synchrotron-Based FTIR Analysis." *Phycologia* 46(5):583–92.

Spudich, J. L. and R. Sager. 1980. "Regulation of the Chlamydomonas Cell-Cycle by Light and Dark." *Journal of Cell Biology* 85(1):136–46.

Suzuki, Nobuhiro, Shai Koussevitzky, Ron Mittler, and Gad Miller. 2012. "ROS and Redox Signalling in the Response of Plants to Abiotic Stress." *Plant, Cell and Environment* 35(2):259–70.

Tamm, Lukas K. and Suren A. Tatulian. 1997. "Infrared Spectroscopy of Proteins and Peptides in Lipid Bilayers." *Quarterly Reviews of Biophysics* 30(4):365–429. Retrieved (http://journals.cambridge.org/abstract_S0033583597003375).

Tanaka, Ayumi et al. 1998. "Chlorophyll a Oxygenase (CAO) Is Involved in Chlorophyll B Formation from Chlorophyll a." *Plant Biology* 95(October):12719–23.

Telfer, Alison. 2014. "Singlet Oxygen Production by PSII Under Light Stress: Mechanism, Detection and the Protective Role of Beta-Carotene." *Plant and Cell Physiology* 55(7):1216–23.

Thompson, G. A. 1996. "Lipids and Membrane Function in Green Algae." *Biochimica Et Biophysica Acta-Lipids and Lipid Metabolism* 1302(1):17–45.

Triantaphylides, C. et al. 2008. "Singlet Oxygen Is the Major Reactive Oxygen Species Involved in Photooxidative Damage to Plants." *Plant Physiology* 148(2):960–68.

Triantaphylides, C. and M. Havaux. 2009. "Singlet Oxygen in Plants: Production, Detoxification and Signaling." *Trends in Plant Science* 14(4):219–28.

Ünlü, Caner, Bartlomiej Drop, Roberta Croce, and Herbert van Amerongen. 2014. "State Transitions in Chlamydomonas Reinhardtii Strongly Modulate the Functional Size of Photosystem II but Not of Photosystem I." *Proceedings of the National Academy of Sciences* 111(9):3460–65. Retrieved (http://www.pnas.org/lookup/doi/10.1073/pnas.1319164111).

Vass, Imre. 2011. "Role of Charge Recombination Processes in Photodamage and Photoprotection of the Photosystem II Complex." *Physiologia Plantarum* 142(1):6–16.

Vieler, A., C. Wilhelm, R. Goss, R. Sub, and J. Schiller. 2007. "The Lipid Composition of the Unicellular Green Alga Chlamydomonas Reinhardtii and the Diatom Cyclotella Meneghiniana Investigated by MALDI-TOF MS and TLC." *Chemistry and Physics of*

*Lipids* 150(2):143–55.

Voigt, J., P. Munzner, and H. P. Vogeler. 1991. “The Cell-Wall Glycoproteins of Chlamydomonas Reinhardtii - Analysis of the in Vitro Translation Products.” *Plant Science* 75(1):129–42.

Voort, F. R., A. A. Ismail, J. Sedman, and G. Emo. 1994. “Monitoring the Oxidation of Edible Oils by Fourier Transform Infrared Spectroscopy.” *J. Am. Oil Chem. Soc.* 71(3):243–53.

Wang, Thomas D. et al. 2007. “Detection of Endogenous Biomolecules in Barrett’s Esophagus by Fourier Transform Infrared Spectroscopy.” *Proceedings of the National Academy of Sciences of the United States of America* 104(40):15864–69.

Weigl, J. W. and R. Livingston. 1953. “Infrared Spectra of Chlorophyll and Related Compounds.” *Journal of the American Chemical Society* 75(9):2173–76.

Wilson, Kenneth E. 2016. “Personal Communication.”

Wilson, Kenneth E. and Norman P. A. Huner. 2000. “The Role of Growth Rate, Redox-State of the Plastoquinone Pool and the Trans-Thylakoid Δph in Photoacclimation of Chlorella Vulgaris to Growth Irradiance and Temperature.” *Planta* 212(1):93–102.

Zer, Hagit and Itzhak Ohad. 2003. “Light, Redox State, Thylakoid-Protein Phosphorylation and Signaling Gene Expression.” *Trends in Biochemical Sciences* 28(9):467–70.

Zhang, Fengqiu, Qing Huang, Jingwen Yan, and Zhu Chen. 2016. “Histone Acetylation Induced Transformation of B-DNA to Z-DNA in Cells Probed through FT-IR Spectroscopy.” *Analytical Chemistry* 88(8):4179–82.